**Universidade do Minho**
I3Bs - Instituto de Investigação em Biomateriais, Biodegradáveis e Biomiméticos

Ana Rita Sobreiro Almeida

# New strategies envisioning functional recovery of the injured kidney

dezembro de 2020

New strategies envisioning functional recovery of the injured kidney
Ana Rita Sobreiro Almeida
UMinho | 2020

**Universidade do Minho**

I3Bs - Instituto de Investigação em Biomateriais, Biodegradáveis e Biomiméticos

Ana Rita Sobreiro Almeida

# New strategies envisioning functional recovery of the injured kidney

Tese de Doutoramento em Engenharia de Tecidos, Medicina Regenerativa e Células Estaminais

Trabalho efetuado sob a orientação de

**Professor Nuno João Meleiro Alves das Neves**

dezembro de 2020

# ACKNOWLEDGMENTS

This PhD has been a long journey, which would had never been possible without the help, support and guidance of several people, whether scientific or personal. This chapter is for them.

First of all, I would like to acknowledge the financial support to the Portuguese Foundation of Science and Technology, not only for my individual grant, but also for the project funding which allowed me to conduct the experimental studies. I also want to express my gratitude to the director of the 3B's Research Group, Prof. Dr. Rui L. Reis, for giving me the opportunity to join this prestigious research group. The scientific experience gathered through these 4 years will definitely be of advantage for my future scientific career. To all 3B's Research Group members that helped me along the way, guiding me in the smallest things, that resulted being bigger. Thank you so much.

I would also like to thank my supervisor, Prof. Dr. Nuno Neves. If I look back 4 years, I see a young naive girl, without experience but with great will. Prof. Nuno was the person that believed in that will from the beginning. He challenged, tested and proved me every time, and even though sometimes I would not understand, now I can see clearly: "Experience is what you get, when you don't get what you want".

I would definitely have to thank to all my co-authors. All of you have been essential for producing the scientific outcomes of this thesis. Thank you for reaching out for me, especially in the hardest moments. A special thanks to Prof. Dr. Paola Romagnani and Prof. Dr. Laura Lasagni. They received me abroad and taught me so much more than what is inside this thesis. Big thanks.

To all my friends, especially to the ones that I made in 3B's. Although we are all different, we share the same feelings, same frustrations, same thoughts and same values. They helped me more than what I can write into words. I care for them all, and I know for sure that this friendship will last. Thank you. To my "forever" friends, although you do not understand most of the politics, you have always been my "escape", making me laugh of the most serious things. You are amazing.

To my partner in crime, Diogo. You have seen my best and my worse, and still you love me. Every problem vanishes when I arrive home. I learned a lot from your hard work and dedication. Thank you for that hug in the hard days. Thank you for lifting me up, every single time. Thank you, half.

At last, but not least, to my family. Their unconditional love, their patience, their advices, the dreams they share with me. They are always there for me, taking the weight off my shoulders, supporting and making me push even harder every time. My will, my ambition, my determination, my way of looking into life and the future, it's all theirs. Special thanks to my mom, which I will never thank enough.

## STATEMENT OF INTEGRITY

I hereby declare having conducted this academic work with integrity. I confirm that I have not used plagiarism or any form of undue use of information or falsification of results along the process leading to its elaboration.

I further declare that I have fully acknowledged the Code of Ethical Conduct of the University of Minho.

## ABSTRACT

Kidney diseases represent a major healthcare burden worldwide. It is estimated that one in ten persons suffer from kidney dysfunction. Indeed, a decline in renal function is considered an independent risk factor for both cardiovascular disease and all-cause mortality. The problem is only aggravated by treatment alternatives, with dialysis and transplantation being the only currently available renal replacement therapies.

Envisioning the functional recovery of the injured kidney, two regenerative resources were explored: porcine-derived kidney decellularized matrices and renal progenitor cells from human origin. For that, the decellularization process was optimized to obtain porcine kidney decellularized tissue. A full characterization of this matrix in terms of morphology, structural integrity, biochemical content, thermal and molecular properties and protein content was performed. Indeed, porcine-derived matrices were validated as an adequate raw material for the production of several decellularized-based substrates. Namely, kidney tissue-derived electrospun membranes were fabricated for the development of a tubular filtration barrier model. Additionally, decellularized tissue was used for the fabrication of a particulate matrix and a bioink, where 3D cultures of isolated renal cells were established envisioning implantation. Indeed, these cells already shown to possess reparative properties when injected into the injured kidney tissue alone, with limited efficacy. They were also used to develop an organoid model of the glomerulus. Overall, renal progenitor cells demonstrated versatility, specific differentiation into renal phenotypes and proliferation capacity when embedded on the matrix substrates.

The works developed in this thesis show that decellularized-based biomaterial substrates may have multiple applications, from modeling systems to moldable implantable scaffolds for tissue engineering strategies. These substrates demonstrated physiological kidney tissue characteristics, allowing cultured cells to represent morphological, phenotypic and functional properties of *in vivo* systems. Ultimately, this thesis allowed for the development of advanced strategies comprising both relevant cells and biomaterial substrates that may have greater implications in the biomedical field as promising solutions to address renal pathologies in its early stages.


**Keywords**: Advanced Therapies, Decellularized Matrices, Kidney Decellularization, Renal Progenitor Cells, Tissue Models

# RESUMO

As doenças renais representam um grande problema económico-social. Está estimado que uma em cada dez pessoas sofre de disfunção renal. São também consideradas um fator de risco para doenças cardiovasculares e para a taxa de mortalidade geral. Este problema é agravado visto que as únicas opções de tratamento atuais são a diálise e transplantação.

Visto que o objetivo inicial da tese é a recuperação do rim lesado, foram explorados dois recursos regenerativos: matriz extracelular de rim de porcino decelularizadas e células progenitoras renais de origem humana. O processo de descelularização foi cuidadosamente otimizado com vista a obter matrizes descelularizadas. Posteriormente, foi feita uma caracterização completa da matriz de porcino em termos de morfologia, integridade estrutural, conteúdo bioquímico, propriedades térmicas e moleculares e ainda conteúdo proteico. Estas matrizes foram usadas como base para produção de diversos biomateriais. Foram fabricadas membranas fibrosas por electrofiação para o desenvolvimento de um modelo *in vitro* da barreira de filtração tubular. A matriz descelularizada foi usada para obter partículas e também uma biotinta, onde foram estabelecidas culturas 3D de células renais isoladas, com o objetivo final de implantação. Estas células demonstraram anteriormente o seu potencial quando injetadas num rim lesado, com limitada eficácia. Nesta tese, as mesmas células foram também usadas para desenvolver um modelo de organoide do glomérulo. As células progenitoras renais demonstraram ter versatilidade, capacidade de diferenciação específica em fenótipos renais e de proliferação quando cultivadas nas matrizes.

Os materiais produzidos a partir da matriz decelularizada demonstraram poder ser usados em múltiplas aplicações, desde modelos para estudos *in vitro* até *scaffolds* implantáveis para estratégias de engenharia de tecidos. Estes biomateriais demonstraram ter uma variabilidade fisiológica semelhante à do rim, o que permitiu às células cultivadas modelar propriedades dos sistemas *in vivo*, nomeadamente morfológicas, fenotípicas e funcionais. Por fim, esta tese permitiu o desenvolvimento de estratégias avançadas compostas por células e biomateriais relevantes, que podem ter imensas implicações biomédicas como soluções promissoras para o tratamento de lesões renais em estágios iniciais.

**Palavras-chave:** Células Progenitoras Renais, Decelularização do Rim, Matrizes Decelularizadas, Modelos de tecido, Terapias Avançadas

TABLE OF CONTENTS

ACKNOWLEDGMENTS III

STATEMENT OF INTEGRITY IV

ABSTRACT V

RESUMO VI

LIST OF ABBREVIATIONS XIII

LIST OF FIGURES XVI

LIST OF SUPPLEMENTARY FIGURES XVIII

LIST OF TABLES XX

LIST OF SUPPLEMENTARY TABLES XX

LIST OF EQUATIONS XX

SHORT *CURRICULUM VITAE* XXI

LIST OF PUBLICATIONS XXII

INTRODUCTION TO THE THESIS FORMAT XXV

SECTION 1 GENERAL INTRODUCTION 1

CHAPTER I RENAL REGENERATION: THE ROLE OF EXTRACELLULAR MATRIX AND CURRENT ECM-BASED TISSUE ENGINEERED STRATEGIES 2

Abstract 3

I-1. Kidneys Function and Disease 4

I-2. Kidney Extracellular Matrix 6

I-2.1. Kidney ECM composition and structure 6

I-2.2. The role of the ECM in kidney remodeling and repair after insult 8

I-3. Kidney tissue engineering strategies 10

I-3.1. Cell-based approaches 10

I-3.2. Biomaterial-based approaches 12

I-3.3. Kidney decellularized matrices 14

I-4. Concluding remarks and perspectives 28

I-5. References 29

SECTION 2 EXPERIMENTAL DESIGN 42

CHAPTER II MATERIALS & METHODS 43

Overview 44

II-1. Materials 45

II-1.1. Decellularized Kidney Matrix 45

II-1.2. Poly(caprolactone) 47

II-2. Methods 48

II-2.1. Biomaterials' assays 48

II-2.2. Biological Assays 62

II-3. References 77

SECTION 3 DEVELOPMENT OF KIDNEY TISSUE MODEL SYSTEMS 84

CHAPTER III EXTRACELLULAR MATRIX ELECTROSPUN MEMBRANES FOR MIMICKING NATURAL RENAL FILTRATION BARRIERS 85

Abstract 86

III-1. Introduction 87

III-2. Experimental 89

III-2.1. Decellularization process 89

III-2.2. Characterization of decellularized kidney extracellular matrix (dKECM) 89

III-2.3. Scaffold fabrication 91

III-2.4. Scaffold characterization 92

III-2.5. Culture of human kidney cells on electrospun membranes 92

III-3. Results 95

III-3.1. dKECM characterization 95

III-3.2. Electrospun dKECM characterization 98

III-3.3. Analysis of HK-2 cell cultures 101

III-4. Discussion 106

III-5. Conclusions 110

III-6. References 111

III-7. Supplementary Information 114

CHAPTER IV CO-CULTURES OF RENAL PROGENITORS AND ENDOTHELIAL CELLS ON KIDNEY DECELLULARIZED MATRICES REPLICATE THE RENAL TUBULAR ENVIRONMENT *IN VITRO* 116

Abstract 117

IV-1. Introduction 118

IV-2. Materials and Methods 119

IV-2.1. Experimental Design 119

IV-2.2. Processing of decellularized kidney electrospun membranes 120

IV-2.3. Biochemical and immunohistochemistry analysis of the dKECM 121

IV-2.4. DKECM electrospun membranes morphological and structural characterization 121

IV-2.5. Isolation and characterization of human renal progenitor cells (hRPC) 122

IV-2.6. Renal endothelium-epithelium mono and bilayer seeding 122

IV-2.7. Evaluation of cellular viability, proliferation and morphology 123

IV-2.8. Immunofluorescence of renal epithelial-related proteins 124

IV-2.9. Real-time quantitative polymerase chain reaction (RT-PCR) of tubular-related genes 124

IV-2.10. Paracellular permeability and albumin reabsorption studies 125

IV-2.11. Nephrotoxicity assessment 125

IV-2.12. Statistical analysis 126

IV-3. Results 126

IV-3.1. dKECM and dKECM-derived membrane characterization 126

IV-3.2. Cellular behaviour of hRPCs on decellularized matrix membranes 127

IV-3.3. Phenotypic characterization of hRPCs over time 129

IV-3.4. Polarization and maturity assessment on proximal tubule cells 131

IV-3.5. Characterization of proximal tubule physiological functions 133

IV-3.6. Model of drug-induced nephrotoxicity 134

IV-4. Discussion 135

IV-5. References 138

IV-6. Supplementary Information 141

CHAPTER V RETINOIC ACID BENEFITS GLOMERULAR ORGANOTYPIC DIFFERENTIATION FROM ADULT RENAL PROGENITOR CELLS *IN VITRO* 144

Abstract 145

V-1. Introduction 146

V-2. Materials and Methods 148

V-2.1. Human renal progenitor cells (hRPCs) isolation 148

V-2.2. Spheroid formation and differentiation 148

V-2.3. Endothelial inclusion on the spheroids 149

V-2.4. Viability and growth over time 149

V-2.5. Flow cytometry characterization 149

V-2.6. Immunocytochemistry and immunohistochemistry 150

V-2.7. Gene expression analysis 150

V-2.8. Statistical analysis 151

V-3. Results 151

V-3.1. Spheroids remain viable and intact during long-time cultures 151

V-3.2. Short maturation time potentiates the effect of retinoic acid 152

V-3.3. Specific markers expression is dependent of the seeding concentration 154

V-3.4. Retinoic acid outstands CHIR99021 on spheroid glomerular differentiation 155

V-3.5. Endothelial inclusion allows for a higher spheroid organizational level 157

V-4. Discussion 159

V-5. Conclusion 162

V-6. References 163

V-7. Supplementary Information 166

SECTION 4 STRATEGIES FOR RENAL REGENERATION 169

CHAPTER VI PARTICULATE KIDNEY EXTRACELLULAR MATRIX: BIOACTIVITY AND PROTEOMIC ANALYSIS OF A NOVEL SCAFFOLD FROM PORCINE ORIGIN 170

**Abstract** 171

**VI-1. Introduction** 172

**VI-2. Materials and Methods** 173

VI-2.1. Processing and characterization of kidney ECM derived powders (pKECM) 173

VI-2.2. *In vitro* renal progenitor cell culture studies on pKECM 175

VI-2.3. Statistical analysis 177

**VI-3. Results** 177

VI-3.1. Evaluation of pKECM substrates 177

VI-3.2. 3D culture of renal progenitor cells and pKECM 183

**VI-4. Discussion** 189

**VI-5. Conclusions** 192

**VI-6. References** 193

**VI-7. Supplementary Information** 196

VI-7.1. Supplementary methods 196

VI-7.2. References 199

VI-7.3. Supplementary Figures and Tables 200

**CHAPTER VII DECELLULARIZED KIDNEY EXTRACELLULAR MATRIX BIOINKS RECAPITULATE RENAL 3D MICROENVIRONMENT *IN VITRO*** 206

**Abstract** 207

**VII-1. Introduction** 208

**VII-2. Methods** 209

VII-2.1. Tissue decellularization and characterization 209

VII-2.2. Bioink development and characterization 210

VII-2.3. Cellular encapsulation on dKECM bioinks 211

VII-2.4. Printing of cell-laden constructs 211

VII-2.5. Evaluation of cellular performance 212

VII-2.6. Evaluation of cellular phenotype 212

VII-2.7. Development of the glomerular model 213

VII-2.8. Statistical Analysis 213

VII-3. Results 213
VII-3.1. Tissue processing and evaluation of decellularization 213
VII-3.2. Effect of dKECM bioink concentration on structural and rheological properties 215
VII-3.3. Printability of dKECM bioink using a support bath 218
VII-3.4. Biological evaluation of dKECM bioinks 221
VII-3.5. Tissue-specific proteins on encapsulated hRPCs 224
VII-3.6. 3D Printing of a pre-glomerular model 225
VII-4. Discussion 227
VII-5. Conclusions 230
VII-6. References 231
VII-7. Supplementary Information 235
SECTION 5 238
GENERAL CONCLUSIONS 238
CHAPTER VIII GENERAL CONCLUSIONS AND FUTURE PERSPECTIVES 239
VIII-1. General conclusions 240
VIII-2. Future Perspectives 242

# LIST OF ABBREVIATIONS

## #

2D – 2-Dimensional
3D – 3-Dimensional
µL – microliter
µm – micrometer
µg $mL^{-1}$ – microgram per milliliter
% – Percentage
5/10/20K – Five/Ten/Twenty thousand

## A

Abs – Absorbance
AB – Alcian Blue
ACN – Acetonitrile
AIM – Anterior Intermediate Mesoderm
AKI – Acute Kidney Injury
ANOVA – Analysis of variance
AP – Anterior-posterior
AQP1 – Aquaporin-1
ASCs – Adipose-derived Stem Cells
ATCC - American Type Culture Collection
ATN – Acute Tubular Necrosis
ATR-FTIR – Attenuated total reflection Fourier Transformed Infrared Spectroscopy

## B

BAK – Bioartificial Kidney
BCA – Bicinchoninic acid
BM – Basement Membrane
BSA – Bovine serum albumin

## C

$CaCl_2$ – Calcium Chloride
Calcein-AM – Calcein-Acetoxymethyl
CD – Cluster of Differentiation
cDNA – Complementary DNA
CHIR99021 – chemical inhibitor of GSK-3 enzyme
CKD – Chronic Kidney Injury
CLC-NKA – Chloride Channel Ka
$cm^{-1}$ – Wavenumber
COL – Collagen
CRISPR – Clustered Regularly Interspaced Short Palindromic Repeats
Ct – Cycle Threshold
CV – Coefficient of Variation

## D

d – Days
Da – Dalton
DAPI – 4',6-diamidino-2-phenylindole
DKD – Diabetic kidney disease
dKECM – Decellularized Kidney Extracellular Matrix
DMMB – Dimethylmethylene blue
DMEM – Dulbecco's modified Eagle's medium
DMF - N,N-dimethylformamide
DMSO – Dimethylsulfoxide
DNA - Deoxyribonucleic Acid
DPBS – Dulbecco's Phosphate-Buffered Saline
DSC – Differential Scanning Calorimetry
dsDNA – Double stranded Deoxyribonucleic Acid

## E

EBM - Endothelial Basal Medium
ECM – Extracellular matrix
EDS – Energy-Dispersive X-ray Spectroscopy
EDTA – Ethylenediamine tetraacetic acid
EGM-MV – Microvascular Endothelial Cell Growth Medium
ESCs – Embryonic Stem Cells
ESRD – End Stage Renal Disease
EtOH - ethanol
eV – electron Volt
Ex/Em – Excitation/Emission

## F

FA – Formic acid
FACIT collagens – Fibril-associated collagens
FBS – Fetal bovine serum
FC – Flow Cytometry
FDA – Food and drug administration
FDR – False Discovery Rate

FE – Fold expression
FG – Fibrinogen
FGF-9 – Fibroblast growth factor 9
FITC – Fluorescein Isothiocyanate
FN – Fibronectin
F1/2/3 – Different fractions of protein extraction

G
g – grams
G – gauge
GAGs – Glycosaminoglycans
GAPDH – Glyceraldehydes-3-phosphate-dehygrogenase
GBM – Glomerular Basement Membrane
GFs – Growth factors
GFR – Glomerular Filtration Rate
GGT1 – γ-glutamyltranspeptidase
GS – Glomerulosclerosis
GSK-3 – Glycogen synthase kinase 3

H
h – Hours
HA – Hyaluronic acid
HCl – Hydrochloric acid
HFIP – 1,1,1,3,3,3- Hexafluoro-2-propanol
HK-2 – Human Kidney-2 cell line
HMDS – 1,1,1,3,3,3-Hexamethyldisilazane
HMECs – Human Microvascular Endothelial Cells
hRPCs – Human renal progenitor cells
HSA – Human Serum Albumin
HSPG – Heparan Sulfate Proteoglycans
HUVECs – Human Umbilical Vein Endothelial Cells
H&E – Hematoxylin–eosin

I
ICU – Intensive Care Unit
IF – Immunofluorescence
IHC – Immunohistochemistry
iPSC – Induced Pluripotent Stem Cell

K
kDa - kiloDalton
kPa - kiloPascal
kV - kiloVolt

L
LAM – Laminin
LASX – Leica Application Software X
LVE – Linear viscoelastic region

M
M – Molar
mg – milligram
mg $mL^{-1}$ – milligram per milliliter
min – minute
mL – Milliliter
mm – Millimeter
$mm^{2/3}$ – square/cubic millimeter
mM – Millimolar
MMPs – Matrix metalloproteases
mm $s^{-1}$ – millimeters per second
MSCs – Mesenchymal Stem Cells
MTS/MTT – Tetrazolium
MT – Masson Trichrome
mTG – microbial transglutaminase
Mw – Molecular weight

N
n – Number of samples
nanoLC-MS/MS – nano-liquid chromatography-tandem mass spectometry
NaOH – Sodium hydroxide
NC domain – Non-collagenous domain
NCC – Na/Cl co-transporter
NID – Nidogen
nm – Nanometer
ng – Nanograms
ng $mL^{-1}$ – nanogram per milliliter
NPHS1 – Nephrin
NPHS2 – Podocin

O

OCT – Optimal cutting temperature
OCT4 – Octamer-binding transcription factor 4

P

PATH – Doctoral Program on Advanced Therapies for Health
PAX2 – Paired box2
PBS – Phosphate buffer saline
PCL – Poly(caprolactone)
PCR – Polymerase Chain Reaction
PGA – Polyglycolic acid
pH - Hydrogenionic potential
PI – Propidium iodide
PIM –Posterior Intermediate Mesoderm
PKD – Polycystic kidney disease
pKECM – Particulate kidney extracellular matrix
PLGA – poly(lactic-co-glycolic acid)
*p* – Statistical level of significance

Q

qPCR – Quantitative polymerase chain reaction

R

RA – Retinoic Acid
REGM – Renal Epithelial Cell Growth Medium
RM – Regenerative Medicine
RNA – Ribonucleic Acid
Rpm – Rotations per minute
RPTECs – Renal Proximal Tubular Epithelial Cells
RT – Room temperature
RT-PCR – Real-time quantitative polymerase chain reaction
RAD – Renal Tubule Assist Device

S

s - seconds
SCID – Severe combined immunodeficient mice
SD – Standard deviation
SDS – Sodium Dodecyl Sulfate
SEM – Scanning electron microscopy
SGLT2 – Sodium glucose transporter
SLC – Solute Carrier Family
SYNPO – Synaptopodin

T

TBM – Tubular Basement Membrane
TCPS – Tissue culture polystyrene
TE – Tissue Engineering
TEER –Transepithelial electrical resistance
TGF-β – Transforming growth factor β
THP – Tamm-Horsfall protein
TJ – Tight Junction
T0/2/5 – Time/Day

U

UV – Ultraviolet

V

V – Volume
v/v – volume/volume
VEGF – Vascular endothelial growth factor
vWF – von Willebrand Factor

W

w/v – weight/volume
w/w –weight/weight
WT1 – Wilms tumor 1

Z

ZO – Zona Occludens

## LIST OF FIGURES

Figure I-1– Schematic representation of a longitudinal section of a whole kidney (left image) and an magnification of the renal medulla and renal cortex, representing two whole nephrons; schematic representation of the glomerular and tubular filtration barriers (right images). _____ 5

Figure I-2 – Major kidney ECM components and the major factors influencing its composition. _____ 8

Figure I-3 – The different uses of kidney decellularized matrices for regenerative medicine strategies. 16

Figure II-1 – Examples of macroscopic aspect of organs before and after decellularization process. __46

Figure II-2 – Ring-opening polymerization of ε-caprolactone into poly(caprolactone). _____47

Figure II-3 – Schematic representation of the decellularization process. _____49

Figure II-4 - Schematic representation of the processing steps after the decellularization process. ___49

Figure II-5 - Schematic representation of the methodology used to obtain ECM fractions. _____55

Figure II-6 – Schematic representation of the co-culture and monoculture cell seeding on the electrospun membranes. _____66

Figure II-7 – Schematic representation of the 3D culture performed on pKECM substrates. _____67

Figure II-8 – Schematic representation of spheroid seeding and differentiation protocol with retinoic acid. _____68

Figure II-9 – Schematic representation of the decellularized matrix bioprinting process using an agarose support bath. _____69

Figure III-1 – Macroscopic evaluation of kidney decellularization. _____89

Figure III-2 – DAPI staining before (A) and after (B) decellularization. _____96

Figure III-3 – Hematoxylin and eosin staining of native and decellularized kidney tissue. _____97

Figure III-4 – SEM micrographs of decellularized tissues. _____97

Figure III-5 – Collagen (A) and sGAG's (B) quantification on native vs. decellularized tissue. _____98

Figure III-6 – SEM micrographs of 70:30 ECM:PCL, 50:50 ECM:PCL, 30:70 ECM:PCL and PCL. __100

Figure III-7 – Mechanical behavior of the produced electrospun meshes. _____101

Figure III-8 – Viability of the HK-2 cells measured by MTS assay. _____101

Figure III-9 – Cell proliferation measured by quantification of DNA with Picogreen kit. 102

Figure III-10 – Protein Intracellular content on HK-2 cells. 103

Figure III-11 – SEM micrographs of HK-2 cells. 104

Figure III-12 – Immunocytochemistry of epithelial marker zona occludens-1 (red) and DAPI (blue). 105

Figure III-13 – Measurement of TEER over a 14-day period. 106

Figure IV-1 - Schematic representation of decellularization process and membranes preparation procedure. 120

Figure IV-2 – dKECM characterization. 127

Figure IV-3 – Behavior of hRPC in contact with decellularized matrix membrane over 21 days. 129

Figure IV-4 – Phenotypic characterization of hRPCs cultured on decellularized membranes. Gene expression of tubular related markers. 131

Figure IV-5 – Assessment of hRPTECs maturity and polarization after 7 days of bilayer assembling. 132

Figure IV-6 – Functional assays on the bilayer model. 133

Figure IV-7 – Cisplatin-induced nephrotoxicity model. 135

Figure V-1 – Spheroids remain viable and intact during long-time cultures. 152

Figure V-2 – Short maturation time potentiates the effect of retinoic acid. 153

Figure V-3 – Specific markers expression is dependent of the seeding concentration. 155

Figure V-4 – Retinoic acid outstands CHIR99021 on spheroid glomerular differentiation. 156

Figure V-5 – Retinoic acid outstands CHIR99021 on spheroid glomerular differentiation. Immunofluorescent staining of hRPC-related markers. 157

Figure V-6 – Endothelial inclusion allows for a higher spheroid organizational level. 158

Figure VI-1 – Sequence of procedures used in the preparation of pKECM. 174

Figure VI-2 – Particulate kidney matrix characterization. 179

Figure VI-3 – Schematic representation of the methodology and the unique profile of the ECM fractions. 181

Figure VI-4 – Quantitative assessment of proteomic profile of pKECM by LC-MS/MS. 183

Figure VI-5 – Cytocompatibility of human renal progenitor cells. _____185

Figure VI-6 – Quantitative analysis of viability and proliferation of hRPCs cultured on pKECM. _____186

Figure VI-7 – Spatial distribution of hRPCs cultured on pKECM substrates. _____188

Figure VII-1 – Representative micrographs of native and decellularized kidney tissue and macroscopic representations of post-decellularization processing. _____215

Figure VII-2 – Rheological characterization of dKECM bioinks using different concentrations._____217

Figure VII-3 – Macroscopic printability evaluation using different 3D models. _____219

Figure VII-4 – Printability of the dKECM bioinks depending of the printing speed. _____220

Figure VII-5 – Cytocompatibility assessment of dKECM and gelatin-encapsulated hRPCs. _____223

Figure VII-6 – Evaluation of differentiation into renal-specific lineages and overall maturation of the constructs. _____225

Figure VII-7 – Development of a pre-glomerular model._____226

## LIST OF SUPPLEMENTARY FIGURES

Figure S III-1 – Viability of the HK-2 cells measured by MTS assay. _____114

Figure S III-2 – Cell proliferation measured by quantification of DNA with Picogreen kit. _____114

Figure S III-3 – Protein intracellular content on HK-2 cells. _____114

Figure S III-4 – SEM micrographs of HK-2 cells seeded on TCPS. _____115

Figure S IV-1 – Human renal progenitor cells (hRPCs) behavior and phenotypic expression when cultured on the decellularized membranes. _____141

Figure S IV-2 – Assessment of hRPTECs maturity and polarization in the monolayer model. (a-b) SEM micrographs of hRPTECs. _____142

Figure S IV-3 – Nephrotoxicity assessment of cisplatin on monocultures._____143

Figure S V-1 – Flow cytometry analysis for non-stimulated conditions. _____166

Figure S V-2 – Flow cytometry analysis for retinoic acid-stimulated conditions (induction)._____167

Figure S V-3 – Higher magnification (x63) images of hRPC spheroids with endothelial cells. _____168

Figure S VI-1 – Quantitative proteomic analysis of the 30 most abundant proteins on decellularized porcine matrix. 200

Figure S VI-2 – Flow cytometry characterization of hRPCs. 201

Figure S VI-3 – Venn diagram representing the overlap and differences between the human and porcine kidney ECM proteome as identified by the study of Louzao-martinez et al. 201

Figure S VI-4 – 3D micrograph of the hRPCs distribution on the pKECM. 202

Figure S VII-1 – Rheological characterization of the agarose support bath. 235

Figure S VII-2 – Scanning Electron micrographs of 1 and 2 % dKECM concentrations with and without microbial transglutaminase (mTG). 235

Figure S VII-3 – Macroscopic printability evaluation using different 3D models. 236

Figure S VII-4 – Histological evaluation of cellular performance inside the dKECM constructs. 236

Figure S VII-5 – Evaluation of differentiation into renal-specific lineages and overall maturation of the constructs. 237

## LIST OF TABLES

Table I-1– An overview of whole recellularized and/or implanted kidney scaffolds from the literature._22

Table II-1 – Antibodies and concentrations used for phenotypic markers analysis of the produced substrates. _____74

Table III-1 – Fiber diameters for the electrospun meshes._____99

## LIST OF SUPPLEMENTARY TABLES

Table S VI-1 – Quantitative proteomic analysis of decellularized porcine kidney ECM. _____203

## LIST OF EQUATIONS

Equation 1 _____60

Equation 2 _____61

Equation 3 _____61

Equation 4 _____75

# SHORT *CURRICULUM VITAE*

Ana Rita Sobreiro Almeida was born on the 6th of December 1992, in Águeda, Portugal. She is currently a PhD student at 3B's Research Group, I3Bs Research Institute on Biomaterials, Biodegradables and Biomimetics, at University of Minho, Headquarters of the European Institute of Excellence on Tissue Engineering and Regenerative Medicine at Avepark at Caldas das Taipas, Guimarães, Portugal.

Rita has graduated in Genetics and Biotechnology at the University of Trás-os-Montes e Alto Douro, Vila Real, Portugal with a final grade of 15/20, in 2013. Her curricular internship was performed in collaboration with Biocant, at the Nex Gen Seq Unit.

She proceeded to a master degree in Biophysics and Bionanosystems at the University of Minho, Braga, Portugal, which was successfully concluded in 2015, with a final grade of 18/20. The dissertation was performed under the scope of the ERASMUS program, at the Center of Biomaterials and Tissue Engineering, in the Universitat Politècnica de València, Spain. During this period, she worked with polymeric particles for bone regeneration, which resulted in a publication. Her master thesis was concluded with a final grade of 19/20.

In 2016, she won a research scholarship under the scope of her master thesis, under the project "ElectroBio", at the Center of Physics of the University of Minho, Braga, Portugal.

Later in 2016, she started her PhD at the 3B's Research Group, University of Minho, Portugal, under the supervision of Prof. Dr. Nuno Neves in the field of ECM-based materials for renal regeneration. During this time, she had the opportunity to go abroad for 9 months for a collaborative work, which was performed at the Department of Biomedical, Experimental and Clinical Medicine "Mario Serio" in the University of Florence, Italy.

Scientifically, Rita has contributed with 5 peer-reviewed papers in international journals (plus 3 submitted). Furthermore, she participated in national and international conferences with 2 oral communications and 6 poster communications.

# LIST OF PUBLICATIONS

The work performed during the PhD period resulted in the publications listed below:

## *INTERNATIONAL PUBLICATIONS IN SCIENTIFIC PEER-REVIEWED JOURNALS*

**Sobreiro-Almeida, Rita;** Melica, Maria Elena; Lasagni, Laura; Osório, Hugo; Romagnani, Paola; Neves, Nuno M. *Particulate kidney extracellular matrix: bioactivity and proteomic analysis of a novel scaffold from porcine origin*. Biomaterials Science, ahead of print, doi: 10.1039/D0BM01272F, 2020;

**Sobreiro-Almeida, Rita;** Melica, Maria Elena; Lasagni, Laura; Romagnani, Paola; Neves, Nuno M. *Co-cultures of renal progenitors and endothelial cells on kidney decellularized matrices replicate the renal tubular environment in vitro*. Acta Physiologica, 230(1):e13491, doi: 10.1111/apha.13491, 2020;

**Sobreiro-Almeida, Rita;** Fonseca, Diana R.; Neves, Nuno M. *Extracellular matrix electrospun membranes for mimicking natural renal filtration barriers*. Materials Science and Engineering: C, 103:109866, doi: 10.1016/j.msec.2019.109866, 2019;

**Sobreiro-Almeida, Rita;** Melica, Maria Elena; Lasagni, Laura; Romagnani, Paola; Neves, Nuno M. *Retinoic acid benefits glomerular organotypic differentiation from adult renal progenitor cells in vitro*. (Under review);

**Sobreiro-Almeida, Rita;** Gómez-Florit, Manuel; Quinteira, Rita; Reis, Rui L.; Gomes, Manuela; Neves, Nuno M. *Decellularized kidney extracellular matrix bioinks recapitulate renal 3D microenvironment in vitro.* (Submitted);

**Sobreiro-Almeida, Rita;** Quinteira, Rita; Neves, Nuno M. *Renal regeneration: the role of extracellular matrix and current ECM-based tissue engineered strategies*. (Submitted)

## *CONFERENCE POSTERS*

**Sobreiro-Almeida, Rita;** Melica, Maria Elena; Lasagni, Laura; Romagnani, Paola; Neves, Nuno M. *Decellularized matrix powders as cell carriers for renal therapy*. TERMSTEM conferece, Braga, Portugal, 2019;

**Sobreiro-Almeida, Rita;** Melica, Maria Elena; Lasagni, Laura; Romagnani, Paola; Neves, Nuno M. *Acellular matrix powders as cell carriers for renal therapy*. 1st Discoveries Forum, Porto, Portugal, 2019;

**Sobreiro-Almeida, Rita;** Fonseca, Diana; Neves, Nuno M. *Decellularized kidney extracellular matrix as a suitable biomaterial for mimicking natural renal filtration barriers*. Chem2Nature Summer School, Porto, Portugal, 2018;

**Sobreiro-Almeida, Rita;** Fonseca, Diana; Neves, Nuno M. *Native extracellular matrix as a promising biomaterial for the creation of constructs to treat kidney injuries*. TERM STEM conference, Porto, Portugal, 2017;

**Sobreiro-Almeida, Rita;** Fonseca, Diana; Neves, Nuno M. *Advanced strategies for the recovery of kidney function after injury*. Chem2Nature second school, Porto, Portugal, 2017.

***AWARDS***

The Portuguese Foundation of Technology (FCT) awarded a PhD grant on the Doctoral Program on Advanced Therapies for Health (PATH) (PD/BD/128102/2016).

*OTHER PUBLICATIONS (work not directly related with the PhD)*

### International Publications in Scientific Peer-Reviewed Journals

Fonseca, Diana R.; **Sobreiro-Almeida, Rita;** Sol, Paula C.; Neves, Nuno M. *Development of non-orthogonal 3D-printed scaffolds to enhance their osteogenic performance.* Biomaterials Science, 223 (115034), doi:10.1039/C8BM00073E, 2018.

**Sobreiro-Almeida, Rita;** Tamaño-Machiavello, Maria N.; Carvalho, Estela; Cordón, Lourdes; Doria, S.; Senent; Correia, Daniela M.; Ribeiro, Clarisse; Lanceros-Méndez, Senentxu; Sabater I Serra, Roser; Gomez-Ribelles, Jose Luis; Sempere, Amparo. *Human Mesenchymal Stem Cells Growth and Osteogenic Differentiation on Piezoelectric Poly(vinylidene fluoride) Microsphere Substrates*. International Journal of Molecular Sciences, 18(11):2391, doi: 10.3390/ijms18112391, 2017.

### Conference Oral Presentations

**Sobreiro-Almeida, Rita;** Tamaño-Machiavello, Maria N.; Senent, Leonor; Cordón, Lourdes; Correia, Daniela M.; Ribeiro, Clarisse; Lanceros-Méndez, Senentxu; Sabater I Serra, Roser; Sempere, Amparo; Gomez-Ribelles, Jose Luis. *Behaviour of hMSC cultured on piezoelectric quasi-3D substrates: growth and osteogenic differentiation*. Frontiers in Bioengineering and Biotechnology 4, doi: 10.3389/conf.FBIOE.2016.01.02160, 10th World Biomaterials Congress, Montréal, Canada, 2016.

**Sobreiro-Almeida, Rita;** Tamaño-Machiavello, Maria N.; Cordón, Lourdes; Senent, Leonor; Correia, Daniela M.; Ribeiro, Clarisse; Lanceros-Méndez, Senentxu; Sabater I Serra, Roser; Gomez-Ribelles, Jose Luis; Sempere, Amparo. *Human Mesenchymal Stem Cells growth and osteogenic differentiation on poly(vinylidenefluoride) substrates*. *Effect of surface topography*. 15th Euroconference on Clinical Cell Analysis, Sicily, Italy, 2015.

### Conference Poster Presentations

**Sobreiro-Almeida, Rita**; Maciel, Marta; Pereira, Ricardo B.; Ribeiro, Sylvie; Correia, Daniela; Ribeiro, Clarisse; Gomez-Ribelles, José Luis; Lanceros-Méndez, Senentxu. *Poly(vinylidene fluoride) as high potential scaffold for Tissue Engineering.* Conferences of the Center of Physics, Braga, Portugal, 2015.

# INTRODUCTION TO THE THESIS FORMAT

The work performed under the scope of this PhD thesis is herein organized into five main **Sections** (**1** to **5**), comprising eight chapters (**I** to **VIII**). This structure allows for a more organized follow-up of the thesis, which is divided according to the nature of each work and its specific aims.

**Section I** includes a general introduction to the extracellular matrix (ECM) of the kidney and the current state-of-the-art on ECM-based strategies for kidney regeneration (**Chapter I**). This section is followed by a detailed overview of Materials and Methods used in the thesis, corresponding to **Section 2** (**Chapter II**). The experimental studies, their specific results, as well as their discussion are presented in **Section 3 and 4**, comprising **Chapters III** to **VII**. These chapters are divided into two main sections according to their main goal, being kidney models (**Section 3**) and strategies for kidney regeneration (**Section 4**). Since they are based on a series of publications published or submitted for publication in international journals, the chapters are presented as an adapted version of the published or submitted manuscript style, keeping its contents, *i.e.* abstract, introduction, experimental section, results, discussion and conclusion. The specific publication is identified in the front page of each chapter and a list of relevant references is also presented at the end of the chapter. **Section 5** (**Chapter VIII**) describes the overall conclusions of the experimental work and future perspectives.

*Section 1 – General introduction*

**Chapter I** – Renal regeneration: the role of extracellular matrix and current ECM-based tissue engineered strategies: This chapter provides an overview on the knowledge gathered so far in kidney ECM. The composition and structure of kidney ECM is associated with its intrinsic capacity of remodeling and repair after insult. The current kidney tissue engineering strategies, whether cell or biomaterial based, will also be reviewed. Moreover, the evolution on the field towards different uses of the ECM as a biological scaffold material are discussed, with emphasis on future directions for clinical validation.

*Section 2 – Experimental Design*

**Chapter II** – Materials and Methods: This chapter provides a detailed description of the materials used, the processing techniques, the strategies used for biomaterials' development and the employed techniques for physicochemical characterization of the decellularized kidney matrix. The biological assays with both cell lines and primary cultures of human renal progenitor cells are also described. Moreover, a

detailed description of the cellular performance after seeding, including evaluation of cellular phenotype and assessment of functionality in model systems is also provided.

*Section 3 – Development of kidney tissue model systems*

**Chapter III** – Extracellular matrix electrospun membranes for mimicking natural renal filtration barriers: This chapter describes the development of electrospun membranes based on renal ECM, obtained from the decellularization of porcine kidneys, and a polymeric biodegradable substrate. Their physicochemical characteristics are explored, as well as their biological characterization with a tubular cell line. The main goal of this work was understanding the biological responses by varying the ratio of renal ECM to polymer.

**Chapter IV** – Co-cultures of renal progenitors and endothelial cells on kidney decellularized matrices replicate the renal tubular environment *in vitro:* As a follow-up study to Chapter III, this work was developed with the main aim of studying the tubular barrier function on the previously developed membranes. The biological activity, specific gene and protein expression of human renal progenitor cells were evaluated. Additionally, functionality studies were performed in order to further validate the model.

**Chapter V** – Retinoic acid benefits glomerular organotypic differentiation from adult renal progenitor cells *in vitro:* The main goal of this study was to further explore the potential of human renal progenitor cells, which are present in the kidney since embryogenesis to adulthood. Since there are no ethical concerns on their use, we explored glomerular organotypic differentiation on 3D spheroids composed uniquely by these cells. We emphasized the achievement of an easy-to-follow protocol and the use of retinoic acid as the differentiative compound.

*Section 4 – Strategies for renal regeneration*

**Chapter VI** – Particulate kidney extracellular matrix: bioactivity and proteomic analysis of a novel scaffold from porcine origin: Herein, the potential of the extracellular matrix itself was explored for renal regeneration. The porcine-derived matrix is processed to obtain a particulate form, which composition is extensively characterized by proteomic approaches. The matrix is further combined with human renal progenitor cells to evaluate their bioactivity and the future potential as an advanced therapy.

**Chapter VII** – Decellularized kidney extracellular matrix bioinks recapitulate renal 3D microenvironment *in vitro:* This chapter describes the development of a bioink composed uniquely of

decellularized kidney matrix. Its printability was evaluated by varying pressure and speed settings, with the aid of a support bath to maintain the integrity of the constructs after printing. Furthermore, their biological activity and specific tubular and glomerular differentiation was evaluated during a 30-day culture.

*Section 5 – Concluding remarks*

Chapter VIII – General Conclusions and Future Perspectives: The general conclusions of the developed experimental works are herein specified. Furthermore, the limitations and potential benefits found during the development of the thesis are discussed, with emphasis on future perspectives and research lines to be followed.

"*O que dá o verdadeiro sentido ao encontro é a busca,*
*e é preciso andar muito para se alcançar o que está perto.*"

*José Saramago*

# SECTION 1

# GENERAL INTRODUCTION

# Chapter I

# Renal regeneration: the role of extracellular matrix and current ECM-based tissue engineered strategies

# Chapter I[1]

## Renal regeneration: the role of extracellular matrix and current ECM-based tissue engineered strategies


### ABSTRACT

The development of tissue engineered advanced therapies for human application frequently relies on the use of extracellular matrix (ECM) components, such as collagens and growth factors, or on the use of different techniques and materials to mimic its intrinsic functionality. However, the complexity of the ECM has proven difficult to be reproduced in its structure and function by synthetic methods. Indeed, natural ECM matrices are currently being studied as an alternative source for organ transplantation or as new solutions for initial-stage repetitive episodes of kidney injury, which can evolve to end-stage renal disease, a life devastating condition.

This chapter provides an overview on the current knowledge in kidney ECM and its usefulness on future investigations. The composition and structure of kidney ECM is associated with its intrinsic capacity of remodeling and repair after insult. The current kidney tissue engineering strategies, whether cell or biomaterial based, will also be reviewed. Moreover, the evolution on the field towards different uses of the ECM as a biological scaffold material will be discussed, with emphasis on future directions for clinical validation.


[1] This chapter is based on the following publications:

**Sobreiro-Almeida, Rita**; Quinteira, Rita; Neves, Nuno M. Renal regeneration: the role of extracellular matrix and current ECM-based tissue engineered strategies. (Submitted)

## I-1. KIDNEYS FUNCTION AND DISEASE

The kidneys are two similar bean-shaped organs found in vertebrates, responsible for removing waste products and uremic toxins from blood. Besides this essential body function, they also play an essential role in maintaining body homeostasis by excreting excess water, regulating fluid osmolality, acid-base balance and concentrations of electrolytes. Important hormones are also produced and/or activated in this organ, such as renin, that helps in maintaining regular blood pressure, erythropoietin, which stimulates red blood cell production, vitamin D, which is involved in bone homeostasis, and prostaglandins.[1] Anatomically, the kidney can be divided into two main sections: the cortex, which is the outer part, and the medulla, the inner part. The medulla drains into the renal pelvis, from where the ureter conducts urine for excretion (Figure I-1).[2] Each kidney comprises an average of 1 million nephrons, which are constituted by a glomerulus and a segmented tubular resorption compartment. The glomerulus is surrounded by the Bowman's capsule and consists of a capillary bed that is covered by a negatively charged glomerular basement membrane (GBM) and specific cells that wrap around the glomerular capillary in an interdigitating structure, named podocytes. Although the fenestrations of the endothelial cells have 70 nm, the filtration slits between the podocytes range from 4 to 15 nm in size, which restricts the passage of blood cells and large or negatively charged solutes. The glomerulus is where the first and main filtration step occurs. This filtrate contains uremic waste products, but also an excess of water and a variety of molecules that need to be reabsorbed, such as glucose and amino acids. The second step of filtration occurs in the tubular system, where several transporters are distributed in a way that a selective resorption and secretion occurs between the ducts and the capillaries.[3] Each tubule is surrounded by capillaries and is divided in different segments, characterized by their different functions, namely the proximal tubule, the loop of Henle and the distal tubule which is connected to a collecting duct. The epithelial tubular cells are attached to a tubular basement membrane (TBM) at the basal side, that overlies the subjacent interstitial connective tissue. The volume and composition of the filtrate changes as it travels along the tubule, mainly because each segment is known to be composed by different types of epithelial cells, expressing different transporters at the basolateral and/or apical side (Figure I-1). Because of this orchestrated function and remarkable control of the filtration, body homeostasis is maintained within toughly controlled margins.

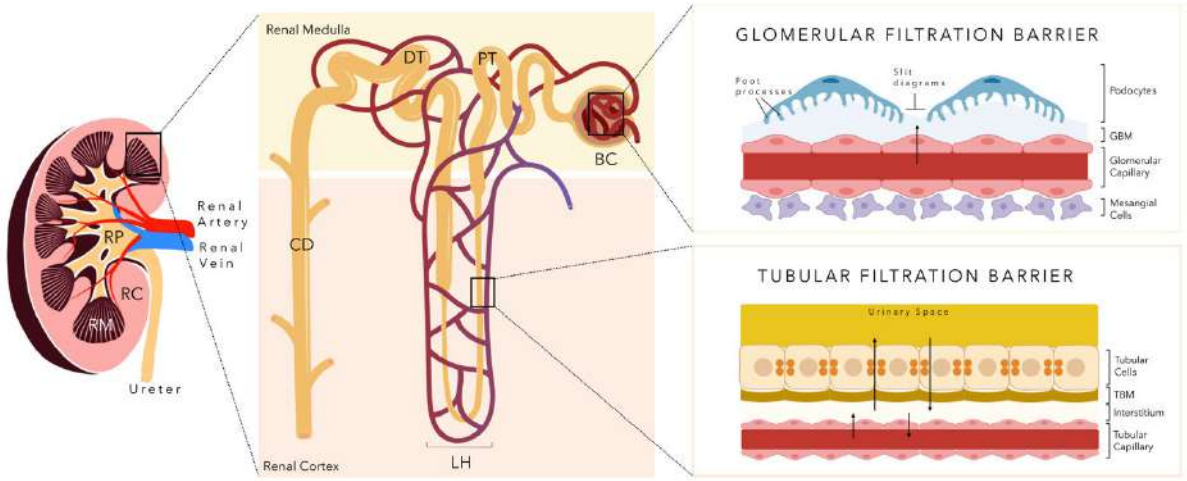


Figure I-1– Schematic representation of a longitudinal section of a whole kidney (left image) and an magnification of the renal medulla and renal cortex, representing two whole nephrons; schematic representation of the glomerular and tubular filtration barriers (right images). RC – Renal Cortex; RM – Renal Medulla; RP – Renal Pelvis; BC –Bowman's Capsule; PT – Proximal Tubule; LH – Loop of Henle; DT – Distal Tubule; CD – Collecting Duct; GBM – Glomerular Basement Membrane; TBM – Tubular Basement Membrane.

Small disturbances can cause the renal function to diminish very quickly. Several injury factors can compromise kidney function, such as sudden interruption of blood flow, the ingestion of nephrotoxic drugs, or obstruction of the urinary tract. Those events can lead to episodes of Acute Kidney Injury (AKI).[4] Generally, AKI is followed by an innate regeneration process. However, repetitive episodes of AKI can lead to irreversible renal damage and evolve into Chronic Kidney Disease (CKD). This disease is defined as the presence of abnormalities in the kidney function or structure for at least 3 months and is a devasting condition involving multiple organs and affecting a variety of systems.[5] Kidney diseases are associated with huge morbidity and mortality. Besides their worldwide prevalence (14 % of the population), there is an increasing risk of developing other diseases such as cardiovascular, diabetes and hypertension, also accompanied by systemic inflammatory responses.[6] The Global Burden of Disease study estimated that in 2015 1.3 million people died from kidney failure, a value that increased 32 % since 2005.[7] When the kidney fails to perform its regular function, that is, end-stage renal disease (ESRD), the current available treatments rely on life-long dialysis or kidney transplantation. Hemodialysis treatment involves regular filtration of the blood by an external machine, which allow patients to live with renal failure for many years. However, there are several kidney functions that will be impaired. Consequently, the decrease in life quality will be evident, with major complications for other organs in the human body.[8] As for transplantation, although this treatment has an overall good outcome, with more than 75 % of the patients surviving eight years after transplantation,[9] the shortage of donor organs is still a major concern. As of December 3rd, 2020, more than one hundred thousand patients are registered

on the organ transplanting list in US, in which more than ninety thousand of them are waiting for kidney transplantation.[10] In fact, 13 people die everyday waiting for a life-saving kidney transplant. This high demand of organs for transplantation has been the driving force for tissue engineering (TE) and regenerative medicine (RM) approaches to develop in the past decades, as these can be a promising solution for this problem.

Herein, we will review the role of the extracellular matrix (ECM) on kidney homeostasis and disease development. We will also focus on the use of the natural ECM, i.e., decellularized kidney matrices in regenerative medicine approaches and how the field has evolved in the past two decades.

## I-2. KIDNEY EXTRACELLULAR MATRIX

The ECM accounts for a substantial proportion of the tissues and organs. Over the years, more than one thousand ECM proteins have been identified in humans and many of these proteins are conserved over species and through evolution.[11] ECM proteins play a crucial role for the coordinated cell and organ function. For this reason, disease phenotypes are often associated with changes in ECM assembly and composition. Herein, we will provide an overview of the composition of kidney ECM and how it affects disease and regeneration.

### I-2.1. Kidney ECM composition and structure

Kidney's highly orchestrated organization requires a specific and unique composition of proteins, glycosaminoglycans and soluble signals to support the function of each section of the organ.[12] The ECM plays an important role not only in the maintenance of tissue integrity and cellular stimulus, but also for signaling after injury episodes.[13]

The GBM is the central, non-cellular layer of the glomerular filtration barrier that is generated, organized and maintained by the three resident cell types: the podocytes, endothelial cells and also mesangial cells. Understanding the interaction between these cells and their surrounding environment is essential to develop new therapies for tissue remodeling and regenerative medicine. Indeed, GBM composition and assembly has shown to be dependent on the crosstalk between podocytes and endothelial cells.[14] This study has shown, by proteomic analysis, that the ECM produced by these cells *in vitro* overlap in 70% with the natural glomerular ECM. The analysis of the glomerular ECM identified

144 distinct proteins, being the most abundant collagens I, IV and VI (specially the $\alpha3\alpha4\alpha5$ (IV) network), laminins (mainly $\alpha5\beta2\gamma1$), nidogen 1 and heparan sulfate proteoglycans (HSPGs) (perlecan, agrin and collagen type XVIII), which are also the core components of basement membranes (BMs).[15] According to the analysis, the GBM is essentially composed of structural and regulatory ECM proteins. By laser capture microdissection of glomeruli, other authors identified 147 ECM proteins, where the majority of structural and BM proteins identified in the previous study were also present, including a number of new matrix-associated proteins such as laminins $\alpha3$ and $\alpha4$.[16] The mesangial cells that compose the glomerulus also secrete ECM that provides structural support to the glomerular vasculature.[17] An important component of the mesangial matrix is tenascin, which has revealed its importance under normal and pathological conditions, being highly expressed on glomeruli.[18] Besides the main components of BMs, the mesangial matrix is also composed of fibronectin, biglycan and decorin. The last two are proteoglycans, which are considered to have a major role in regulating the electrical charge in the glomerulus.

The ECM of the tubulointerstitial matrix is composed by tubular BMs, directly associated with tubular epithelium, and the ECM between the nephrons and the vasculature (Figure I-1). Different ECM components were found to be present in distinct segments of the nephron, thereby evidencing possible implications of the ECM heterogeneity on the functional specificity observed in the kidney.[12] Our group has also studied the behavior of renal tubular cells cultured on membranes composed of a synthetic polymer compared with membranes composed of decellularized ECM.[19] The presence of the matrix revealed to be essential to maintain the cellular phenotype. Although the main components are believed to be the same composing the glomerulus,[11] specific-tubular ECM has not yet been studied by proteomic approaches. This characterization would enable a broader understanding of the mechanisms underlying tubular cell function, development and disease.

Besides the overall ubiquitous ECM composition of the kidneys in adulthood, this complex niche can also vary with racial background and sex, therefore being different in each individual (Figure I-2). In fact, genetic background was already proven to be a key influencer of the glomerular ECM composition.[20] Age was found to influence ECM composition in other organs,[21] a type of interaction which was also verified in the kidney.[22] Collagen type IV and I were found to have increased accumulation with age, which correlates with an increase of interstitial fibrosis.[23] Although poorly understood, cells, particularly undifferentiated cells, demonstrate being sensitive to tissue or niche-specific matrix, which will be herein reviewed. Minor differences between ECMs supporting different cellular types in the kidney could be the

key to understand the specificity and function associated with the cellular organization and a further step to its *in vitro* replication and *in vivo* regeneration.

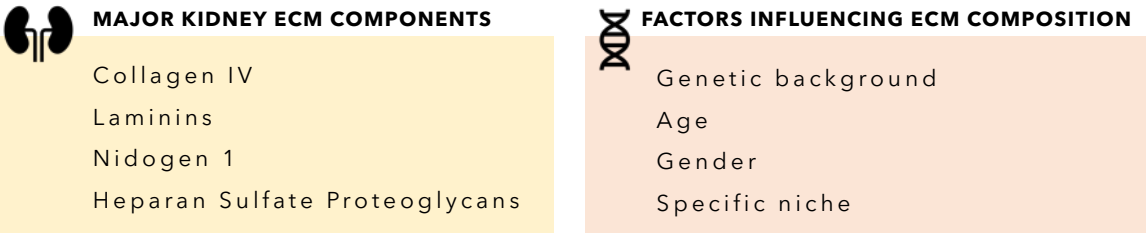


Figure I-2 – Major kidney ECM components and the major factors influencing its composition.

## I-2.2. The role of the ECM in kidney remodeling and repair after insult

The ECM molecules and their receptors exert a dynamic role not only by providing structural support for the spatial organization of cells, but also on organ development and remodeling. Tissue remodeling requires synthesis and deposition of ECM and also their proteolytic breakdown. The repair after injury is another process that requires several structural and functional changes on the ECM. Upon recovering from injury events, some ECM components regulate fundamental signal transduction pathways, being the injured cells replaced with new cells that restore tissue integrity. These cells, characterized by high mitogenic activity, migrate to the injured sites and stop dividing, acquiring the phenotype of the original tubule epithelium.[24] Many of these events recapitulate tissue growth and maturation events taking place during embryonic development. In fact, it is postulated that kidney repair can recapitulate some genetic mechanisms taking part during development, in order to reestablish its function after injury. For instance bcl-2, vimentin, pax-2, leukemia inhibitory factor and Wnt4 are highly expressed proteins during early development which are also overexpressed in adult kidneys after injury episodes.[25]

For the normal function of the kidneys, the tubular epithelial cells and podocytes require adhesive interactions with the underlying BMs. When these interactions are absent or with abnormal remodeling, the kidney becomes injured and its function is compromised. Regenerative processes also depend on this underlying ECM as a physical substratum for these events. In fact, glomerular mesangial cells were shown to undergo apoptosis when deprived of cell-matrix adhesions.[26] Besides the structural role and support, the ECM molecules also take a huge part in signaling pathways through the interaction with cellular integrins. Growth factors are known to interfere with reparative and remodeling processes in all organs, being also important in the kidney. The ECM, and particularly proteoglycans may serve as reservoirs for growth factors and are also known to regulate their biological activity.[27] The readers

interested in this aspect are referred to a review on renotropic factors.[28] Among the identified growth factors are hepatocyte growth factor (HGF), epidermal growth factor (EGF), insulin-like growth factor-I (IGF-I), heparin-binding EGF-like growth factor (HB-EGF) and PDGF that were all shown to contribute to the renal regeneration process and repair.

The continuous remodeling of the ECM is performed by the proteolytic activity of metalloproteases (MMPs) and their inhibitors (tissue inhibitor of metalloprotease, TIMPs). The MMPs are a large family of zinc-dependent endopeptidases capable of degrading ECM proteins.[29] First, the degradation of the ECM by MMPs facilitates cell migration, which promotes tissue regeneration and progenitor differentiation on specific tissue sites. Second, the products generated by ECM degradation have shown to display new recognition sites for cell surface ECM receptors, which can trigger signals promoting cellular migration and differentiation.[30] MMPs were also found to interact with several other non-ECM molecules, including growth factor precursors, cytokines and cell surface adhesion receptors, implying their indirect participation in cellular regulatory mechanisms.[29] The role of different proteases in kidney homeostasis and diseases was reviewed elsewhere.[31] Because MMPs interact with a wide range of substrates, they are implicated in a diverse array of biological processes and cellular events. Consequently, their activity was already shown to be altered in several kidney diseases. ECM remodeling can be also promoted by components of the serine protease family. Plasminogen activators are serine proteases that catalyze the activation of plasmin, which in turn can degrade several ECM components. These enzymes were also found to influence ECM production and degradation *in vivo* by activating MMPs and influence the post-translational activation of several growth factors including TGFβ-1 and HGF.[32]

In addition to the usual kidney remodeling after an injury episode, the kidney engages different mechanisms in order to reverse tissue damage. Following AKI episodes studied in animal models, several genes encoding for ECM molecules were found to be *up-regulated* and to have an important role in the following regeneration stage, including osteopontin,[33] laminin-5[34] Gpnmb glycoprotein,[35] and fibronectin[36]. Indeed, TGF-β1 expression was also found to be enhanced in post-ischemic kidney and to influence the expression of plasminogen activators, fibronectin, collagen IV and TIMP-1,[37] therefore demonstrating its deep involvement on kidney ECM homeostasis and regeneration events. Galectin-3 and ghrelin were also found to ameliorate kidney function after AKI by inhibiting renal tubular epithelial cell apoptosis.[38, 39] Other molecules including palladin, a component of actin-containing microfilaments has also shown to have an important role on epithelial cell migration after injury.[40] Recently, the Wnt family of secreted growth factors was also demonstrated to be dramatically *up-regulated* after ischemic

kidney injury.[41] This data suggests that all of these identified molecules are involved in re-epithelialization events and kidney regeneration. Nevertheless, some ECM molecules including type I collagen and fibronectin are known to be over expressed in injured tissue, promoting fibrosis and tissue dysfunction. A good balance between inflammation and ECM remodeling is essential to maintain homeostasis and to restore essential functions after injury.

## I-3. KIDNEY TISSUE ENGINEERING STRATEGIES

We have already demonstrated that the kidney has some intrinsic capacity of regeneration after injury, by using cellular processes such as dedifferentiation, migration and re-differentiation of remnant healthy cells. However, in comparison to other organs such as skin, the kidney has a very limited regenerative capacity. This, adding to the fact that the only currently available treatment for patients reaching ESRD is transplantation or dialysis, makes the urgent need for the discovery of new therapies envisioning renal repair and regeneration after injury. The tissue-engineered strategies currently being developed for kidney are herein divided in two major categories: cell and biomaterial-based approaches. We will review the major achievements in the area and then focus our attention on the use of decellularized matrices for kidney regenerative strategies.

### I-3.1. Cell-based approaches

#### I-3.1.1. Cellular injection

Cell-based approaches are a promising treatment option for kidney diseased patients, either by transplanting cells alone or by implantation with a tissue engineered biomaterial. Within the field of cellular therapies alone, bone-marrow mesenchymal stem cells have been extensively described as renotropic. They have shown to help on the recovery from AKI episodes,[42] protect against CKD,[43] prevent nephropathy in type I diabetic mice[44] and to enhance glomerular healing in experimental glomerulonephritis.[45] The mechanism through which the MSCs improve kidney function is still not well elucidated. Some authors claim that effects of MSC are primarily mediated via complex paracrine actions,[46] and/or microvesicles,[47] whereas others demonstrate their differentiation towards specific renal phenotypes.[48] Other authors also claim that MSCs can attenuate inflammation-related injury by modulating inflammatory response.[49, 50] Indeed, several clinical trials have been completed, once

more evidencing the benefit of using these cells for recovery of renal function and also for decreasing the incidence of acute rejection after transplantation, which was extensively reviewed elsewhere.[51] Other cells including adipose-derived stem cells,[52] umbilical cord mesenchymal stem cells,[53] embryonic renal multipotent progenitors,[54] amniotic fluid-derived stem cells,[55, 56] induced pluripotent stem cells,[57] endothelial progenitor cells,[58] and primary renal cells[59] have all been explored for their renal regenerative potential *in vivo*, demonstrating favorable results on recovering and/or protecting renal function. Several authors also reported the existence of a subset of multipotent progenitors in the adult kidney, preserved from developmental stages.[60–62] Although their classification and characterization is not yet unified, these cells have already demonstrated to significantly ameliorate kidney function after injury.[63–65]

### I-3.1.2. Bottom-up approaches

The injection of exogenous cells alone has a number of shortcomings. Without a substrate to attach, many cells are lost in the process or migrate out of the intended site of action and frequently there is insufficient cell engraftment to obtain clinically relevant efficacy. In this way, the neo-kidney research has been gaining interest in the past few years, augmenting our understanding on organogenesis mechanisms, with the main goal of *in vivo* implantation and/or *in vitro* models. Stem/pluripotent cell manipulation was already exploited to build organoids, which are presented as replicas of the human renal developmental stages, creating mini-kidneys.[66] Some important works in this area of research have been recently published, enlightening the use of adult urine-derived stem cells[67] or embryonic stem cells[68] for the recreation of tubular organoids. The recapitulation of embryonic branching morphogenesis[69, 70] and glomerular 3D mature structures[71] from pluripotent stem cells was also reported. Additionally, is it important to highlight the replication of kidney disease phenotypes in pluripotent-derived organoids by CRISPR technology[72] and the use of high-throughput techniques[73] and/or bioreactors[74] for multidimensional phenotypic screening of organoids.

Xenoembryos and blastocyst complementation are two bottom-up approaches that rely on the use of another species embryo to theoretically grow patient's own cells for *de novo* organogenesis.[75, 76] Although these techniques are promising, no major developments were accomplished in the last decade, which is possibly due to the challenging ethical barriers. Despite all of the advances in the area, these approaches have not yet achieved the kidney complexity with a fully developed collecting duct system able to filter solutes and produce urine.

## I-3.2. Biomaterial-based approaches

### I-3.2.1. Bioartificial Substitutes

Patients undergoing dialysis treatment have limited life expectancy and poor patient prognosis due to acute tubular necrosis, which results in the loss of kidney's immunoregulatory functions, such as red blood cell production, hormones secretion and activation of vitamin $D_3$. Being these functions not substitutable by the dialysis equipment, tissue integrity and host defense is weaker over time.[77] Consequently, the usual cause of death in these patients is the development of sepsis or bacterial infection, which will provoke a systemic inflammatory response and result in cardiovascular collapse and multiorgan failure.[78] Therefore, in the last decades, researchers focused efforts on the development of new filtration devices with incorporated cell monolayers, so that blood filtration occurs in a less thrombogenic and more physiological manner. These bioartificial devices represent the intersection between regenerative medicine and renal replacement therapy. Some of these were named Renal Tubule Assist Devices (RADs). RADs consist in synthetic hemofiltration cartridges supported in series by a bioreactor unit containing renal cells performing their physiological solute excretion and reabsorption role, while exerting the above mentioned functions.[79] So far, one research group has been successful in bringing this technology into patients. Initially, a phase I/II clinical study was completed in 10 ICU patients in an *ex vivo* setting. The results indicated that RAD maintained durability and viability during the treatment with metabolic and endocrinological activity, but also reported events of hypoglycemia, thrombocytopenia and hypotension.[80] In 2008, a phase II multicenter, randomized, controlled open-label trial involving 58 patients suggested a 50% reduction in mortality risk when employing the RAD up to 72 h.[81] Recently, the same group has developed and tested in a sheep *in vivo* model a wearable second-generation device, with a portable and cryopreservable format. This device relies on peritoneal dialysis fluid for supporting cellular viability and delivery of cellular therapies while providing uremic control.[82] Another wearable device was also developed and tested on a 24-hour clinical trial comprising 10 patients.[83] Despite effective uremic solute clearance and maintenance of electrolyte and fluid homeostasis, the device demonstrated having technical problems. Besides device development, research is also focused on improving several techniques for the production of filtering membranes which could be applied on these devices. Electrospinning techniques,[19, 84] ECM coatings,[85, 86] supramolecular biomaterials functionalization,[87, 88] immune modulation,[89] graphene oxide dopping,[90] silicone nanoporous membranes,[91] and even a functional computational model[92] have all been explored as functional

and promising "living" membrane substitutes for composing dialysis equipment's. Although no effective dialysis device substitute has yet been developed for a daily-basis clinical usage, it's clear that the combination of regenerative medicine and bioengineering offers a promising strategy to overcome the current limitation on the field.

### I-3.2.2. Biomaterials for implantation

Another approach for kidney regeneration is the implantation of tissue substitutes. These can either be of natural or synthetic origin and can also act as cell carriers. The main aim of implantation can be to substitute tissue that was removed due to the presence of tumors or injection of a therapy *in situ* to reduce fibrosis and promote functional recovery of the kidney. Herein, we will review the major therapies that were developed in the last decades, highlighting the evolution in manufacturing techniques. In 2002, a group of researchers first demonstrated the *in vivo* reconstitution and structural remodeling of renal tissues from cloned kidney cells. The cells were seeded into renal devices with collecting systems that produced urinelike fluid and demonstrated unidirectional secretion and concentration of urea nitrogen and creatinine.[93] Although this strategy seems promising, it could not be applied in humans because of ethical concerns. Thus, researchers have been developing scaffolds capable of supporting cultures of cell or tissue segments for posterior *in vivo* implantation or *in vitro* tissue modeling. Indeed, kidney morphogenesis was already studied in a type IV collagen matrix,[94] in a ECM-derived gel,[95] in a growth factor-loaded polymeric hydrogel,[96] and in another soft matrix consisting of heparin crosslinked to starPEG [97], demonstrating the potential of these biomaterials. Collagen matrices were also used to study 3D culture of primary renal cells,[98] which when implanted *in vivo* allowed cells to migrate towards the parenchyma and integrate into glomerular and interstitial structures.[99] Regarding the use of synthetic materials, polyglycolic acid (PGA), poly(lactic-co-glycolic acid) (PLGA) and poly(caprolactone) (PCL) are preferred for *in vivo* implantation, being highly biocompatible and biodegradable polymers.[100, 101] A series of biomaterials of different origins and structures were already tested *in vivo* as neo-kidney augment prototypes, including particles and beads of PLGA, PCL, gelatin and hyaluronic acid (HA).[102] Recently, a PCL biomimetic renal scaffold was developed based on a vascular corrosion casting technique. The material was coated with collagen and endothelial cells before being embedded on a 3D collagen matrix. After this, a cortical defect was created and the constructs were implanted on the renal cortex, which integrated in the tissue and promoted the formation of renal tubules after 14 days.[103]

Another approach for kidney regeneration using biomaterials is to target renal tissues for specific drug delivery. Anionized polyvinylpyrrolidone (PVP),[104] gold nanoparticles,[105] catechol-functional chitosan nanocomplexes,[106] supramolecular hydrogels,[107] poly(D,L-lactic-co-hydroxymethyl glycolic acid) (PLHMGA) microspheres[108] and IL-10 loaded HA hydrogels[109] were developed to target kidney tissue, which all demonstrated being safe drug carriers, indicating minimal tissue response in the cases of subcapsular implantation. Not only drugs, but also stem cells delivery were tested on alginate-HA microbeads, which were shown to be biocompatible after 14 days of *in vivo* subcapsular implantation.[110] The delivery of MSCs was also tested *in vivo* on collagen/poly(γ-glutamic acid) hydrogels, demonstrating therapeutic effects against renal dysfunction, namely attenuating the level of blood urea nitrogen and creatinine.[111] In another study, hydrogels composed of chitosan with a reactive sequence of IGF were mixed together with ASCs and demonstrated to substantially ameliorate renal function in a AKI model, by the promotion of stem cell survival and angiogenesis.[112] Other polymeric based scaffolds were also studied as carriers for kidney cells[113] and non-viral genes.[114]

The use of biomaterials for the development of new tissue augments and/or drug and cell delivery into the kidneys is a very promising area of research. Although no current technology seems near clinical translation, a lot of efforts have been made in the last decade which hopefully will guide our research into a new era of kidney regeneration for the benefits of patients.

### I-3.3. Kidney decellularized matrices

The *in vitro* culture of cells has changed dramatically in recent years. Since scientists have understood that each cell type needs a particular niche to maintain its specific phenotype, many efforts have been performed to mimic the ECM, including diverse biomaterial processing strategies. Nowadays, the use of 2D cell cultures for regenerative strategies is decreasing, because they fail to recapitulate the complex environment of *in vivo* systems. Instead, sponges, electrospun meshes, hydrogels and porous 3D scaffolding systems are produced using different materials, different mechanical characteristics and several combinations with biomolecules.[115] However, the ECM bioactive and dynamic structure is still difficult to mimic. For these reasons, naturally derived ECM obtained through decellularization processing has gained interest in the TE field. These matrices are able to retain the majority of proteins, glycosaminoglycans and growth/secreted factors present in the native tissue, lacking the immunogenic components of the cells.[116] Decellularized tissues were first patented on 1996 for cardiac valves[117] and since then many discoveries were found on the ECM of several tissues, including skin,[118]

liver,[119] kidney,[120] lung,[121] cartilage[122] or heart.[123] FDA already approved for human use several decellularized matrices and their commercialization. For a comprehensive review on the decellularized matrices approved by the FDA, the reader is referred to reference 124. Overall, these studies reflect the advances on regenerative medicine approaches necessary to fulfill the needs of patients awaiting for organ transplantation.

In this section we will review the major achievements of using decellularized matrices for tissue engineering purposes (Figure I-3). We will focus on the use of decellularized matrices to guide progenitor or stem cell differentiation, especially in the kidney. We will also discuss the contribution of whole organ engineering and scaffolding systems produced from decellularized matrices on the development of new advanced therapies for treating kidney diseased patients.

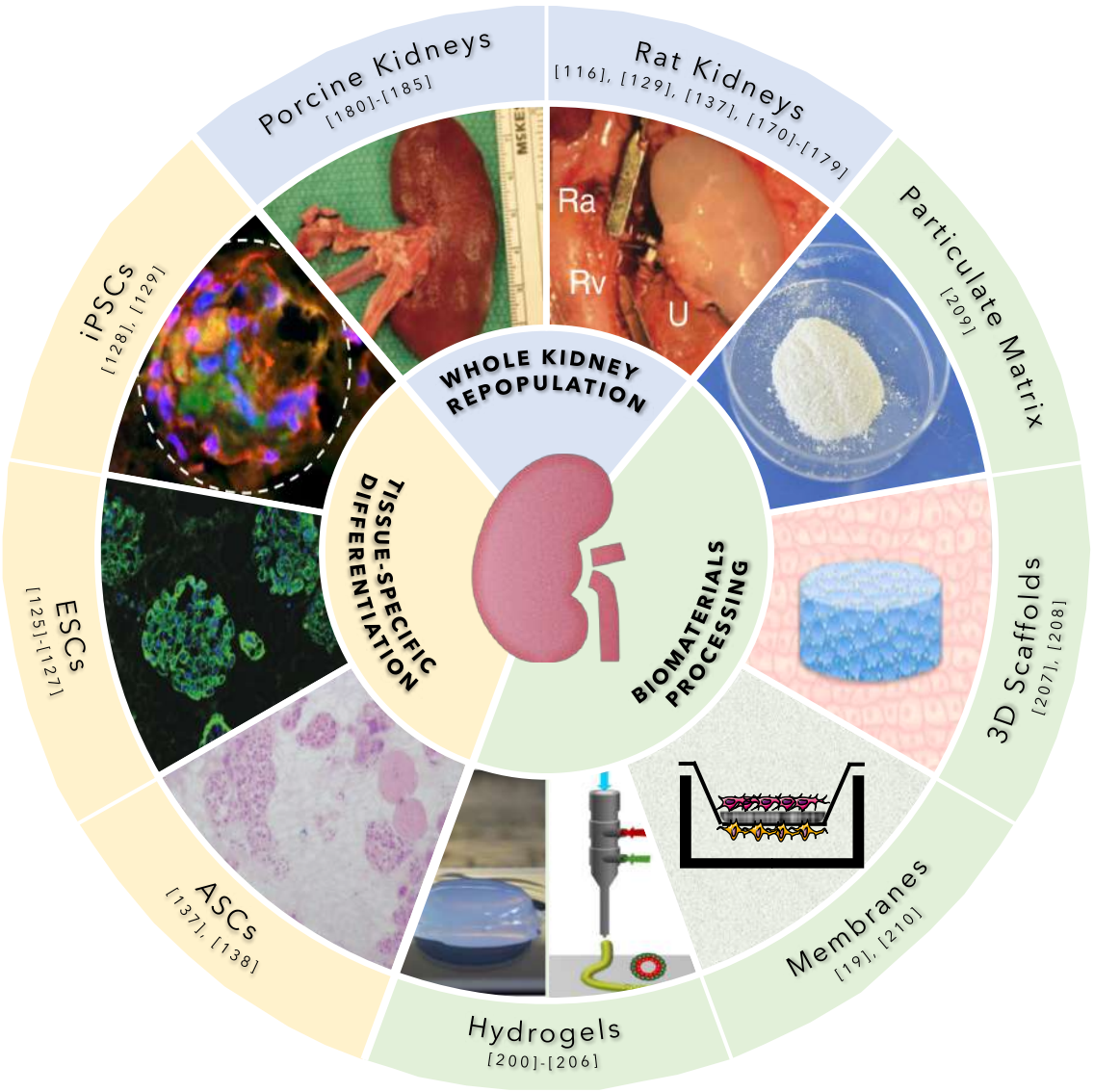


Figure I-3 – Different examples of kidney decellularized matrices uses for regenerative medicine strategies. The major achievements in the area rely on three major areas. The decellularized matrices can be used for whole kidney recellularization (mainly in porcine and rat kidneys), on tissue-specific differentiation of progenitor/stem cells and as a substrate for fabrication of several structures, which can serve as therapeutic implants for in situ renal regeneration or as components of *in vitro* renal tissue models.

### I-3.3.1. Decellularized ECM guiding tissue-specific cellular differentiation

Tissue specificity is known to drive specific cellular differentiation. However, it is important to establish which are the tissue properties that potentiate lineage specification during recellularization experiments or cell cultures in specific matrices. Therefore, we will review studies that have demonstrated the power of the ECM to determine tissue specification of different progenitor/stem cells.

The effect of different decellularization protocols has shown to produce matrices with varying histological properties in paraffin slices, which in turn influenced the differentiation of seeded embryonic stem cells (ESCs) towards the renal lineages.[125] This study provides new insights on the importance of optimizing decellularization protocols. These cells were also cultured on decellularized kidney scaffolds, demonstrating efficient recellularization with loss of cell pluripotency and differentiation towards meso-endodermal lineages.[126] By seeding ESCs on decellularized matrices of lung and kidney, resulted on cells' up-regulation of key lung and kidney-associated genes, respectively.[127] Overall, ESCs cells have shown to be sensitive to cues existing on the surrounding matrix, being highly versatile.

Human induced pluripotent stem cells (iPSC) are reprogrammed to be pluripotent cells through inducing genes and factors. The main advantage of using these cells relies on its origin, given that they are derived from adult somatic cells, obviating the ethical dilemmas surrounding the use of ESCs. These cells already demonstrated reestablishment of organ-specific functionality by culturing them in decellularized matrices. A recent study shows that the commitment of iPSC-derived embryonic stage mesodermal precursor cells is dependent on the organ substrate, when cultured without additional supplementation.[128] The cells were directly differentiated into a variety of specific renal cells that compose the glomerulus, proximal and distal tubules, loop of Henle, collecting ducts and also endothelial cells only by seeding in kidney decellularized matrices. It was noticed that the revealed organ-specific differentiation was demonstrated to be exclusively due to HSPGs embedded on the matrix, which could be extremely useful for future research on therapies based on decellularized matrices. iPSC-derived renal progenitor cells also exhibited upregulation of regulatory key genes involved in kidney development, a cellular response that was mediated by the presence of endothelial cells.[129] These results suggest a regulatory role of endothelial cells, which is an important finding for this field. The iPSCs have also demonstrated their tissue-specific differentiation potential for regenerative strategies when cultured on decellularized matrices of livers,[130] lungs,[131, 132] pancreas[133] and human cardiac ECM.[134]

The use of embryonic and/or pluripotent stem cells is of extreme importance for breakthrough advances in cell development and differentiation. But although they demonstrated unlimited cell growth and potency, strong ethical concerns are raised by their use. Moreover, iPSCs have already demonstrated to be tumorigenic, which limits their translational potential.[135] Besides that, non-kidney cells such as neurons and muscle were already found when performing differentiative assays.[136] Although these cells may be more sensitive to the surrounding niche, it is important to consider adult stem cells studies.

Having own-patient cells implanted on a foreign matrix for *in situ* implantation would be a closer step on their clinical use.

Kidney ECM has shown to influence the differentiation of induced-intermediate mesoderm adipose-derived stem cells (ASCs) into tubular-like and podocyte-like cells.[137] Their differentiation into endothelial and tubular cells in a rat decellularized kidney scaffold was also demonstrated, being important to notice the contribution of stromal cell-derived factor-1 on enhanced cell attachment.[138] The importance of the ECM in the cellular fate decisions of ASCs was studied by culturing these cells on secreted decellularized ECM substrates. Cells have demonstrated up-regulation of genes expressed during early events of differentiation into osteogenic and adipogenic lineages, where integrin subunits alpha-6 and beta-1 were found to be involved in the interaction of cells with the ECM.[139] The influence of different cell types on lung decellularization-based therapies was shown in a study in which higher expression of lung cell-related progenitor genes was found in ASCs, comparing with bone marrow-derived MSCs.[140] Adult stem cells from kidney tissue obtained from clonal nephrospheres have also demonstrated to spontaneously differentiate into parenchymal and endothelial cell populations in kidney ECM scaffolds by 30 days of culture time, demonstrating the time-dependent role of ECM in cellular differentiation.[141] The engraftment and differentiation of different adult stem cells was already demonstrated in decellularized matrices of vascular grafts,[142] human cornea scaffolds,[143] pig esophagus,[144] in an aortic patch,[145] blood vessels,[146] myocardium scaffolds,[147, 148] cardiac ECM,[149] small intestine,[150] lung,[151] and tracheal allografts.[152]

As decellularized matrices have shown to provide adequate stimulus for uncommitted and committed cells to adhere, proliferate and differentiate into the specific organ-lineages, it was noticed that these matrices do not only preserve the specificity of tissues, but also the stage of development of the organ. Further studies will have to focus their research on the leading differentiative cues provided by the surrounding matrix. Understanding cellular responses and cross-talking mechanisms between the matrix and cells will hopefully guide the next era of clinical therapies.

### I-3.3.2. Using xenogeneic ECM for regenerative purposes

The first uses of xenogeneic tissues and organs on human medicine dates from more than 100 years ago. Curiously, one of the first reports of xenotransplantation describes the transplant of kidney rabbit slices into a child with chronic kidney disease.[153] Nowadays, xenotransplantation remains one of the

major challenges in medicine, and no current effective treatment of xenogeneic whole organs has been developed for the routine use of these sources. However, porcine and bovine substitutes of heart valves and myocardial patches for the treatment of post-infarction aneurysms are available and used on the clinical practice after glutaraldehyde chemical treatment. This treatment is performed in order to prevent immune rejection and prolong the durability of the prostheses.[154] The major motivation behind the use of xenogeneic organs relies on the huge transplant waiting list and on the easy availability of these sources. Nevertheless, there are many concerns about immune rejection and ethical issues to be addressed before the implementation of this strategy. In the past few years, the improvement of decellularization and recellularization strategies of whole organs has provided a theoretical means for the creation of patient-specific artificial organs that could address the current donor shortage while potentially alleviating the need for immunosuppressants. Indeed, a recent study demonstrated that decellularized xenogeneic tissues outperform glutaraldehyde-fixed tissues in the reduction of the humoral immune response in patients who were submitted to heart valve implantation.[155] For the effective removal of nucleic material, a tissue is considered decellularized if the content of dsDNA is quantified less than 50 ng/mg of tissue.[156] However, this analysis does not inform about xenogeneic antigenicity. Other report established a threshold level of 92 % of lipid antigen removal as necessary to overcome recipient graft-specific adaptive humoral immune response.[157] The innate immune system was also found to tolerate minor changes in protein organization as long as that molecular structure is maintained, which is an important finding for the use of decellularized xenogeneic organs.

Recently, some researchers have been focused on the study of species mismatch and its potential applications in regenerative medicine. Although the use of pigs as xenogeneic donor sources has shown promising results,[158] a recent study has demonstrated that lung tissues of primate sources demonstrate much more similarities to that of the human tissue than porcine and rat sources.[159] Not only the species but also the method of decellularization or antigen removal and the source of the recellularized cells will provoke different humoral effects on the recipient.[160, 161] Numerous decellularization methodologies were described in the literature. For the use of xenogeneic sources, a species and tissue-specific protocol has to be uniformized, in order to maintain all of the mechanical features of the organ without compromising its biological activity.[162] Indeed, although the use of xenogeneic sources seems promising, a lot of issues have to be addressed for their future use on clinical practice. The development of decellularization and recellularization strategies on xenogeneic kidneys and their implantation success will be reviewed in the next section.

### I-3.3.3. Whole kidney decellularization and repopulation

Whole kidney engineering can be described as the fabrication of a kidney with its intact architecture and function ready for transplantation.[163] The kidney has a complex architecture with a fine intrinsic vascularization network, a specific cortex and medullar organization and more than 20 specialized cell types. Because of the difficulty in recreating such an organ, we are still far from the clinical translation of this technology. The decellularization of whole organs is an interesting approach that suffered its major development in the last decade. It is postulated that upon decellularization, organ-derived intact ECMs capture the histoarchitecture and physiological cues that best represent the *in vivo* environment.[164] Theoretically, these scaffold ECMs could be repopulated with cells of human origin – matching those of the recipient –, which would migrate towards specific sites and differentiate towards the lineages of interest by responding to the retained ECM cues on the tissue.[165] The kidney highly complex microarchitecture makes its repopulation and consequent functionality a very difficult objective.[166] There are several parameters that can be modified to fine tune the strategy for having a fully repopulated and functional kidney. Currently, the most efficient and robust method for decellularization is the use of chemical infusion through manual or pump perfusion. The method is highly tunable, beginning with the choice and concentration of the administered solutions, the duration and pressure of the perfusion and also the flow rates. Then, after whole decellularization is achieved, washing solutions and sterilization processes are additional steps to be performed. The last stage, but one of the more important parameters, are the cells. Selecting the "right" cells to repopulate a kidney is a critical task. The renal corpuscle is composed of endothelial cells, mesangial cells, podocytes, and parietal epithelial cells, besides the cells that comprise the juxtaglomerular apparatus. The epithelial cells that compose the tubule are divided into renal proximal tubular cells and cells that form the distal tubules, and each one of them is further divided into different segments. Each of these segments presents specific cell types, with different functions related to their ultrastructural characteristics. An overview of kidney decellularization procedures is available elsewhere.[167] Herein, we will review the published literature on recellularized kidney matrices and/or *in vivo* implanted kidney scaffolds. We will focus mainly on comparing the source of the scaffold versus the seeded cells and the major outcomes (Table I-1). As demonstrated in Table I-1, the majority of studies were performed using rodent kidneys, and the strongest morphological and functionality results were obtained by orthotopic transplantation of a rat recellularized kidney,[116] which is very limited in terms of evidence for clinical translation. Furthermore, only one study was performed so far in human matrices, and other on primate matrices, which were seeded with iPSC-derived endothelial cells and

ESCs, respectively. Besides the ethical and tumorigenic concerns raised by the use of these cells, these scaffolds not yet implanted *in vivo*, limiting the conclusions that can be taken from these studies for further clinical translation.

In 10 years, researchers expect that whole kidney recellularization studies complete the preclinical phase, representing a high potential for translation compared to other tissue engineering approaches to kidney repair, such as renal organoids or 3D bioprinting.[168] However, despite all efforts performed in the field, not many studies have shown successful outcomes. Although the efforts on recellularizing kidneys demonstrates its limitations, the field is evolving trough the development of new bioreactors and new recellularizing strategies, which could be very valuable in the near future for the treatment of ESRD.

Table I-1 – An overview of whole recellularized and/or implanted kidney scaffolds from the literature. RA: Renal artery; RV: Renal Vein; SDS: Sodium Dodecyl Sulfate; VEGF: Vascular Endothelial Growth Factor.

| Kidney Source | Decellularization Method | Cell Source for Recellularization | Recellularization Strategy | *In vivo* implantation | Overall Results | Reference |
|---|---|---|---|---|---|---|
| **Mouse** | Perfusion of 1% SDS and 1% Triton X-100 | Renal Progenitor Cells (RPCs) and endothelial cells, both differentiated from iPSCs | Manual injection of $4 \times 10^6$ cells through the RA (1:1 proportion of endothelial and RPCs) | Yes | Expression of renal-associated genes and successful *in vivo* implantation with excretion of urea and creatinine and albumin reabsorption | [129] |
| | Peristaltic pump perfusion of 0.1% SDS and 0.1% Triton X-100 | mESC-derived metanephric mesenchyme cells | Vacuum was applied for cell loading through the ureter | No | Cells organized and differentiated into several kidney structures | [169] |
| **Rat** | Peristaltic pump perfusing 1% SDS | Murine ESCs (mESCs) | Perfusion through different sites (RA, RV and/or ureter) at the same time or alone at different densities and flow rates | Yes. Acellular | *In vitro* recellularization resulted in inconsistent cell seeding. Acellular scaffolds implanted *in vivo* could not be repopulated with cells. | [170] as a follow-up of [126] |
| | | Human iPSC-derived endothelial cells | Perfusion of 4 suspensions of $7.5 \times 10^6$ cells through the RA and another 4 suspensions through the RV | No | Cells were able to cover 89% of the glomeruli and extensively repopulate peritubular capillaries | [171] |
| | Peristaltic pump perfusing 1% Triton X-100 and 0.1% SDS | iPSC and immortalized human renal cortical tubular epithelial cells (RCTE) | Injection of $5 \times 10^6$ iPSC or bioreactor infusion of $40 \times 10^6$ RCTE through de RA | Yes | *In vitro* repopulation was supported by acellular scaffolds. *In vivo* transplanted scaffolds maintained 3h of leak-free blood flow. | [172] |
| | Perfusion of 1% SDS and 1% of Triton X-100 | HUVECs and rat neonatal kidney cells | Bioreactor seeding of $50.67 \times 10^6$ HUVECs through the RA. After o/n incubation, seeding of | Yes | *In vitro* scaffolds demonstrated successful reendothelialization and nephrogenesis. *In vivo* transplantation provided urine production and clearance | [116] |

| Kidney Source | Decellularization Method | Cell Source for Recellularization | Recellularization Strategy | *In vivo* implantation | Overall Results | Reference |
|---|---|---|---|---|---|---|
| Rat | | | 60.71 × $10^6$ neonatal cells through the ureter | | of metabolites. No thrombosis was observed. | |
| | Perfusion of 0.5% SDS | mESCs | Seeding of 5 × $10^7$ through the RA and the ureter | Yes | Cells populated and proliferated into all kidney structures *in vitro*. *In vivo* implantation resulted in easily reperfusion and urine production with no blood leakage after 2 weeks. | [173] |
| | Perfusion of 3% Triton X-100, DNase and 4% SDS | Murine ESCs | Manual injection of 2 × $10^6$ cells through the RA | No | *In vitro* cell seeding demonstrated population into all kidney structures and endothelial differentiation. Co-localization with mouse BM proteins was observed. | [174] as a follow-up of [166] |
| | Bioreactor system with perfusion of 1% SDS and 0.2 mg/mL DNase into cryopreserved kidneys | Murine $C_3H_{10}T^{1/2}$ pluripotent stem cells | Injection of 2 × $10^6$ cells through the RA or directly in the kidney | No | *In vitro* recellularization supported cellular attachment and growth | [175] |
| | Peristaltic pump perfusing 50U/mL heparin, 0.1% Triton X-100 and 0.8% SDS | Not applied | Not applied | Yes. Acellular | *In vivo* implantation in a partially nephrectomized rat resulted in significant recovery of renal function after 6 weeks | [176] |
| | Bioreactor perfusion with specific reagents as described in [172] | Immortalized Madin-Darby canine kidney (MDCK) cells and primary human | Manual high-pressure injection of 40 × $10^6$ MDCK cells and 6.25 × $10^6$ CD133/1+ cells into the RA | No | Xenogeneic recellularization was successful, maintaining growth and proliferation for 7 days | [177] |

| Kidney Source | Decellularization Method | Cell Source for Recellularization | Recellularization Strategy | *In vivo* implantation | Overall Results | Reference |
|---|---|---|---|---|---|---|
| Rat | | renal papillae-derived CD133/1+ cells | | | | |
| | Perfusion of 0.125% SDS | Rat primary renal cells or mesenchymal stromal cells | Multistep bolus injections of 50 × $10^6$ cells trough the RA | No | Successful *in vitro* recellularization with no evidence of cellular differentiation | [178] |
| | Peristaltic pump perfusion of 0.5% SDS | hASC-derived intermediate mesoderm cells | Injection of 1 × $10^7$ cells through the RA and the ureter | No | Differentiation into several kidney lineages was verified as well as homogeneous distribution of cells in all kidney structures after 10 days | [137] as a follow-up of [138] |
| | Perfusion of 0.5% SDS and 1 mg/mL of collagen binding peptide-heparin | HUVECs | Injection of 25 × $10^6$ cells through the RA | No | Endothelial cells were found to be attached to the scaffold after 7 days. Clot formation and thrombosis was not observed through whole blood perfusion | [179] |
| Porcine | Peristaltic pump perfusing SDS | Not applied | Not applied | Yes. Acellular | Scaffold implantation was well tolerated after 2 weeks with non-specific inflammatory response. Thrombosis was observed | [180] |
| | Bioreactor system with perfusion of 0.5% SDS and 0.0025% DNase | Primary porcine renal cells isolated from harvested tissue | Injection of 400 × $10^6$ cells into the cortical region. Bioreactor culture was performed afterwards. | No | Renal tubular structures with some functional capacities were formed | [181] as a follow-up of [182] |
| | | Primary murine endothelial cells isolated | Antibody conjugation of vasculature prior to a combination of static and ramping (50 × $10^6$ cells for | Yes | Uniform coverage and retention of endothelial cells *in vitro.* Clot formation | [183] |

| Kidney Source | Decellularization Method | Cell Source for Recellularization | Recellularization Strategy | *In vivo* implantation | Overall Results | Reference |
|---|---|---|---|---|---|---|
| **Porcine** | | from pancreatic islets (MS1) | each one) perfusion cell seeding. | | was observed after 2 h of *in vivo* implantation | |
| | Bioreactor system with perfusion of 1% Triton X-100 and 0.5% SDS | | Antibody conjugation of vasculature prior to a combination of static and ramping ($150 \times 10^6$ cells for each one) perfusion cell seeding | No | Preservation of vascular structures with partial cell detachment after *in vitro* blood perfusion | [184] |
| | Kidney sections decellularized in 1% Triton X-100 and DNase | Primary human renal cells | $1 \times 10^6$ cells were seeded onto the scaffolds in a shaking incubator | Yes. Acellular | *In vivo* implantation a partially nephrectomized mice resulted in glomeruli-like structure formation and neovascularity | [185] |
| **Monkey** | Perfusion of 100 USP/mL of heparin and 1% SDS | Human ESCs | Bioreactor perfusion of $20 \times 10^6$ cells through the RA and/or the ureter | No | Recellularization was successful in medullary vascular or tubular lumens but not in outer cortical tubules or glomeruli. Differentiation into several renal lineages was observed | [186] |
| **Human** | Perfusion of 1% SDS, 2000E DNase and 1% Triton X-100 | Human iPSC-derived endothelial cells | After perfusion with VEGF o/n, $60 \times 10^6$ cells were perfused through the RV and $70 \times 10^6$ cells were perfused trough the RA | No | Reendothelialization of the kidney vasculature, including the glomerular and peritubular capillaries was observed. Perfusion with human whole blood was achieved | [187] |

### I-3.3.4. Decellularized matrices as biomaterials

Biological materials composed of decellularized ECM have already demonstrated to facilitate remodeling of different tissues. Indeed, FDA already approved the use of several xenogeneic or allogeneic decellularized matrices for tissue regeneration, including LifeCell's AlloDerm® Regenerative Tissue Matrix (human dermal graft), DSM's Meso BioMatrix® Surgical Mesh (porcine mesothelium) and CryoLife's SynerGraft® (human pulmonary heart valve), which are currently clinically available. Because the matrix retains most of its essential components when lyophilized, researchers have been processing it into different structures, according to the intended application. Although some claim that these biomaterials lose their inherent bioactivity when processed, several works demonstrate that the structure and bioactivity of the processed ECM can be preserved throughout the processing steps. Different tissues including cartilage,[188] neuronal tissue,[189] adipose,[190] urinary bladder,[191] dermal tissue,[192] lung,[193] liver,[194] cardiac tissue,[195] and small intestine submucosa[196] were already used for biomaterials production. Because ECM-derived biomaterials usually offer poor mechanical properties, they are often combined with biodegradable polymers, such as PCL or PLGA, which will also help on handling and to decrease their fast degradability.[164] The degradability can also be controlled by the use of crosslinking agents, by treatments such as EDC-NHS chemistry[188] or methacrylation,[197] which makes these ECM-based biomaterials very versatile. However, collagen-based matrices have an inherent capacity to crosslink and obtain a gel-like consistency after acidic digestion, neutralization and incubation at 37 °C. The driving force for this phenomenon is protein and peptide self-assembly. The polymerization of long fibrillar structures is regulated by both electrostatic and hydrophobic interactions that promote the collagen fibers to crosslink.[198] This intrinsic property has led researchers to explore ECM-based hydrogels for specific tissue regeneration, including in the kidney.

Kidney ECM-based materials were first patented in 2015,[199] and region specificity of kidney stem cells in these same materials was studied.[200] These authors decellularized porcine kidney and separated the ECM obtained from renal papilla, renal medulla and renal cortex. The ECM was used either in its native from, in the form of a hydrogel or in its solubilized from. After, these materials were used to study regional specificity, where kidney stem cells were shown to be more sensitive to the papillary ECM. In follow-up studies, these hydrogels were further explored for different applications, including in flow-directed microphysiological systems, by using them to mimic the 3D microvascular environment of the kidney.[201] A more specific response was also studied on these hydrogels by glomerular endothelial cell

encapsulation.[202] The fibrillar architecture of kidney hydrogels was also investigated by macromolecular crowding, where researchers have found that the inclusion of a crowding agent resulted in greater diameters and alignment of matrix fibrils, which consequently lead greater capillary network formation by HUVECs (in the presence of VEGF) and morphogenesis of mouse kidney stem cells into highly branched aggregates.[203] Recently, the investigation on kidney-derived hydrogels has evolved by producing bioinks from these hydrogels.[204] A group of researchers methacrylated kidney ECM before mixing it with gelatin, hyaluronic acid and glycerol, producing a kidney ECM-based bioink.[205] Other authors created a 3D model of a renal tubule by co-axial cell printing of endothelial and epithelial cells in the decellularized bioink mixed with alginate.[206] Although being far from clinical application, these 3D printed constructs have great potential for the future of functional renal tissue bioengineering. Its *in vivo* application demonstrated maintenance of the structure, infiltration of host vasculature and functional marker expression after 8 weeks of implantation. Moreover, they have demonstrated antifibrotic potential of these bioinks when implanted on a unilateral ureteral obstruction mouse model.[206] The application of these bioinks in microfluidic devices for disease modelling was also validated by the creation of a vascularized renal proximal tubule-on-a-chip, which would be extremely helpful for further studies of *ex vivo* chronic kidney disease model.[206]

The production of structures from decellularized kidney matrices extends beyond hydrogels. 3D scaffolds composed of PLGA comprising 10 % of kidney ECM in its composition were developed.[207] Although these authors have not established a renal disease model, they have implanted the construct in a partially nephrectomized mouse model. The results revealed renal glomerular tissue regeneration with low inflammatory responses, which is a promising result for the future of renal advanced therapies.[208] Our group has also explored this potential by creating a 3D particulate ECM scaffold which could act as an injectable cell carrier for renal therapies.[209] The results revealed that particulate kidney ECM is able to modulate the morphology and phenotypic expression of renal progenitor cells, which are reparative renal cells existing in adult kidney tissue.[60] We have also explored the potential of kidney matrices to fabricate electrospun membranes which could be valuable substitutes of basement membranes *in vitro*.[19] These membranes demonstrated to potentiate cell performance when comparing to bare PCL membranes and also to support functional bilayer co-cultures of endothelial and epithelial cells useful for nephrotoxicity screening and disease modelling.[210]

ECM biomaterials derived from the kidney have already demonstrated to influence the growth and metabolism of kidney cells and the *in vivo* kidney remodeling and functional recovery after injury. Although

this area of research has recently emerged, it has already demonstrated its potential for future development of biomaterials applications in kidney repair and regeneration strategies. These ECM-derived biomaterials can be used for delivering and directing the differentiation of reparative cells to address renal pathologies and also for *ex vivo* 3D modelling and nephrotoxicity screening. Although their versatility and regenerative potential are very attractive for researchers, we have not yet been able to bring these new kidney therapies to the clinic. Most importantly, we must build a deeper understanding of the changes that occur with such materials following its *in vivo* implantation. This success and clinical validation of biomaterials fabrication from natural matrices will largely depend on our ability to understand and take advantage of their inherent properties, thereby maximizing their regenerative potential.

## I-4. CONCLUDING REMARKS AND PERSPECTIVES

The literature herein reviewed clarifies the dynamic and active role of the ECM and its composition in kidney remodeling and regeneration. Improving our understanding on the role of the ECM on remodeling processes and mechanisms leading to the deposition of altered ECM is extremely important to obtain new strategies to treat kidney diseases or creating functional kidneys. We have demonstrated that a large part of kidney diseases is caused or involves ECM alterations and although new targets are being identified, current therapies are still not able to reverse ECM changes and fibrosis. In the past few years, researchers identified new ECM-related disease biomarkers that could lead to an early diagnostic and, consequently, a more effective treatment to prevent future organ loss. Also, several innovative research studies are ongoing to address the limitations of current renal replacement therapies. Because kidney ECM can be obtained from relatively easy-to-implement decellularization processes, recently researchers have been applying it in regenerative medicine strategies. Despite the early encouraging results, there are several hurdles that need to be addressed in whole kidney bioengineering, such as thrombosis and/or efficient niche-specific cellular distribution and differentiation, which makes this technology far from its clinical applicability. Nevertheless, the use of processed ECM from xenogeneic origin as a component of diverse biomaterials has recently emerged, already revealing promising results in small animal models. In the next years, the field is expected to evolve to a successful utilization of mammalian kidney ECM in the clinic, taking advantage of the inherent repair capacity of the kidney. To achieve this goal, new animal disease models will have to be developed, mimicking in a more faithful way the advance of renal diseases in humans. Furthermore, new scaled-up recellularization strategies and new advanced therapies for partial kidney implantation are required to bring ECM-based therapies to a

new level of clinical research. Herein, we have shown the important role of the ECM on tissue remodeling, disease and how researchers can take advantage of it. Either by identifying new therapeutic targets and/or producing a new generation of clinically applicable materials, researchers are now able to use ECM in order to change the course of kidney therapies.

## I-5. REFERENCES


1. Lote CJ (2013) Principles of renal physiology, 5th ed. Springer, New York
2. Marieb EN, Hoehn K (2007) Human anatomy & physiology, 7th ed. Pearson
3. Scott RP, Quaggin SE (2015) The cell biology of renal filtration. J Cell Biol 209:199–210. https://doi.org/10.1083/jcb.201410017
4. Bellomo R, Kellum JA, Ronco C, et al (2012) Acute kidney injury. Lancet (London, England) 380:756–66. https://doi.org/10.1016/S0140-6736(11)61454-2
5. Webster AC, Nagler E V., Morton RL, Masson P (2017) Chronic Kidney Disease. Lancet 389:1238–1252. https://doi.org/10.1016/S0140-6736(16)32064-5
6. Luyckx VA, Tonelli M, Stanifer JW (2018) The global burden of kidney disease and the sustainable development goals. Bull World Health Organ 96:414-422D. https://doi.org/10.2471/BLT.17.206441
7. Wang H, Naghavi M, Allen C, et al (2016) Global, regional, and national life expectancy, all-cause mortality, and cause-specific mortality for 249 causes of death, 1980-2015: a systematic analysis for the Global Burden of Disease Study 2015. Lancet (London, England) 388:1459–1544. https://doi.org/10.1016/S0140-6736(16)31012-1
8. Grams ME, Rabb H (2012) The distant organ effects of acute kidney injury. Kidney Int 81:942–948. https://doi.org/10.1038/ki.2011.241
9. Mayor S (2016) Survival after kidney transplant from non-matching live donor is good. BMJ 352:i1476. https://doi.org/10.1136/BMJ.I1476
10. U.S. Department of Health & Human Services (2020) Organ Procurement and Transplantation Network. https://optn.transplant.hrsa.gov/data/
11. Lennon R (2017) Extracellular Matrix Biology Applied to the Kidney. In: Kidney Transplantation, Bioengineering, and Regeneration: Kidney Transplantation in the Regenerative Medicine Era, 1st ed. Academic Press, p 1252
12. Miner JH (1999) Renal basement membrane components. Kidney Int 56:2016–2024. https://doi.org/10.1046/j.1523-1755.1999.00785.x
13. Klein G, Ekblom P (1990) Extracellular matrix composition during kidney development. Contrib Nephrol 80:17–31. https://doi.org/10.1159/000418624
14. Byron A, Randles MJ, Humphries JD, et al (2014) Glomerular Cell Cross-Talk Influences Composition and Assembly of Extracellular Matrix. J Am Soc Nephrol 25:953–966. https://doi.org/10.1681/ASN.2013070795
15. Lennon R, Byron A, Humphries JD, et al (2014) Global Analysis Reveals the Complexity of the Human Glomerular Extracellular Matrix. J Am Soc Nephrol 25:939–951. https://doi.org/10.1681/ASN.2013030233
16. Hobeika L, Barati MT, Caster DJ, et al (2017) Characterization of glomerular extracellular matrix by proteomic analysis of laser-captured microdissected glomeruli. Kidney Int 91:501–511. https://doi.org/10.1016/j.kint.2016.09.044

17. Kim BW (2017) Clinical regenerative medicine in urology, 1st ed. Springer
18. Truong LD, Pindur J, Barrios R, et al (1994) Tenascin is an important component of the glomerular extracellular matrix in normal and pathologic conditions. Kidney Int 45:201–210. https://doi.org/10.1038/ki.1994.24
19. Sobreiro-Almeida R, Fonseca DR, Neves NM (2019) Extracellular matrix electrospun membranes for mimicking natural renal filtration barriers. Mater Sci Eng C 103:109866. https://doi.org/10.1016/J.MSEC.2019.109866
20. Randles MJ, Woolf AS, Huang JL, et al (2015) Genetic Background is a Key Determinant of Glomerular Extracellular Matrix Composition and Organization. J Am Soc Nephrol 26:3021–3034. https://doi.org/10.1681/ASN.2014040419
21. de Castro Brás LE, Toba H, Baicu CF, et al (2014) Age and SPARC Change the Extracellular Matrix Composition of the Left Ventricle. Biomed Res Int 810562:1–7. https://doi.org/10.1155/2014/810562
22. Nakayama KH, Batchelder CA, Lee CI, Tarantal AF (2011) Renal tissue engineering with decellularized rhesus monkey kidneys: age-related differences. Tissue Eng Part A 17:2891–901. https://doi.org/10.1089/ten.TEA.2010.0714
23. Eikmans M, Baelde HJ, De Heer E, Bruijn JA (2001) Effect of age and biopsy site on extracellular matrix mrna and protein levels in human kidney biopsies. Kidney Int 60:974–981. https://doi.org/10.1046/j.1523-1755.2001.060003974.x
24. Safirstein R (1999) Renal regeneration: Reiterating a developmental paradigm. Kidney Int 56:1599–1600. https://doi.org/10.1046/j.1523-1755.1999.00718.x
25. Basile DP, Liapis H, Hammerman MR (1997) Expression of bcl-2 and bax in regenerating rat renal tubules following ischemic injury. Am J Physiol - Ren Physiol 272:F640–F647. https://doi.org/10.1152/ajprenal.1997.272.5.f640
26. Makino H, Sugiyama H, Kashihara N (2000) Apoptosis and extracellular matrix–cell interactions in kidney disease. Kidney Int 58:S67–S75. https://doi.org/10.1046/J.1523-1755.2000.07711.X
27. Kanwar YS, Carone FA, Kumar A, et al (1997) Role of extracellular matrix, growth factors and proto-oncogenes in metanephric development. Kidney Int 52:589–606. https://doi.org/10.1038/ki.1997.372
28. Maeshima A, Nakasatomi M, Nojima Y (2014) Regenerative medicine for the kidney: Renotropic factors, renal stem/progenitor cells, and stem cell therapy. Biomed Res Int 595493:1–10. https://doi.org/10.1155/2014/595493
29. Stamenkovic I (2003) Extracellular matrix remodelling: The role of matrix metalloproteinases. J Pathol 200:448–464. https://doi.org/10.1002/path.1400
30. Giannelli G, Falk-Marzillier J, Schiraldi O, et al (1997) Induction of cell migration by matrix metalloprotease-2 cleavage of laminin-5. Science (80- ) 277:225–8. https://doi.org/10.1126/science.277.5323.225
31. Tan RJ, Liu Y (2012) Matrix metalloproteinases in kidney homeostasis and diseases. Am J Physiol - Ren Physiol 302:F1351–F1361. https://doi.org/10.1152/ajprenal.00037.2012
32. Lelongt B, Ronco P (2003) Role of extracellular matrix in kidney development and repair. Pediatr Nephrol 18:731–742. https://doi.org/10.1007/s00467-003-1153-x
33. Padanilam BJ, Martin DR, Hammerman MR (1996) Insulin-like growth factor I-enhanced renal expression of osteopontin after acute ischemic injury in rats. Endocrinology 137:2133–2140. https://doi.org/10.1210/endo.137.5.8612558
34. Zuk A, Matlin KS (2002) Induction of a laminin isoform and $\alpha$ 3 $\beta$ 1-integrin in renal ischemic injury and repair in vivo. Am J Physiol - Ren Physiol 283:F971 – F984. https://doi.org/10.1152/ajprenal.00176.2002

35. Li B, Castano AP, Hudson TE, et al (2010) The melanoma-associated transmembrane glycoprotein Gpnmb controls trafficking of cellular debris for degradation and is essential for tissue repair. FASEB J 24:4767–4781. https://doi.org/10.1096/fj.10-154757
36. Zuk A, Bonventre J V., Matlin KS (2001) Expression of fibronectin splice variants in the postischemic rat kidney. Am J Physiol - Ren Physiol 280:F1037–F1053. https://doi.org/10.1152/ajprenal.2001.280.6.f1037
37. Basile DP, Martin DR, Hammerman MR (1998) Extracellular matrix-related genes in kidney after ischemic injury: Potential role for TGF-$\beta$ in repair. Am J Physiol - Ren Physiol 275:F894–F903. https://doi.org/10.1152/ajprenal.1998.275.6.f894
38. Zhang W, Shu L (2016) Upregulation of miR-21 by Ghrelin Ameliorates Ischemia/Reperfusion-Induced Acute Kidney Injury by Inhibiting Inflammation and Cell Apoptosis. DNA Cell Biol 35:417-425Up-regulation of galectin-3 in acute renal. https://doi.org/10.1089/dna.2016.3231
39. Nishiyama J, Kobayashi S, Ishida A, et al (2000) Up-regulation of galectin-3 in acute renal failure of the rat. Am J Pathol 157:815–823. https://doi.org/10.1016/S0002-9440(10)64595-6
40. Chang EH, Gasim AH, Kerber ML, et al (2015) Palladin is Upregulated in Kidney Disease and Contributes to Epithelial Cell Migration after Injury. Sci Rep 5:7695. https://doi.org/10.1038/srep07695
41. He YX, Diao TT, Song SM, et al (2018) Wnt4 is significantly upregulated during the early phases of cisplatin-induced acute kidney injury. Sci Rep 8:10555. https://doi.org/10.1038/s41598-018-28595-4
42. Morigi M, Introna M, Imberti B, et al (2008) Human Bone Marrow Mesenchymal Stem Cells Accelerate Recovery of Acute Renal Injury and Prolong Survival in Mice. Stem Cells 26:2075–2082. https://doi.org/10.1634/stemcells.2007-0795
43. Gatti S, Bruno S, Deregibus MC, et al (2011) Microvesicles derived from human adult mesenchymal stem cells protect against ischaemia-reperfusion-induced acute and chronic kidney injury. Nephrol Dial Transplant 26:1474–1483. https://doi.org/10.1093/ndt/gfr015
44. Ezquer FE, Ezquer ME, Parrau DB, et al (2008) Systemic Administration of Multipotent Mesenchymal Stromal Cells Reverts Hyperglycemia and Prevents Nephropathy in Type 1 Diabetic Mice. Biol Blood Marrow Transplant. https://doi.org/10.1016/j.bbmt.2008.01.006
45. Kunter U, Rong S, Djuric Z, et al (2006) Transplanted mesenchymal stem cells accelerate glomerular healing in experimental glomerulonephritis. J Am Soc Nephrol 17:2202–2212. https://doi.org/10.1681/ASN.2005080815
46. Tögel F, Hu Z, Weiss K, et al (2005) Administered mesenchymal stem cells protect against ischemic acute renal failure through differentiation-independent mechanisms. Am J Physiol - Ren Physiol 289:F31–F42. https://doi.org/10.1152/ajprenal.00007.2005
47. Bruno S, Grange C, Collino F, et al (2012) Microvesicles derived from mesenchymal stem cells enhance survival in a lethal model of acute kidney injury. PLoS One 7:e33115. https://doi.org/10.1371/journal.pone.0033115
48. Qian H, Yang H, Xu W, et al (2008) Bone marrow mesenchymal stem cells ameliorate rat acute renal failure by differentiation into renal tubular epithelial-like cells. Int J Mol Med 22:325–332. https://doi.org/10.3892/ijmm_00000026
49. Franquesa M, Herrero E, Torras J, et al (2012) Mesenchymal stem cell therapy prevents interstitial fibrosis and tubular atrophy in a rat kidney allograft model. Stem Cells Dev 21:3125–3135. https://doi.org/10.1089/scd.2012.0096
50. Semedo P, Correa-Costa M, Cenedeze MA, et al (2009) Mesenchymal stem cells attenuate renal fibrosis through immune modulation and remodeling properties in a rat remnant kidney model. Stem Cells 27:3063–3073. https://doi.org/10.1002/stem.214

51. Perico N, Casiraghi F, Remuzzi G (2018) Clinical Translation of Mesenchymal Stromal Cell Therapies in Nephrology. J Am Soc Nephrol 29:362–375. https://doi.org/10.1681/ASN.2017070781
52. Chen YT, Sun CK, Lin YC, et al (2011) Adipose-Derived Mesenchymal Stem Cell Protects Kidneys against Ischemia-Reperfusion Injury through Suppressing Oxidative Stress and Inflammatory Reaction. J Transl Med 9:51. https://doi.org/10.1186/1479-5876-9-51
53. Zhou Y, Xu H, Xu W, et al (2013) Exosomes released by human umbilical cord mesenchymal stem cells protect against cisplatin-induced renal oxidative stress and apoptosis in vivo and in vitro. Stem Cell Res Ther 4:34. https://doi.org/10.1186/scrt194
54. Lazzeri E, Crescioli C, Ronconi E, et al (2007) Regenerative potential of embryonic renal multipotent progenitors in acute renal failure. J Am Soc Nephrol 18:3128–3138. https://doi.org/10.1681/ASN.2007020210
55. Sedrakyan S, Da Sacco S, Milanesi A, et al (2012) Injection of amniotic fluid stem cells delays progression of renal fibrosis. J Am Soc Nephrol 23:661–673. https://doi.org/10.1681/ASN.2011030243
56. Hauser P V., De Fazio R, Bruno S, et al (2010) Stem cells derived from human amniotic fluid contribute to acute kidney injury recovery. Am J Pathol 177:2011–2021. https://doi.org/10.2353/ajpath.2010.091245
57. Lee PY, Chien Y, Chiou GY, et al (2012) Induced pluripotent stem cells without c-Myc attenuate acute kidney injury via downregulating the signaling of oxidative stress and inflammation in ischemia-reperfusion rats. Cell Transplant 21:2569–2585. https://doi.org/10.3727/096368912X636902
58. Chade AR, Zhu X, Lavi R, et al (2009) Endothelial progenitor cells restore renal function in chronic experimental renovascular disease. Circulation 119:547–557. https://doi.org/10.1161/CIRCULATIONAHA.108.788653
59. Yamaleyeva LM, Guimaraes-Souza NK, Krane LS, et al (2012) Cell Therapy with Human Renal Cell Cultures Containing Erythropoietin-Positive Cells Improves Chronic Kidney Injury. Stem Cells Transl Med 1:373–383. https://doi.org/10.5966/sctm.2011-0048
60. Sagrinati C, Netti GS, Mazzinghi B, et al (2006) Isolation and Characterization of Multipotent Progenitor Cells from the Bowman's Capsule of Adult Human Kidneys. J Am Soc Nephrol 17:2443–2456. https://doi.org/10.1681/ASN.2006010089
61. Bussolati B, Bruno S, Grange C, et al (2005) Isolation of renal progenitor cells from adult human kidney. Am J Pathol 166:545–555. https://doi.org/10.1016/S0002-9440(10)62276-6
62. Oliver JA, Maarouf O, Cheema FH, et al (2004) The renal papilla is a niche for adult kidney stem cells. J Clin Invest 114:795–804. https://doi.org/10.1172/JCI20921
63. Herrera MB, Bussolati B, Bruno S, et al (2007) Exogenous mesenchymal stem cells localize to the kidney by means of CD44 following acute tubular injury. Kidney Int 72:430–441. https://doi.org/10.1038/sj.ki.5002334
64. Lin F, Moran A, Igarashi P (2005) Intrarenal cells, not bone marrow-derived cells, are the major source for regeneration in postischemic kidney. J Clin Invest 115:1756–1764. https://doi.org/10.1172/JCI23015
65. Ronconi E, Sagrinati C, Angelotti ML, et al (2009) Regeneration of glomerular podocytes by human renal progenitors. J Am Soc Nephrol 20:322–332. https://doi.org/10.1681/ASN.2008070709
66. Takasato M, Er PX, Chiu HS, Little MH (2016) Generation of kidney organoids from human pluripotent stem cells. Nat Protoc 11:1681–1692. https://doi.org/10.1038/nprot.2016.098
67. Schutgens F, Rookmaaker MB, Margaritis T, et al (2019) Tubuloids derived from human adult kidney and urine for personalized disease modeling. Nat Biotechnol 37:303–313. https://doi.org/10.1038/s41587-019-0048-8

68. Tan Z, Shan J, Rak-Raszewska A, Vainio SJ (2018) Embryonic Stem Cells Derived Kidney Organoids as Faithful Models to Target Programmed Nephrogenesis. Sci Rep 8:16618. https://doi.org/10.1038/s41598-018-34995-3
69. Taguchi A, Nishinakamura R (2017) Higher-Order Kidney Organogenesis from Pluripotent Stem Cells. Cell Stem Cell 21:730–746. https://doi.org/10.1016/j.stem.2017.10.011
70. Taguchi A, Kaku Y, Ohmori T, et al (2014) Redefining the in vivo origin of metanephric nephron progenitors enables generation of complex kidney structures from pluripotent stem cells. Cell Stem Cell 14:53–67. https://doi.org/10.1016/j.stem.2013.11.010
71. Hale LJ, Howden SE, Phipson B, et al (2018) 3D organoid-derived human glomeruli for personalised podocyte disease modelling and drug screening. Nat Commun 9:5167. https://doi.org/10.1038/s41467-018-07594-z
72. Freedman BS, Brooks CR, Lam AQ, et al (2015) Modelling kidney disease with CRISPR-mutant kidney organoids derived from human pluripotent epiblast spheroids. Nat Commun 6:8715. https://doi.org/10.1038/ncomms9715
73. Czerniecki SM, Cruz NM, Harder JL, et al (2018) High-Throughput Screening Enhances Kidney Organoid Differentiation from Human Pluripotent Stem Cells and Enables Automated Multidimensional Phenotyping. Cell Stem Cell 22:929-940.e4. https://doi.org/10.1016/j.stem.2018.04.022
74. Przepiorski A, Sander V, Tran T, et al (2018) A Simple Bioreactor-Based Method to Generate Kidney Organoids from Pluripotent Stem Cells. Stem Cell Reports 11:470–484. https://doi.org/10.1016/j.stemcr.2018.06.018
75. Usui JI, Kobayashi T, Yamaguchi T, et al (2012) Generation of kidney from pluripotent stem cells via blastocyst complementation. Am J Pathol 180:2417–2426. https://doi.org/10.1016/j.ajpath.2012.03.007
76. Yokoo T, Ohashi T, Jin SS, et al (2005) Human mesenchymal stem cells in rodent whole-embryo culture are reprogrammed to contribute to kidney tissues. Proc Natl Acad Sci U S A 102:3296–3300. https://doi.org/10.1073/pnas.0406878102
77. Pino CJ, Humes HD (2017) Renal Replacement Devices. In: Kidney Transplantation, Bioengineering, and Regeneration: Kidney Transplantation in the Regenerative Medicine Era, 1st ed. Academic Press, p 1252
78. O'Hare AM, Kurella Tamura M, Lavallee DC, et al (2019) Assessment of Self-reported Prognostic Expectations of People Undergoing Dialysis. JAMA Intern Med 179:1325–1333. https://doi.org/10.1001/jamainternmed.2019.2879
79. Humes HD, Buffington DA, MacKay SM, et al (1999) Replacement of renal function in uremic animals with a tissue- engineered kidney. Nat Biotechnol 17:451–455. https://doi.org/10.1038/8626
80. Humes HD, Weitzel WF, Bartlett RH, et al (2004) Initial clinical results of the bioartificial kidney containing human cells in ICU patients with acute renal failure. Kidney Int 66:1578–1588. https://doi.org/10.1111/j.1523-1755.2004.00923.x
81. Tumlin J, Wali R, Williams W, et al (2008) Efficacy and safety of renal tubule cell therapy for acute renal failure. J Am Soc Nephrol 19:1034–1040. https://doi.org/10.1681/ASN.2007080895
82. Johnston KA, Westover AJ, Rojas-Pena A, et al (2017) Development of a wearable bioartificial kidney using the Bioartificial Renal Epithelial Cell System (BRECS). J Tissue Eng Regen Med 11:3048–3055. https://doi.org/10.1002/term.2206
83. Gura V, Rivara MB, Bieber S, et al (2016) A wearable artificial kidney for patients with end-stage renal disease. JCI Insight 1:e86397. https://doi.org/10.1172/jci.insight.86397

84. Jansen K, Castilho M, Aarts S, et al (2019) Fabrication of Kidney Proximal Tubule Grafts Using Biofunctionalized Electrospun Polymer Scaffolds. Macromol Biosci 19:e1800412. https://doi.org/10.1002/mabi.201800412
85. Zhang H, Tasnim F, Ying JY, Zink D (2009) The impact of extracellular matrix coatings on the performance of human renal cells applied in bioartificial kidneys. Biomaterials 30:2899–2911. https://doi.org/10.1016/J.BIOMATERIALS.2009.01.046
86. Modi A, Verma SK, Bellare J (2018) Extracellular matrix-coated polyethersulfone-TPGS hollow fiber membranes showing improved biocompatibility and uremic toxins removal for bioartificial kidney application. Colloids Surfaces B Biointerfaces 167:457–467. https://doi.org/10.1016/j.colsurfb.2018.04.043
87. van Gaal RC, Fedecostante M, Fransen PPKH, et al (2019) Renal Epithelial Monolayer Formation on Monomeric and Polymeric Catechol Functionalized Supramolecular Biomaterials. Macromol Biosci 19:1800300. https://doi.org/10.1002/mabi.201800300
88. Mollet BB, Bogaerts ILJ, van Almen GC, Dankers PYW (2017) A bioartificial environment for kidney epithelial cells based on a supramolecular polymer basement membrane mimic and an organotypical culture system. J Tissue Eng Regen Med 11:1820–1834. https://doi.org/10.1002/term.2080
89. Chevtchik N V., Mihajlovic M, Fedecostante M, et al (2018) A bioartificial kidney device with polarized secretion of immune modulators. J Tissue Eng Regen Med 12:1670–1678. https://doi.org/10.1002/term.2694
90. Modi A, Verma SK, Bellare J (2018) Graphene oxide-doping improves the biocompatibility and separation performance of polyethersulfone hollow fiber membranes for bioartificial kidney application. J Colloid Interface Sci 514:750–759. https://doi.org/10.1016/j.jcis.2017.12.044
91. Kim S, Feinberg B, Kant R, et al (2016) Diffusive silicon nanopore membranes for hemodialysis applications. PLoS One 11:e0159526. https://doi.org/10.1371/journal.pone.0159526
92. Refoyo R, Skouras ED, Chevtchik N V., et al (2018) Transport and reaction phenomena in multilayer membranes functioning as bioartificial kidney devices. J Memb Sci 565:61–71. https://doi.org/10.1016/j.memsci.2018.08.007
93. Lanza RP, Chung HY, Yoo JJ, et al (2002) Generation of histocompatible tissues using nuclear transplantation. Nat Biotechnol 20:689–696. https://doi.org/10.1038/nbt703
94. Rosines E, Johkura K, Zhang X, et al (2010) Constructing kidney-like tissues from cells based on programs for organ development: Toward a method of in vitro tissue engineering of the kidney. Tissue Eng - Part A 16:2441–2455. https://doi.org/10.1089/ten.tea.2009.0548
95. Kitamura S, Sakurai H, Makino H (2015) Single adult kidney stem/progenitor cells reconstitute three-dimensional nephron structures in vitro. Stem Cells 33:774–784. https://doi.org/10.1002/stem.1891
96. Gheisari Y, Yokoo T, Matsumoto K, et al (2010) A thermoreversible polymer mediates controlled release of glial cell line-derived neurotrophic factor to enhance kidney regeneration. Artif Organs 34:642–647. https://doi.org/10.1111/j.1525-1594.2009.00928.x
97. Weber HM, Tsurkan M V., Magno V, et al (2017) Heparin-based hydrogels induce human renal tubulogenesis in vitro. Acta Biomater 57:59–69. https://doi.org/10.1016/j.actbio.2017.05.035
98. Lü SH, Lin Q, Liu YN, et al (2012) Self-assembly of renal cells into engineered renal tissues in collagen/Matrigel scaffold in vitro. J Tissue Eng Regen Med 6:786–792. https://doi.org/10.1002/term.484
99. Guimaraes-Souza NK, Yamaleyeva LM, Aboushwareb T, et al (2012) In vitro reconstitution of human kidney structures for renal cell therapy. Nephrol Dial Transplant 27:3082–3090. https://doi.org/10.1093/ndt/gfr785

100. Kim SS, Park HJ, Han J, et al (2003) Renal tissue reconstitution by the implantation of renal segments on biodegradable polymer scaffolds. Biotechnol Lett 25:1505–1508. https://doi.org/10.1023/A:1025490718221
101. Casanova MR, Alves da Silva M, Costa-Pinto AR, et al (2019) Chondrogenesis-inductive nanofibrous substrate using both biological fluids and mesenchymal stem cells from an autologous source. Mater Sci Eng C 98:1169–1178. https://doi.org/10.1016/j.msec.2019.01.069
102. Basu J, Genheimer CW, Rivera EA, et al (2011) Functional evaluation of primary renal cell/biomaterial neo-kidney augment prototypes for renal tissue engineering. Cell Transplant 20:1771–1790. https://doi.org/10.3727/096368911X566172
103. Huling J, Min S il, Kim DS, et al (2019) Kidney regeneration with biomimetic vascular scaffolds based on vascular corrosion casts. Acta Biomater 95:328–336. https://doi.org/10.1016/j.actbio.2019.04.001
104. Kodaira H, Tsutsumi Y, Yoshioka Y, et al (2004) The targeting of anionized polyvinylpyrrolidone to the renal system. Biomaterials 25:4309–4315. https://doi.org/10.1016/j.biomaterials.2003.10.097
105. Choi CHJ, Zuckerman JE, Webster P, Davis ME (2011) Targeting kidney mesangium by nanoparticles of defined size. Proc Natl Acad Sci U S A 108:6656–6661. https://doi.org/10.1073/pnas.1103573108
106. Qiao H, Sun M, Su Z, et al (2014) Kidney-specific drug delivery system for renal fibrosis based on coordination-driven assembly of catechol-derived chitosan. Biomaterials 35:7157–7171. https://doi.org/10.1016/j.biomaterials.2014.04.106
107. Dankers PYW, van Luyn MJA, Huizinga-van der Vlag A, et al (2012) Development and in-vivo characterization of supramolecular hydrogels for intrarenal drug delivery. Biomaterials 33:5144–5155. https://doi.org/10.1016/j.biomaterials.2012.03.052
108. Kazazi-Hyseni F, Zandstra J, Popa ER, et al (2015) Biocompatibility of poly(d,l-lactic-co-hydroxymethyl glycolic acid) microspheres after subcutaneous and subcapsular renal injection. Int J Pharm 482:99–109. https://doi.org/10.1016/j.ijpharm.2014.12.014
109. Soranno DE, Rodell CB, Altmann C, et al (2016) Delivery of interleukin-10 via injectable hydrogels improves renal outcomes and reduces systemic inflammation following ischemic acute kidney injury in mice. Am J Physiol - Ren Physiol 311:F362–F372. https://doi.org/10.1152/ajprenal.00579.2015
110. Amirian J, Van TTT, Bae SH, et al (2017) Examination of in vitro and in vivo biocompatibility of alginate-hyaluronic acid microbeads As a promising method in cell delivery for kidney regeneration. Int J Biol Macromol 105:143–153. https://doi.org/10.1016/j.ijbiomac.2017.07.019
111. Cho SH, Noh JR, Cho MY, et al (2017) An injectable collagen/poly( $\gamma$ -glutamic acid) hydrogel as a scaffold of stem cells and $\alpha$ -lipoic acid for enhanced protection against renal dysfunction. Biomater Sci 5:285–294. https://doi.org/10.1039/c6bm00711b
112. Feng G, Zhang J, Li Y, et al (2016) IGF-1 C domain-modified hydrogel enhances cell therapy for AKI. J Am Soc Nephrol 27:2357–2369. https://doi.org/10.1681/ASN.2015050578
113. Burton TP, Callanan A (2018) A Non-woven Path: Electrospun Poly(lactic acid) Scaffolds for Kidney Tissue Engineering. Tissue Eng Regen Med 15:301–310. https://doi.org/10.1007/s13770-017-0107-5
114. Madl CM, Keeney M, Li X, et al (2014) Co-release of cells and polymeric nanoparticles from sacrificial microfibers enhances nonviral gene delivery inside 3D hydrogels. Tissue Eng - Part C Methods 20:798–805. https://doi.org/10.1089/ten.TEC.2013.0669
115. Santos E, Orive G, M R, Luis J (2011) Cell-Biomaterial Interaction: Strategies To Mimic The Extracellular Matrix. In: On Biomimetics. IntechOpen, pp 529–558

116. Song JJ, Guyette JP, Gilpin SE, et al (2013) Regeneration and experimental orthotopic transplantation of a bioengineered kidney. Nat Med 19:646–51. https://doi.org/10.1038/nm.3154
117. Campbell TD, Landeen LK, Naughton BA, et al (1996) WO/1996/008213 - Three-dimensional human cell cultures on cardiac valve frameworks and their uses
118. Reing JE, Brown BN, Daly KA, et al (2010) The effects of processing methods upon mechanical and biologic properties of porcine dermal extracellular matrix scaffolds. Biomaterials 31:8626–8633. https://doi.org/10.1016/j.biomaterials.2010.07.083
119. Baptista PM, Siddiqui MM, Lozier G, et al (2011) The use of whole organ decellularization for the generation of a vascularized liver organoid. Hepatology 53:604–617. https://doi.org/10.1002/hep.24067
120. Nakayama KH, Batchelder CA, Lee CI, Tarantal AF (2010) Decellularized rhesus monkey kidney as a three-dimensional scaffold for renal tissue engineering. Tissue Eng - Part A 16:2207–2216. https://doi.org/10.1089/ten.tea.2009.0602
121. Price AP, England KA, Matson AM, et al (2010) Development of a decellularized lung bioreactor system for bioengineering the lung: The matrix reloaded. Tissue Eng - Part A 16:2581–2591. https://doi.org/10.1089/ten.tea.2009.0659
122. Yang Q, Peng J, Guo Q, et al (2008) A cartilage ECM-derived 3-D porous acellular matrix scaffold for in vivo cartilage tissue engineering with PKH26-labeled chondrogenic bone marrow-derived mesenchymal stem cells. Biomaterials 29:2378–2387. https://doi.org/10.1016/j.biomaterials.2008.01.037
123. Wainwright JM, Czajka CA, Patel UB, et al (2010) Preparation of cardiac extracellular matrix from an intact porcine heart. Tissue Eng - Part C Methods 16:525–532. https://doi.org/10.1089/ten.tec.2009.0392
124. Heath DE (2019) A Review of Decellularized Extracellular Matrix Biomaterials for Regenerative Engineering Applications. Regen Eng Transl Med 5:155–166. https://doi.org/10.1007/s40883-018-0080-0
125. Ofenbauer A, Sebinger DDR, Prewitz M, et al (2015) Dewaxed ECM: A simple method for analyzing cell behaviour on decellularized extracellular matrices. J Tissue Eng Regen Med 9:1046–1055. https://doi.org/10.1002/term.1658
126. Bonandrini B, Figliuzzi M, Papadimou E, et al (2014) Recellularization of well-preserved acellular kidney scaffold using embryonic stem cells. Tissue Eng - Part A 20:1486–1498. https://doi.org/10.1089/ten.tea.2013.0269
127. Nakayama KH, Lee CCI, Batchelder CA, Tarantal AF (2013) Tissue Specificity of Decellularized Rhesus Monkey Kidney and Lung Scaffolds. PLoS One 8:e64134. https://doi.org/10.1371/journal.pone.0064134
128. Ullah I, Busch JF, Rabien A, et al (2020) Adult Tissue Extracellular Matrix Determines Tissue Specification of Human iPSC-Derived Embryonic Stage Mesodermal Precursor Cells. Adv Sci 7:1901198. https://doi.org/10.1002/advs.201901198
129. Du C, Narayanan K, Leong MF, et al (2016) Functional Kidney Bioengineering with Pluripotent Stem-Cell-Derived Renal Progenitor Cells and Decellularized Kidney Scaffolds. Adv Healthc Mater 5:2080–2091. https://doi.org/10.1002/adhm.201600120
130. Minami T, Ishii T, Yasuchika K, et al (2019) Novel hybrid three-dimensional artificial liver using human induced pluripotent stem cells and a rat decellularized liver scaffold. Regen Ther 10:127–133. https://doi.org/10.1016/j.reth.2019.03.002
131. Ghaedi M, Le A V., Hatachi G, et al (2018) Bioengineered lungs generated from human iPSCs-derived epithelial cells on native extracellular matrix. J Tissue Eng Regen Med 12:e1623–e1635. https://doi.org/10.1002/term.2589

132. Gilpin SE, Ren X, Okamoto T, et al (2014) Enhanced lung epithelial specification of human induced pluripotent stem cells on decellularized lung matrix. Ann Thorac Surg 98:1721–1729. https://doi.org/10.1016/j.athoracsur.2014.05.080
133. Wan J, Huang Y, Zhou P, et al (2017) Culture of iPSCs derived pancreatic $\beta$ -like cells in vitro using decellularized pancreatic scaffolds: A preliminary trial. Biomed Res Int 4276928. https://doi.org/10.1155/2017/4276928
134. Oberwallner B, Brodarac A, Anić P, et al (2015) Human cardiac extracellular matrix supports myocardial lineage commitment of pluripotent stem cells. Eur J Cardio-thoracic Surg 47:416–425. https://doi.org/10.1093/ejcts/ezu163
135. Lo B, Parham L (2009) Ethical issues in stem cell research. Endocr Rev 30:204–213. https://doi.org/10.1210/er.2008-0031
136. Freedman BS (2019) Better Being Single? Omics Improves Kidney Organoids. Nephron 141:128–132. https://doi.org/10.1159/000496009
137. Zhang J, Li K, Kong F, et al (2019) Induced Intermediate Mesoderm Combined with Decellularized Kidney Scaffolds for Functional Engineering Kidney. Tissue Eng Regen Med 16:501–512. https://doi.org/10.1007/s13770-019-00197-9
138. Xue A, Niu G, Chen Y, et al (2018) Recellularization of well-preserved decellularized kidney scaffold using adipose tissue-derived stem cells. J Biomed Mater Res - Part A 106:805–814. https://doi.org/10.1002/jbm.a.36279
139. Guneta V, Zhou Z, Tan NS, et al (2018) Recellularization of decellularized adipose tissue-derived stem cells: Role of the cell-secreted extracellular matrix in cellular differentiation. Biomater Sci 6:168–178. https://doi.org/10.1039/c7bm00695k
140. Mendez JJ, Ghaedi M, Steinbacher D, Niklason LE (2014) Epithelial cell differentiation of human mesenchymal stromal cells in decellularized lung scaffolds. Tissue Eng - Part A 20:1735–1746. https://doi.org/10.1089/ten.tea.2013.0647
141. Bombelli S, Meregalli C, Scalia C, et al (2018) Nephrosphere-Derived Cells Are Induced to Multilineage Differentiation when Cultured on Human Decellularized Kidney Scaffolds. Am J Pathol 188:184–195. https://doi.org/10.1016/j.ajpath.2017.09.012
142. Lin CH, Hsia K, Tsai CH, et al (2019) Decellularized porcine coronary artery with adipose stem cells for vascular tissue engineering. Biomed Mater 14:045014. https://doi.org/10.1088/1748-605X/ab2329
143. Alio del Barrio JL, Chiesa M, Garagorri N, et al (2015) Acellular human corneal matrix sheets seeded with human adipose-derived mesenchymal stem cells integrate functionally in an experimental animal model. Exp Eye Res 132:91–100. https://doi.org/10.1016/j.exer.2015.01.020
144. Nayakawde NB, Methe K, Banerjee D, et al (2020) In Vitro Regeneration of Decellularized Pig Esophagus Using Human Amniotic Stem Cells. Biores Open Access 9:22–36. https://doi.org/10.1089/biores.2019.0054
145. Gao LP, Du MJ, Lv JJ, et al (2017) Use of human aortic extracellular matrix as a scaffold for construction of a patient-specific tissue engineered vascular patch. Biomed Mater 12:065006. https://doi.org/10.1088/1748-605X/aa801b
146. Dong J De, Huang JH, Gao F, et al (2011) Mesenchymal stem cell-based tissue engineering of small-diameter blood vessels. Vascular 19:206–213. https://doi.org/10.1258/vasc.2011.oa0283
147. Pawan KC, Shah M, Liao J, Zhang G (2017) Prevascularization of decellularized porcine myocardial slice for cardiac tissue engineering. ACS Appl Mater Interfaces 9:2196–2204. https://doi.org/10.1021/acsami.6b15291

148. Wang B, Wang G, To F, et al (2013) Myocardial scaffold-based cardiac tissue engineering: Application of coordinated mechanical and electrical stimulations. Langmuir 29:11109–11117. https://doi.org/10.1021/la401702w
149. Baghalishahi M, Efthekhar-vaghefi S hasan, Piryaei A, et al (2018) Cardiac extracellular matrix hydrogel together with or without inducer cocktail improves human adipose tissue-derived stem cells differentiation into cardiomyocyte–like cells. Biochem Biophys Res Commun 502:215–225. https://doi.org/10.1016/j.bbrc.2018.05.147
150. Patil PB, Chougule PB, Kumar VK, et al (2013) Recellularization of Acellular Human Small Intestine Using Bone Marrow Stem Cells. Stem Cells Transl Med 2:307–315. https://doi.org/10.5966/sctm.2012-0108
151. Crabbé A, Liu Y, Sarker SF, et al (2015) Recellularization of decellularized lung scaffolds is enhanced by dynamic suspension culture. PLoS One 10:e0126846. https://doi.org/10.1371/journal.pone.0126846
152. Haykal S, Zhou Y, Marcus P, et al (2013) The effect of decellularization of tracheal allografts on leukocyte infiltration and of recellularization on regulatory T cell recruitment. Biomaterials 34:5821–5832. https://doi.org/10.1016/j.biomaterials.2013.04.044
153. Princeteau M (1905) Greffe renale. J Med Bordeaux 549
154. Kueri S, Kari FA, Fuentes RA, et al (2019) The use of biological heart valves. Dtsch Aerzteblatt Int 116:423–430. https://doi.org/10.3238/arztebl.2019.0423
155. Böer U, Schridde A, Anssar M, et al (2015) The immune response to crosslinked tissue is reduced in decellularized xenogeneic and absent in decellularized allogeneic heart valves. Int J Artif Organs 38:199–209. https://doi.org/10.5301/ijao.5000395
156. Crapo PM, Gilbert TW, Badylak SF (2011) An overview of tissue and whole organ decellularization processes. Biomaterials 32:3233–3243. https://doi.org/10.1016/j.biomaterials.2011.01.057
157. Dalgliesh AJ, Parvizi M, Lopera-Higuita M, et al (2018) Graft-specific immune tolerance is determined by residual antigenicity of xenogeneic extracellular matrix scaffolds. Acta Biomater 79:253–264. https://doi.org/10.1016/j.actbio.2018.08.016
158. O'Neill JD, Anfang R, Anandappa A, et al (2013) Decellularization of human and porcine lung tissues for pulmonary tissue engineering. Ann Thorac Surg 96:1046–1055. https://doi.org/10.1016/j.athoracsur.2013.04.022
159. Balestrini JL, Gard AL, Gerhold KA, et al (2016) Comparative biology of decellularized lung matrix: Implications of species mismatch in regenerative medicine. Biomaterials 102:220–230. https://doi.org/10.1016/j.biomaterials.2016.06.025
160. Papalamprou A, Chang CW, Vapniarsky N, et al (2016) Xenogeneic cardiac extracellular matrix scaffolds with or without seeded mesenchymal stem cells exhibit distinct in vivo immunosuppressive and regenerative properties. Acta Biomater 45:155–168. https://doi.org/10.1016/j.actbio.2016.07.032
161. Wong ML, Wong JL, Vapniarsky N, Griffiths LG (2016) In vivo xenogeneic scaffold fate is determined by residual antigenicity and extracellular matrix preservation. Biomaterials 92:1–12. https://doi.org/10.1016/j.biomaterials.2016.03.024
162. VeDepo MC, Buse EE, Quinn RW, et al (2017) Species-specific effects of aortic valve decellularization. Acta Biomater 50:249–258. https://doi.org/10.1016/j.actbio.2017.01.008
163. Yamanaka S, Yokoo T (2015) Current bioengineering methods for whole kidney regeneration. Stem Cells Int 2015:724047. https://doi.org/10.1155/2015/724047
164. Badylak SF, Freytes DO, Gilbert TW (2015) Reprint of: Extracellular matrix as a biological scaffold material: Structure and function. Acta Biomater 23:S17–S26. https://doi.org/10.1016/j.actbio.2015.07.016

165. McKee RA, Wingert RA (2016) Repopulating decellularized kidney scaffolds: An avenue for ex vivo organ generation. Materials (Basel) 9:190. https://doi.org/10.3390/ma9030190
166. Ross EA, Williams MJ, Hamazaki T, et al (2009) Embryonic stem cells proliferate and differentiate when seeded into kidney scaffolds. J Am Soc Nephrol 20:2338–2347. https://doi.org/10.1681/ASN.2008111196
167. Destefani AC, Sirtoli GM, Nogueira BV (2017) Advances in the Knowledge about Kidney Decellularization and Repopulation. Front Bioeng Biotechnol 5:34. https://doi.org/10.3389/fbioe.2017.00034
168. Laurence J, Baptista PM, Atala A, Van Beusekom M (2015) Translating Regenerative Medicine to the Clinic, 1st ed. Academic Press
169. Sambi M, Chow T, Whiteley J, et al (2017) Acellular Mouse Kidney ECM can be Used as a Three-Dimensional Substrate to Test the Differentiation Potential of Embryonic Stem Cell Derived Renal Progenitors. Stem Cell Rev Reports 13:513–531. https://doi.org/10.1007/s12015-016-9712-2
170. Remuzzi A, Figliuzzi M, Bonandrini B, et al (2017) Experimental Evaluation of Kidney Regeneration by Organ Scaffold Recellularization. Sci Rep 7:43502. https://doi.org/10.1038/srep43502
171. Ciampi O, Bonandrini B, Derosas M, et al (2019) Engineering the vasculature of decellularized rat kidney scaffolds using human induced pluripotent stem cell-derived endothelial cells. Sci Rep 9:8001. https://doi.org/10.1038/s41598-019-44393-y
172. Caralt M, Uzarski JS, Iacob S, et al (2015) Optimization and critical evaluation of decellularization strategies to develop renal extracellular matrix scaffolds as biological templates for organ engineering and transplantation. Am J Transplant 15:64–75. https://doi.org/10.1111/ajt.12999
173. Guan Y, Liu S, Sun C, et al (2015) The effective bioengineering method of implantation decellularized renal extracellular matrix scaffolds. Oncotarget 6:36126–36138. https://doi.org/10.18632/oncotarget.5304
174. Ross EA, Abrahamson DR, St John PL, et al (2012) Mouse stem cells seeded into decellularized rat kidney scaffolds endothelialize and remodel basement membranes. Organogenesis 8:49–55. https://doi.org/10.4161/org.20209
175. Chani B, Puri V, Sobti RC, et al (2017) Decellularized scaffold of cryopreserved rat kidney retains its recellularization potential. PLoS One 12:e0173040. https://doi.org/10.1371/journal.pone.0173040
176. Yu YL, Shao YK, Ding YQ, et al (2014) Decellularized kidney scaffold-mediated renal regeneration. Biomaterials 35:6822–6828. https://doi.org/10.1016/j.biomaterials.2014.04.074
177. Uzarski JS, Bijonowski BM, Wang B, et al (2015) Dual-Purpose Bioreactors to Monitor Noninvasive Physical and Biochemical Markers of Kidney and Liver Scaffold Recellularization. Tissue Eng - Part C Methods 21:1032–1043. https://doi.org/10.1089/ten.tec.2014.0665
178. He M, Callanan A, Lagaras K, et al (2017) Optimization of SDS exposure on preservation of ECM characteristics in whole organ decellularization of rat kidneys. J Biomed Mater Res - Part B Appl Biomater 105:1352–1360. https://doi.org/10.1002/jbm.b.33668
179. Wang M, Bao L, Qiu X, et al (2018) Immobilization of heparin on decellularized kidney scaffold to construct microenvironment for antithrombosis and inducing reendothelialization. Sci China Life Sci 61:1168–1177. https://doi.org/10.1007/s11427-018-9387-4
180. Orlando G, Farney AC, Iskandar SS, et al (2012) Production and implantation of renal extracellular matrix scaffolds from porcine kidneys as a platform for renal bioengineering investigations. Ann Surg 256:363–370. https://doi.org/10.1097/SLA.0b013e31825a02ab
181. Abolbashari M, Agcaoili SM, Lee M-KK, et al (2016) Repopulation of porcine kidney scaffold using porcine primary renal cells. Acta Biomater 29:52–61. https://doi.org/10.1016/j.actbio.2015.11.026

182. Sullivan DC, Mirmalek-Sani S-H, Deegan DB, et al (2012) Decellularization methods of porcine kidneys for whole organ engineering using a high-throughput system. Biomaterials 33:7756–7764. https://doi.org/10.1016/j.biomaterials.2012.07.023
183. Ko IK, Abolbashari M, Huling J, et al (2014) Enhanced re-endothelialization of acellular kidney scaffolds for whole organ engineering via antibody conjugation of vasculatures. TECHNOLOGY 02:243–253. https://doi.org/10.1142/s2339547814500228
184. Zambon JP, Ko IK, Abolbashari M, et al (2018) Comparative analysis of two porcine kidney decellularization methods for maintenance of functional vascular architectures. Acta Biomater 75:226–234. https://doi.org/10.1016/J.ACTBIO.2018.06.004
185. Choi SH, Chun SY, Chae SY, et al (2015) Development of a porcine renal extracellular matrix scaffold as a platform for kidney regeneration. J Biomed Mater Res - Part A 103:1391–1403. https://doi.org/10.1002/jbm.a.35274
186. Batchelder CA, Martinez ML, Tarantal AF (2015) Natural scaffolds for renal differentiation of human embryonic stem cells for kidney tissue engineering. PLoS One 10:e0143849. https://doi.org/10.1371/journal.pone.0143849
187. Leuning DG, Witjas FMR, Maanaoui M, et al (2019) Vascular bioengineering of scaffolds derived from human discarded transplant kidneys using human pluripotent stem cell–derived endothelium. Am J Transplant 19:1328–1343. https://doi.org/10.1111/ajt.15200
188. Almeida H V., Cunniffe GM, Vinardell T, et al (2015) Coupling Freshly Isolated CD44 + Infrapatellar Fat Pad-Derived Stromal Cells with a TGF- $\beta$ 3 Eluting Cartilage ECM-Derived Scaffold as a Single-Stage Strategy for Promoting Chondrogenesis. Adv Healthc Mater 4:1043–1053. https://doi.org/10.1002/adhm.201400687
189. Baiguera S, Del Gaudio C, Lucatelli E, et al (2014) Electrospun gelatin scaffolds incorporating rat decellularized brain extracellular matrix for neural tissue engineering. Biomaterials 35:1205–1214. https://doi.org/10.1016/j.biomaterials.2013.10.060
190. Choi JS, Yang H-J, Kim BS, et al (2009) Human extracellular matrix (ECM) powders for injectable cell delivery and adipose tissue engineering. J Control Release 139:2–7. https://doi.org/10.1016/j.jconrel.2009.05.034
191. Gilbert TW, Stolz DB, Biancaniello F, et al (2005) Production and characterization of ECM powder: implications for tissue engineering applications. Biomaterials 26:1431–1435. https://doi.org/10.1016/j.biomaterials.2004.04.042
192. Hong Y, Takanari K, Amoroso NJ, et al (2012) An elastomeric patch electrospun from a blended solution of dermal extracellular matrix and biodegradable polyurethane for rat abdominal wall repair. Tissue Eng Part C Methods 18:122–32. https://doi.org/10.1089/ten.TEC.2011.0295
193. Pouliot RA, Link PA, Mikhaiel NS, et al (2016) Development and characterization of a naturally derived lung extracellular matrix hydrogel. J Biomed Mater Res - Part A 104:1922–1935. https://doi.org/10.1002/jbm.a.35726
194. Deegan DB, Zimmerman C, Skardal A, et al (2016) Stiffness of hyaluronic acid gels containing liver extracellular matrix supports human hepatocyte function and alters cell morphology. J Mech Behav Biomed Mater 55:87–103. https://doi.org/10.1016/j.jmbbm.2015.10.016
195. Fong AH, Romero-López M, Heylman CM, et al (2016) Three-Dimensional Adult Cardiac Extracellular Matrix Promotes Maturation of Human Induced Pluripotent Stem Cell-Derived Cardiomyocytes. Tissue Eng Part A 22:1016–25. https://doi.org/10.1089/ten.TEA.2016.0027
196. Wang W, Zhang X, Chao N-N, et al (2016) Preparation and characterization of pro-angiogenic gel derived from small intestinal submucosa. Acta Biomater 29:135–148. https://doi.org/10.1016/j.actbio.2015.10.013

197. Beck EC, Barragan M, Tadros MH, et al (2016) Approaching the compressive modulus of articular cartilage with a decellularized cartilage-based hydrogel. Acta Biomater 38:94–105. https://doi.org/10.1016/j.actbio.2016.04.019
198. Claudio-Rizo JA, Delgado J, Quintero-Ortega IA, et al (2018) Decellularized ECM-Derived Hydrogels: Modification and Properties. In: Hydrogels, 1st ed. IntechOpen, pp 3–22
199. Freytes DO, Vunjak-Novakovic G, O'Neill J (2015) US2015/0037434A1 - Biomaterials derived from tissue extracellular matrix
200. O'Neill JD, Freytes DO, Anandappa AJ, et al (2013) The regulation of growth and metabolism of kidney stem cells with regional specificity using extracellular matrix derived from kidney. Biomaterials 34:9830–9841. https://doi.org/10.1016/j.biomaterials.2013.09.022
201. Nagao RJ, Xu J, Luo P, et al (2016) Decellularized Human Kidney Cortex Hydrogels Enhance Kidney Microvascular Endothelial Cell Maturation and Quiescence. Tissue Eng Part A 22:1140–1150. https://doi.org/10.1089/ten.TEA.2016.0213
202. Su J, Satchell SC, Shah RN, Wertheim JA (2018) Kidney decellularized extracellular matrix hydrogels: Rheological characterization and human glomerular endothelial cell response to encapsulation. J Biomed Mater Res - Part A 106A:2448–2462. https://doi.org/10.1002/jbm.a.36439
203. Magno V, Friedrichs J, Weber HM, et al (2017) Macromolecular crowding for tailoring tissue-derived fibrillated matrices. Acta Biomater 55:109–119. https://doi.org/10.1016/j.actbio.2017.04.018
204. Pati F, Jang J, Ha DH, et al (2014) Printing three-dimensional tissue analogues with decellularized extracellular matrix bioink. Nat Commun 5:3935. https://doi.org/10.1038/ncomms4935
205. Ali M, Anil Kumar PR, Yoo JJ, et al (2019) A Photo-Crosslinkable Kidney ECM-Derived Bioink Accelerates Renal Tissue Formation. Adv Healthc Mater 8(7):e1800992. https://doi.org/10.1002/adhm.201800992
206. Singh NK, Han W, Nam SA, et al (2020) Three-dimensional cell-printing of advanced renal tubular tissue analogue. Biomaterials 232:119734. https://doi.org/10.1016/j.biomaterials.2019.119734
207. Lih E, Park KW, Chun SY, et al (2016) Biomimetic Porous PLGA Scaffolds Incorporating Decellularized Extracellular Matrix for Kidney Tissue Regeneration. ACS Appl Mater Interfaces 8:21145–21154. https://doi.org/10.1021/acsami.6b03771
208. Lih E, Park W, Park KW, et al (2019) A Bioinspired Scaffold with Anti-Inflammatory Magnesium Hydroxide and Decellularized Extracellular Matrix for Renal Tissue Regeneration. ACS Cent Sci 5:458–467. https://doi.org/10.1021/acscentsci.8b00812
209. Sobreiro-Almeida R, Melica ME, Lasagni L, et al (2020) Cytocompatibility, Bioactivity and Proteomic Analysis of Particulate Porcine Kidney Extracellular Matrix. Advance Ar: https://doi.org/10.1039/D0BM01272F
210. Sobreiro‐Almeida R, Elena Melica M, Lasagni L, et al (2020) Co‐cultures of renal progenitors and endothelial cells on kidney decellularized matrices replicate the renal tubular environment in vitro. Acta Physiol 230:e13491. https://doi.org/10.1111/apha.13491210.

# SECTION 2

# EXPERIMENTAL DESIGN

# Chapter II

# Materials & Methods

# Chapter II

# Materials and Methods

## OVERVIEW

This chapter provides a detailed description of the materials and methodologies used for the development of the experimental studies presented on Chapters III to VII. This information is complementary to the "Materials and Methods" of those chapters, giving a deeper insight on the methodological fundaments and rationale followed throughout the thesis.

A description of the main materials used, namely decellularized kidney matrix and poly(caprolactone) can be found in the first part of this section. In the second part, the necessary methods and optimizations for the development of the decellularized biomaterial structures will be described. The different characterization techniques applied to assess the physicochemical properties of the materials will also be addressed. Moreover, the methodologies followed to assess the biological performance of those materials are also herein detailed. This chapter aims to justify the selected methodology to answer specific research questions.

## II-1. MATERIALS

The biomaterials used in this thesis are herein described. The description of their main properties will help understanding their selection as candidate biomaterials. All of the reagents used on this thesis were acquired from Sigma Aldrich, unless otherwise specified.

### II-1.1. Decellularized Kidney Matrix

Organ- and tissue-derived extracellular matrices (ECM) represent the ideal template for all regenerative medicine strategies, as they contain a very similar composition to that of the surrounding cellular niche of a specific tissue or organ.[1] Decellularized tissues were first patented in 1996 for cardiac valves (WO/1996/008213).[2] Since then, they have been extensively used in the regenerative medicine field. Indeed, FDA already approved the use of several xenogeneic or allogeneic decellularized matrices aimed at tissue regeneration. These matrices can be obtained by using combinations of completely different methodologies, from physical to chemical and enzymatic treatments.[3] Physical treatments include perfusion, sonication, agitation, mechanical pressure or freezing and thawing. Chemical treatments are usually based on the use of acids, detergents, organic solvents, chelating agents and hypotonic/hypertonic solutions. Enzymatic treatments use proteases or nucleases to cleave the peptide or nucleotide bonds. All of these methodologies include several advantages and disadvantages on their use and are usually combined to maximize the decellularization procedure.[4] The main goal of a decellularization protocol is to have a good balance between nuclear material removal and preservation of the composition, biological activity, integrity and biomechanical properties of the ECM (Figure II-1).

Another important aspect of a decellularized tissue is its immunogenicity. For a successful implantation, decellularized tissues or derived biomaterials should not be toxic or elicit any immunological response. Some authors have already performed kidney decellularization optimization in non-human primates,[5] although no proteomic analysis was performed for comparison with human sources. Despite the genetically and evolutionarily similarity, this source is not plentiful and sustainable. Therefore, rat and porcine kidneys have been commonly explored for decellularization optimizations [6, 7] and for *in vivo* implantation of whole decellularized kidneys.[8, 9] The knowledge gathered so far on rodents kidneys' decellularization was important for the development on the field, which enabled the optimization of the strategies for decellularization. This includes the use of combined detergent solutions to maximize the decellularization potential,[10] which was also implemented on this thesis. Nevertheless, porcine kidneys

have numerous advantages over other sources, including the easy availability, higher breeding potential of the species and the larger amount of raw material that can be obtained after decellularization, and that was the main reason behind our source choice. Nevertheless, one of the main concerns of using porcine sources is the human immune rejection of porcine antigens, namely the α-Gal epitope.[11] Fortunately, research has evolved to study immunogenicity provoked by these scaffolds, and a study has reported that porcine-derived ECM elevates serum antibody level, but no adverse reaction upon tissue remodeling was reported in a non-human primate model.[12] Besides, chemical treatment was also reported to reduce immunogenicity of the decellularized matrices, a treatment which was also included in the preparation of the herein developed decellularized ECM.[13]

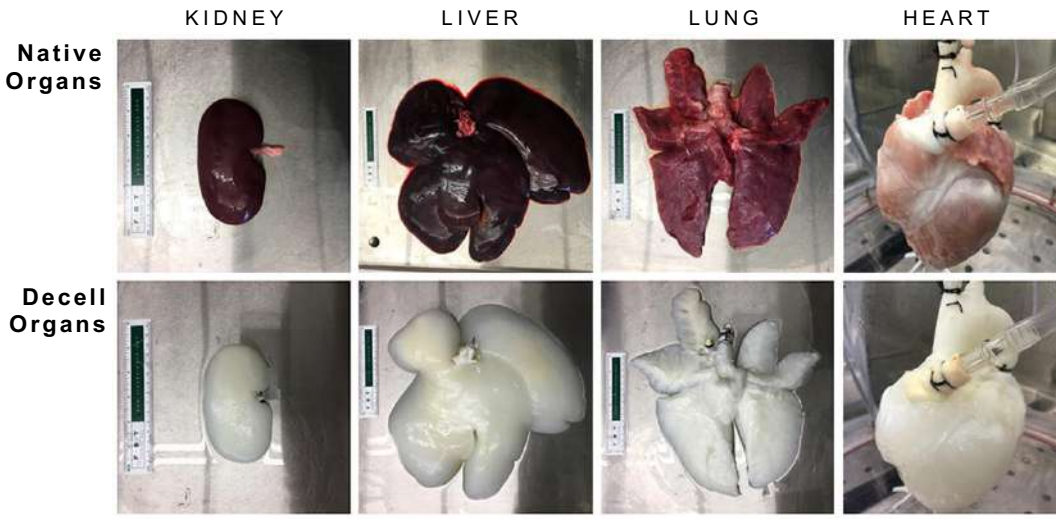


Figure II-1 – Examples of macroscopic images of organs before and after decellularization process. Adapted from[14].

After optimizing the best strategy for the decellularization of a specific tissue, decellularized tissues can be repopulated with cells of interest, with the main goal of generating a functional organ.[9] Besides representing a possible alternative to organ transplantation, the composition and versatility of the decellularized matrices enables their use as a basis to fabricate several types of biomaterial structures, without losing their bioactive factors and retaining their structure and function.[1] These biomaterials can represent a unique alternative for tissue engineering and regenerative medicine approaches, in order to partially regenerate an organ and restore its lost function.

Herein, the decellularization process was optimized to obtain well-preserved decellularized matrices from porcine kidneys, from which we have produced different biomaterial structures, as will be further described in the methods section.

## II-1.2. Poly(caprolactone)

Poly(caprolactone) (PCL) is a biodegradable hydrophobic and semicrystalline polymer. It can be synthetized via ring opening polymerization using ε-caprolactone as a monomer (Figure II-2).[15] Its chemical nature, allows the hydrolysis of ester linkages under physiological conditions, which enables its use for biomedical applications.[16] Indeed, since its approval by the Food and Drug Administration (FDA), is has been commonly used as a component for long-term implantable devices, such as sutures, and drug release applications. Additionally, its melting point around 60 °C, and its excellent solubility in common organic solvents, allows for a fine tuning of its shape and mechanical properties into a wide range of 3D scaffolding platforms. However, its hydrophobicity often results in poor cell adhesion and its slow degradation rate can compromise the intended application.[17] Therefore, PCL is frequently blended with other natural-based materials such as starch,[18] chitosan[19] and gelatin[20] in order to increase the mechanical properties of the natural materials and the degradation rate of the polymer.

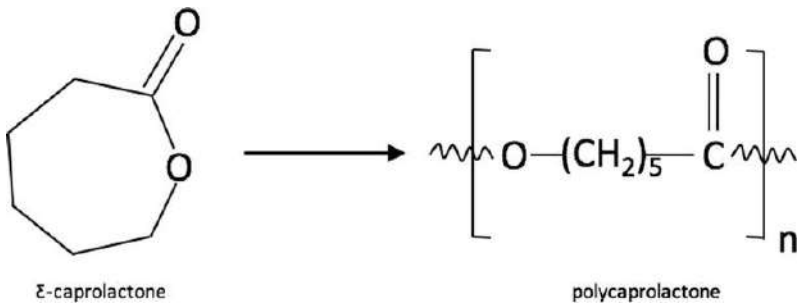


Figure II-2 – Ring-opening polymerization of ε-caprolactone into poly(caprolactone).[21]

The inclusion of a biodegradable polymer on this thesis was primarily intended for improving the mechanical stability of the developed tubular basement membrane models. PCL selected as a candidate material, as its degradation has already shown causing no harmful effects to the human body and its combination with other decellularized matrices such as small intestinal submucosa,[22] meniscus,[23] and adipose tissue [24] was already reported as non-cytotoxic. Being a biodegradable material, as the decellularized matrix, the mixing of both components would enable the creation of a unique model, with both similar mechanical and compositional properties to that of the human kidney. Thus, we have used PCL to combine it with the decellularized kidney matrix and develop a suitable tubular filtration barrier, decreasing degradability rates of the matrix and increasing the stability of a bilayer model for prolonged studies, as will be further described.

# II-2. METHODS

## II-2.1. Biomaterials' assays

This section discriminates all the necessary processing steps for obtaining the biomaterials developed in this thesis. Additionally, their specific physicochemical characterization is herein described, with additional focus on the different applied techniques, and how they have demonstrated to be suitable on fulfilling our characterization goal.

### II-2.1.1. Decellularized kidney matrix-derived biomaterials development

This section describes the established procedures for the obtention of biomaterial structures derived from kidney matrix. From obtention of the kidneys until their final processing for *in vitro* validation, all the steps were carefully optimized and herein summarized.

#### II-2.1.1.1 *Porcine kidney's decellularization and processing*

Whole porcine kidneys were obtained from a local slaughterhouse and kept at 4 °C. When they were not used immediately, they were frozen at -20 °C for a maximum period of 6 months. All the steps were performed in a sterile environment. To start the decellularization process, kidneys were cut in horizontal sections after removal of renal capsules and renal pelvis. Kidney sections were rinsed in cold sterile Milli-Q water and transferred into sterile containers, after which the decellularization process was started. The containers were filled with different solutions for 14 days and kept in an orbital shaker at 4 °C. The nature and duration of the immersing solutions are shown on Figure II-3. All the solutions were changed twice a day and the containers were washed to remove cellular debris. Remnants of nucleic material were removed by immersing kidney sections in DNase buffer overnight under the same conditions (0.0025 w/v% DNase in 100 mM Tris hydrochloride, pH = 7.5, 2.5 mM magnesium chloride and 0.5 mM calcium chloride). After completing the decellularization process, decellularized kidney extracellular matrix (dKECM) sections were cut into smaller pieces and used immediately for characterization or frozen at -80°C for further processing. Frozen sections of decellularized tissue were freeze-dried for 48 h (Figure II-4-A). Lyophilized tissue was grinded in a cryogenic mill (SPEX SamplePrep) to yield a particulate matrix

(pKECM, Figure II-4-B). This matrix was stored at -20 °C until further use or sterilized by ethylene oxide gas (42 °C, 3 h exposure) for cell culture studies.

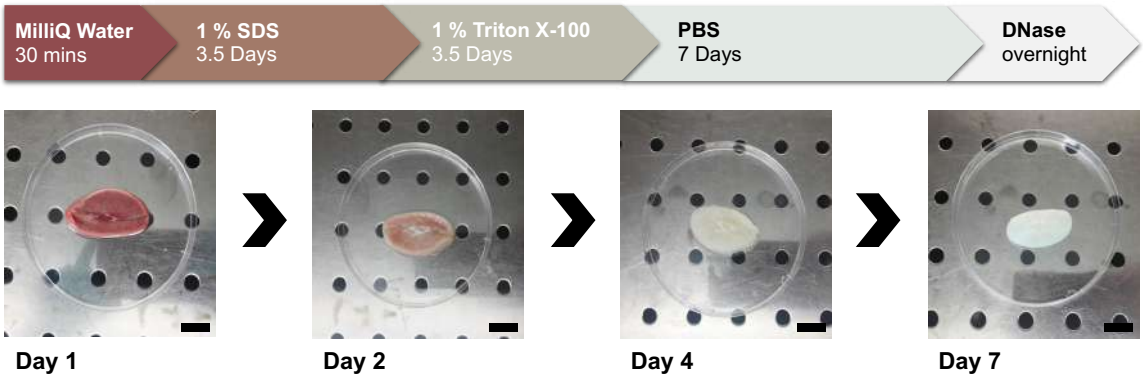


Figure II-3 – Schematic representation of the decellularization process. The above flowchart shows the solutions and reagents used to immerse kidney sections during a 14-Day process. The sections are kept inside a sterile container under agitation (120 rpm) at 4 °C. Below the flowchart, the macroscopic changes happening during the decellularization process are presented. Although at day 7 the sections are already decellularized, the process is prolonged for one more week for ensuring the removal of remaining detergent solutions. Scale bar: 1cm.


Figure II-4 - Schematic representation of the processing steps after the decellularization process. The matrix is lyophilized (A) and ground into a fine powder (B) which is then solubilized in a pepsin-containing acidic solution, acquiring a gel-like consistency (C).

### II-2.1.1.2 *Development of dKECM-based electrospun meshes*

The electrospinning process relies on the use of electrostatic forces to stretch a viscous solution through a needle, which forms a stable jet that solidifies when reaching the collector. At this stage, the solvent was partially evaporated and the fibers are formed and deposited at the surface of the collector as a non-woven web of small fibers – a mesh.[25] Herein, the use of this technique enabled developing an analogue of a tubular barrier. First, it enabled mixing two components in one solvent, adding mechanical stability to a mesh that could not be electrospun without the use of a polymeric material.

Second, it was thought as an advantageous technique to fabricate porous membranes, similar to the basement membranes found in the human kidney.[26] Other techniques, such as solvent casting, would not enable obtaining the indispensable porosity for barrier studies, such as the ones we were trying to replicate.

Powdered dKECM was solubilized in HFIP (1,1,1,3,3,3-Hexafluoro-2-propanol ≥99%) at a concentration of 100 mg $mL^{-1}$. Polycaprolactone (PCL, 80kDa) was dissolved in the same reagent at a concentration on 15 w/v%. The two were mixed in the different proportions, starting with 30 %, 50 % and finally 70 % of dKECM to PCL. The mixture was electrospun through a 21 G needle at 18 kV, establishing a distance of 15 cm between the needle tip and the ground collector, a flow rate of 0.5 $mL.h^{-1}$ and collecting the random fiber mesh on a flat aluminium foil. After 2 h of dKECM/PCL deposition, the meshes were left to dry for one day in a fume hood to evaporate all the remaining solvent. To avoid a fast degradation of the dKECM in the meshes, vapors of glutaraldehyde were applied to the meshes in a desiccator under vacuum for 24 h. Afterwards, the meshes were cut into 1.2 x 1.2 mm squares and introduced on 24-well plate inserts (CellCrown™). The inserts with the membranes were immersed in a 0.1 M glycine aqueous solution for 1 h to decrease the toxicity of residue aldehyde groups to cells, followed by sterilization using 70 v/v% of ethanol and 30 min UV exposure/each side.

#### II-2.1.1.3 *Development of dKECM bioink*

Bioprinting is a technique which enables the layer-by-layer spatial deposition of several biomaterials, biomolecules and cells to fabricate tissue analogues. There are several advantages on the use of this technique, being the most relevant the tunning of a specific 3D architecture, via a computer controlled dispensing system.[27] Herein, the development of a bioink and derived bioprinted constructs was thought to address several issues already reported on the literature. First, it would enable the construction of a tissue analogue with a certain degree of porosity, through an adequate 3D porous model, which is not possible to obtain when cells are encapsulated in a hydrogel. Second, it would enable tunning of the specific architecture and encapsulating different types of cells. This allows for specific spatial placement of these cells, which is very important for mimicking tissue functionality.[24] Because of this, the regenerative medicine potential of using bioinks is wide, from using the bioprinted constructs for drug screening to organ reconstruction/transplantation, biomolecule/cellular delivery and disease modeling. Herein, the development of a bioink composed uniquely of kidney matrix intends to address the gap existent on the literature on the development of these inks, which were frequently combined with other

materials. This combination could compromise their *in vivo* application and/or specific tissue functionality.

To develop the bioink, kidney decellularized particulate matrix was digested in acidic environment. Two concentrations were produced to test injectability and rheological properties. 1 and 2 % (w/v) of dKECM was digested for 48 h in 0.01 M hydrochloric acid together with 0.1 and 0.2 % (w/w) of pepsin (Enzymatic), respectively. The digestion was taken for 48 h at room temperature. After 48 h, the matrix was brought-up to physiological pH by addition of cold 10x PBS and 0.1 N NaOH (Enzymatic) in proportions of 1:9 and 1:10, respectively (Figure II-4-C). Before bioprinting, dKECM bioinks were centrifuged at 4000 rpm to pellet non-digested pieces.

### II-2.1.2. Decellularized kidney matrix characterization

This section describes the performed assays that were used to validate the process of decellularization. The protein content of the matrix was carefully studied and characterized by several approaches. Additionally, it was necessary to characterize the physicochemical properties of the matrix before and after processing into different biomaterial structures.

#### II-2.1.2.1 *DNA extraction and quantification*

The measurement of DNA content on the decellularized tissues is the most important step of validation mainly because residual nucleic material may contribute to cause cytocompatibility problems and adverse host responses *in vivo*. According to published data, a tissue is considered decellularized when the content of dsDNA is less than 50 ng $mg^{-1}$ of ECM dry weight.[28] This value was based upon the findings of studies in which host responses were not significant, while an *in vivo* constructive remodeling response has been observed.[28] Other works refer to the percentage regarding the native tissue,[29] being that 90 % of nucleic material removal is the accepted minimum value for a tissue to be considered decellularized. Herein, we followed the rationale of several published works,[24, 29, 30] and assessed DNA contents on fresh tissues and processed matrix after lyophilization.

For the detection of dsDNA, decellularized tissue pieces or lyophilized particulate ECM were digested for 2 h at 56 °C with proteinase K and the remaining DNA extraction was performed using DNeasy blood and tissue kit (Qiagen) according to manufacturer's instructions. Native kidney pieces were also digested

as controls. Each sample (n=3) was derived for different decellularization batches and weighted before the digestion step. The extracted DNA was quantified using Quanti-iT PicoGreen dsDNA assay kit (Invitrogen). Values were extrapolated using a standard curve of dsDNA and sample fluorescence was read in a microplate reader (excitation: 485/20 nm; emission: 530/25 nm). Alternatively, the nanodrop equipment (ThermoScientific) was also used for direct DNA quantification.

#### II-2.1.2.2 *Collagen and glycosaminoglycan's quantification*

The quantification of collagen and glycosaminoglycan's (GAG's) are rapid and easy-to-follow techniques which can be useful for the validation of our decellularization methodology. The maintenance of these components is of utmost importance since these are key players in maintaining the integrity and function of the tissues.[31] It is important to keep a good balance between matrix preservation and complete cellular removal, which is why these quantifications are required. Herein, we have used Sircol Collagen Assay Kit and 1,9-dimethymethylene blue (DMMB) dye binding assay for quantification of collagen and GAG's, respectively. Other kits such as the hydroxyproline detection kit for collagens and the Blyscan Glycosaminoglycan Assay kit or the alcian blue colorimetric assay for GAG's are available on the market and were also used for quantification on decellularized tissues.[23, 32] These specific assays were chosen as they were already described in the literature for quantification of decellularized tissues and demonstrated being effective protocols enabling obtaining accurate results.[33–35]

Acid and pepsin-soluble collagens were quantified using Sircol Collagen Assay Kit (Biocolor) according to manufacturer's instructions. Native and decellularized kidneys were cut into 8 mm circles with a thickness of approximately 2 mm. Collagen isolation and concentration was performed overnight at RT by immersing the tissue in 0.1 mg $mL^{-1}$ of pepsin (Enzymatic) in 0.5 M acetic acid (VWR). After releasing and recovery of the Collagen Bound Dye, absorbance was measured in a microplate reader at 555 nm against reagent blanks and standards. Tissue collagen concentrations were obtained from a collagen type I standard curve.

Glycosaminoglycans were quantified using DMMB dye binding assay. Kidneys were cut as described for collagen quantification and were placed in digestion buffer in a thermomixer at 60 °C and 300 rpm overnight. The buffer consisted in a solution of 200 mM phosphate buffer containing 1 mM of ethylenediamine tetraacetic acid (EDTA, pH 6.8), 500 µg $mL^{-1}$ of papain and 960 µg $mL^{-1}$ of n-acetyl cysteine. After digestion, the samples were centrifuged and the supernatants was used for quantification.

DMMB dye was added to the ECM digests at a 1:10 ratio of digests to dye. A standard curve was plotted using chondroitin sulphate. Absorbance was measured in a microplate reader at 525 nm and concentrations were obtained from the standard curve.

#### II-2.1.2.3 *Histological stainings*

In order to fully characterize the decellularized matrix, quantification assays were coupled with imaging methods. The histological assessment is widely used in combination with quantitative biochemical analysis to corroborate the removal of nuclear material and the preservation of important components of the matrix, such as collagen and GAG's, as previously mentioned. Indeed, many reports demonstrate that a combination of both strategies is effective for the assessment of matrix content after decellularization.[9, 36, 37] Following the rationale of these works, we have chosen to perform Hematoxylin and eosin (H&E), Masson's Trichrome (MT) and Alcian Blue (AB) stainings as these are effective stainings to detect DNA, Collagen and GAG's.

H&E is one of the main tissue stains used in histology and is the most widely used stain in medical diagnosis. Hematoxylin stains cell nuclei in blue, and eosin stains the extracellular matrix and cytoplasm in pink.[38] Herein, this stain was employed to assess if the nuclear material was completely removed, with preservation of ECM. As a complement, MT staining was also performed using a commercially available kit, in which four different stains are used: Weigert's iron hematoxylin for nuclei, picric acid for erythrocytes, a mixture of acid dyes for cytoplasm and aniline blue for connective tissue. Overall, these solutions produce a blue stain for collagen, a light red or pink stain for the cytoplasm and black stain for cell nuclei.[38] AB staining was also performed on decellularized tissue sections. In this staining, the bluish-green color indicates the presence of acidic polysaccharides such as glycosaminoglycans. Since the decellularization aims at preserving the ECM content while removing cell nuclei, these histology stainings enable a triple assessment of the tissue by imaging.

For the stainings, kidney sections were cut into smaller pieces with a 8 mm diameter biopsy punch and immersed in a 10 % neutral buffered formalin solution (Thermo Scientific) for 24 h at room temperature. Pieces of decellularized and native tissues were embedded in paraffin and cut into 5 µm-thick sections. These sections were deparaffinized, rehydrated and stained with working solutions of H&E, AB and a MT staining kit (Bio-optica), according to manufacturer's instructions.

Particulate kidney samples were also assessed by H&E and MT stainings of frozen sections. The samples were fixed for 30 min with 10 % neutral-buffered formalin before being embedded in OCT compound (Bio-optica). After this, they were snap-freezed in liquid nitrogen and cut into 10 µm sections using a cryostat. Sections were stained as previously mentioned. After staining, sections were dehydrated through a series of ethanol concentrations (50, 75, 95 and 100 %) and further mounted.

#### II-2.1.2.4 *Immunofluorescence*

Immunofluorescence is one of the most used techniques in biology. It allows the imaging of the distribution of a target molecule throughout a sample. For this, specific antibodies target the antigen of interest and fluorescent dyes produce a fluorescent signal, allowing for a very specific detection through imaging methods. This technique was also performed in several reports of tissue decellularization, enabling confirming the previously described assays.[5, 39, 40] Herein, we have only used secondary immunofluorescence, in which a secondary antibody is needed to emit fluorescence.[41] The substrates were analyzed by embedding the particulate matrix in OCT, as previously described (section II-2.1.2.3). After washing the OCT compound, particulate kidney ECM sections were blocked with 3 % bovine serum albumin (BSA) in PBS before being incubated with primary antibodies for immunofluorescent analysis as follows: anti-Collagen IV (1:100; ab6586), anti-Fibronectin (1:100, ab2413) and anti-Collagen I (1:40, ab765). After a washing step, secondary antibody Alexa Fluor 488 (1:500) was incubated with DAPI (1:1000) for 1 hour at RT before being mounted and analyzed under a confocal microscope.

#### II-2.1.2.5 *Total protein extraction and quantification*

The extraction of total protein is a critical step for the quantitative analysis by mass spectrometry. Ensuring that even the most insoluble proteins in the common buffers can be successfully extracted will result in a more accurate quantification of proteins present in the matrix.[42] Therefore, the process was optimized to yield the maximum quantity of protein without compromising protein stability and avoiding degradation, as represented in Figure II-5. With this protocol, we aim to evaluate if the proteins present in the insoluble part of the decellularized ECM are extracted and also to avoid the effect of the initial sonication and enzymatic digestion on sensitive proteins. Therefore, total protein extraction was performed on the particulate matrix substrates (pKECM) in three fractions. Approximately 5 mg of pKECM from different decellularization processes was processed in triplicate. One mL of Urea Extraction Buffer

(8 M Urea, 10 mM ammonium bicarbonate and 25 mM of tris(2-carboxyethyl)phosphine, pH 8.0) supplemented with 10 mg $mL^{-1}$ of dithiothreitol (abcr GmbH) and 20 µL $mL^{-1}$ of protease inhibitors were used to homogenize the matrix with a tissue grinder (Nippon Genetics). After, the matrix was incubated in the buffer overnight in agitation. The homogenized pKECM was centrifuged at 12700 rpm and the supernatant, referred as Fraction 1, was removed and saved. The pellet was once again homogenized and centrifuged. The resultant supernatant was joined to the soluble Fraction 1 (F1). Urea extraction buffer was again added to the resultant pellet and vortexed. The mixture was sonicated at 40 % amplitude while being refrigerated. After centrifuging, the supernatant was saved as Fraction 2 (F2). The remaining pellet was digested with trypsin as described in section II-2.1.2.6 to yield Fraction 3 (F3).

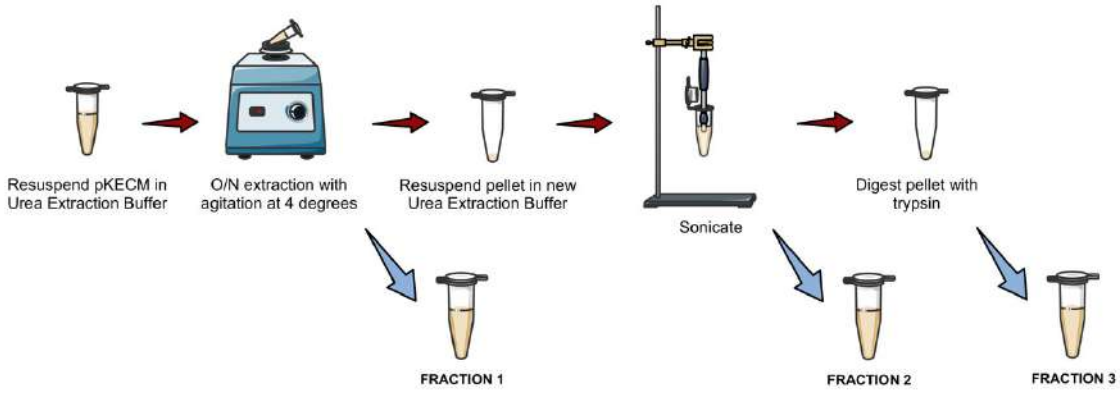


Figure II-5 - Schematic representation of the methodology used to obtain ECM fractions. Fraction 1 was obtained by homogenization with Urea Extraction Buffer, Fraction 2 was obtained after sonication of the remaining pellet and Fraction 3 was obtained after tryptic digestion of the Fraction 2 pellet.

For accurate protein quantification we used a commercial kit based on the Bradford coomassie-binding (ThermoFisher).[43] Briefly, this technique relies on the formation of a complex between Coomassie brilliant blue G-250 dye and proteins in an acidic solution. When the reaction happens, an immediate shift in color from brown to blue is held, and protein concentration can be estimated by the use of an absorbance reader. Herein, after protein extraction, 250 µL of Coomasie Reagent of sample was added to 5 µL of each sample in triplicate and quantified by measuring absorbance at 595 nm in a microplate reader. The protein concentration of each sample was calculated using a bovine serum albumin (BSA) standard curve.

### II-2.1.2.6 *Characterization and relative quantification of protein composition by nano-liquid chromatography–tandem mass spectrometry (nanoLC- MS/MS)*

Liquid chromatography (LC) coupled with mass spectrometry (MS) is an analytical chemistry technique that combines the physical separation capabilities of LC with the mass analysis capabilities of MS. As this technique evolved over time, it was modified to enhance its sensitivity. Nano-LC columns usually have smaller internal diameters and handle very low liquid flows in order to allow for a more efficient molecule separation. In tandem MS (MS/MS), two spectrometers are used to identify and separate ions that have very similar mass-to-charge (m/z) ratios. The molecules of a given sample are ionized and the first spectrometer separates these ions by their m/z ratio. Ions are then split into smaller fragments and then introduced into the second mass spectrometer, which in turn repeats the fragment separation process and detects them. The sensitivity of this technique has advantages over conventional LC-MS that allows for the analysis of peptide mixtures in sample-limited situations, with higher sensitivity.[44]

In this work, each sample was reduced and alkylated and processed for proteomics analysis following the solid-phase-enhanced sample-preparation (SP3) protocol as described in PMID30464214.[45] Enzymatic digestion was performed with Trypsin/LysC (2 µg) overnight at 37 °C. Protein identification and quantitation was performed by nanoLC-MS/MS. This equipment is composed by an Ultimate 3000 liquid chromatography system coupled to a Q-Exactive Hybrid Quadrupole-Orbitrap mass spectrometer (Thermo Scientific, Bremen, Germany). Samples were loaded onto a trapping cartridge (Acclaim PepMap C18 100Å, 5 mm x 300 µm i.d., 160454, Thermo Scientific) in a mobile phase of 2 % acetonitrile (ACN), 0.1% formic acid (FA) at 10 µL $min^{-1}$. After 3 min loading, the trap column was switched in-line to a 50 cm by 75 µm inner diameter EASY-Spray column (ES803, PepMap RSLC, C18, 2 µm, Thermo Scientific, Bremen, Germany) at 250 nL $min^{-1}$. Separation was generated by mixing A: 0.1% FA, and B: 80 % ACN, with the following gradient: 5 min (2.5 % B to 10 % B), 120 min (10 % B to 30 % B), 20 min (30 % B to 50 % B), 5 min (50 % B to 99 % B) and 10 min (hold 99 % B). Subsequently, the column was equilibrated with 2.5 % B for 17 min. Data acquisition was controlled by Xcalibur 4.0 and Tune 2.9 software (Thermo Scientific, Bremen, Germany).

The raw data was processed using Proteome Discoverer 2.4.0.305 software (Thermo Scientific) and searched against the UniProt database for the Sus scrofa Proteome 2019_11. The Sequest HT search engine was used to identify tryptic peptides. The ion mass tolerance was 10 ppm for precursor ions and 0.02 Da for fragment ions. Maximum allowed missing cleavage sites was set to 2. Cysteine

carbamidomethylation was defined as constant modification. Methionine oxidation and protein N-terminus acetylation were defined as variable modifications. Peptide confidence was set to high. The processing node Percolator was enabled with the following settings: maximum delta Cn 0.05; decoy database search target FDR 1 %, validation based on q-value. Protein label free quantitation was performed with the Minora feature detector node at the consensus step. Precursor ions quantification was performing at the processing step with the following parameters: unique plus razor peptides were considered for quantification, precursor abundance was based on intensity and normalization was based on total peptide amount.

The total number of proteins identified in each fraction was obtained by filtering peptide identifications at > 95.0 % confidence interval with at least two peptides per protein. Gene ontology analysis (GO) was performed manually using AmiGO online platform.[46, 47] Following categorization, non-ECM proteins were excluded to perform graphical analysis. Coefficient of variation (CV) values were calculated by dividing the standard deviation by the mean values of the ECM proteins identified on each kidney sample. The mass spectrometry proteomics data was deposited in the ProteomeXchange Consortium via the PRIDE[48] partner repository with the dataset identifier PXD019122.

#### II-2.1.2.7 *Scanning Electron Microscopy (SEM)*

The principle of SEM relies on the interaction between an electron beam and the atoms at the sample surface. A focused beam of electrons scans the surface by interacting with its atoms in a raster scan. When scanning a conductive material, this beam is scattered, producing signals which are detectable by the SEM equipment, and transformed into a 2D image. By the position of the detected beam and the intensity of the signal, the produced image reflects the topographic details of the sample with high magnifications.[49] Although the produced image can give us useful information about three-dimensionality and topographical detail, all samples have to be prepared before being placed in the vacuum chamber, which is not ideal for biological samples. These samples must be dehydrated, and sputter coated with a conductive material, steps that can result in artifacts which are very difficult to identify and/or eliminate.

Herein, the morphology and ultrastructure of the dKECM fresh tissues and derived biomaterial structures was analyzed by SEM (JSM-6010 LV, JEOL). All samples were fixed in 2.5 % (v/v) glutaraldehyde (VWR) in a PBS solution for 24 h. After removing the residual fixation reagent, fresh tissues and dKECM bioinks were dehydrated through a series of ethanol gradient solutions and submitted to

critical point drying (Autosamdri-815, Tousimis) for a 45 min cycle. DKECM membranes and particulate matrix were also analyzed without prior dehydration. All samples were sputter coated with gold prior to analysis and micrographs were obtained using an accelerating voltage of 10 kV (coater 108 A, Cressington, United States). The SEM micrographs were further used to calculate the average fiber diameter of the dKECM electrospun membranes. By using a computed image analyzer (ImageJ), at least 200 fibers were randomly measured in 3 samples from different fabrication batches.

#### II-2.1.2.8 *Mechanical testing*

Testing the mechanical properties of biomaterials is of extreme importance in biomedicine. It allows assessing the biomaterials response to stress, its strength and also how it sustains mechanical stretching. By performing a tensile test, we can obtain a stress/strain curve which reflects the reaction of the material to the increasing stresses being applied, giving information about the point of failure, the modulus of elasticity and the yield strength.[50] It was important to apply this test in order to determine the mechanical properties of dKECM-derived meshes for its use as a model of the tubular barrier. The membranes (containing 0, 30, 50 and 70% of dKECM to PCL) were tested using a universal mechanical testing machine (5543 K2942, 5543, Instron) equipped with a 1 kN load cell in tensile mode. Firstly, samples of each membrane (n = 5) were cut into testing specimens with length of 2 cm and width of 0.6 cm and then were fixed in paper frames with a square window of 1.2 × 1.2 cm. The frames were then mounted onto the tester grips with a gauge length of 1.2 cm. The lateral sides of the paper frame were cut before testing the sample at a crosshead speed of 0.5 $mm.min^{-1}$. The Young's Modulus (E) was calculated from the stress–strain curve as the maximum slope of the initial linear portion of the curve, neglecting any toe region due to the initial mechanical conditioning of the specimen.

#### II-2.1.2.9 *Fourier Transformed Infrared Spectroscopy (ATR-FTIR)*

FTIR technique enables obtaining the absorption or reflectance infrared spectrum of a certain solid, liquid or gas. In the infrared region, the sample molecules selectively absorb radiation and undergo a vibrational transition, which refers to the excitation of a molecule to a higher vibrational state. Therefore, by analyzing the vibrational absorption bands in infrared spectrum, it is possible to detect functional groups and identify chemical structures.[51] Unlike other spectroscopy techniques, in FTIR, instead of irradiating the sample with a monochromatic beam of light, the beam contains many frequencies of

infrared radiation at once, allowing for a rapid measurement of the spectrum of a sample. This process is repeated many times so that the beam contains different combinations of frequencies.[52] The attenuated total reflectance (ATR) is sampling technique that can be coupled to the FTIR equipment. Fundamentally, it relies on the internal reflection of the incident radiation, which is attenuated by a crystal, creating an evanescent wave. The beam is then collected by a detector as it exits the crystal.[53] This feature allows to examine a sample directly without prior preparation, which is a great advantage for biological samples. Also, samples can be used directly in their solid or liquid state, being useful for studying conformational changes in proteins,[54] which was our main goal in performing this analysis. Thus, the infrared spectra of pKECM before and after sterilization was analyzed by ATR-FTIR (IRPrestige 21, Shimadzu), with a spectral range of 500-4000 $cm^{-1}$ in reflection mode to characterize the composition and molecular conformation of the pKECM (n = 3). The number of samples was used to confirm that different decellularization batches do not interfere with the obtained spectra.

#### II-2.1.2.10 *Differential Scanning Calorimetry (DSC)*

DSC technique measures the amount of energy (or heat flow) required to maintain a sample and a reference at the same temperature, while the temperature is changing trough a predefined heating rate. The basic principle of this technique relies on performing a scan of temperatures which provoke physical transformations on the sample. When this happens, the sample will require more or less heat flow comparing with the reference, which denotes an endothermic or exothermic process.[55] Therefore, it allows for the determination of enthalpies of transitions by the analysis of the resulting curve of heat flux vs. temperature. For proteins, the thermogram can be used to identify the temperatures at which denaturation processes occur. Upon heating, proteins unfold with disruption of hydrogen bonds, hydrophobic interactions, and non-covalent interactions. The necessary energy (enthalpy) for this disruption can be calculated from the thermogram.[56] Thus, we have measured the thermal properties of native lyophilized kidneys and pKECM substrates before and after sterilization by using a DSC equipment (Q100, TA Instruments). Approximately 2 mg of native, sterile and non-sterile pKECM (n = 3) were transferred into an aluminum pan and the sample was scanned with a modulated heating method. Samples were heated until 250 °C at a heating rate of 10 °C $min^{-1}$ and then cooled down to 10 °C. The sample chamber was purged with nitrogen at a flow rate of 50 mL $h^{-1}$.

### II-2.1.2.11 *Porosity, weight loss and water uptake studies*

A liquid displacement technique was used to calculate DKECM membranes porosity.[57] The rationale behind this measurement relies on the volume that the membrane soaks after immersion on a liquid. This volume, that occupies the "empty" spaces in the membrane is removed simultaneously with the membrane, which generates a difference from the initial volume that can be calculated. This is an important measurement for biological membranes, especially in the tubule, since they need to allow solute and water passage to ensure normal filtration function.[58] Therefore, porosity was calculated following equation 1, where $V_1$ is the initial liquid volume, $V_2$ is the volume after soaking the membrane and all the pores are filled and $V_3$ is the volume after membrane soaking and removal.

$$Porosity\ (\%) = \frac{V_1 - V_3}{V_2 - V_3} \times 100 \qquad \text{Equation 1}$$

Biodegradable materials can also undergo several changes in their physicochemical properties as a result of degradation, which may compromise the desired function. As a result, it is necessary to characterize the changes that occur at different stages of degradation over time.[59] There are important measurements that can be performed to characterize these changes, being one of them the quantity of water that one material can absorb. This absorption will cause dimensional changes and influence the speed of degradation. Additionally, it may give us useful information about the materials' hydrophilicity. Herein, we determined weight loss and water uptake of the dKECM membranes. Membranes were initially weighted ($m_i$) and soaked in an isotonic solution of sodium chloride (0.154 M, pH 7.4), in order to simulate the body environment. After, membranes were incubated at 37 °C for 30 days. These conditions were optimized to simulate the human body environment. After predefined periods of time, the membranes were weighted in their wet state and the percentage of water uptake was calculated using the equation 2, where $m_w$ is their wet weight and $m_i$ is the initial dry weight. Membranes were then placed on the incubator for another hour to dry before being weighted again. Weight loss percentage was calculated using equation 3, where $m_f$ is their final weight after immersing and drying, and $m_i$ is the initial dry weight.

$$Water\ uptake\ (\%) = \frac{m_w - m_i}{m_i} \times 100 \qquad \text{Equation 2}$$

$$Weight\ loss\ (\%) = \frac{m_i - m_f}{m_i} \times 100 \qquad \text{Equation 3}$$

#### II-2.1.2.12 *Rheological characterization*

Rheology is the science which allows studying the deformation and flow of certain materials which cannot be completely described by either classic solid or liquid mechanics, but instead demonstrate a viscoelastic behavior.[60] Understanding the shear response of hydrogels and the potential changes in their bulk characteristics in response to stress is extremely important for biomedical applications. There are several measurements that can be performed in a rheometer, the most relevant being dynamic frequency sweeps, temperature sweeps and viscosity. Frequency sweeps are performed over a range of oscillation frequencies at a constant oscillation amplitude and temperature, giving information about several parameters, such as the Storage (Elastic) Modulus (G') and/or the Viscous (Loss) Modulus (G''). Because hydrogels may undergo macro- or micro-structural rearrangement with time, this measurement is essential to study the maintenance of the shape and mechanical integrity over time. Temperature sweeps are particularly important for temperature-sensitive samples, since it allows for the study of samples' gelation kinetics, as well as their modulus before and after the crosslinking process. Viscosity is another useful rheology measurement, since it measures the material's resistance to deformation as function of shear rate or stress. This measurement is especially important for samples which are subjected to a variety of shear rates, such as nozzle extrusion during the printing process.

Evaluation of the bioink rheological properties was performed on 1 and 2 % dKECM using a rheometer (Kinexus Prot, Malvern). 20 mm diameter parallel plates and 1 mm gap size was used for all the measurements. To mimic bioprinting crosslinking conditions, transglutaminase was added at a final concentration of 10 mg $mL^{-1}$ of dKECM neutralized solution. The gelation kinetics of the samples was measured by temperature sweeps.[24] First, the linear viscoelastic region (LVE) was determined by a strain sweep. dKECM bioinks were then subjected to oscillatory shear stress (by setting the strain to 1% and angular frequency to 10 rad $s^{-1}$) during heating from 4 to 37 °C. A linear ramp of 5 °C $min^{-1}$ was set, while there were two incubation periods at 15 °C and 37 °C for 5 and 40 min, respectively. Dynamic

frequency sweep analysis was performed after a 30 min incubation at 37 °C, by setting the applied strain at 1% and sweeping the frequency from 100 to 0.1 rad $s^{-1}$. Finally, shear rate sweeps were conducted to access viscosity, by varying the shear rate from 0.01 to 500 $s^{-1}$ at room temperature. Mineral oil (Fisher Scientific) was used as solvent trap.

### II-2.2. Biological Assays

After the optimization of the biomaterials production, it is important to ensure that these are non-cytotoxic and relevant for maintaining and/or inducing renal phenotypes. This section will elucidate the biological validation of the biomaterial structures produced in this thesis in a descriptive way. After a short introduction to each cell type that was employed, the cell seeding protocols and respective optimizations are described. Then, the assays that were conducted to evaluated cellular performance, phenotype and functionality over time are also explained.

#### II-2.2.1. Cells employed in the study

The removal of cells from an animal or plant and their subsequent growth in a favorable artificial environment enables the development of cell culture tests *in vitro*, which are extremely important before any *in vivo* validation. Cells may be removed from the tissue directly and disaggregated by enzymatic or mechanical means – which are named as primary cells – or they can be chemically or virally induced to acquire the ability to divide indefinitely – named cell lines. This section comprises a brief description of the cells that were used throughout this thesis. Their nature, origin and the subculturing method for following *in vitro* validation assays will be herein explained.

##### II-2.2.1.1 *Human Kidney cell line 2 (HK-2)*

Herein, we employed a human kidney cortex/proximal tubule established cell line derived from normal kidney, HK-2 (American Type Culture Collection, ATCC). These cells were immortalized by transduction with human papilloma virus 16 (HPV-16) E6/E7 genes and have already proved to retain functional and morphologic characteristics of normal adult proximal tubular epithelium,[61] being a valuable resource for the *in vitro* proof-of-concept studies. These cells are seeded and expanded in

Keratinocyte Serum Free Medium supplemented with 0.05 mg $mL^{-1}$ Bovine Pituitary Extract and 5 ng $mL^{-1}$ of Epidermal Growth Factor (Gibco).

#### II-2.2.1.2 *Human Renal Progenitor Cells (hRPCs)*

Human renal progenitors are a subset of cells present in adult human kidney that are conserved since early morphogenesis.[62] They are characterized by the expression of the specific surface markers CD133 and CD24 in the absence of lineage-specific markers of differentiation.[63] Additionally, they demonstrate functional properties characteristic of stem cells, such as self-renewal capacity, high clonogenic activity and multidifferentiation potential. Their ability to differentiate towards renal epithelial cells of the cortical nephron, including glomerular or tubular epithelial cell lineages was already demonstrated.[64, 65] Indeed, these cells have also exhibited differentiation capacity into osteogenic cells, adipocytes and neuronal cells, upon specific supplementation.[63] When injected into immunodeficient mice with different disease models of glomerular or tubular damage, human RPC could engraft in the damaged kidney and integrate/differentiate within tubules and replace lost podocytes.[63, 66] More importantly, the injection of these cells alone has shown to ameliorate morphologic and functional kidney damage. Thus, this subset of multipotent cells can be very valuable for the development of new therapies for kidney diseases, being used throughout this thesis combined with various biomaterials.

For isolating hRPCs, human kidney fragments were obtained in agreement with the Ethical Committee on human experimentation of the Azienda Ospedaliero-Universitaria Careggi, Florence, Italy. All subjects gave their informed consent for inclusion before they participated in the study. The study was conducted in accordance with the Declaration of Helsinki, and the protocol was approved by the Ethics Committee on Human Experimentation of the Azienda Ospedaliero-Universitaria Careggi, Florence, Italy (project identification code 2015/0009082 from 25/03/2015). After obtaining kidney fragments, the cortex was minced before proceeding to an enzymatic digestion with collagenase solution type IV 750 U $mL^{-1}$ for 45 min at 37 °C. After digestion, the solution was sieved through graded mesh screens (60 and 80 μm). The cellular suspension was collected, washed and plated on petri dish containing complete medium. The medium is composed by Microvascular Endothelial Cell Growth Medium (EGM-MV, Lonza) supplemented with 20 % HyClone Fetal Bovine Serum (FBS, GE Healthcare). After 4-5 days of culture, the cells that adhered to the plate were subcultured. Cultures were checked for simultaneous expression

of CD133 and CD24 by flow cytometry at different passages, as will be further described in section 2.2.4.1. These cells were used between passages 1-3.

According to previously published reports, hRPCs take 30 days to differentiate into human renal proximal tubular epithelial cells (hRPTECs), when in specific cell culture conditions.[63] Thus, for cell culture studies with hRPTECs, differentiation on tissue culture plastic was performed before cell seeding in the biomaterial structures. For 23 days, hRPCs were cultured in Renal Epithelial Cell Growth Medium (REGM, Lonza) supplemented with 50 ng $mL^{-1}$ of hepatocyte growth factor (HGF, Peprotech), after which cell culture was continued on the membranes for 7 more days as will be further described in section 2.2.2.1.

#### II-2.2.1.3 *Human Umbilical Vein Endothelial Cells (HUVECs)*

HUVECs are frequently selected for the study of normal endothelial biology and mechanisms underlying vascular pathology. They present several advantages, including being primary non-immortalized cells of human origin and are relatively easy to isolate without contamination of other cell types. Besides, the source tissue is readily available, with no need for invasive techniques.[67] These were first isolated in 1973,[68] and since then several authors published protocols using different isolation techniques and different culture mediums.

We have obtained the cells from Cascade Biologics, Inc., which were directly isolated from 14 days or less newborn umbilical veins. They represent a pool from multiple donors which were cryopreserved at the end of the primary culture. After being thawed, HUVECs were cultured and expanded in EGM-MV media supplemented with 20 % FBS before being seeded. Passages between 1-6 were used on our experiments.

#### II-2.2.1.4 *Human Microvascular Endothelial Cells (HMECs)*

For more specific glomerular studies, we have employed a microvascular endothelial cell line, HMEC-1 (ATCC Cat# CRL-10636, RRID:CVCL_0307). These cells were isolated from human foreskins and transfected with pSVT vector, a pBR-322 based plasmid containing the coding region for Simian virus 40A gene product, large T antigen, being able to immortalize them.[69] They are well characterized and

show to retain morphologic, phenotypic and functional characteristics of normal human microvascular endothelial cells, being an interesting resource for our glomerular barrier studies.

These cells were expanded and cultured in EGM-MV media supplemented with 20 % FBS before being seeded together with hRPCs for differentiation studies. Passages between 26-30 were used in the experiments.

### II-2.2.2. Cell seeding

Before establishing cell culture studies, some important parameters have to be optimized. The seeding strategy needs to be adjusted depending on the substrate area and on whether it is a 2D or 3D seeding. Additionally, the cell size, growth and phenotype will also influence the evolution of the culture and are key parameters to be taken into account. All the seeding strategies herein described were optimized according to the substrates' nature and the type of cells being seeded.

#### II-2.2.2.1 *Seeding on electrospun membranes (mono and co-culture studies)*

DKECM-based electrospun membranes mounted on 24 well-plate inserts were cells obtained from three different origins. In a first proof-of-concept study, HK-2 cells were seeded within a concentrated drop containing $50 \times 10^3$ cells, which were left to adhere for 4 h at 37 °C. After this time, expansion medium was added, and the culture was maintained during 7 days (Figure II-6-A).

HRPCs were seeded on the membranes at a density of $3 \times 10^3$ cells/insert in endothelial basal medium (EBM, Lonza) supplemented with 10 % FBS (HyClone, GE Healthcare) and expanded for 21 days (Figure II-6-B). For co-culture studies, primary HUVECs (Cascade Biologics, Inc) were plated at a density of $7.5 \times 10^3$ cells/well in the day before hRPCs were seeded within the same expansion medium (Figure II-6-C). The cell seeding concentration was optimized to obtain a confluent monoculture of hRPCs at the end of the culture time.

For *in vitro* culture of the bilayer model, HUVECs were seeded on inverted inserts at a density of $2 \times 10^5$ cells $mL^{-1}$ and allowed to attach 3 hours before being reverted. Then, hRPCs with 23 days of differentiation supplementation were cultured at a density of $1.3 \times 10^5$ cells $mL^{-1}$ on the reverse side of the HUVECs insert for 7 days. The medium consisted of a mixture of 1:1 HGF-supplemented REGM with EBM plus 10 % of FBS (Figure II-6-D).

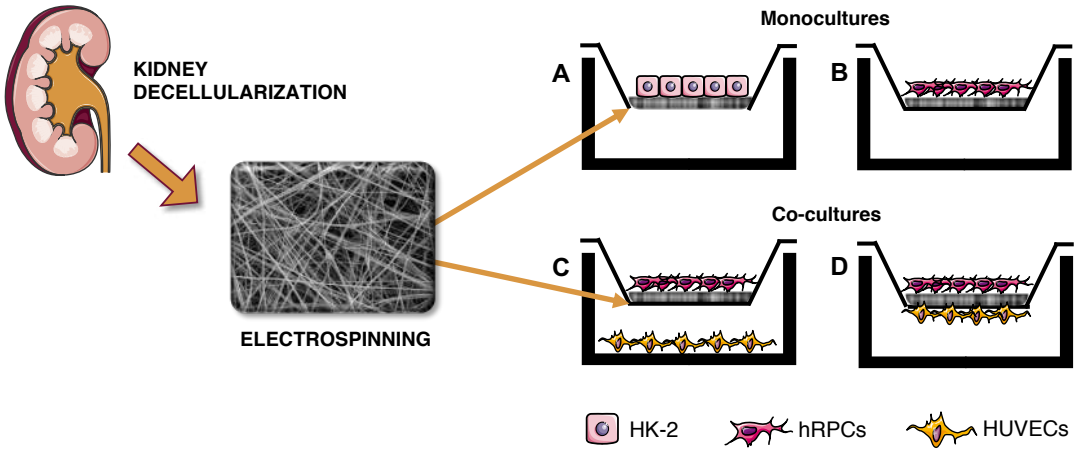


Figure II-6 – Schematic representation of the co-culture and monoculture cell seeding on the electrospun membranes.

### II-2.2.2.2 *3D non-adherent culture on particulate kidney ECM (pKECM)*

The effect of pKECM on cell behavior was analyzed having 3 different ratios of pKECM to hRPCs (Figure II-7). Suspension tissue culture 48-well plates were used in this study. 1, 2 and 4 mg of pKECM were weighted and added to each well before being rehydrated with complete medium for 30 min at 37 °C. A cell suspension of 50 µL containing $1 \times 10^5$ hRPC was added to each well and left 30 min at 37 °C to adhere to pKECM substrates. After that, complete medium composed by EGM-MV supplemented with 20 % HyClone™ FBS was added. Non-adherent cultures were performed by coating culture plates with a thin layer of 1.5 % agarose gel which was left to gelify overnight at 4 °C. The same cell concentration was seeded without the presence of pKECM in tissue culture treated polystyrene plates for the adherent cultures (2D control). The medium was changed every 2 or 3 days.

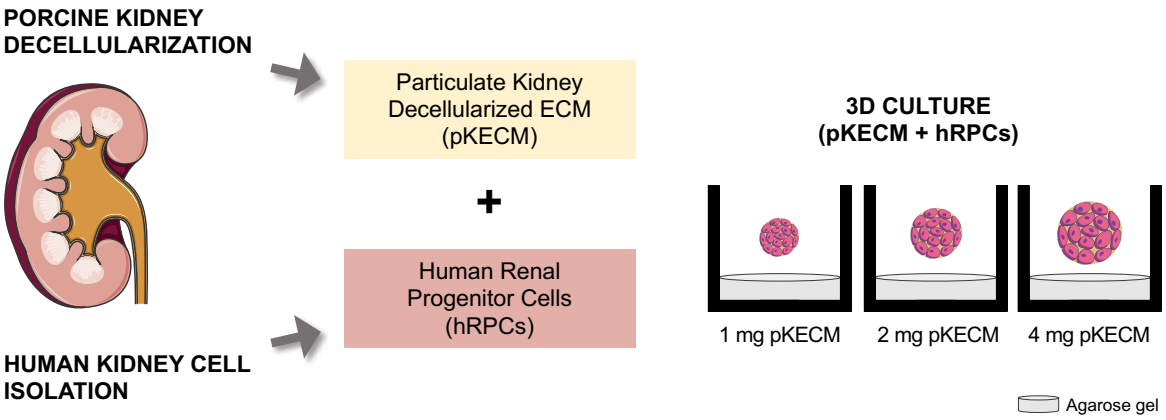


Figure II-7 – Schematic representation of the 3D culture performed on pKECM substrates.

### II-2.2.2.3 *Spheroids seeding and optimization*

hRPCs between P0 and P2 were used on this study. Cells were culture by hanging drop method.[70] Briefly, hRPCs were plated in hanging drops of 20 µL containing EGM-MV medium with 5, 10 and 20 × $10^3$ cells/drop. The different initial densities of cells per spheroid were defined taking into account previously reported protocols.[71, 72] Podocyte differentiation was conducted in DMEM-F12, supplemented with 10 % FBS and all-trans retinoic acid (RA, 100 µM) [65] and applied to the spheroids for a maximum of 48 h (Figure II-8). Similarly, an highly selective glycogen synthase kinase-3 (GSK-3) inhibitor, CHIR99021, was used as a WNT agonist to induce differentiation according to a previously published protocol.[73] Spheroid cultures were supplemented for 1 h in DMEM-F12 medium supplemented with 10 % FBS and 5 µM of CHIR99021 (R&D Systems). After, the medium was changed to include 10 % of FBS and 200 ng $mL^{-1}$ of FGF9 (R&D Systems) as supplements for 5 days. To obtain spheroid derived cells, spheroids were incubated with trypsin/EDTA for 5–20 min in a 37 °C water bath while pipetting every 2–3 min. For experiments using endothelial cells, we employed the HMEC-1 cell line. Briefly, $5\times10^4$ HMEC-1 were mixed with $15\times10^4$ hRPCs and seeded on hanging drops as previously described. The culture was either maintained for 4 days in EGM-MV media or stimulated with DMEM-F12 RA-containing media after 2 days of seeding time, for 48h, as previously described. After 4 days of co-culture, spheroids were retrieved for immunofluorescence or histology assessment.

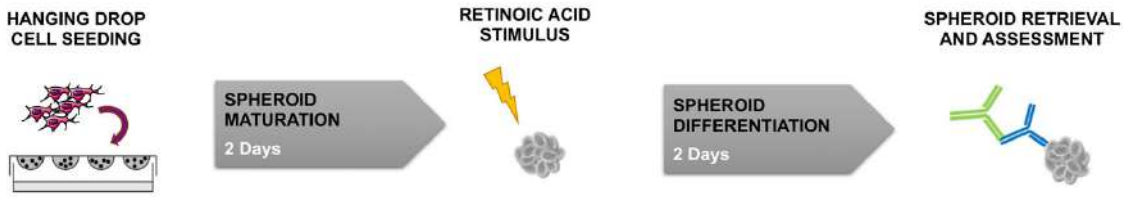


Figure II-8 – Schematic representation of spheroid seeding and differentiation protocol with retinoic acid.

#### II-2.2.2.4 *Bioink cell encapsulation and printing*

Before bioprinting, dKECM bioinks were centrifuged at 4000 rpm to pellet non-digested pieces. For cellular encapsulation, $1 \times 10^6$ hRPCs were resuspended in each 1 mL of 2% dKECM matrix. Cell-laden bioinks were loaded in sterile cartridges (CELLINK) for printing. Gelatin-laden bioinks were used as a control. Briefly, a 10 % gelatin solution was dissolved in PBS under constant stirring at 60 °C for 30 min and then cooled to 37 °C, before being mixed with $10^6$ hRPCs per mL and loaded in sterile cartridges. Constructs were printed using a bioprinter (BIO X, CELLINK). A scheme of the bioprinting process is shown in Figure II-9. The bioprinting process was performed using a support bath, as previously reported.[74] Briefly, a 0.5 % agarose solution (Lonza) containing 11 mM $CaCl_2$ (Sigma-Aldrich) was prepared and autoclaved. Immediately after, the solution was cooled down to room temperature under constant agitation at 700 rpm to form agarose microparticles. The solution was stored at 4 °C or used directly after cooling. 0.5 w/v % of microbial transglutaminase (Ajinomoto) was added to the agarose bath and left to solubilize for 20 min before printing. Printability was tested using a 25G needle with a varying printing speed from 8 to 12 mm $s^{-1}$ and a varying pressure from 5 to 10 kPa. The gelatin-containing printhead was heated at 37 °C, and hRPCs-laden gelatin was printing at a constant pressure of 5 kPa and a printing speed of 10 mm $s^{-1}$. Based on the printability tests, a square solid construct of $10 \times 10 \times 1$ $mm^3$ was printed inside sterile plates loaded with the support bath (Figure II-9). After printing, the constructs were crosslinked by incubation at 37 °C for 2 h, followed by agarose bath removal and fresh culture media addition. Cultures were maintained for 30 days, with specific timepoints to evaluate the evolution of the cellular performance.

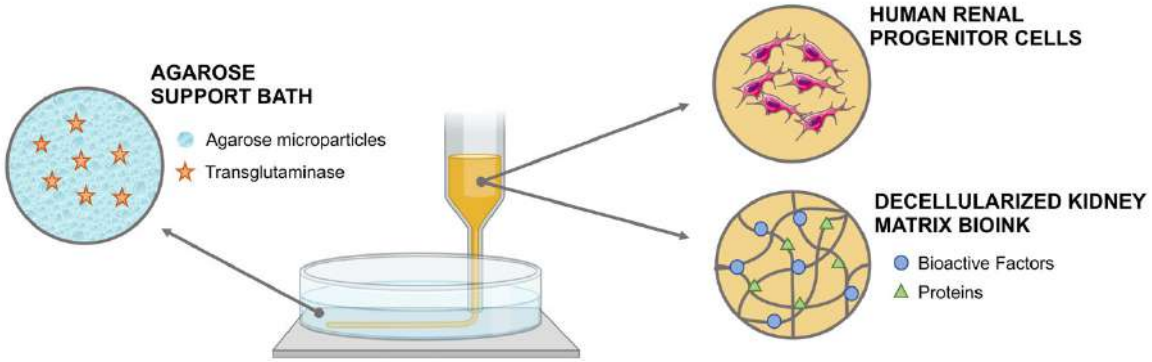


Figure II-9 – Schematic representation of the decellularized matrix bioprinting process using an agarose support bath.

### II-2.2.3. Cellular performance

The microenvironment in which cells are cultured, whether is a 2D or 3D culture, plays a primary role in defining cell fate during culture time. First, the biomaterial structures need to be tested for their cytotoxicity. Additionally, cell growth, proliferation, morphology and overall performance were evaluated, and those tests are herein briefly described.

#### II-2.2.3.1 *Cellular metabolic activity quantification*

Cellular viability assays are often used for screening cytotoxic effects that eventually lead to cell death. These effects can be a result of contacting with certain molecules or existing/released compounds during the culture time. Several assays can be performed to evaluate the cellular viability. The majority of them display a direct dependence on other parameters such as the incubation period, the number of cells and their metabolic activity.[75] Herein, MTS, MTT and alamarBlue® were used as quantitative assays of cellular metabolic activity, from which overall viability can also be inferred.

MTT (3-(4,5-dimethylthiazol-2-yl)-2,5-diphenyltetrazolium bromide) assay is based on the reduction of MTT tetrazolium dye to insoluble formazan (with a purple color) by NAD(P)H enzymes present in cells.[76] In this work, spheroids were incubated with a mixture of 1:5 MTT reagent:DMEM-F12 and incubated for 4 h at 37 °C. After that, the mixture was removed and 100 µL of DMSO were used to dissolve the dye. Absorbance was read in a microplate reader at 570 nm.

MTS (3-(4,5-dimethylthiazol-2-yl)-5-(3-carboxymethoxyphenyl)-2-(4-sulfophenyl)-2H-tetrazolium) was selected to evaluate HK-2 metabolic activity on dKECM electrospun membranes. This assay is described

as a "one-step" MTT, as the formazan products generated are directly soluble in culture media, simplifying the assay.[75] However, this advantage also makes MTS assay more susceptible to colorimetric interferences. HK-2 cells cultured above the dKECM electrospun membranes were incubated in a 5:1 proportion of MTS (Promega) to DMEM without phenol red for 4 h at 37 °C in the dark. Then, the supernatant was used to determine the absorbance at 490 nm. Cells cultured on glass coverslips were used as a negative control for cell metabolic activity.

AlamarBlue® is a commercially available kit that enables measuring the metabolic activity by the reduction of resazurin, a cell permeable redox indicator. Viable cells with active metabolism reduce this compound to resofurin, a pink soluble compound, which fluorescence can be directly measured on a microplate reader.[77] The great advantage of resazurin reduction relies on the fact that cells are not affected by the substrate after the assay, offering the possibility of performing other assays or continuing to evaluate cell culture over time. Herein, alamarBlue® was applied on hRPCs cultured on dKECM electrospun membranes, pKECM and dKECM bioinks. At day 7, 14 and 21 of culture, the hRPC-seeded dKECM membranes were removed from the inserts, washed with DPBS and placed on new 24 well-plates. Fresh culture medium containing 10 % of alamarBlue reagent was added to each well and incubated for 4 hours at 37 °C. The hRPCs-seeded pKECM assay was performed on cell suspensions after 1, 2, 4 and 7 days of culture using the same protocol, with 7 h of incubation time. Finally, bioink-encapsulated hRPCs metabolic activity was also measured using alamarBlue®, with an incubation time of 4 h and 30 min. For all conditions, supernatants were used to determine the fluorescence intensity in a microplate reader (excitation: 530/25 nm; emission: 590/25 nm).

#### II-2.2.3.2 *Live/Dead Assay*

The Live/Dead assay is a qualitative measurement of viability that can be used as a complementary assay to quantitative measurements. This test is usually performed using two fluorescent compounds, one indicating live cells in green, calcein, and another indicating dead cells in red, propidium iodide (PI). Calcein-AM is the acetomethoxy form of calcein, a highly lipophilic, cell membrane permeable dye. It requires the presence of intracellular esterases for the desterification of calcein AM and also plasma membrane integrity for the retention of the fluorescent calcein product.[78] On the contrary, PI is cell membrane impermeable and thus requires damaged cell membranes or dead cells to enter and bind to DNA. The fluorescence produced by PI when bound to DNA is enhanced 40-fold, enabling its detection by fluorescence microscopy. Herein, we performed live/dead assay on hRPCs cultured on pKECM

substrates and dKECM-derived bioinks. Briefly, the fluorescent dyes were incubated with the constructs at a concentration of 1 μg $mL^{-1}$ for PI and 2 μg $mL^{-1}$ for Calcein, AM in DPBS for 30 min at 37 °C. After this time, the constructs were analyzed using a confocal microscope (Leica, Wetzlar, Germany). Images were recorded digitally and further processed using LASX software (Leica) and ImageJ.[79]

#### II-2.2.3.3 *Cellular proliferation quantification*

Quantifying cell proliferation is of extreme importance to understand the effect that different biomaterials can have on the mitotic capacity of the cultured cells. It can also be used to plot a calibration curve correlating the number of cells with the amount of DNA at the beginning of the seeding. This can give us information about the number of cells throughout the culture time. Several methods for measuring cellular proliferation are available, but nucleic acid binding dyes have been widely used because of their high sensitivity.[80] Herein, we have employed the commercially available kit Quant-iT™ PicoGreen™ dsDNA Assay (ThermoFisher) to evaluate cellular proliferation on dKECM membranes, pKECM substrates and spheroids. When bound to dsDNA, PicoGreen has a maximum fluorescence enhancement, with little or no interference by ECM proteins produced by the cells. Briefly, all the cell-containing substrates were washed with DPBS, immersed in Milli-Q water and frozen at -80 °C. In this process, cells are lysed by osmotic shock. The resulting supernatant was used for the assay. The fluorescence of each specimen was measured by incubating samples with Picogreen for 10 min, according to manufacturer instructions. Fluorescence was measured using a microplate reader at an excitation wavelength of 485 nm, and an emission wavelength of 528 nm. The DNA concentration for each sample was calculated using a standard curve.

#### II-2.2.3.4 *Total protein synthesis quantification*

Total protein produced by cultured cells can be performed as a complementary measurement to their proliferative capacity. It can also be used as a background measurement for other assays dependent on protein concentration. Although this assay cannot quantify the type of proteins produced, it can give a first insight on differentiative stage of the seeded cells together with other complementary assays. There are several methods for quantifying proteins, which usually work within a high detection range. Herein, we employed a microBCA™ commercially available kit for quantifying lower amounts of intracellular proteins.[81] The amount of protein is determined by their ability to reduce $Cu^{2+}$ to $Cu^{1+}$ in an alkaline

environment, which then reacts with bicinchoninic acid (BCA) creating a purple color. This change in color can be detected on a microplate reader. Protein quantification was performed on hRPCs and HK-2 cells seeded on dKECM membranes. Using the same supernatants as previously described for DNA quantification, total protein content was quantified by incubating samples with BCA compound at 37 °C, according to the manufacturer's instructions. After 2 h of sample incubation with the substrate, absorbance was measured at 562 nm in a microplate reader. The concentration of total protein in the samples was calculated using a standard curve of Bovine Serum Albumin.

#### II-2.2.3.5 *Cellular morphology and distribution*

The morphology adopted by cells in response to different environments and/or biomaterials is extremely important for the validation of the developed biomaterial structures. These changes can be used to predict the phenotypic impact of different biomaterials or compounds.[82] Additionally, cell distribution analysis can give useful insights on the monolayer of cells, which is important for the functionality of tubular models.[83] In this way, we have studied the distribution and morphology on HK-2 cells and hRPCs seeded on dKECM-derived electrospun meshes, particulate matrix and bioinks by SEM and IHC.

In order to evaluate the cellular adhesion on the electrospun meshes, after 1, 3 and 7 days of cell culture membranes were removed from the inserts, washed with PBS and fixed in with 2.5% (v/v) of a glutaraldehyde solution (VWR) for 1 h. After this, they were washed again and dehydrated through an alcohol series before being treated with 1,1,1,3,3,3-Hexamethyldisilazane (HMDS). As for microstructure analysis of the cellular adhesion onto different quantities of pKECM, after 7 days of culture, constructs were washed with DPBS and fixed in 2.5 % (v/v) glutaraldehyde for 1 h at 4 °C. After the fixation step, they were washed again and dehydrated through a gradient of ethanol concentrations. All samples were sputter coated with gold prior to analysis and micrographs were obtained by scanning electron microscopy (SEM, JSM-6010 LV, JEOL). For the histological analysis of the distribution of the cells on the particulate matrix after 7 days, constructs were fixed in 10 % neutral buffered formalin, and embedded in OCT compound for cryosectioning. H&E and MT stainings were performed on the constructs as previously described in section II-2.1.2.3. Staining intensity and cell distribution were observed by light microscopy (DM750, Leica).

### II-2.2.4. Evaluation of cellular phenotype

Evaluating cell phenotype changes a very important assay in stem cell biology. Understanding what is the main stimulus behind phenotype change enables studying the effect of our biomaterial substrates and should also improve our understanding of stem cell differentiation towards a specific phenotype for the purpose of therapeutic applications.[84] Herein, we will describe several methods that were used to evaluate specific proteins or genes, which enabled us to evaluate the therapeutic potential of the produced substrates and/or culture methodology.

#### II-2.2.4.1 *Flow cytometry characterization*

Flow cytometry (FC) is a technique that allows for the characterization of a population of cells or particles. This laser-based technology is able to characterize different cell types in a heterogeneous population as well as their cellular size and volume. Basically, cells are resuspended and stained with fluorescent antibodies. When the cell suspension is introduced into the equipment, it flows through a small nozzle, causing the cells to pass through a laser beam one at a time. The light scattered by the cells or particles as well as the emitted fluorescence of the positively stained cells is detected as they pass through the laser beam, which is then translated into a dot plot for further analysis.[85] In this work, cultures were checked for simultaneous expression of CD133 and CD24 at different passages, according to previously published methods for characterizing hRPCs.[64] Briefly, cells were washed with PBS containing 0.5 % BSA and blocking was performed with FcR Blocking Reagent (Miltenyi Biotec). Primary antibodies anti-CD133/2 (Miltenyi Biotec) and anti-CD24 (Santa Cruz) were incubated for 15 min along with respective isotypes. Secondary antibodies added and incubated for 15 min in the dark. A total of 4 $\times$ $10^4$ events for each sample were acquired. Dead cells were excluded by propidium iodide positive staining (Miltenyi Biotec). Only populations expressing $\geq$ 90 % CD133+CD24+ cells were used on this study.

#### II-2.2.4.2 *Immunofluorescence of phenotypic markers*

To perform immunocytochemistry, dKECM membranes, pKECM, spheroids and bioinks were fixed at the end of culture time with 10 % neutral buffered formalin and kept at 4 °C until further use. A permeabilization step was performed for intracellular proteins by soaking substrates in 0.5 % TWEEN®

20 for 30 min. After this, the blocking step was performed with 3 % BSA for another 30 min. Primary antibodies were diluted in 3 % BSA and incubated overnight at 4 °C (Table II-1). Secondary antibodies Alexa Fluor 488 or 594 (1:500, Alfagene) were diluted in PBS and incubated for 1 h at RT in the dark. When required, DAPI (1:1000, Sigma Aldrich) and Phalloidin (1:200, Alfagene) were incubated along with the secondary antibody. After several rinses in PBS, constructs were analyzed under Leica confocal microscope (Leica, Wetzlar, Germany). Images were recorded digitally and further processed using LASX software (Leica).

Immunohistochemistry was also performed after the fixation step. Briefly, spheroids were embedded in Histogel™ (ThermoFisher) before being processed and embedded in paraffin for sectioning. 5 µm thick sections were stained with Hematoxylin & Eosin (H&E) or deparaffinized and rehydrated to perform immunofluorescence. A blocking step was performed with 3 % BSA and primary antibodies were incubated for 1 h at RT in 0.5 % TWEEN® 20. Secondary antibodies Alexa Fluor 488 or 594 were incubated among with DAPI and Phalloidin for 1 h in the dark. After several rinses in PBS, slides were mounted with VECTASHIELD® and analyzed under a confocal microscope.

Table II-1 – Antibodies and concentrations used for phenotypic markers analysis of the produced substrates.

| Antibody | Concentration | Antibody | Concentration |
|---|---|---|---|
| *Zona Occludens-1 (ZO-1)* | 1:100 | *Na/Cl co-transporter (NCC)* | 1:25 |
| *Sodium-dependent glucose transporter 2 (SGLT2)* | 1:30 | *Paired box gene 2 (PAX2)* | 1:100 |
| *Aquaporin-1 (AQP-1)* | 1:100 | *Nephrin 1 (NPHS1)* | 1:200 |
| *Chloride channel Ka (CLC-NKA)* | 1:25 | *CD133* | 1:2.5 |
| *Von Willebrand Factor (vWF)* | 1:100 | *Tamm–Horsfall protein (THP)* | 1:25 |
| *Synaptopodin (SYNPO)* | 1:10 | *Podocin (NPHS2)* | 1:65 |

#### II-2.2.4.3 *Real-time quantitative polymerase chain reaction (RT-PCR)*

Polymerase chain reaction, or PCR, is a widely used technique in molecular biology. It allows amplifying a small amount of DNA in several cycles, enabling detailed studies of gene expression. First, the RNA has to be isolated and transcribed to cDNA by using reverse transcription. After that, the cDNA

enters a series of temperature cycles which enable denaturation, separating the two cDNA chains, annealing of the primers and amplification by the DNA polymerase. Using real-time PCR, we are able to monitor the results during the PCR, as a fluorescent signal is emitted every time there is amplification.[86] There are two major methodologies for the detection of amplification in real-time PCR, being the first non-specific fluorescent dyes that intercalate with any double-stranded DNA (e.g. SYBR Green) and the second sequence-specific DNA probes consisting of oligonucleotides that are labelled with a fluorescent reporter (Taqman probes). Herein, we have used Taqman technology as it detects specific amplification products only. For that, total RNA was extracted using RNeasy Microkit (Qiagen) and quantified using a Nanodrop spectrophotometer (ThermoFisher Scientific). For the spheroid's studies, after predefined periods of differentiation, 50 spheroids for each condition were collected, centrifuged, trypsinzed and frozen until analysis. For the studies on dKECM membranes, after 7, 14 and 21 days of culture, membranes in monoculture or in co-culture systems were removed from the inserts and frozen until analysis. After, the cell pellets and dKECM membranes were thaw and resuspended in buffer RTL (composing the kit) containing β-mercaptoethanol for efficient cell lysis. For the spheroids, RNA corresponding to the same number of cells per condition was used. In the membranes work, as it was not possible to make an effective count of the number of cells, 52 ng of RNA per condition were used. After, RNA was retrotranscribed using TaqMan™ Reverse Transcription Reagents (ThermoFisher) following manufacturer's instructions. TaqMan RT-PCR was performed using a 7900HT Real Time PCR System (Applied Biosystems).[87, 88] Paired box2 (*PAX2*), Octamer-binding transcription factor 4 (*OCT4*), Wilms tumor 1 (*WT1*), Synaptopodin (*SYNPO*) and Nephrin1 (*NPHS1*) quantification were performed for spheroids. Na/K/Cl co-transporter (*SLC12A1*), amino acid transport protein (*SLC3A1*), γ-glutamyltranspeptidase (*GGT1*) and Na/H exchanger (*SLC9A3*) quantification were performed for hRPC-seeded dKECM membranes. Commercially available Assay on Demand kits (Applied Biosystems) were used. Fold expression (FE) was determined using the following equation:

$$Fold\ Expression\ (FE) = 2^{-\Delta\Delta Ct} \qquad \text{Equation 4}$$

where ΔCt = Ct gene of interest – Ct housekeeping gene, glyceraldehyde-3-phosphate dehydrogenase (GAPDH), and ΔΔCt = Ct sample of interest – Ct control sample, which was considered the gene expression level at the seeding day.

### II-2.2.5. Functionality Assessment

After the confirmation of cell phenotype changes, it is important to measure if differentiated cells are performing their physiological function. Herein, the function of tubular cells was measured by confirming the monolayer formation and the reabsorption of albumin. Nephrotoxicity measurements were also performed. These assays allow obtaining a deeper understanding on the behavior of cells and the likely utilization of the dKECM membrane as a bilayer model of the tubular filtration barrier.

#### II-2.2.5.1 *Transepithelial electrical resistance measurement*

Studying transepithelial electrical resistance (TEER) allows for the functional characterization of a monolayer of epithelial cells. The paracellular transport *in vivo* is mediated along the tubular cells' tight junctions and the lateral intercellular spaces. Thus, this measurement is important for the validation of *in vitro* models, especially when modeling leaky epithelia such as the proximal tubule.[89] Herein, we determined the barrier properties of the HK-2 monolayers cultured on dKECM membranes. TEER was measured over a 14-day period using a Millicell® ERS-2 Volt-Ohm Meter (MA, USA) with the same sets of inserts over time in PBS. Values were multiplied by the surface area of the membrane occupied by cells.

#### II-2.2.5.2 *Paracellular permeability assay*

The study of paracellular permeability is complementary to the TEER measurement. It allows studying if the monolayer of epithelial cells is not leaking and performing its natural barrier function. For that, some molecules such as inulin can be used, as it is not actively taken up by tubular epithelial cells.[90] Herein, we studied inulin leakage on the bilayer model composed of RPTECs and HUVECs cultured on the dKECM membranes. Thus, at day 7 of co-culture, 400 µL of media containing 25 µg $mL^{-1}$ of fluorescein isothiocyanate (FITC)-conjugated inulin was applied to the top compartment, while 600 µL of medium was applied to the bottom compartment. Cells were incubated at 37 °C for 5 hours. Every hour, samples were drawn from both compartments and fluorescence intensity was measured in a microplate reader (excitation: 485/25 nm; emission: 530/25 nm) to quantify the passage of inulin through the monolayer.

#### II-2.2.5.3 *Albumin reabsorption quantification*

Serum albumin is commonly found protein in blood that helps clearing uremic toxins. When it reaches the kidneys, some is filtered through the glomeruli and reabsorbed by the proximal tubule cells by receptor-mediated endocytosis.[91] When the kidney is dysfunctional, this function becomes compromised. Thus, albumin reabsorption is a relevant indicator of a functional layer of tubular epithelial cells. Herein, we studied albumin reabsorption on the bilayer model composed of RPTECs and HUVECs cultured on the dKECM membranes. FITC-conjugated human serum albumin (HSA) was applied to the top compartment at a concentration of 40 μg $mL^{-1}$ and the initial fluorescence was measured in the total volume of the well. After 5 hours, inserts were drawn from the wells and the remaining concentration of HSA in the well was measured by fluorescence intensity in a microplate reader (excitation: 485/25 nm; emission: 530/25 nm).

#### II-2.2.5.4 *Nephrotoxicity assessment*

One of the major goals in developing a reliable *in vitro* model of the tubule is to have a consistent response to drugs which are known to induce nephrotoxicity. In this way, it will be possible to predict drug toxicity in humans with *in vitro* tests. Cisplatin is a known nephrotoxic drug that accumulates in the renal parenchyma by active transport into proximal tubular cells.[92, 93] Thus, we evaluated its effect on the bilayer model as a functionality test. Cisplatin was applied to the top compartment of confluent monocultures of hRPTEC and to the co-cultures with HUVEC. 0, 50, 100 and 150 μM of cisplatin in REGM complete medium were added to the inserts after 7 days of bilayer culture. The range of values was selected according to previously published papers which also performed nephrotoxicity assays, with the main aim of evaluating cell response to the increasing concentration of cisplatin.[94, 95] Cellular metabolic activity was assessed by alamarBlue as previously described and presented as a percentage of control values (the inserts that were subjected to 0 μM of cisplatin). To further evaluate the effect of cisplatin, live/dead assay and immunofluorescence of DAPI and Phalloidin were also performed, as previously described.

## II-3. REFERENCES

1. Badylak SF, Freytes DO, Gilbert TW (2015) Reprint of: Extracellular matrix as a biological scaffold

material: Structure and function. Acta Biomater 23:S17–S26. https://doi.org/10.1016/j.actbio.2015.07.016
2. Campbell TD, Landeen LK, Naughton BA, et al (1996) WO/1996/008213 - Three-dimensional human cell cultures on cardiac valve frameworks and their uses
3. Gilbert TW, Sellaro TL, Badylak SF (2006) Decellularization of tissues and organs. Biomaterials 27:3675–3683. https://doi.org/10.1016/j.biomaterials.2006.02.014
4. Gilpin A, Yang Y (2017) Decellularization Strategies for Regenerative Medicine: From Processing Techniques to Applications. Biomed Res Int 2017:9831534. https://doi.org/10.1155/2017/9831534
5. Nakayama KH, Batchelder CA, Lee CI, Tarantal AF (2010) Decellularized rhesus monkey kidney as a three-dimensional scaffold for renal tissue engineering. Tissue Eng - Part A 16:2207–2216. https://doi.org/10.1089/ten.tea.2009.0602
6. He M, Callanan A, Lagaras K, et al (2017) Optimization of SDS exposure on preservation of ECM characteristics in whole organ decellularization of rat kidneys. J Biomed Mater Res - Part B Appl Biomater 105:1352–1360. https://doi.org/10.1002/jbm.b.33668
7. Guan Y, Liu S, Liu Y, et al (2015) Porcine kidneys as a source of ECM scaffold for kidney regeneration. Mater Sci Eng C 56:451–456. https://doi.org/10.1016/j.msec.2015.07.007
8. Orlando G, Farney AC, Iskandar SS, et al (2012) Production and implantation of renal extracellular matrix scaffolds from porcine kidneys as a platform for renal bioengineering investigations. Ann Surg 256:363–370. https://doi.org/10.1097/SLA.0b013e31825a02ab
9. Song JJ, Guyette JP, Gilpin SE, et al (2013) Regeneration and experimental orthotopic transplantation of a bioengineered kidney. Nat Med 19:646–51. https://doi.org/10.1038/nm.3154
10. Caralt M, Uzarski JS, Iacob S, et al (2015) Optimization and critical evaluation of decellularization strategies to develop renal extracellular matrix scaffolds as biological templates for organ engineering and transplantation. Am J Transplant 15:64–75. https://doi.org/10.1111/ajt.12999
11. Cooper DKC, Koren E, Oriol R (1994) Oligosaccharides and Discordant Xenotransplantation. Immunol Rev 141:31–58. https://doi.org/10.1111/j.1600-065X.1994.tb00871.x
12. Daly KA, Stewart-Akers AM, Hara H, et al (2009) Effect of the αgal epitope on the response to small intestinal submucosa extracellular matrix in a nonhuman primate model. Tissue Eng - Part A 15:3877–3888. https://doi.org/10.1089/ten.tea.2009.0089
13. Kim H, Park MN, Kim J, et al (2019) Characterization of cornea-specific bioink: high transparency, improved in vivo safety. J Tissue Eng 10:2041731418823382. https://doi.org/10.1177/2041731418823382
14. Taylor DA, Sampaio LC, Ferdous Z, et al (2018) Decellularized matrices in regenerative medicine. Acta Biomater 74:74–89. https://doi.org/10.1016/j.actbio.2018.04.044
15. Gurlek AC, Sevinc B, Bayrak E, Erisken C (2017) Synthesis and characterization of polycaprolactone for anterior cruciate ligament regeneration. Mater Sci Eng C 71:820–826. https://doi.org/10.1016/j.msec.2016.10.071
16. Dwivedi R, Kumar S, Pandey R, et al (2020) Polycaprolactone as biomaterial for bone scaffolds: Review of literature. J Oral Biol Craniofacial Res 10:381–388. https://doi.org/10.1016/j.jobcr.2019.10.003
17. Guarino V, Gentile G, Sorrentino L, Ambrosio L (2017) Polycaprolactone: Synthesis, Properties, and Applications. In: Encyclopedia of Polymer Science and Technology, 4th ed. John Wiley & Sons
18. Shen Z, Wang J (2011) Biological denitrification using cross-linked starch/PCL blends as solid carbon source and biofilm carrier. Bioresour Technol 102:8835–8838. https://doi.org/10.1016/j.biortech.2011.06.090
19. Cooper A, Bhattarai N, Zhang M (2011) Fabrication and cellular compatibility of aligned chitosan-

PCL fibers for nerve tissue regeneration. Carbohydr Polym 85:149–156. https://doi.org/10.1016/j.carbpol.2011.02.008
20. Zhang Y, Ouyang H, Lim CT, et al (2005) Electrospinning of gelatin fibers and gelatin/PCL composite fibrous scaffolds. J Biomed Mater Res 72B:156–165. https://doi.org/10.1002/jbm.b.30128
21. Osathanon T, Chanjavanakul P, Kongdecha P, et al (2017) Polycaprolactone-Based Biomaterials for Guided Tissue Regeneration Membrane. In: Periodontitis - A Useful Reference. IntechOpen, pp 171–188
22. Hong S, Kim G (2010) Electrospun micro/nanofibrous conduits composed of poly(ε-caprolactone) and small intestine submucosa powder for nerve tissue regeneration. J Biomed Mater Res Part B Appl Biomater 94:421–428. https://doi.org/10.1002/jbm.b.31670
23. Gao S, Guo W, Chen M, et al (2017) Fabrication and characterization of electrospun nanofibers composed of decellularized meniscus extracellular matrix and polycaprolactone for meniscus tissue engineering. J Mater Chem B 5:2273–2285. https://doi.org/10.1039/c6tb03299k
24. Pati F, Jang J, Ha DH, et al (2014) Printing three-dimensional tissue analogues with decellularized extracellular matrix bioink. Nat Commun 5:3935. https://doi.org/10.1038/ncomms4935
25. Doshi J, Reneker DH (1995) Electrospinning process and applications of electrospun fibers. J Electrostat 35:151–160. https://doi.org/10.1016/0304-3886(95)00041-8
26. Abrahamson DR, Leardkamolkarn V (1991) Development of kidney tubular basement membranes. Kidney Int 39:382–393. https://doi.org/10.1038/KI.1991.50
27. Choudhury D, Tun HW, Wang T, Naing MW (2018) Organ-Derived Decellularized Extracellular Matrix: A Game Changer for Bioink Manufacturing? Trends Biotechnol 36:787–805. https://doi.org/10.1016/j.tibtech.2018.03.003
28. Crapo PM, Gilbert TW, Badylak SF (2011) An overview of tissue and whole organ decellularization processes. Biomaterials 32:3233–3243. https://doi.org/10.1016/j.biomaterials.2011.01.057
29. Baiguera S, Del Gaudio C, Lucatelli E, et al (2014) Electrospun gelatin scaffolds incorporating rat decellularized brain extracellular matrix for neural tissue engineering. Biomaterials 35:1205–1214. https://doi.org/10.1016/j.biomaterials.2013.10.060
30. Yin H, Wang Y, Sun Z, et al (2016) Induction of mesenchymal stem cell chondrogenic differentiation and functional cartilage microtissue formation for in vivo cartilage regeneration by cartilage extracellular matrix-derived particles. Acta Biomater 33:96–109. https://doi.org/10.1016/j.actbio.2016.01.024
31. Kruegel J, Miosge N (2010) Basement membrane components are key players in specialized extracellular matrices. Cell Mol Life Sci 67:2879–2895. https://doi.org/10.1007/s00018-010-0367-x
32. Pouliot RA, Link PA, Mikhaiel NS, et al (2016) Development and characterization of a naturally derived lung extracellular matrix hydrogel. J Biomed Mater Res - Part A 104:1922–1935. https://doi.org/10.1002/jbm.a.35726
33. Deegan DB, Zimmerman C, Skardal A, et al (2016) Stiffness of hyaluronic acid gels containing liver extracellular matrix supports human hepatocyte function and alters cell morphology. J Mech Behav Biomed Mater 55:87–103. https://doi.org/10.1016/j.jmbbm.2015.10.016
34. Lu Q, Li M, Zou Y, Cao T (2014) Delivery of basic fibroblast growth factors from heparinized decellularized adipose tissue stimulates potent de novo adipogenesis. J Control Release 174:43–50. https://doi.org/10.1016/j.jconrel.2013.11.007
35. Beck EC, Barragan M, Tadros MH, et al (2016) Approaching the compressive modulus of articular cartilage with a decellularized cartilage-based hydrogel. Acta Biomater 38:94–105. https://doi.org/10.1016/j.actbio.2016.04.019
36. Sullivan DC, Mirmalek-Sani S-H, Deegan DB, et al (2012) Decellularization methods of porcine

kidneys for whole organ engineering using a high-throughput system. Biomaterials 33:7756–7764. https://doi.org/10.1016/j.biomaterials.2012.07.023
37. Su J, Satchell SC, Shah RN, Wertheim JA (2018) Kidney decellularized extracellular matrix hydrogels: Rheological characterization and human glomerular endothelial cell response to encapsulation. J Biomed Mater Res - Part A 106A:2448–2462. https://doi.org/10.1002/jbm.a.36439
38. Ross M, Pawlina W (2010) Histology: A Text and Atlas, with Correlated Cell and Molecular Biology, 8th ed. Lippincott Williams & Wilkins
39. Nagao RJ, Xu J, Luo P, et al (2016) Decellularized Human Kidney Cortex Hydrogels Enhance Kidney Microvascular Endothelial Cell Maturation and Quiescence. Tissue Eng Part A 22:1140–1150. https://doi.org/10.1089/ten.TEA.2016.0213
40. Xue A, Niu G, Chen Y, et al (2018) Recellularization of well-preserved decellularized kidney scaffold using adipose tissue-derived stem cells. J Biomed Mater Res - Part A 106:805–814. https://doi.org/10.1002/jbm.a.36279
41. Shakes DC, Miller DM, Nonet ML (2012) Immunofluorescence Microscopy. In: Methods in Cell Biology, 1st ed. Academic Press, pp 35–66
42. Johnson TD, Hill RC, Dzieciatkowska M, et al (2016) Quantification of decellularized human myocardial matrix: A comparison of six patients. Proteomics - Clin Appl 10:75–83. https://doi.org/10.1002/prca.201500048
43. Bradford MM (1976) A rapid and sensitive method for the quantitation of microgram quantities of protein utilizing the principle of protein-dye binding. Anal Biochem 72:248–254. https://doi.org/10.1016/0003-2697(76)90527-3
44. Gaspari M, Cuda G (2011) Nano LC-MS/MS: a robust setup for proteomic analysis. Methods Mol Biol 790:115–26. https://doi.org/10.1007/978-1-61779-319-6_9
45. Hughes CS, Moggridge S, Müller T, et al (2019) Single-pot, solid-phase-enhanced sample preparation for proteomics experiments. Nat Protoc 14:68–85. https://doi.org/10.1038/s41596-018-0082-x
46. Carbon S, Ireland A, Mungall CJ, et al (2009) AmiGO: Online access to ontology and annotation data. Bioinformatics 25:288–289. https://doi.org/10.1093/bioinformatics/btn615
47. Carbon S, Douglass E, Dunn N, et al (2019) The Gene Ontology Resource: 20 years and still GOing strong. Nucleic Acids Res 47:D330–D338. https://doi.org/10.1093/nar/gky1055
48. Perez-Riverol Y, Csordas A, Bai J, et al (2019) The PRIDE database and related tools and resources in 2019: Improving support for quantification data. Nucleic Acids Res 47:D442–D450. https://doi.org/10.1093/nar/gky1106
49. Reimer L (1998) Scanning Electron Microscopy: Physics of Imaging Formation and Microanalysis, 2nd ed. Springer-Verlag Berlin Heidelberg
50. Davis JR (2004) Tensile testing, 2nd ed. ASM International
51. Dutta A (2017) Fourier Transform Infrared Spectroscopy. Spectrosc Methods Nanomater Charact 73–93. https://doi.org/10.1016/B978-0-323-46140-5.00004-2
52. Griffiths PR, De Haseth JA (2007) Fourier Transform Infrared Spectrometry, 2nd ed. Wiley-Interscience
53. Baker MJ, Trevisan J, Bassan P, et al (2014) Using Fourier transform IR spectroscopy to analyze biological materials. Nat Protoc 9:1771–1791. https://doi.org/10.1038/nprot.2014.110
54. Oberg KA, Fink AL (1998) A new attenuated total reflectance fourier transform infrared spectroscopy method for the study of proteins in solution. Anal Biochem 256:92–106. https://doi.org/10.1006/abio.1997.2486
55. Bershtein VA., Egorov VM, Leib G V, et al (1994) Differential Scanning Calorimetry of Polymers: Physics, Chemistry, Analysis, Technology. Ellis Horwood Ltd

56. Chiu M, Prenner E (2011) Differential scanning calorimetry: An invaluable tool for a detailed thermodynamic characterization of macromolecules and their interactions. J Pharm Bioallied Sci 3:39–59. https://doi.org/10.4103/0975-7406.76463
57. Salehi M, Naseri-Nosar M, Ghorbani S, et al (2017) Wet-electrospun PCL/PLLA Blend Scaffolds: Effects of Versatile Coagulation Baths on Physicochemical and Biological Properties of the Scaffolds. 2:1–7. https://doi.org/10.22037/rrr.v2i1.15431
58. Prozialeck WC, Edwards JR, Lamar PC, Smith CS (2006) Epithelial barrier characteristics and expression of cell adhesion molecules in proximal tubule-derived cell lines commonly used for in vitro toxicity studies. Toxicol Vitr 20:942–953. https://doi.org/10.1016/j.tiv.2005.11.006
59. Azevedo H, Reis R (2005) Understanding the Enzymatic Degradation of Biodegradable Polymers and Strategies to Control Their Degradation Rate. In: Biodegradable Systems in Tissue Engineering and Regenerative Medicine. CRC Press, pp 177–201
60. McLemore R (2011) Rheological properties of injectable biomaterials. In: Injectable Biomaterials: Science and Applications. Woodhead Publishing, pp 46–60
61. Ryan MJ, Johnson G, Kirk J, et al (1994) HK-2: An immortalized proximal tubule epithelial cell line from normal adult human kidney. Kidney Int 45:48–57. https://doi.org/10.1038/ki.1994.6
62. Lazzeri E, Crescioli C, Ronconi E, et al (2007) Regenerative potential of embryonic renal multipotent progenitors in acute renal failure. J Am Soc Nephrol 18:3128–3138. https://doi.org/10.1681/ASN.2007020210
63. Sagrinati C, Netti GS, Mazzinghi B, et al (2006) Isolation and Characterization of Multipotent Progenitor Cells from the Bowman's Capsule of Adult Human Kidneys. J Am Soc Nephrol 17:2443–2456. https://doi.org/10.1681/ASN.2006010089
64. Angelotti ML, Ronconi E, Ballerini L, et al (2012) Characterization of Renal Progenitors Committed Toward Tubular Lineage and Their Regenerative Potential in Renal Tubular Injury. Stem Cells 30:1714–1725. https://doi.org/10.1002/stem.1130
65. Ronconi E, Sagrinati C, Angelotti ML, et al (2009) Regeneration of glomerular podocytes by human renal progenitors. J Am Soc Nephrol 20:322–332. https://doi.org/10.1681/ASN.2008070709
66. Lasagni L, Angelotti ML, Ronconi E, et al (2015) Podocyte Regeneration Driven by Renal Progenitors Determines Glomerular Disease Remission and Can Be Pharmacologically Enhanced. Stem Cell Reports 5:248–263. https://doi.org/10.1016/j.stemcr.2015.07.003
67. Jiménez N, Krouwer VJD, Post JA (2013) A new, rapid and reproducible method to obtain high quality endothelium in vitro. Cytotechnology 65:1–14. https://doi.org/10.1007/s10616-012-9459-9
68. Jaffe EA, Nachman RL, Becker CG, Minick CR (1973) Culture of human endothelial cells derived from umbilical veins. Identification by morphologic and immunologic criteria. J Clin Invest 52:2745–2756. https://doi.org/10.1172/JCI107470
69. Ades EW, Candal FJ, Swerlick RA, et al (1992) HMEC-1: Establishment of an immortalized human microvascular endothelial cell line. J Invest Dermatol 99:683–690. https://doi.org/10.1111/1523-1747.ep12613748
70. Bartosh TJ, Ylöstalo JH, Mohammadipoor A, et al (2010) Aggregation of human mesenchymal stromal cells (MSCs) into 3D spheroids enhances their antiinflammatory properties. Proc Natl Acad Sci U S A 107:13724–13729. https://doi.org/10.1073/pnas.1008117107
71. Nishikawa M, Kimura H, Yanagawa N, et al (2018) An optimal serum-free defined condition for in vitro culture of kidney organoids. Biochem Biophys Res Commun 501:996–1002. https://doi.org/10.1016/j.bbrc.2018.05.098
72. Taguchi A, Kaku Y, Ohmori T, et al (2014) Redefining the in vivo origin of metanephric nephron progenitors enables generation of complex kidney structures from pluripotent stem cells. Cell Stem Cell 14:53–67. https://doi.org/10.1016/j.stem.2013.11.010

73. Takasato M, Er PX, Chiu HS, Little MH (2016) Generation of kidney organoids from human pluripotent stem cells. Nat Protoc 11:1681–1692. https://doi.org/10.1038/nprot.2016.098
74. Mendes BB, Gómez-Florit M, Hamilton AG, et al (2020) Human platelet lysate-based nanocomposite bioink for bioprinting hierarchical fibrillar structures. Biofabrication 12:015012. https://doi.org/10.1088/1758-5090/ab33e8
75. Riss TL, Moravec RA, Niles AL, et al (2013) Cell Viability Assays. In: Assay Guidance Manual [Internet]. Bethesda (MD): Eli Lilly & Company and the National Center for Advancing Translational Sciences, p eBook
76. Berridge M V., Herst PM, Tan AS (2005) Tetrazolium dyes as tools in cell biology: New insights into their cellular reduction. Biotechnol Annu Rev 11:127–152. https://doi.org/10.1016/S1387-2656(05)11004-7
77. Rampersad SN (2012) Multiple applications of alamar blue as an indicator of metabolic function and cellular health in cell viability bioassays. Sensors (Basel) 12:12347–12360. https://doi.org/10.3390/s120912347
78. Green PS, Perez EJ, Calloway T, Simpkins JW (2000) Estradiol attenuation of β-amyloid-induced toxicity: A comparison of MTT and calcein AM assays. J Neurocytol 29:419–423. https://doi.org/10.1023/A:1007173509470
79. Schneider CA, Rasband WS, Eliceiri KW (2012) NIH Image to ImageJ: 25 years of Image Analysis. Nat Methods 9:671–675. https://doi.org/10.1038/nmeth.2089
80. Quent VMC, Loessner D, Friis T, et al (2010) Discrepancies between metabolic activity and DNA content as tool to assess cell proliferation in cancer research. J Cell Mol Med 14:1003–1013. https://doi.org/10.1111/j.1582-4934.2010.01013.x
81. Smith PK, Hermanson GT, Gartner FH, et al (1985) Measurement of Protein Using Bicinchoninic Acid. Anal Biochem 150:76–85. https://doi.org/10.1016/0003-2697(85)90442-7
82. Nassiri I, McCall MN (2018) Systematic exploration of cell morphological phenotypes associated with a transcriptomic query. Nucleic Acids Res 46:e116. https://doi.org/10.1093/nar/gky626
83. Sobreiro-Almeida R, Fonseca DR, Neves NM (2019) Extracellular matrix electrospun membranes for mimicking natural renal filtration barriers. Mater Sci Eng C 103:109866. https://doi.org/10.1016/J.MSEC.2019.109866
84. Tosh D, Slack JMW (2002) How cells change their phenotype. Nat Rev Mol Cell Biol 3:187–194. https://doi.org/10.1038/nrm761
85. Adan A, Alizada G, Kiraz Y, et al (2017) Flow cytometry: basic principles and applications. Crit Rev Biotechnol 37:163–176. https://doi.org/10.3109/07388551.2015.1128876
86. Arya M, Shergill IS, Williamson M, et al (2005) Basic principles of real-time quantitative PCR. Expert Rev Mol Diagn 5:209–219. https://doi.org/10.1586/14737159.5.2.209
87. Lazzeri E, Ronconi E, Angelotti ML, et al (2015) Human Urine-Derived Renal Progenitors for Personalized Modeling of Genetic Kidney Disorders. J Am Soc Nephrol 26:1961–1974. https://doi.org/10.1681/ASN.2014010057
88. Sobreiro-Almeida R, Elena Melica M, Lasagni L, et al (2020) Co-cultures of renal progenitors and endothelial cells on kidney decellularized matrices replicate the renal tubular environment in vitro. Acta Physiol 230:e13491. https://doi.org/10.1111/apha.13491
89. Aydin S, Signorelli S, Lechleitner T, et al (2008) Influence of microvascular endothelial cells on transcriptional regulation of proximal tubular epithelial cells. Am J Physiol Physiol 294:C543–C554. https://doi.org/10.1152/ajpcell.00307.2007
90. Brakeman P, Miao S, Cheng J, et al (2016) A modular microfluidic bioreactor with improved throughput for evaluation of polarized renal epithelial cells. Biomicrofluidics 10:064106. https://doi.org/10.1063/1.4966986
91. Tojo A, Kinugasa S (2012) Mechanisms of glomerular albumin filtration and tubular reabsorption.

Int J Nephrol 2012:481520. https://doi.org/10.1155/2012/481520
92. Ishida S, Lee J, Thiele DJ, Herskowitz I (2002) Uptake of the anticancer drug cisplatin mediated by the copper transporter Ctr1 in yeast and mammals. Proc Natl Acad Sci 99:14298–14302. https://doi.org/10.1073/pnas.162491399
93. Ludwig T, Riethmüller C, Gekle M, et al (2004) Nephrotoxicity of platinum complexes is related to basolateral organic cation transport. Kidney Int 66:196–202. https://doi.org/10.1111/j.1523-1755.2004.00720.x
94. Czerniecki SM, Cruz NM, Harder JL, et al (2018) High-Throughput Screening Enhances Kidney Organoid Differentiation from Human Pluripotent Stem Cells and Enables Automated Multidimensional Phenotyping. Cell Stem Cell 22:929-940.e4. https://doi.org/10.1016/j.stem.2018.04.022
95. Jang K-J, Mehr AP, Hamilton GA, et al (2013) Human kidney proximal tubule-on-a-chip for drug transport and nephrotoxicity assessment. Integr Biol 5:1119–1129. https://doi.org/10.1039/c3ib40049b

# SECTION 3

# DEVELOPMENT OF KIDNEY TISSUE MODEL SYSTEMS

# Chapter III

# Extracellular matrix electrospun membranes for mimicking natural renal filtration barriers

# Chapter III

## Extracellular matrix electrospun membranes for mimicking natural renal filtration barriers [†]


### ABSTRACT

Kidney diseases are recognized as a major health problem, which affect 10 % of the population. Because currently available therapies have many limitations, some tissue engineering strategies have been emerging as promising approaches in this field.

In this work, porcine kidneys were decellularized to obtain decellularized kidney extracellular matrix (dKECM). Our results demonstrate a successful protocol of decellularization characterized by the removal of nucleic acid material and preservation of collagen and glycosaminoglycans. Blends of polycaprolactone (PCL) and dKECM were prepared by electrospinning and characterized. The biological performance of the membranes was tested with a human kidney cell line (HK-2) for 7 days. It was observed that cellular metabolic activity, proliferation and protein content increased with an increase in dKECM concentrations (30, 50 and 70 %). Additionally, the expression of zona occludens-1 was revealed on dKECM-containing membranes but not on pure PCL membranes.

To the best of our knowledge this is the first time that natural extracellular matrix is used to mimic the kidney basement membrane as an *in vitro* model. This could be a valuable tool for regenerative nephrology and may have an impact on the development of kidney advanced therapies in the future.


[†]This chapter is based on the following publication:

**Sobreiro-Almeida, Rita;** Fonseca, Diana R.; Neves, Nuno M. Extracellular matrix electrospun membranes for mimicking natural renal filtration barriers. *Materials Science and Engineering: C*, 103:109866, doi: 10.1016/j.msec.2019.109866, 2019.

## III-1. INTRODUCTION

The extracellular matrix (ECM) is a multifunctional network of molecules produced by resident cells of each tissue. Their specific structure gives the tissues their structural and biochemical support. The ECM is known to play an essential role in tissue development, remodeling and function, being therefore essential for the appropriate environment of the tissues in the human body.[1] It was previously demonstrated that the ECM plays a crucial role in embryonic and fetal development.[2] The ECM is also important in orchestrating complex remodeling functions by interacting with receptors of stem cells driving its proliferation, migration and differentiation.[3–5] The composition of the ECM varies depending on the tissue considered, since different cell types will secrete specific cues for the correct functioning of the tissue and its surrounding microenvironment. However, some molecules are more abundant in the connective tissues, such as collagen type I and IV and a variety of glycosaminoglycans (GAGs).[6]

Tissue engineering strategies have been developed to enable obtaining tissue regeneration and remodeling in the context of various diseases. Several techniques and materials were developed with the purpose of mimicking diverse features of the ECM, including its architecture, structural organization and biochemical cues. However, the complexity of the ECM has proven difficult to be reproduced in its structure and function by synthetic methods. In general, synthetic materials can only mimic the ECM structure by using techniques such as electrospinning [7] or cues by integrating some soluble morphogens [8], which have difficulties in mimicking accurately the properties of the native ECM.

An effective alternative to the use of synthetic-derived scaffolds is using the ECM itself as a biological scaffold material. For that, decellularization techniques have been developed to remove the cellular content of tissues and organs perfusing the vasculature with detergents to decellularize it and further with medium containing cells to repopulate the matrix. This strategy was already performed in several organs, such has the kidney [9] and heart [10] and successfully implanted *in vivo* envisioning whole organ repopulation. Although it is still in its infancy, this is a promising approach for the production of whole transplantable organs, since primary immunogenic factors are in theory fully removed. Decellularized organs were used to extract and process the ECM in order to create detailed architectures adapted to a specific tissue defect.[6] These include engineered soft tissue applications,[11, 12] cartilage [13, 14] or improving vascularization.[15] Different studies already demonstrated the value of renal ECM on modulating cell proliferation and differentiation when cultured on native tissues.[16–19] Also, renal ECM-based scaffolds have been proposed to study the effect of regional specificity of mouse stem cells [20] and hydrogels have been developed to study endothelial cell maturation and quiescence.[15]

Basement membranes are the first fully differentiated ECM-composed structures to appear during embryonic development and are highly preserved during adulthood life.[21] In the kidney, several drugs and their metabolites are absorbed in the proximal tubule and therefore the function of basement membranes is of utmost importance for the excretory function. These metabolites are prone to cause damage to the glomerulus and proximal tubular cells, eventually compromising the renal filtration capacity and clearance of toxins.[22] Ultimately, the accumulation of uremic toxins can give rise to Acute Tubular Necrosis (ATN) and Acute Kidney Injury (AKI), a disease associated with great morbidity and mortality.[23] Therefore, *in vitro* systems capable of replicating the proximal tubule filtration capacity have great interest not only for pharmacological industry as models of disease but also on developing new devices for replacement of the conventional hemo- or peritoneal dialysis treatment modalities. Several researchers have been focused on the development of bioartificial kidneys (BAK) containing specific renal cells to better replicate kidney function.[24–26] One of the most important components of these devices are the membranes, since it is essential that the proximal tubule cells assemble into a monolayer with epithelial functional characteristics. Also, it has already been demonstrated that there is an improved cell performance when renal cells are cultured in contact with extracellular matrix coatings.[27] However, the behavior of renal cells when seeded on membranes having a composition similar to that of the kidney ECM was not previously reported in the literature. Also, to the best of our knowledge, no BAK strategy using components of decellularized ECM was performed, despite being already known that changes in the ECM are liked to cause altered proximal tubule cell behavior. [27]

Nephrons are complex structures composed of linings of epithelial cells, which act as a selective permeable tissue barrier regulating the transport of solutes and ions not only paracellularly, but also across the tubule wall during filtrate reabsorption. This capacity of selective absorption and electrolyte balance in the tubules is mainly dependent on tissue integrity maintained by the coordinated assembly of tight junction (TJ) complexes between epithelial cells.[28] Hence, AKI if often associated with derangements of the tubule cell cytoskeleton, which will impair the filtration capacity and cause a depression on the Glomerular Filtration Rate (GFR), leading to injury.[29] For this reason, mimicking this complex matrix to obtain differentiated monolayers of proximal tubule epithelial cells *in vitro* is an essential step in kidney engineering.

In this work, porcine kidneys were decellularized with the goal of using the obtained ECM to produce electrospun porous membranes. An immortalized proximal tubule renal cell line was used to test its biological activity when cultured on ECM derived membranes in comparison to synthetic ones. Monolayer

formation and epithelial functional characterization was investigated to propose these membranes for developing a realistic *in vitro* kidney model.

## III-2. EXPERIMENTAL

### III-2.1. Decellularization process

Whole porcine kidneys were obtained from a local slaughterhouse and kept at 4 °C before being frozen at −20 °C. Afterwards, they were cut in horizontal sections (Figure III-1) and the renal capsules were removed. Kidney sections were rinsed in cold Milli-Q water and kept in an agitated bath at 100 rpm immersed in a solution of 1 % SDS at 4 °C. The solution was changed twice daily. After the decellularization process was completed, sections were transferred to cold Milli-Q water under the same conditions. The water was changed twice a day for 1 week. Decellularized kidney sections were used immediately for characterization or stored at −80 °C until use.

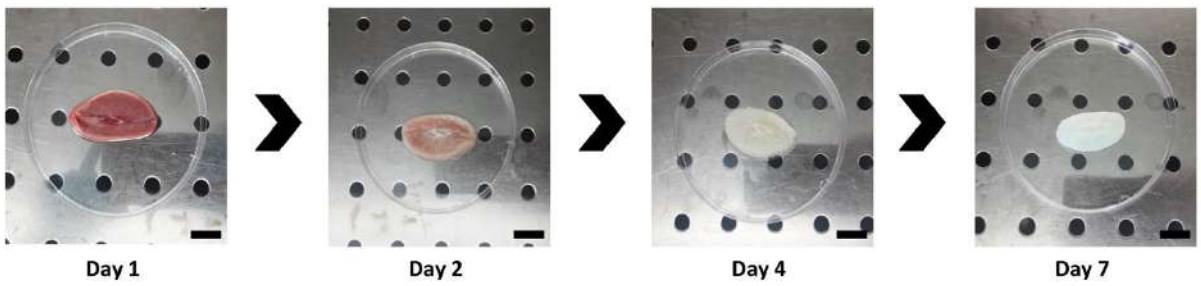


Figure III-1 – Macroscopic evaluation of kidney decellularization. Scale bar: 1.5 cm.

### III-2.2. Characterization of decellularized kidney extracellular matrix (dKECM)

#### III-2.2.1. Assessment of cellular content

DAPI (4′,6-diamidino-2-phenylindole) staining was performed both in native (n = 3) and in decellularized tissue sections (n = 3) to assess if remaining DNA fragments were present on the decellularized sections. Kidney sections were cut into smaller pieces with an 8 mm diameter biopsy punch and immersed in a 10 % neutral buffered formalin solution (Thermo Scientific) for 24 h at room temperature. Pieces of decellularized and native tissues were embedded in paraffin and cut into 5 µm thick sections. These sections were deparaffinized, rehydrated and stained with DAPI (VWR) (diluted 1:10000) for 10 min in the dark. The sections were further analyzed by fluorescence microscopy.

### III-2.2.2. Scanning electron microscopy

To analyze the structure of the decellularized tissue, native and decellularized sections were fixed in 2.5 %(v/v) of glutaraldehyde (VWR) in a buffered PBS solution for 24 h. After removing the residual fixation reagent, samples were dehydrated through a series of ethanol gradient solutions and submitted to critical point drying (Autosamdri- 815, Tousimis) for a 45 min cycle. Samples were further mounted, sputter coated with gold and analyzed by scanning electron microscopy (SEM, JSM-6010 LV, JEOL).

### III-2.2.3. DNA quantification

The DNA content in both native and decellularized tissue was extracted using the DNeasy Blood and Tissue kit (Quiagen) according to manufacturer instructions. Each sample (n = 3) was weighted before digestion of the tissue. To quantify the double stranded DNA concentration on each sample, nanodrop equipment (ThermoScientific) was used.

### III-2.2.4. Collagen content measurement

Acid and pepsin-soluble collagens were quantified using Sircol Collagen Assay Kit (Biocolor) according to manufacturer's instructions. Briefly, kidneys were cut into 8 mm punches with approximately 2 mm thick. Native tissue was kept at −80 °C until quantification and the remaining tissue proceeded to the decellularization process, as above mentioned. The extraction was performed overnight at RT by immersing the tissue in 0.1 mg $mL^{-1}$ of pepsin (Enzymatic) in 0.5 M acetic acid (VWR). Absorbance was measured at 555 nm against reagent blanks and standards. Tissue collagen concentrations were obtained from a collagen I standard curve.

### III-2.2.5. Sulfated glycosaminoglycans (sGAG) content measurement

Glycosaminoglycans were quantified using 1,9-dimethylmethylene blue (DMMB) dye binding assay. Kidneys were cut as described for collagen quantification and were digested in 500 µg $mL^{-1}$ of papain (Sigma) in phosphate buffer overnight at 60 °C under agitation. DMMB dye was added to the ECM digests at a 1:10 ratio of digests to dye. A standard curve was plotted using chondroitin sulphate (Sigma). Absorbance was measured at 525 nm and concentrations were obtained from a standard curve.

## III-2.3. Scaffold fabrication

### III-2.3.1. dKECM processing

Frozen sections of decellularized tissue were freeze-dried and grinded to yield a powder which was stored until use. To remove any residual detergent, dKECM was resuspended on 70% ethanol and vigorously vortexed. The suspension was centrifuged at 12900 rpm for 5 min and fresh ethanol was added to the pellet in order to resuspend and wash again. This procedure was repeated 3 times. Afterwards, the pellet was left to dry and was further lyophilized.

To ensure that dKECM was efficiently digested, the washed powder was added to a solution of 0.01 M of HCl (Laborspirit) at a concentration of 10 mg $mL^{-1}$ and pepsin (Enzymatic) was added at a concentration of 1 mg $mL^{-1}$. The powder was left to digest for 48 h at room temperature. The digested matrix was then neutralized with 10× PBS and 0.1 M NaOH (Enzymatic) in proportions of 1:10 and 1:9, respectively. This solution was freeze-dried for further use.

### III-2.3.2. Electrospinning processing

The processed kidney ECM was solubilized in HFIP (1,1,1,3,3,3- Hexafluoro-2-propanol ≥99%) (Sigma-Aldrich) at a concentration of 100 mg $mL^{-1}$. Polycaprolactone (PCL, 80 kDa, Sigma Aldrich) was dissolved in the same reagent at a concentration on 15 %(w/v). The two were mixed in the following proportions 70:30, 50:50, 30:70 of dKECM and PCL respectively. The blends were electrospun through a 21 G needle at 18 kV, establishing a distance of 15 cm between the needle tip and the ground collector, a flow rate of 0.5 mL $h^{-1}$ and collecting the random fiber mesh on a flat aluminum foil. After 2 h of dKECM/PCL deposition, the meshes were left to dry for one day in a fume hood to evaporate all the remaining solvent.

### III-2.3.3. Scaffold crosslinking and sterilization

To avoid a fast degradation of the dKECM in the meshes, vapors of glutaraldehyde were applied to the meshes in a desiccator under vacuum for 24 h. Afterwards, the meshes were cut into 1.2 × 1.2 mm squares and introduced on 24 well plate inserts (CellCrownTM) to proceed to the sterilization processing. Before this, they were immersed in a 0.1 M glycine aqueous solution (Sigma Aldrich) for 1 h to decrease

the toxicity of residue aldehyde groups to cells, followed by sterilization using 70 %(v/v) ethanol and 1 h UV exposure/each side.

### III-2.4. Scaffold characterization

#### III-2.4.1. Morphological characterization and fiber diameter

The microstructure of the PCL meshes as well as the different blends of dKECM/PCL was evaluated by scanning electron microscopy (SEM; JSM-6010 LV, JEOL, Japan). Samples were sputter coated with gold (coater 108 A, Cressington, United States) prior to examination. The micrographs were taken at an accelerating voltage of 10kV. The average diameter of 100 fibers per condition were measured by ImageJ software using the SEM pictures with magnification of 2000 times.

#### III-2.4.2. Mechanical testing

The mechanical properties were determined using a universal mechanical testing machine (5543 K2942, 5543, Instron) equipped with a 1 kN load cell in tensile mode. Firstly, samples of each membrane (n = 5) were cut into testing specimens with length of 2 cm and width of 0.6 cm and then were fixed in paper frames with a square window of 1.2 × 1.2 cm. The frames were then mounted onto the tester grips at a gauge length of 1.2 cm, and the lateral sides of the frame were cut before testing at crosshead speed of 0.5 mm $min^{-1}$. Five samples per condition were tested. The Young's Modulus (E) was then calculated from the stress–strain curve as the slope of the initial linear portion of the curve, neglecting any toe region due to the initial conditioning of the specimen.

### III-2.5. Culture of human kidney cells on electrospun membranes

#### III-2.5.1. Study design

To evaluate the behavior of cells seeded on electrospun dKECM/PCL meshes, a human kidney cortex/proximal tubule established cell line derived from normal kidney was used, HK-2 (American Type Culture Collection, ATCC). These cells were immortalized by transduction with human papilloma virus 16 (HPV-16) E6/E7 genes. They were expanded in the company recommended medium, Keratinocyte

Serum Free Medium supplemented with 0.05 mg $mL^{-1}$ Bovine Pituitary Extract and 5 ng $mL^{-1}$ of Epidermal Growth Factor (Gibco) until a sufficient number was archived to initiate the assays.

Scaffolds were seeded with a concentrated drop containing 50000 cells, which were left to adhere for 4 h at 37 °C in a humidified atmosphere containing 5% $CO_2$. After this time, expansion medium was added, and the culture was maintained for 7 days. Also, after 1 and 3 days of culture, cell-seeded meshes were collected to perform cellular assays. Three independent experiments were performed with three replicates for each sample in each experiment.

### III-2.5.2. Cellular metabolic activity

HK-2 metabolic activity was evaluated by 3-(4,5-dimethylthiazol-2-yl)-5-(3-carboxymethoxyphenyl)-2-(4-sulfophenyl)-2H-tetrazolium (MTS) assay. The cells were further incubated with a 5:1 proportion of MTS (Promega) to DMEM without phenol red (ThermoFisher) for 4 h at 37 °C in dark. Then, the supernatant was used to determine the absorbance at 490nm. Cells cultured on glass coverslips were used as a negative control for cell viability.

### III-2.5.3. Cellular proliferation

Cell proliferation was quantified by the total amount of double-stranded DNA, assessed using Quant-iT PicoGreen dsDNA assay kit, according to the manufacturer's instructions. First, cell-seeded electrospun meshes washed with PBS and immersed in Milli-Q water. In this process, cells became lysed by thermal and osmotic shock. The resulting supernatant was used for the assay. The fluorescence of each specimen was measured by incubating samples with Picogreen for 10 min. Fluorescence was measured using a microplate reader at an excitation wavelength of 485 nm, and an emission wavelength of 528 nm. The DNA concentration for each sample was calculated using a standard curve.

### III-2.5.4. Protein content measurement

The amount of protein synthesized by the cells seeded on the different meshes was determined by their ability to reduce $Cu^{2+}$ in an alkaline environment, which is detected by bicinchoninic acid (BCA). Thus, using the same lysates as previously described for DNA quantification, total protein content was measured by Micro BCA Protein Assay Kit (Thermo Scientific), according to the manufacturer's

instructions. After 2 h of sample incubation with the substrate, absorbance was measured at 562 nm in a microplate reader. The concentration of total protein in the samples was calculated using a standard curve of Bovine Serum Albumin.

### III-2.5.5. Morphology examination

In order to evaluate cellular adhesion onto different percentages of ECM on electrospun meshes, after 1, 3 and 7 days of cell culture membranes were removed from the inserts, washed with PBS and fixed in with 2.5 %(v/v) of a glutaraldehyde solution (VWR) for 1 h. After this, they were washed again and dehydrated through an alcohol series before being treated with 1,1,1,3,3,3-Hexamethyldisilazane (HMDS, Sigma Aldrich). Samples were sputter coated with gold prior to analysis.

### III-2.5.6. Phenotypic markers expression analysis

Immunocytochemistry was performed after 7 days of culture to evaluate if the cells cultured in meshes produced with the different blends of ECM/PCL electrospun meshes change the phenotypic expression of epithelial tight junction marker zona occludens (ZO)-1. Briefly, cells were fixed in 10 % neutral buffered formalin (ThermoFisher) for 1 h at 4 °C and then washed in PBS. Cells were further incubated with antibody against the tight-junction marker ZO-1 (Abcam; 1:100 diluted in 1 % BSA/PBS) at 4 °C overnight. The next day, cells were washed with PBS and incubated with the secondary antibody

Alexa Fluor 594 (Alfagene; 1:500 diluted in 1 % BSA/PBS) at RT in the dark for 1 h. After several rinses in PBS, DAPI was incubated (VWR, 1:10000) for 10 min in the dark. HK-2 cells cultured over the meshes were analyzed under a fluorescence microscope (Zeiss, Axio Imager Z1m), the images were recorded digitally and further processed using Zen Lite Software (Zeiss).

### III-2.5.7. Transepithelial electrical resistance (TEER)

To determine the maximum barrier properties for the monolayers, TEER was measured over a 14-day period. TEER was measured in with the Millicell® ERS-2 Volt-Ohm Meter (MA, USA) with the same sets of inserts over time in PBS. Values were multiplied by the surface area of the membrane occupied by cells.

### III-2.5.8. Statistics

Statistical analyses were performed with GraphPad Prism 7 (GraphPad Software, California, USA). Data were expressed as means ± standard deviation of experiments with at least three independent treatments per cellular assay. Differences between groups were analyzed by unpaired t-test or two-way analysis of variance (ANOVA) in case of experiments conducted over time, using Tukey test for post hoc assessments of the differences between samples. Statistical significance was defined as $p < 0.05$.

## III-3. RESULTS

### III-3.1. dKECM characterization

#### III-3.1.1. Evaluation of cellular content and retention of the native structure on decellularized kidney matrices

Porcine kidneys were decellularized in sections on an orbital shaker for 7 days. Macroscopic evaluation of native kidneys throughout time indicates significant loss of cellular components by the appearance, characteristic of decellularized matrices (Figure III-1). The microscopic assessment by immunofluorescence staining corroborated this evaluation by the absence of fluorescence on DAPI staining (Figure III-2-B), when compared to the round-intact nucleus seen in the native tissues (Figure III-2-A). Some level of non-specific fluorescence by DAPI appears on these decellularized kidney sections. This was already reported on kidney tissues [15] and heart valves,[30] as a result of the strong protein binding to dodecyl sulphate during decellularization.[31] Unlike nuclear staining, the staining present on these decellularized kidney sections is diffuse and rare, suggesting traces of residual anionic residues from the detergent that was employed in the decellularization protocol.

Additionally, DNA quantification on these tissues demonstrated that this decellularization process resulted in the effective removal of nucleic acid material, where >95 % of the DNA was removed, when comparing with the native tissue (Figure III-2-C).

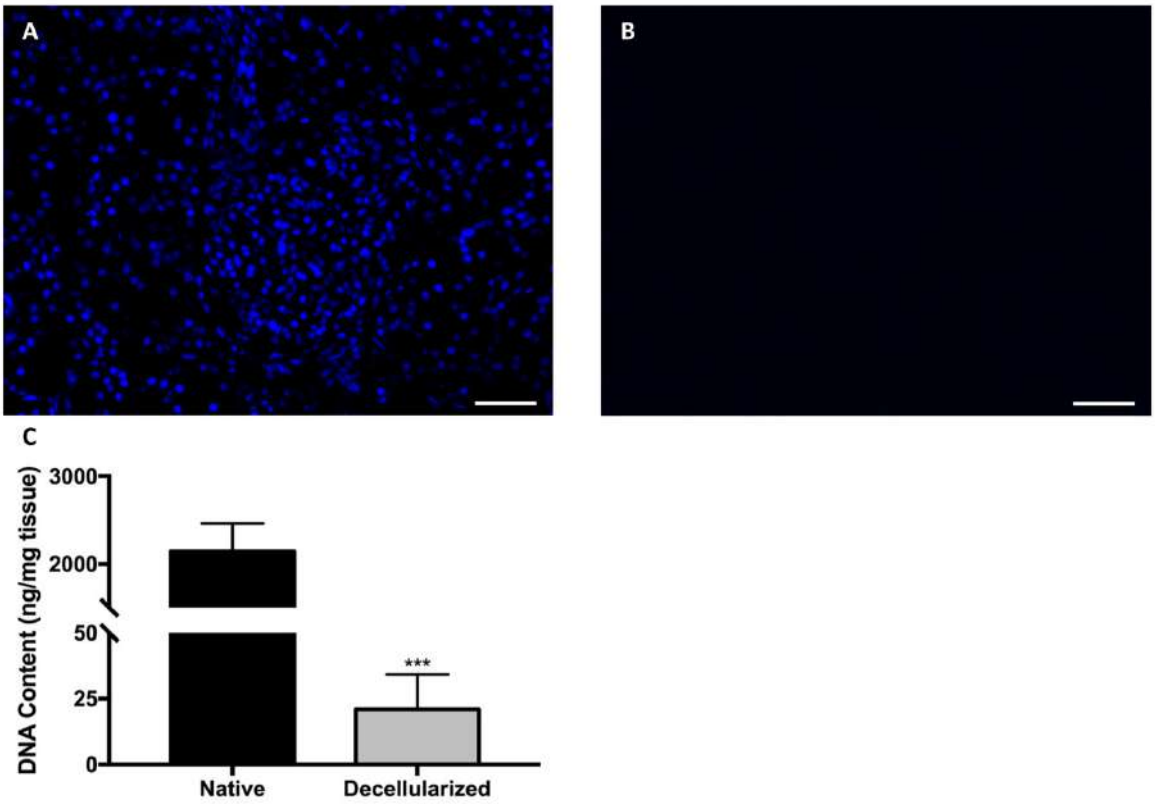


Figure III-2 – DAPI staining before (A) and after (B) decellularization. Scale bar: 50 µm. (C) DNA quantification by nanodrop of native and decellularized kidney tissue. Results are normalized by tissue mass. Unpaired t-test was employed. $^{***}p \leq 0.001$.

The preservation of the microscopic structures of the native tissue was confirmed by histological methods. Empty spaces which were once occupied by cells can be observed, evidencing the peritubular and the glomerular basement membrane preservation. Intact decellularized glomerulus can also be identified (Figure III-3-B and D - asterisks), as well as vessels (cardinals), which have their microarchitecture preserved. When compared with the native tissue, decellularized tissues are very similar, retaining the most functional components of the kidney. Hematoxylin nuclei counterstaining clearly revealed the absence of nucleic material, which corroborates what is said about DAPI non-specific binding. Preservation of the structure was also confirmed by scanning electron microscopy (SEM) (Figure III-4-A and B), where even after processing, glomerulus can be seen intact (Figure III-4-A - asterisk) with mesangial cells removed.

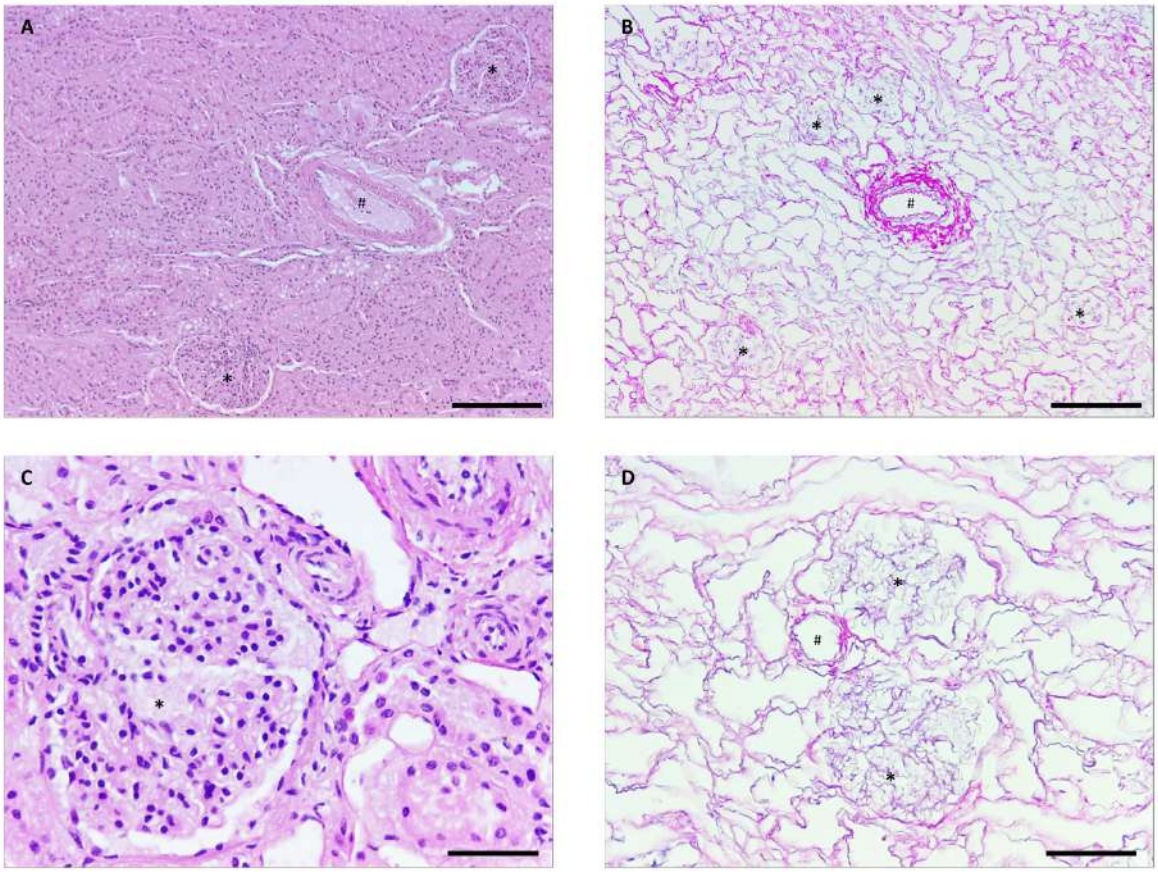


Figure III-3 – Hematoxylin and eosin staining of native (A and C) and decellularized kidney tissue (B and D). Intact decellularized glomerulus (*), blood vessels (#). Scale bar: 200 µm (A and B), 50 µm (C and D).

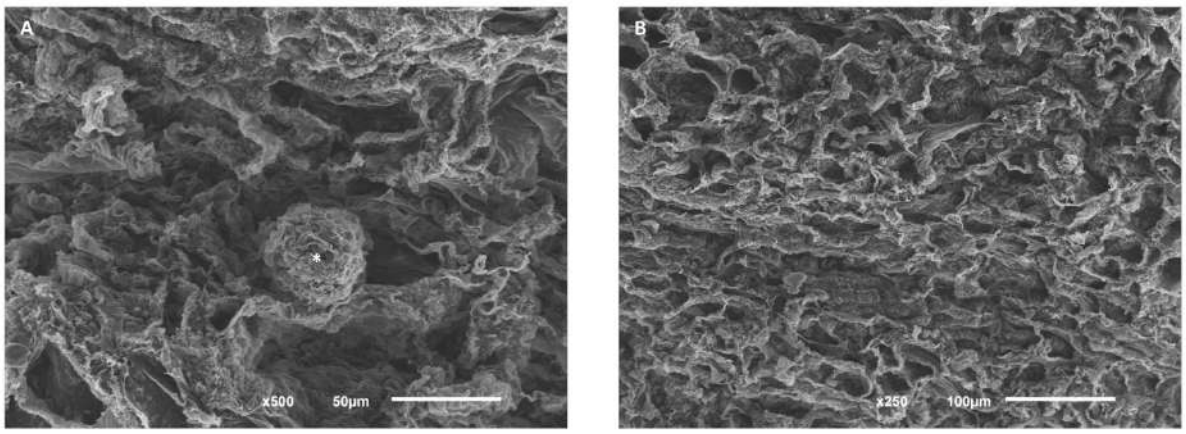


Figure III-4 – SEM micrographs of decellularized tissues. Intact glomerulus can be spotted (A*) and empty spaces evidencing cell removal are also seen through the whole tissue (B).

### III-3.1.2. Collagen and glycosaminoglycan's (GAG's) assessment

In order to utilize the decellularized matrix to produce scaffolds, the preservation of most proteins and components of the matrix is of utmost importance. Since there are several steps involved in the

process to obtain the powdered matrix, lyophilized tissues were used for these quantifications. The preservation of collagen, the main structural protein existent in the kidneys,[15] and GAG's will be essential to regulate cell adhesion, growth and proliferation on the supports manufactured from extracellular matrices. Although some loss of collagen was expected with the decellularization process, a good balance between matrix preservation and complete cellular removal was obtained with this protocol (Figure III-5-A). Also, GAG's quantification revealed that the tissue was well preserved, being these matrices suitable for producing natural ECM membranes (Figure III-5-B). Because there is loss of weight during decellularization, values were not normalized to tissue weight since the results would be masked by this effect.

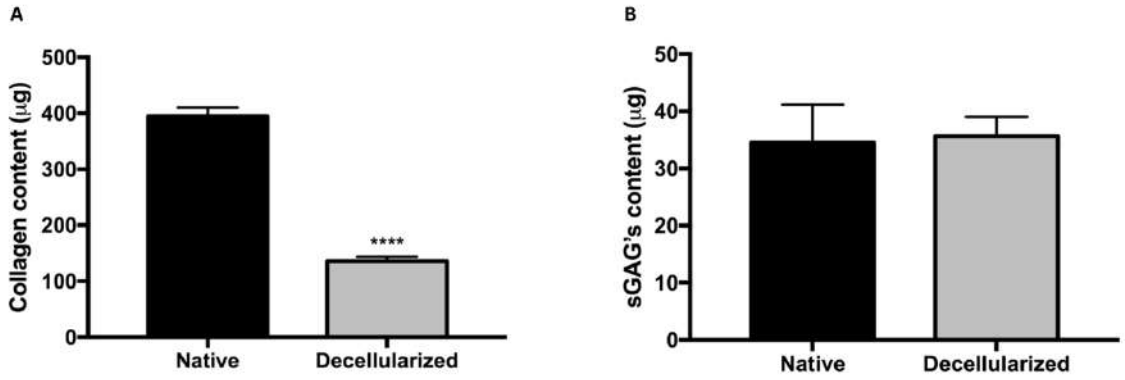


Figure III-5 – Collagen (A) and sGAG's (B) quantification on native vs. decellularized tissue. Unpaired t-test was employed. $^{****}p \leq 0.0001$ vs. Native.

## III-3.2. Electrospun dKECM characterization

The process of obtaining solubilized decellularized kidney ECM (dKECM) for electrospinning processing was the result of several optimization steps. To wash off the possible residual SDS on the tissues, after milling, the powder was submitted to several rinses in 70 % ethanol. After this washing step, we analyzed the powders by Energy-Dispersive X-ray Spectroscopy (EDS) if the sulphate (S) peak was eliminated (data not shown), showing the absence of SDS on the decellularized matrix. Also, digesting the ECM with pepsin allowed obtaining a homogeneous solubilized matrix formation, which was not possible when dissolving the matrix directly on HFIP. The ECM concentration was selected according to the viscosity of the solution, since fiber diameter and its variability greatly depends strongly on this parameter.[32] Lower concentrations prevented the formation of a homogeneous mesh, resulting in small fragments of fibers being deposited on the collector, with a large distribution of fiber diameters. On the

other hand, with higher concentrations, beaded fibers started to appear, compromising our goal of having a homogeneous fiber morphology along the mesh. The inclusion of PCL in our formulations aided the electrospinning processing, allowing obtaining a much more precise tailoring of fiber diameters and facilitating obtaining homogeneous fibers. The blends of PCL and ECM were selected to enable modulating the mechanical and biological performance of the meshes by varying its composition.

### III-3.2.1. Morphology and fiber diameter of electrospun meshes

The morphology of electrospun dKECM:PCL blends was assessed by means of SEM analysis. Uniform porous fiber meshes with random orientation were obtained by electrospinning, as confirmed by SEM micrographs (Figure III-6). Fiber diameters are very similar when comparing the different blends of PCL and dKECM, not having statistical differences between them, proving that the conditions optimized for electrospinning were reproducible and have uniform outcomes (Table III-1). This result is important to discard possible influence of different diameters on cell behavior. By SEM images, an effect of the increasing amount of PCL on the fibers can be analyzed. Straighter fibers and less lumps are observed as the amount of PCL on the blends increase. This can be related to the heterogeneity on the composition of the dKECM and possible fragments of insoluble matrix that were incorporated. On the other hand, PCL meshes were free of lumps, straighter and deposited in random orientation. Additionally, on the electrospun blends of dKECM and PCL, a sub-population of fibers with much smaller diameter appear, which were not quantified for diameter analysis, but still important to promote cell adhesion on a nanometer scale.

Table III-1 – Fiber diameters for the electrospun meshes.

| **Type of Mesh** | 70:30 ECM:PCL | 50:50 ECM:PCL | 30:70 ECM:PCL | PCL |
|---|---|---|---|---|
| **Diameter (μm)** | 0.400 ± 0.093 | 0.383 ± 0.073 | 0.389 ± 0.074 | 0.397 ± 0.075 |

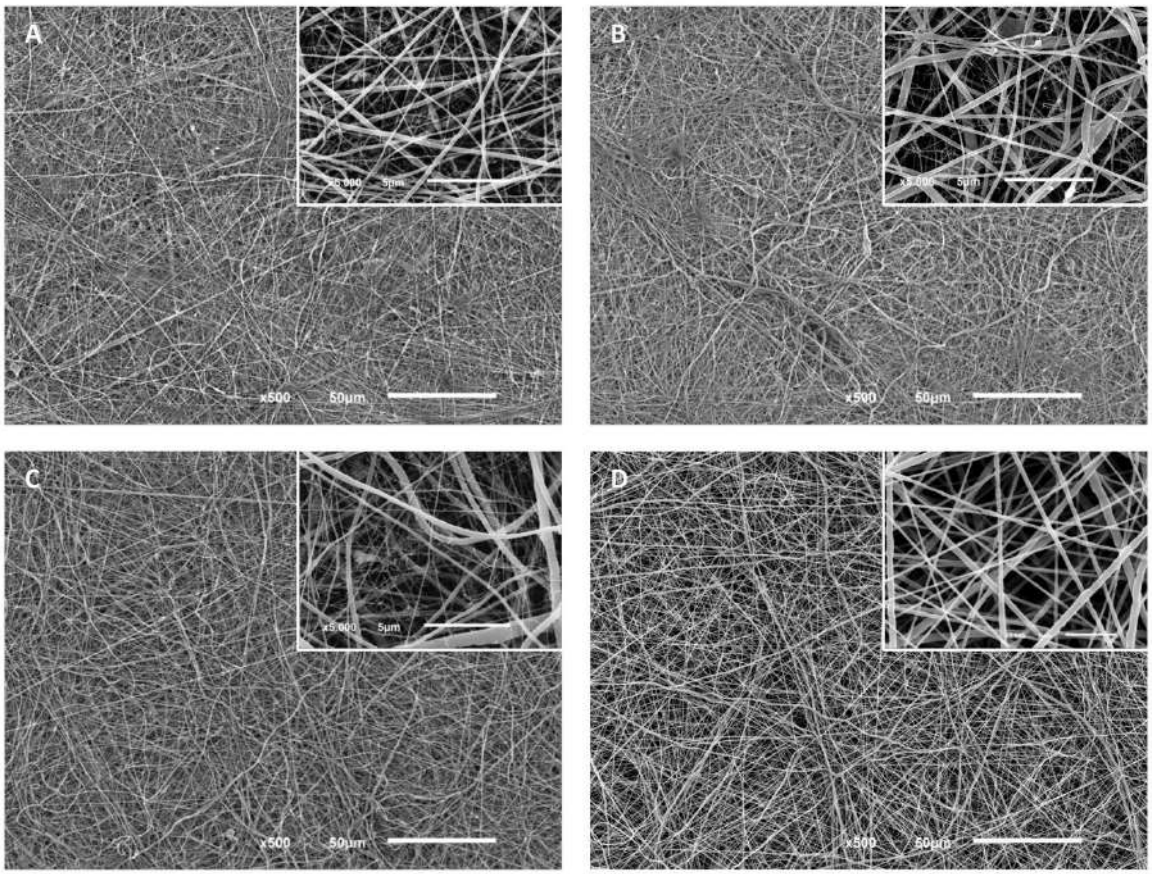


Figure III-6 – SEM micrographs of (A) 70:30 ECM:PCL, (B) 50:50 ECM:PCL, (C) 30:70 ECM:PCL and (D) PCL. Scale bar: 50 µm for the background images; 5 µm for the insert images.

### III-3.2.2. Mechanical analysis

The mechanical behavior of the dKECM blends and PCL meshes was characterized using a uniaxial compression test (Figure III-7). The results indicate that pure PCL meshes have the highest E modulus (E = 25.42 ± 4.69 MPa), which is approximately 4-fold higher com- paring with the blends. Between the meshes composed of dKECM and PCL, there is an increasing effect on the E modulus value related to the increasing amount of PCL on the blends (30:70 ECM:PCL E = 6.7 ± 1.37 MPa, 50:50 ECM:PCL E = 6.3 ± 0.9 MPa and 70:30 ECM:PCL E = 3.99 ± 0.7 MPa) although not statistically significant ($p < 0.05$). A major decrease on E can be detected when the blend is only composed by 30 % of PCL, which corroborates the fact that PCL aids on electrospinning processing, preventing fiber breakage and the formation of heterogeneous meshes, therefore increasing the mechanical properties.

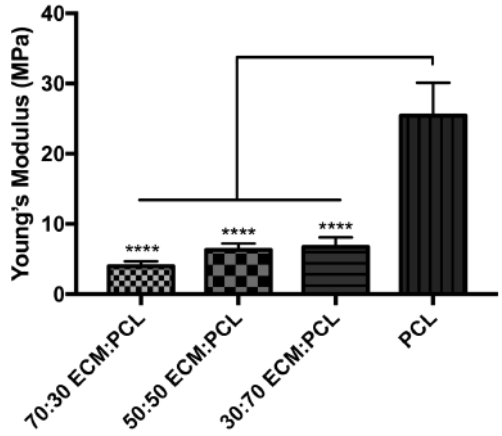


Figure III-7 – Mechanical behavior of the produced electrospun meshes. ****$p \leq 0.0001$.

## III-3.3. Analysis of HK-2 cell cultures

### III-3.3.1. Metabolic activity

DKECM meshes with different proportions of PCL shown being cytocompatible for 7days *in vitro* HK-2 cell culture studies (

Figure III-8). Throughout time there is a clear tendency of increasing metabolic activity in all samples. On day 1 and 3, cells cultured on tissue culture polystyrene (TCPS) exhibited significantly higher metabolic activity when compared to cells cultured on meshes (Figure S III-1). However, on the 3rd and 7th day of culture, cells seeded on 70:30 ECM:PCL membranes seem to outperform the other electrospun membranes in terms of metabolic activity, being significantly higher. Also, cells seeded on PCL membranes demonstrated much lower activity overtime, suggesting a positive effect of the dKECM on the metabolic activity of cells cultured on these substrates.

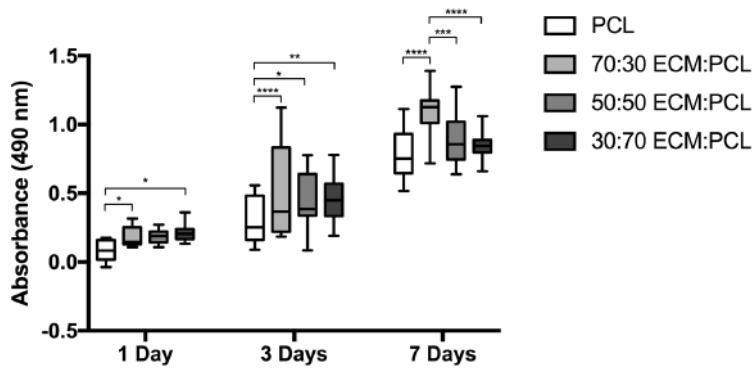


Figure III-8 – Viability of the HK-2 cells measured by MTS assay. These results were compared to control cultures grown on TCPS. *$p \leq 0.05$, **$p \leq 0.01$, ***$p \leq 0.001$, ***$p \leq 0.0001$.

### III-3.3.2. Cell proliferation

HK-2 proliferation on the membranes was assessed by DNA Quantification (Figure III-9). The amount of DNA for each sample increases over time. Indeed, the same tendency for TCPS can be observed here, where from day 1 to 3 the amount of DNA quantified is higher when compared to cells seeded on the electrospun membranes (Figure S III-2). Moreover, from day 3 to 7 the amount of DNA doubled for all samples, evidencing a relevant role of the fibers on the proliferation of these cells. Additionally, in all of the timepoints, cells seeded on membranes composed of PCL alone stand with much lower values for this quantification, being this difference statistically relevant since the very 1st day of culture (****$p <$ 0.0001). This points out to a relevant role of the ECM composed membranes over cell behavior and proliferation. Between the dKECM composed membranes, no relevant difference is found in all of timepoints, except for the 7th day of culture, where HK-2 seeded on 70:30 ECM:PCL membranes outperform cells seeded on the other membranes. Also, at the 7th day of culture on 30:70 ECM:PCL meshes the cells demonstrate slightly higher proliferation when compared to 50:50 ECM:PCL seeded cells. This can be related to the mechanical performance of the membranes composed of a higher percentage of PCL, making a good balance between mechanical properties and dKECM composition.

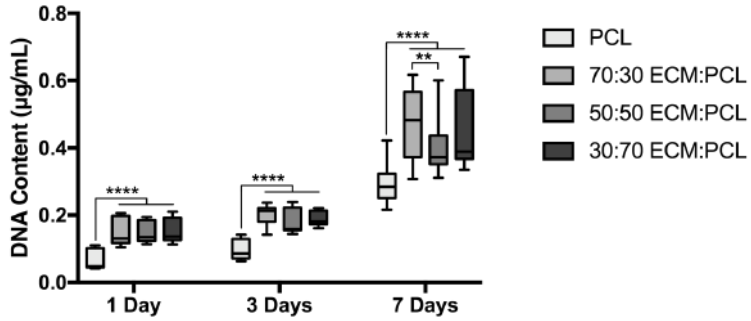


Figure III-9 – Cell proliferation measured by quantification of DNA with Picogreen kit. **$p \leq 0.01$, ****$p \leq 0.0001$.

### III-3.3.3. Protein content

The total protein content was measured to enable correlating the proliferative capacity of the cells with their inner regulation of transcription and translation onto proteins. What can be observed is a plateau phase from day 1 to day 3 in every sample, with values increasing in a small proportion when compared to the increase from day 3 to 7 (Figure III-10). On the 7th day of culture, electrospun membranes display 2-fold the values for TCPS (Figure S III-3). Cells seeded and cultured on membranes composed of PCL only express lower protein content since the 3rd day of culture, being this difference enhanced at the 7th

day of culture. Corroborating the results for metabolic activity and proliferation, 70:30 ECM:PCL seeded cells outperform the other ones at the last timepoint.

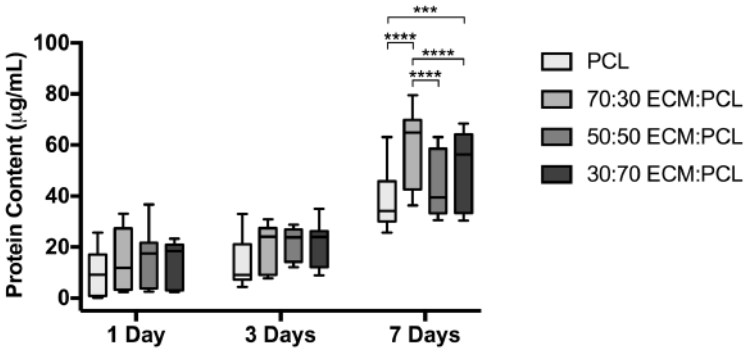


Figure III-10 – Protein Intracellular content on HK-2 cells. ***$p \leq 0.001$, ****$p \leq 0.0001$.

### III-3.3.4. Cell morphology and distribution

The morphology of the HK-2 cells was analyzed by SEM on days 1, 3 and 7 of culture. An evolution on the number of cells is clearly seen from the first until the last day of culture in all the samples. On the 1st day, by these micrographs, it is evidenced that cells are able to attach to the fibers since the 1st day of culture. Yet, cells seeded on 50:50 ECM:PCL membranes seem having a higher cell seeding efficiency (Figure III-11-D), demonstrated by a larger surface area occupied by the cells. The higher magnification micrographs show that cells are also assuming their natural polygonal-shaped epithelial morphology when seeded on the membranes composed of dKECM (Figure III-11-A,D,G). On the other hand, on PCL membranes, cells do not seem to be adapting very well, assuming an irregular morphology (Figure III-11-J). Taking into account the evolution from day 1 to day 3, it can be said that these cells seem to rapidly adapt to the meshes, since they are well spread all over the membranes, particularly on the 70:30 ECM:PCL (Figure III-11-B) and PCL conditions (Figure III-11-K). This can be justified first by a higher content of dKECM on the former, and secondly by a good mechanical support on the latter. By day 7, on dKECM-composed membranes cells are covering almost all of the mesh, forming a homogeneous monolayer (Figure III-11-C,F,I). In some sites cells are even overlapping each other, which can be demonstrated by the round-shaped morphology. However, on the PCL meshes, some spaces unoccupied by cells can be seen, proving that is more difficult for the cells seeded on these meshes to grow into a continuous monolayer (Figure III-11-L). Unlike what is observed for cells seeded on electrospun membranes, cells cultured on TCPS seem to form clusters over time, which can be due to the lack of

adhesion points on smooth surfaces such as tissue culture plastic (Figure S III-4). Some apoptotic cells and debris can also be seen on these surfaces by day 7.

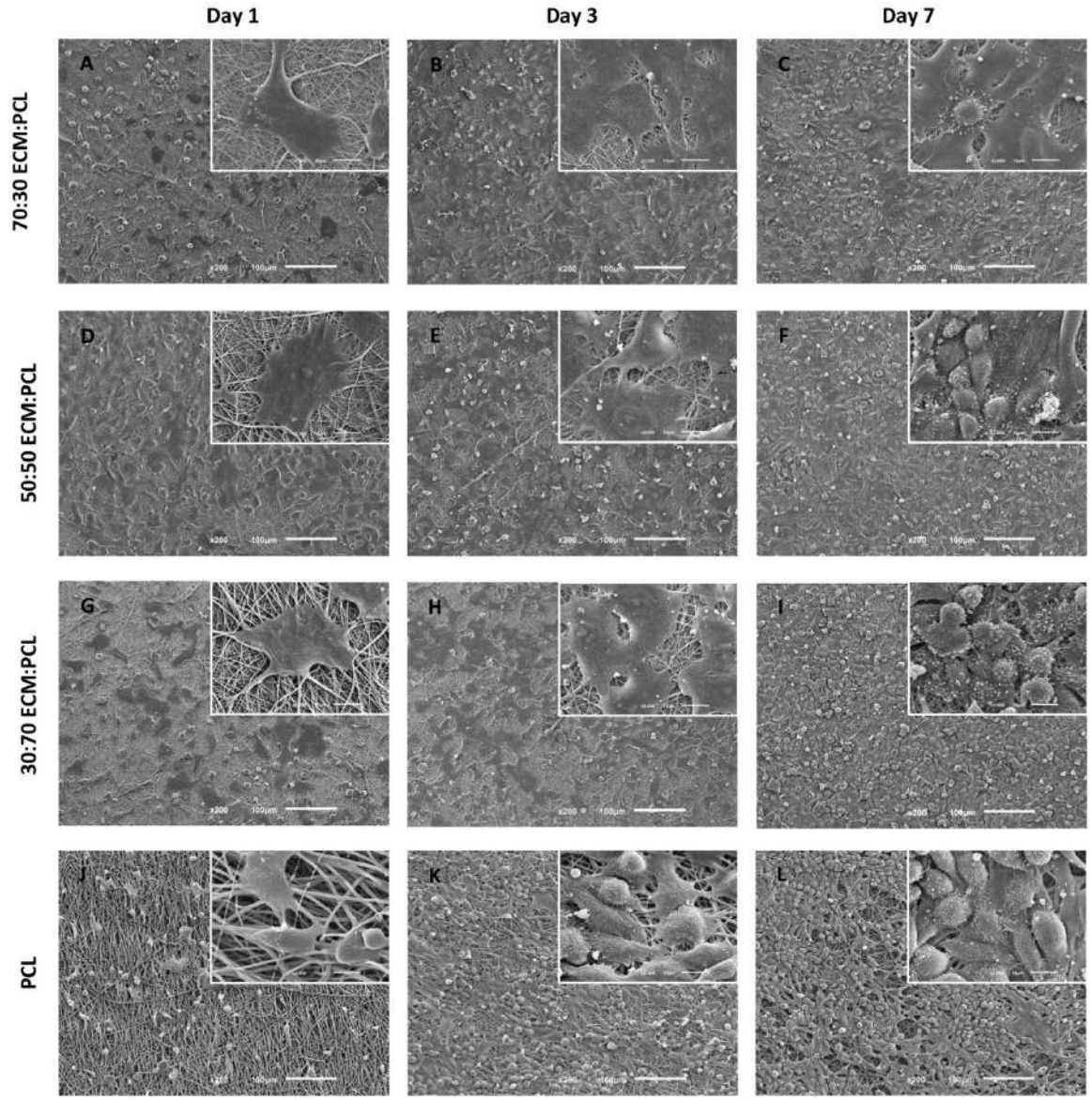


Figure III-11 – SEM micrographs of HK-2 cells on (A)-(C) 70:30 ECM:PCL membranes, (D)-(F) 50:50 ECM:PCL membranes, (G)-(I) 30:70 ECM:PCL membranes and (J)-(L) PCL membranes. Left, middle and right row represent cells after 1, 3 and 7 days of culture, respectively. Scale bar: 100 μm for higher magnification images, 10 μm for the insert images.

### III-3.3.5. Expression of ZO-1 on cell monolayers

Kidney homeostasis and nephron adequate permeability is dependent on the assembly of specific cell-cell tight junctions, where ZO-1 plays a major role.[28] Therefore, we analyzed the expression of this protein on our cell culture studies after the formation of a monolayer of cells. Corroborating SEM

micrographs, DAPI and phalloidin staining (data not shown), confirmed the presence of a monolayer was after 7 days of culture on the electrospun membranes. The same could not be seen on TCPS, as previously observed on SEM micrographs, these cells assembled in clusters. ZO-1 (in red) was found to be expressed on the dKECM-composed electrospun membranes along cell boundaries by representative z-scans (Figure III-12-A,B,C). Since electrospun membranes are not flat, cells reside in different planes and sometimes even below the fibers. This can explain the empty spaces on each micrograph. However, expression of the epithelial marker ZO-1 is clear on dKECM composed membranes and absent on PCL membranes (Figure III-12-D), which highlights the need of a natural component the membranes for these cells to emphasize their epithelial character. Moreover, 70:30 ECM:PCL membranes seem to demonstrate an higher expression of this molecule (Figure III-12-A).

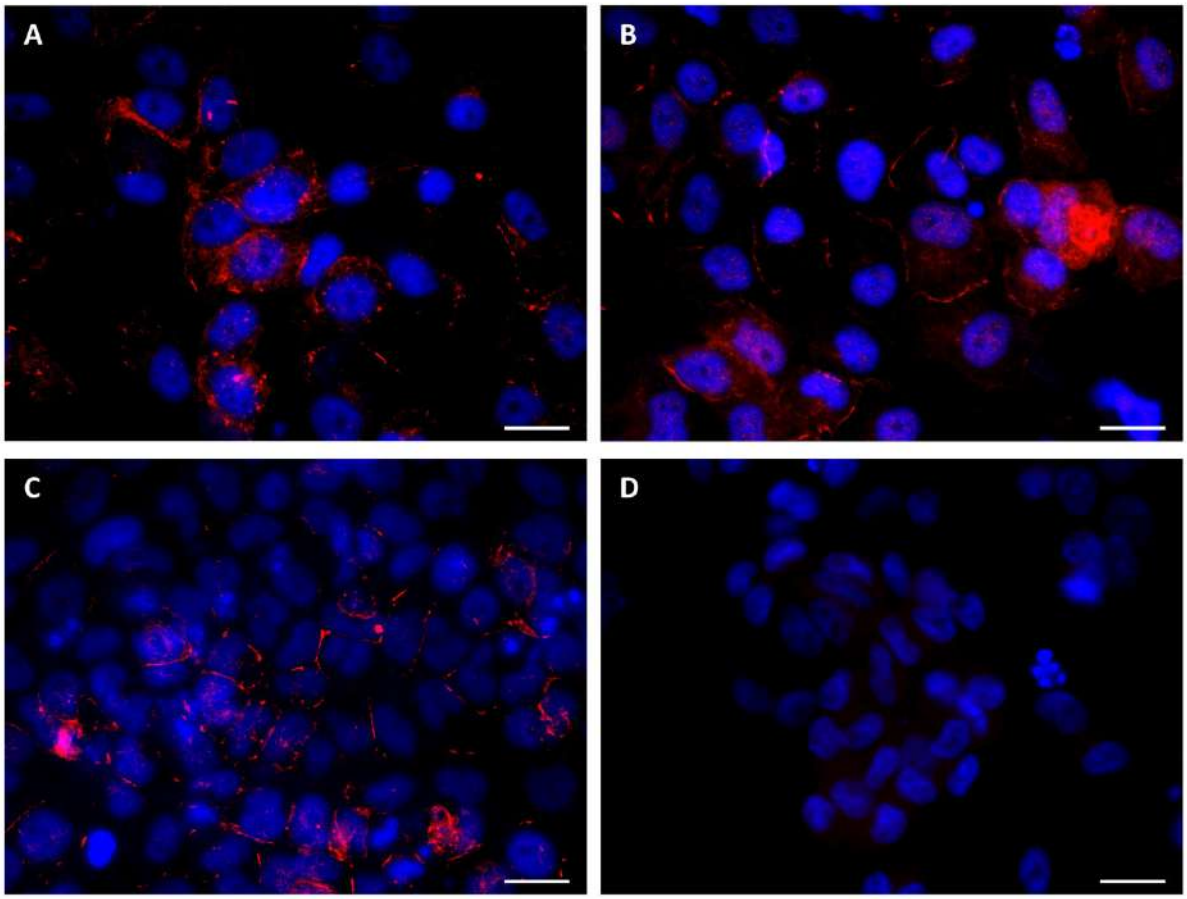


Figure III-12 – Immunocytochemistry of epithelial marker zona occludens-1 (red) and DAPI (blue). (A) 70:30 ECM:PCL, (B) 50:50 ECM:PCL, (C) 30:70 ECM:PCL; (D) PCL. Scale bar: 20 μm.

### III-3.3.6. Transepithelial barrier function

Further changes on TEER and permeability on epithelial cells were tested measuring the TEER over time (Figure III-13). It was found that monocultures of human kidney cells augmented TEER values significantly from day 1 to day 3 of culture, reaching a plateau phase from this point on. This indicates greater tight junction's formation and faster cell growth at this time. Between the membranes, it can be observed that 70:30 ECM:PCL seeded cells adapted faster and exhibited higher TEER at day 3. At the 7th day of culture, 50:50 ECM:PCL membranes exhibit a higher value for TEER, followed by 70:30 ECM:PCL membranes and 30:70 ECM:PCL membranes. At this timepoint, the cells seeded on 50:50 ECM:PCL membranes exhibit a statistically significant difference (** $p < 0.01$) when compared to PCL membranes. Additionally, the TEER value is higher in all timepoints for the membranes composed with a higher ECM fraction, but the 50:50 ECM:PCL membranes have the highest TEER. This condition is the only having statistically significant differences when compared with the others.

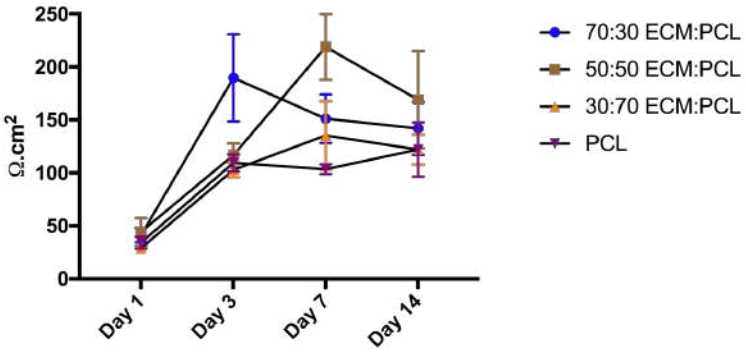


Figure III-13 – Measurement of TEER over a 14-day period. Results are expressed as mean ± SEM.

## III-4. DISCUSSION

In this study we investigated whether ECM-rich electrospun membranes could be a suitable support for mimicking the renal basement membrane and potentially to be applied on the clinical translation of several kidney treatments. We successfully cultured *in vitro* a monolayer of proximal tubule kidney epithelial cells on ECM-based electrospun membranes and studied their phenotype. To the best of our knowledge, this is the first study employing natural decellularized tissues to use as basement membranes and also the first report of using dKECM on electrospun meshes. This gave us the possibility of exploring natural fibrous scaffolds of natural ECM on the expansion, proliferation and functionality of human kidney

cells. While decellularized tissues have been the subject of intensive research efforts for their use in whole organ transplantation,[9, 10] not much is known about the use of these matrices for other applications.

The methods by which tissues are decellularized and ECM is processed to obtain different biomaterials can influence their composition, architecture and properties. Therefore, the biological material (dKECM) was first characterized in terms of nucleic material, collagen and GAG's content. Our results shown that the nucleic material was successfully removed, as observed by H&E and DAPI staining, where no specific nuclear staining was found on these tissues (Figure III-2 and 4). Also, by DNA extraction and quantification it was confirmed that > 95% of the nucleic material was removed (Figure III-3). Several reported techniques of decellularization have employed more than one detergent and/or DNase, serine proteases and solutions to activate endogenous nucleases and remove residues of bulky nuclear material. We observed by optimization that these techniques may be successful when performing decellularization by perfusion. However, since we were decellularizing kidney portions, the most non-destructive method to do it was to use an SDS solution, performing several cycles of washing until it was fully decellularized, as previously reported.[15] This decellularization method has shown to preserve the three-dimensional morphology (Figure III-4) and the histoarchitecture of the native tissue, even microscopically (Figure III-3). Moreover, the matrix content evaluation has shown that, after decellularization, the tissue retains a great amount of GAG's (Figure III-5-B) and had some loss of collagen (Figure III-5-A), which was previously reported in the literature.[20, 33] The maintenance of these components is of utmost importance since these are key players in maintaining the integrity and function of basement membranes.[21] Thus, it is to expect that changes in ECM composition will greatly influence cell adhesion, migration, proliferation and gene expressing, being essential for the formation of a homogeneous monolayer of epithelial cells.

In this work, different proportions of dKECM conjugated with PCL were used in order to study the effect of having increasing biological material and decreasing fraction of synthetic material on a mesh. Being a synthetic biodegradable polymer, PCL is well characterized among the scientific community and has shown its utility for tissue engineering applications either alone [34, 35] or in combination with other materials.[36, 37] Therefore, we have developed ECM membranes composed by renal specific decellularized ECM to evaluate the response of renal epithelial cells. The membranes were successfully optimized using the electrospinning equipment. Pure dKECM was not suitable to be processed by electrospinning given its low viscosity, which makes the solution to spit on the collector, making it difficult to have reproducible conditions for the deposition of uniform meshes. In this work, the inclusion of PCL within the ECM enabled the production of meshes capable of mimicking the size and shape parameters

of *in vivo* matrices, such as nanoscale dimensions, large surface area and interconnected porosity (Figure III-6). Moreover, blending dKECM with another material reduces the amount of matrix needed for the fabrication of these scaffolds. DKECM composed meshes were crosslinked with glutaraldehyde to guarantee the maintenance of the majority of natural ECM proteins on the mesh and to avoid loss over culture time, which was not desirable. The fibrous structure was maintained after crosslinking. We avoided immersing meshes on crosslinking solutions and instead we created a vacuum atmosphere with the crosslinker, which helped on maintaining the mechanical properties of the meshes and avoiding dissolution of material.

Mechanical testing revealed increasing elastic modulus with the increasing amount of PCL on the meshes. This was somewhat expectable giving the complex mixture of natural non-living materials composing the ECM, usually poorer in mechanical properties when compared with synthetic materials. Thus, PCL membranes had an elastic modulus of approximately 74 % higher that of 30:70 ECM:PCL membranes, suggesting that dKECM interferes with PCL structure after mixing the two solutions and processing by electrospinning. However, we could also observe that we could augment the elastic modulus of dKECM membranes by increasing the amount of PCL in them, which was our main goal by joining a synthetic polymer on our formulations. This was important to assess the ease of membranes manipulation in order to proceed with *in vitro* biological assays.

To investigate the biological performance of the produced samples, a human proximal tubule epithelial cell line, HK-2, was cultured on dKECM electrospun membranes. First, it was important to assess the *in vitro* cytocompatibility. We utilized an assay which measures metabolic activity to assess cell viability. From these values we were able to evidence an increasing activity over time in culture. Interestingly, at day 7, 70:30 ECM:PCL membranes exhibited approximately 27 % higher cell metabolic activity when compared to PCL membranes and approximately 20 % higher when compared to the other dKECM membranes, suggesting that renal ECM was more suitable for the growth of HK-2 cells than a synthetic biocompatible polymer such as PCL (

Figure III-8). The same occurred with dsDNA quantification, where dKECM membranes exhibited overall 34 % higher DNA content after 7 days comparing with PCL membranes alone, suggesting that not only dKECM membranes improved cytocompatibility but also had an important role on cell proliferation (Figure III-9). Additionally, 70:30 ECM:PCL membranes outperformed the other dKECM composed membranes, completing the results for metabolic activity. The protein content was also quantified, and the main difference was observed after 7 days of culture between cells seeded on PCL and on dKECM

composed membranes, which further confirmed the other biological data (Figure III-10). Additionally, a huge difference was found between cells cultured on TCPS and cells cultured on electrospun meshes, as the former were quantified with approximately half of the value for protein quantification comparing with electrospun meshes (Figure S III-3). These results may be related to the morphology that cells adopted on the tissue culture plastic, being more elongated and fibroblastic-like (Figure S III-4). Indeed, protein content was already proven to be correlated with cell mass and volume.[38] This may happen due to the higher surface area that dKECM fibers provided for cells to attach and spread, unlike TCPS surfaces. Consequently, cells do not spread as a monolayer but instead as clusters, as revealed by SEM micrographs (Figure S III-4). This was a non-desirable outcome, since changing morphology can many times mean a change on cell phenotype and/or epithelial-to-mesenchymal transition.[39] Furthermore, day 1 micrographs demonstrated that 70:30 ECM:PCL membranes were the ones with less cell seeding efficiency, since less surface area of the mesh was occupied with cells. This could have been a result of the enzymatic degradation of bioactive matrices, despite being crosslinked. The increasing matrix content lead to a faster membrane degradability by the seeded cells, having more infiltrated cells than on the surface. Indeed, on day 3, membranes seem equally populated and on day 7 a monolayer of cells can be seen on the dKECM membranes. SEM results confirm that fibrous scaffolds were preferred by proximal tubule cells to form a monolayer of cells instead of flat surfaces such as TCPS.

The biological assays performed demonstrated improved biocompatibility and proliferation results for the dKECM membranes, validating our initial hypothesis. This can be attributed to the intrinsic bioactivity of the natural ECM, which was retained after electrospinning, enabling higher cell affinity by the more abundant adhesion peptides present at the surface of collagen and other proteins.

Additionally, to validate cellular functionality, expression of ZO-1 was evaluated on HK-2 seeded membranes. The structural organization of tight junctions is determined by the interaction of ZO proteins and occludin. This will create a barrier to the diffusion of solutes through the paracellular pathway.[40] Therefore, analyzing expression of ZO-1 in cell monolayers was an essential step to validate cell phenotype and interaction on dKECM membranes, which was confirmed. By immunocytochemistry images (Figure III-12) expression of ZO-1 (in red) was observed in dKECM composed membranes but not on PCL membranes, proving the value of natural-derived components on the behavior and phenotype of these cells.

The transepithelial barrier function was confirmed by measurement of TEER (Figure III-13). Studying transepithelial resistance allows for a better understanding of a monolayer of epithelial cells, since it

measures its electrical resistance. *In vivo*, the paracellular transport is mediated along the TJ and the lateral intercellular spaces. Thus, this measurement is essential, especially when studying leaky epithelia such as the proximal tubule.[41] Another method to measure paracellular permeability is inulin leakage, which is typically inversely proportional to TEER.[42] Here, we could observe higher TEER for the dKECM composed membranes in all timepoints, corroborating all of the performed biological assays. A slightly decrease in TEER after 14 days could have been due to the static culture conditions, since there is lack of shear-mediated calcium signaling, which has already been seen in previous studies.[43]

Recent studies have developed membranes for removal of uremic metabolites with the final aim of modelling the proximal tubule or even the glomerulus.[43, 44] These reports have demonstrated organic cation transport and an *in vivo*-like behavior with the development a microfluidic device. However, these membranes lack similarity with the nephrons' underlying basement membranes, since they are composed only by synthetic materials. The materials' combination developed throughout this work gives a new insight into the kidney and nephron research with the incorporation of natural materials in their composition, improving already developed strategies.

## III-5. CONCLUSIONS

This study describes a novel scaffold composed of extracellular matrix of renal origin. By the presented protocol, we were able to decellularize kidney tissue, preserving the most important biochemical cues which are known to have an important role on cell proliferation, differentiation, adhesion and migration in biological processes. Indeed, our findings suggest that renal cells cultured on membranes composed of a higher fraction of ECM have a stronger biological performance, when compared with bare synthetic PCL membranes in cell affinity, adhesion, proliferation and migration, maintaining healthy cellular morphological features. This work demonstrates the potential of using kidney decellularized ECM as a substrate to develop tubule functionality. These membranes would potentially be a valuable tool to improve kidney advanced therapies in the future.

## Acknowledgements

This work was supported by the European Regional Development Fund (ERDF) on the project FROnTHERA (NORTE-01-0145-FEDER- 000023); the Portuguese Foundation for Science and Technology

(FCT), under the scope of the project SPARTAN (PTDC/CTM-BIO/4388/2014); and the FCT PhD Grant on the Doctoral Program on Advanced Therapies for Health (PATH) (PD/169/2013).

## III-6. REFERENCES

1. Hynes RO (2009) The extracellular matrix: not just pretty fibrils. Science 326:1216–9. https://doi.org/10.1126/science.1176009
2. Lelongt B, Ronco P (2003) Role of extracellular matrix in kidney development and repair. Pediatr Nephrol 18:731–742. https://doi.org/10.1007/s00467-003-1153-x
3. He F, Pei M (2013) Extracellular matrix enhances differentiation of adipose stem cells from infrapatellar fat pad toward chondrogenesis. J Tissue Eng Regen Med 7:73–84. https://doi.org/10.1002/term.505
4. Tang C, Jin C, Xu Y, et al (2016) Chondrogenic Differentiation Could Be Induced by Autologous Bone Marrow Mesenchymal Stem Cell-Derived Extracellular Matrix Scaffolds Without Exogenous Growth Factor. Tissue Eng - Part A 22:222–232. https://doi.org/10.1089/ten.tea.2014.0491
5. Narayanan K, Lim VY, Shen J, et al (2014) Extracellular matrix-mediated differentiation of human embryonic stem cells: Differentiation to insulin-secreting beta cells. Tissue Eng - Part A 20:424–433. https://doi.org/10.1089/ten.tea.2013.0257
6. Badylak SF, Freytes DO, Gilbert TW (2015) Reprint of: Extracellular matrix as a biological scaffold material: Structure and function. Acta Biomater 23:S17–S26. https://doi.org/10.1016/j.actbio.2015.07.016
7. Alamein MA, Liu Q, Stephens S, et al (2013) Nanospiderwebs: Artificial 3D Extracellular Matrix from Nanofibers by Novel Clinical Grade Electrospinning for Stem Cell Delivery. Adv Healthc Mater 2:702–717. https://doi.org/10.1002/adhm.201200287
8. Oliveira C, Costa-Pinto AR, Reis RL, et al (2014) Biofunctional Nanofibrous Substrate Comprising Immobilized Antibodies and Selective Binding of Autologous Growth Factors. Biomacromolecules 15:2196–2205. https://doi.org/10.1021/bm500346s
9. Song JJ, Guyette JP, Gilpin SE, et al (2013) Regeneration and experimental orthotopic transplantation of a bioengineered kidney. Nat Med 19:646–51. https://doi.org/10.1038/nm.3154
10. Ott HC, Matthiesen TS, Goh S-K, et al (2008) Perfusion-decellularized matrix: using nature's platform to engineer a bioartificial heart. Nat Med 14:213–221. https://doi.org/10.1038/nm1684
11. Stankus JJ, Freytes DO, Badylak SF, Wagner WR (2008) Hybrid nanofibrous scaffolds from electrospinning of a synthetic biodegradable elastomer and urinary bladder matrix. J Biomater Sci Polym Ed 19:635–652. https://doi.org/10.1163/156856208784089599
12. Francis MP, Sachs PC, Madurantakam PA, et al (2012) Electrospinning adipose tissue-derived extracellular matrix for adipose stem cell culture. J Biomed Mater Res Part A 100A:1716–1724. https://doi.org/10.1002/jbm.a.34126
13. Garrigues NW, Little D, Sanchez-Adams J, et al (2014) Electrospun cartilage-derived matrix scaffolds for cartilage tissue engineering. J Biomed Mater Res Part A 102:3998–4008. https://doi.org/10.1002/jbm.a.35068
14. Almeida H V., Cunniffe GM, Vinardell T, et al (2015) Coupling Freshly Isolated CD44+ Infrapatellar Fat Pad-Derived Stromal Cells with a TGF-$\beta$ 3 Eluting Cartilage ECM-Derived Scaffold as a Single-Stage Strategy for Promoting Chondrogenesis. Adv Healthc Mater 4:1043–1053. https://doi.org/10.1002/adhm.201400687

15. Nagao RJ, Xu J, Luo P, et al (2016) Decellularized Human Kidney Cortex Hydrogels Enhance Kidney Microvascular Endothelial Cell Maturation and Quiescence. Tissue Eng Part A 22:1140–1150. https://doi.org/10.1089/ten.TEA.2016.0213
16. Ross EA, Williams MJ, Hamazaki T, et al (2009) Embryonic stem cells proliferate and differentiate when seeded into kidney scaffolds. J Am Soc Nephrol 20:2338–2347. https://doi.org/10.1681/ASN.2008111196
17. Abolbashari M, Agcaoili SM, Lee M-KK, et al (2016) Repopulation of porcine kidney scaffold using porcine primary renal cells. Acta Biomater 29:52–61. https://doi.org/10.1016/j.actbio.2015.11.026
18. Peloso A, Petrosyan A, Da Sacco S, et al (2015) Renal Extracellular Matrix Scaffolds from Discarded Kidneys Maintain Glomerular Morphometry and Vascular Resilience and Retains Critical Growth Factors. Transplantation 99:1807–1816. https://doi.org/10.1097/TP.0000000000000811
19. Orlando G, Booth C, Wang Z, et al (2013) Discarded human kidneys as a source of ECM scaffold for kidney regeneration technologies. Biomaterials 34:5915–5925. https://doi.org/10.1016/j.biomaterials.2013.04.033
20. Wang H, Naghavi M, Allen C, et al (2016) Global, regional, and national life expectancy, all-cause mortality, and cause-specific mortality for 249 causes of death, 1980-2015: a systematic analysis for the Global Burden of Disease Study 2015. Lancet (London, England) 388:1459–1544. https://doi.org/10.1016/S0140-6736(16)31012-1
21. Kruegel J, Miosge N (2010) Basement membrane components are key players in specialized extracellular matrices. Cell Mol Life Sci 67:2879–2895. https://doi.org/10.1007/s00018-010-0367-x
22. Masereeuw R, Mutsaers HAM, Toyohara T, et al (2014) The Kidney and Uremic Toxin Removal: Glomerulus or Tubule? Semin Nephrol 34:191–208. https://doi.org/10.1016/j.semnephrol.2014.02.010
23. Bonventre J V, Yang L (2011) Cellular pathophysiology of ischemic acute kidney injury. J Clin Invest 121:4210–4221. https://doi.org/10.1172/JCI45161
24. David HH (2003) US20030119184 - Bioartificial filtration device for filtering blood to mimic kidney function
25. Zink D, Zay YO (2015) US20150076066 - Bioreactor unit for use in bioartificial kidney device
26. Akira S, Aung YT (2009) US20090209019 - Bioartificial Renal Tubule
27. Zhang H, Tasnim F, Ying JY, Zink D (2009) The impact of extracellular matrix coatings on the performance of human renal cells applied in bioartificial kidneys. Biomaterials 30:2899–2911. https://doi.org/10.1016/J.BIOMATERIALS.2009.01.046
28. Kirk A, Campbell S, Bass P, et al (2010) Differential expression of claudin tight junction proteins in the human cortical nephron. Nephrol Dial Transplant 25:2107–19. https://doi.org/10.1093/ndt/gfq006
29. Kwon O, Nelson WJ, Sibley R, et al (1998) Backleak, tight junctions, and cell- cell adhesion in postischemic injury to the renal allograft. J Clin Invest 101:2054–64. https://doi.org/10.1172/JCI772
30. Cebotari S, Tudorache I, Jaekel T, et al (2010) Detergent Decellularization of Heart Valves for Tissue Engineering: Toxicological Effects of Residual Detergents on Human Endothelial Cells. Artif Organs 34:206–210. https://doi.org/10.1111/j.1525-1594.2009.00796.x
31. Pitt-Rivers R, Impiombato FS (1968) The binding of sodium dodecyl sulphate to various proteins. Biochem J 109:825–30. https://doi.org/10.1042/bj1090825
32. Martins A, Reis RL, Neves NM (2008) Electrospinning: processing technique for tissue engineering scaffolding. Int Mater Rev 53:257–274. https://doi.org/10.1179/174328008X353547

33. Wen X, Wang Y, Guo Z, et al (2015) Cauda equina-derived extracellular matrix for fabrication of nanostructured hybrid scaffolds applied to neural tissue engineering. Tissue Eng Part A 21:1095–105. https://doi.org/10.1089/ten.TEA.2014.0173
34. Alves da Silva M, Martins A, Costa-Pinto AR, et al (2017) Electrospun Nanofibrous Meshes Cultured With Wharton's Jelly Stem Cell: An Alternative for Cartilage Regeneration, Without the Need of Growth Factors. Biotechnol J 12:1700073. https://doi.org/10.1002/biot.201700073
35. Puppi D, Piras AM, Chiellini F, et al (2011) Optimized electro- and wet-spinning techniques for the production of polymeric fibrous scaffolds loaded with bisphosphonate and hydroxyapatite. J Tissue Eng Regen Med 5:253–263. https://doi.org/10.1002/term.310
36. Guimarães A, Martins A, Pinho ED, et al (2010) Solving cell infiltration limitations of electrospun nanofiber meshes for tissue engineering applications. Nanomedicine 5:539–554. https://doi.org/10.2217/nnm.10.31
37. Moura D, Souza MT, Liverani L, et al (2017) Development of a bioactive glass-polymer composite for wound healing applications. Mater Sci Eng C 76:224–232. https://doi.org/10.1016/j.msec.2017.03.037
38. Milo R (2013) What is the total number of protein molecules per cell volume? A call to rethink some published values. Bioessays 35:1050–5. https://doi.org/10.1002/bies.201300066
39. Kalluri R, Weinberg RA (2009) The basics of epithelial-mesenchymal transition. J Clin Invest 119:1420–8. https://doi.org/10.1172/JCI39104
40. Kim S, Kim G-H (2017) Roles of claudin-2, ZO-1 and occludin in leaky HK-2 cells. PLoS One 12:e0189221. https://doi.org/10.1371/journal.pone.0189221
41. Denker BM, Sabath E (2011) The biology of epithelial cell tight junctions in the kidney. J Am Soc Nephrol 22:622–5. https://doi.org/10.1681/ASN.2010090922
42. Aydin S, Signorelli S, Lechleitner T, et al (2008) Influence of microvascular endothelial cells on transcriptional regulation of proximal tubular epithelial cells. Am J Physiol Physiol 294:C543–C554. https://doi.org/10.1152/ajpcell.00307.2007
43. Sakolish CM, Mahler GJ (2017) A novel microfluidic device to model the human proximal tubule and glomerulus. RSC Adv 7:4216–4225. https://doi.org/10.1039/C6RA25641D
44. Jansen J, De Napoli IE, Fedecostante M, et al (2015) Human proximal tubule epithelial cells cultured on hollow fibers: living membranes that actively transport organic cations. Sci Rep 5:16702. https://doi.org/10.1038/srep16702

## III-7. SUPPLEMENTARY INFORMATION

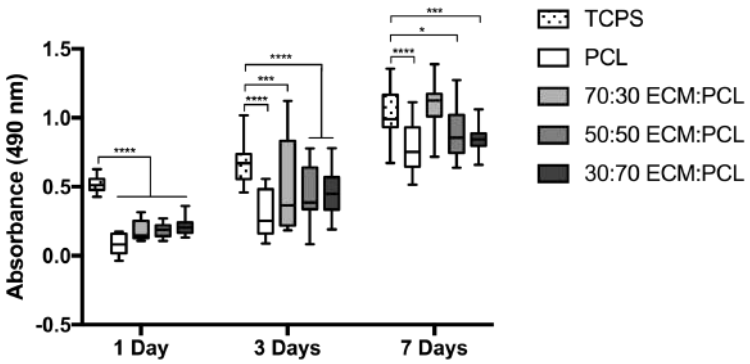


Figure S III-1 – Viability of the HK-2 cells measured by MTS assay. Statistical significance demonstrated only against TCPS. n=9. *$p < 0.05$, ***$p < 0.001$, ****$p < 0.0001$.

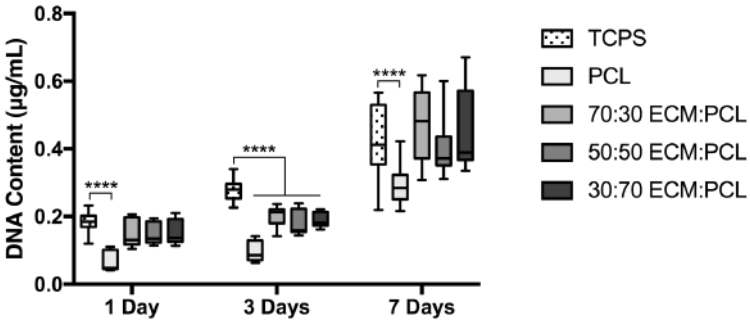


Figure S III-2 – Cell proliferation measured by quantification of DNA with Picogreen kit. Statistical significance demonstrated only against TCPS. n=9. ****$p < 0.0001$.

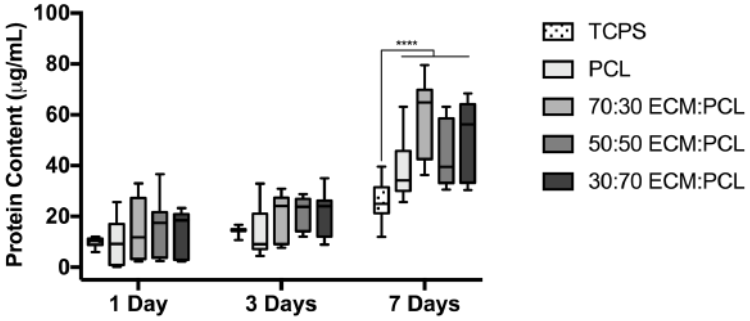


Figure S III-3 – Protein intracellular content on HK-2 cells. Statistical significance demonstrated only against TCPS. n=9. ****$p < 0.0001$.

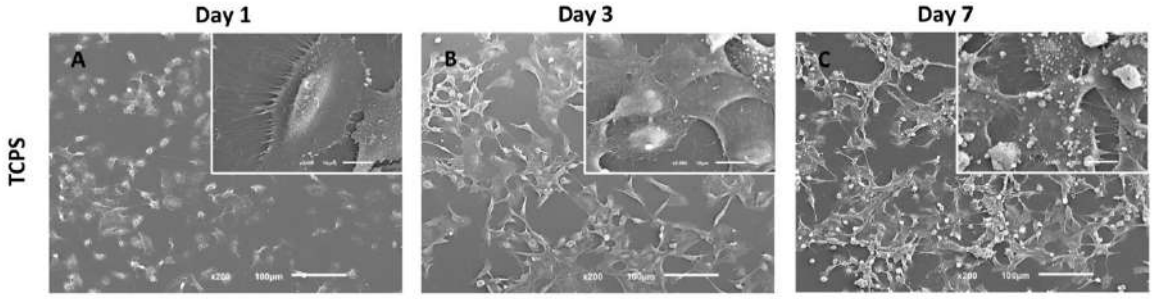


Figure S III-4 – SEM micrographs of HK-2 cells seeded on TCPS. Left, middle and right row represent cells after 1, 3 and 7 days of culture, respectively. Scale bar: 100 μm for higher magnification images, 10 μm for the insert images.

# Chapter IV

# Co-cultures of renal progenitors and endothelial cells on kidney decellularized matrices replicate the renal tubular environment *in vitro*

# Chapter IV

## Co-cultures of renal progenitors and endothelial cells on kidney decellularized matrices replicate the renal tubular environment *in vitro* ‡


### ABSTRACT

Aim: Herein we propose creating a bilayer tubular kidney *in vitro* model. It is hypothesized that membranes composed of decellularized porcine kidney extracellular matrix are valid substitutes of the tubular basement membrane by mimicking the physiological relevance of the *in vivo* environment and disease phenotypes. Methods: Extracellular matrix was obtained from decellularized porcine kidneys. After processing by lyophilization and milling, it was dissolved in an organic solvent and blended with poly(caprolactone). Porous membranes were obtained by electrospinning and seeded with human primary renal progenitor cells to evaluate phenotypic alterations. To create a bilayer model of the *in vivo* tubule, the same cells were differentiated into epithelial tubular cells and co-cultured with endothelial cells in opposite sites. Results: Our results demonstrate increasing metabolic activity, proliferation and total protein content of renal progenitors over time. We confirmed the expression of several genes encoding epithelial transport proteins and we could also detect tubular-specific proteins by immunofluorescence stainings. Functional and transport assays were performed trough the bilayer by quantifying both human serum albumin uptake and inulin leakage. Furthermore, we validated the chemical modulation of nephrotoxicity on this epithelium-endothelium model by cisplatin exposure. Conclusion: The use of decellularized matrices in combination with primary renal cells was shown to be a valuable tool for modeling renal function and disease *in vitro*. We successfully validated our hypothesis by replicating the physiological conditions of an *in vitro* tubular bilayer model. The developed system may contribute significantly for the future investigation of advanced therapies for kidney diseases.


‡ This chapter is based on the following publication:

**Sobreiro-Almeida, Rita;** Melica, Maria Elena; Lasagni, Laura; Romagnani, Paola; Neves, Nuno M. Co-cultures of renal progenitors and endothelial cells on kidney decellularized matrices replicate the renal tubular environment *in vitro*. *Acta Physiologica*, 230(1):e13491, doi: 10.1111/apha.13491, 2020;

.

## IV-1. INTRODUCTION

The human kidney filters nearly 2 L of primary urine from plasma every day, in which millions of nephrons work together to regulate the complex process of filtration. As part of the nephron unit, the tubules are mainly responsible to maintain normal physiological homeostasis and electrolyte balance by regulating the volume and reabsorption of solutes. [1] The epithelial cells that compose the cellular barrier of the tubule express several ion and water channels as well as transporters which can modify the composition of the filtrate according to the physiological needs.[2] This vital function makes the tubules highly susceptible to damage induced from drugs, toxins and bloodborne diseases, which frequently lead to cell death and tubular dysfunction.[3, 4]

The ability to develop *in vitro* models that can recapitulate the renal tubular environment would be of great interest for therapeutic development and discovery but also to understand mechanisms underlying kidney pathology and homeostasis. Tubular cells are attached to an underlying basement membrane (BM), composed by typical elements of the extracellular matrix (ECM), which when dysregulated can affect cell attachment, proliferation, differentiation and migration. Indeed, changes on the composition and thickness of the BM are linked with pathological conditions, such as inflammatory processes, renal fibrosis and epithelial-to-mesenchymal transitions.[5] Major efforts have been accomplished in this area, namely the creation of functional kidney microtissues,[6] microphysiological fluidic kidney systems,[7, 8] or even strategies to mimic the organic cation transport.[9] Although these systems were developed with the main aim of preclinical screening, they are far from replicating the *in vivo* contact with the BM and the cellular crosstalk between endothelial and epithelial cells, both crucial factors on the filtration process of the kidney.[1] The endothelium and/or peritubular capillaries are in close proximity to the tubular epithelium, not only when considering physiological processes, but also under pathophysiological conditions.[10] Several studies have demonstrated the importance of the endothelium for a normal kidney function. A complex communication network between epithelial cells composing the tubule and endothelial cells of the vasculature has already been demonstrated to influence solute transport, angiogenesis and enriched expression of specific genes.[10–13] These co-culture systems proved not only the importance of having endothelial cells on an *in vitro* model, but also the importance of recapitulating the BM permeability and constitution. Although in the past few years huge advances were reported in co-culture systems, their standardization is still difficult. Not only these systems face the problem of epithelial dedifferentiation but also they are composed by synthetic materials which

frequently fail to reproduce the *in vivo* structure and function, being the majority of times coated with different ECM proteins.[14, 15]

Previously, we proposed the use of electrospun membranes combining poly(caprolactone) (PCL) and decellularized porcine kidney ECM (1:1) as valuable replicas of renal basement membranes. We have demonstrated their value by comparing proximal tubular cellular performance on these meshes with bare PCL electrospun meshes.[16] Herein, we propose a study focused on the cellular performance with renal progenitor cells and a second study focused on establishing an *in vitro* bilayer model to further validate our initial hypothesis. We hypothesize that this membrane would be extremely valuable to recapitulate the physiological environment, in such a way that would provide cues to renal progenitor cells (hRPCs) to differentiate and form a functional epithelial monolayer. These cells represent a subset of multipotent progenitors present in the Bowman's capsule, which can be purified from cultured capsulated glomeruli. They were already shown to differentiate into several lineages including osteogenic cells, adipocytes and cells that exhibit phenotypic and functional features of neuronal cells.[17] Additionally, their differentiation potential was further extended for proximal and/or distal tubule cells and podocytes, upon culture with specific supplementation.[18] Indeed, hRPCs were demonstrated to be involved in the regeneration of different portions of the nephron after injury.[19] Accordingly, we hypothesize that we can achieve tubular differentiation from hRPCs without supplementation on our membranes. Additionally, we focused our study on demonstrating transport properties and induction of disease phenotypes on a bilayer model, composed of epithelial and endothelial cells, mimicking the organization of an *in vivo* tubule. Considering the findings that we have found, these models are proposed as valuable tools for integrating dialysis equipment's or bioartificial kidneys in the future.

## IV-2. Materials and Methods

### IV-2.1. Experimental Design

Kidneys were decellularized and the matrix was further processed to be used in electrospinning, after which and membranes of 1:1 decellularized kidney ECM (dKECM) to poly(caprolactone) (PCL) were obtained and sterilized. A brief scheme of the processing steps is represented in Figure IV-1.

For the cell culture assays, human renal progenitor cells (hRPCs) were used to validate the model. We applied two separate and yet complementary approaches; initially, hRPCs were assessed for their

spontaneous differentiation into cells of the tubular lineage. We compared how these cells behaved when in mono or co-culture with human umbilical vein endothelial cells (HUVECs, Figure IV-1a). In a parallel study, the same cells were stimulated to differentiate in 2D substrates into renal proximal tubular epithelial cells (hRPTECs) and were again co-cultured, each cell type in one side of the membrane, creating a bilayer model of an *in vivo* tubule (Figure IV-1b).

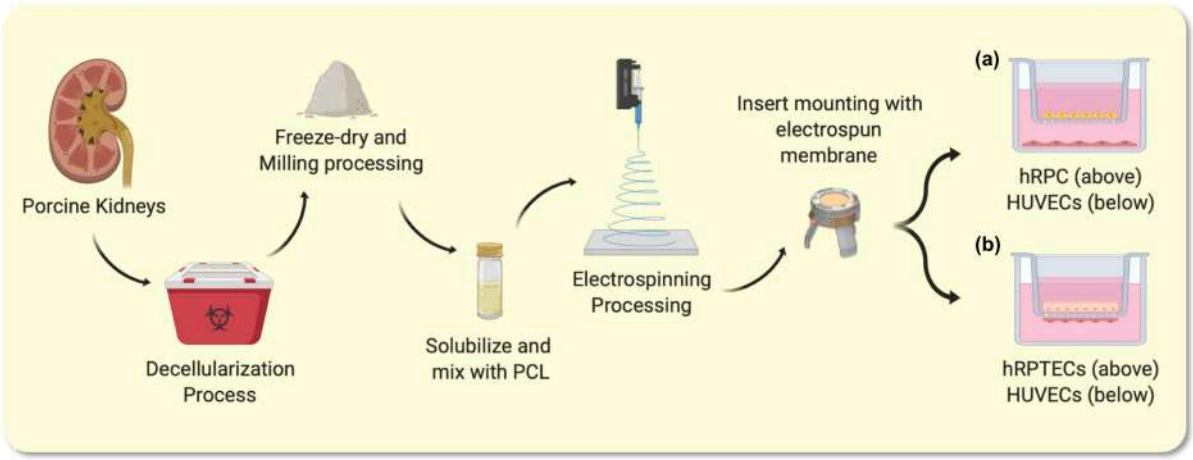


Figure IV-1 - Schematic representation of decellularization process and membranes preparation procedure. Porcine kidneys are obtained on a local butcher. They were chopped and decellularized in different detergent solutions before being processed by freeze drying and with a cryogenic mill to obtain a powder. In order to have a suitable solution for electrospinning process, the powdered matrix is blended with a PCL solution at 1:1 ratio in an organic solvent. After the production of the membranes, these are mounted in 24-well inserts and sterilized. In this work, we developed two kinds of cultures (a) to evaluate hRPCs interaction with HUVECs and (b) a bilayer model composed of differentiated epithelial tubular cells (hRPTECs) and HUVECs to better mimic the *in vivo* tubulointerstitial environment.

## IV-2.2. Processing of decellularized kidney electrospun membranes

Porcine kidneys were obtained from a local slaughterhouse. The decellularized matrix was processed as previously described,[16] with minor modifications. Briefly, kidney portions were immersed in a solution of 1 % SDS before being changed to another solution of 1 % Triton X-100. The solutions were placed in an orbital shaker and changed twice a day. After the decellularization process, the matrix was washed, freeze-dried and reduced to powder. The powdered matrix was solubilized in HFIP (1,1,1,3,3,3-Hexafluoro-2-propanol ≥99 %) (Sigma-Aldrich) at a concentration of 100 mg $mL^{-1}$. Polycaprolactone (PCL, 80 kDa, Sigma Aldrich) was dissolved in the same reagent at a concentration on 15 % (w/v). Both solutions were mixed 1:1 and electrospinning process was performed as previously described.[16] The membranes were cut in squares and placed on 24-well inserts (CellCrown™) before being sterilized by immersion in 70 % ethanol and 30 min exposure to UV on each insert side.

### IV-2.3. Biochemical and immunohistochemistry analysis of the dKECM

Samples were fixed for 30 min with 10 % neutral buffered formalin before being embedded in OCT compound (Bio-optica). After this, they were snap-freezed in liquid nitrogen and cut into 10 µm sections using a cryostat. Sections were incubated with primary antibodies for immunofluorescent analysis as follows: anti-Collagen IV (1:100; ab6586), anti-Fibronectin (1:100, ab2413) and anti-Collagen I (1:40, ab765). Secondary antibody Alexa Fluor 488 (1:500) was incubated with 4,6-diamidino-2-phenylindole (1:1000, DAPI) for 1 h at RT before being analyzed under a confocal microscope.

Total protein content was quantified with Pierce™ Coomassie (Bradford) Protein Assay Kit (Thermo Scientific), according to the manufacturer´s instructions. After sample incubation with the substrate, absorbance was measured at 562 nm in a microplate reader. The concentration of total protein in the samples was extrapolated using a standard curve of bovine serum albumin.

### IV-2.4. DKECM electrospun membranes morphological and structural characterization

The morphology of the membranes was observed by scanning electron microscope (SEM, JSM-6010 LV, JEOL). Samples were sputter coated with gold prior to analysis and micrographs were obtained using an accelerating voltage of 10 kV. The fiber average diameter was statistically calculated using a computed image analyzer (ImageJ) by measuring at least 200 fibers randomly in 3 samples from different fabrication batches.

Membrane porosity was determined as previously described.[20] A liquid displacement technique was used a porosity was calculated following equation 1, where $V_1$ is the initial liquid volume, $V_2$ is the volume after soaking the membrane and all the pores are filled and $V_3$ is the volume after membrane soaking and removal. Membrane cross sections were obtained by immersing fibers in liquid nitrogen and cutting immediately do avoid deformation. Average membrane thicknesses were calculated from SEM micrographs of cross sections with ImageJ software.

$$Porosity\ (\%) = \frac{V_1 - V_3}{V_2 - V_3} \times 100 \qquad \text{Equation 1}$$

To determine weight loss and water uptake of the membranes, these were initially weighted ($m_i$) and soaked in an isotonic solution of sodium chloride (Sigma Aldrich). After, membranes were incubated

at 37 °C for 30 days. These conditions were optimized to simulate the human body environment. After known periods of time, membranes were weighted in their wet state ($m_w$) and the percentage of water uptake was calculated using the equation 2. Membranes were then placed on the incubator for another hour to dry before being weighted again ($m_f$). Weight loss percentage was calculated using equation 3.

$$Water\ uptake\ (\%) = \frac{m_w - m_i}{m_i} \times 100 \qquad \text{Equation 2}$$

$$Weight\ loss\ (\%) = \frac{m_i - m_f}{m_i} \times 100 \qquad \text{Equation 3}$$

### IV-2.5. Isolation and characterization of human renal progenitor cells (hRPC)

Human kidney fragments were obtained in agreement with the Ethical Committee on human experimentation of the Azienda Ospedaliero-Universitaria Careggi, Florence, Italy. All subjects gave their informed consent for inclusion before they participated in the study. The study was conducted in accordance with the Declaration of Helsinki, and the protocol was approved by the Ethics Committee on Human Experimentation of the Azienda Ospedaliero-Universitaria Careggi, Florence, Italy (project identification code 2015/0009082 from 25/03/2015). Human RPCs were obtained and cultured as previously described with minor modifications.[17] Briefly, the cortex was minced before proceeding to an enzymatic digestion with collagenase solution type IV 750 U $mL^{-1}$ (Sigma Aldrich) for 45 min at 37 °C. After digestion, the solution was sieved through graded mesh screens (60 and 80 mesh). The cellular suspension was collected, washed and plated on petri dish containing complete medium. The medium is composed by Microvascular Endothelial Cell Growth Medium (EGM™-MV, Lonza) supplemented with 20 % HyClone™ Fetal Bovine Serum (FBS, GE Healthcare). After 4 to 5 days of culture, cells that adhered to the plate were subcultured. Cultures were checked for simultaneous expression of CD133 and CD24 by flow cytometry at different passages, according to previously published methods for characterizing hRPCs.[17]

### IV-2.6. Renal endothelium-epithelium mono and bilayer seeding

HRPCs were seeded on the membranes at a density of $3\times10^3$ cells/insert in endothelial basal medium (EBM, Lonza) supplemented with 10 % FBS (HyClone™, GE Healthcare) and expanded for 21

days. For co-culture studies, primary HUVECs (Cascade Biologics, Inc.) were plated at a density of $7.5\times10^{3}$ cells/well in the day before hRPCs were seeded. The cell seeding concentration was optimized to obtain a confluent monoculture of hRPCs at the end of the culture time.

For cell culture studies with hRPTECs, differentiation on tissue culture plastic was performed before cell seeding on the inserts. Briefly, hRPCs were cultured in Renal Epithelial Cell Growth Medium (REGM™, Lonza) supplemented with hepatocyte growth factor (HGF, Peprotech) at a concentration of 50 ng $mL^{-1}$. HUVECs were seeded on inverted inserts at a density of $2\times10^{5}$ cells $mL^{-1}$ and allowed to attach 3 h before being reverted. According to previously published reports, hRPCs take 30 days to differentiate into hRPTECs, when in specific cell culture conditions.[19] Therefore, hRPCs with 23 days of differentiation supplementation were cultured at a density of $1.3\times10^{5}$ cells $mL^{-1}$ on the reverse side of the HUVECs insert for 7 days. The medium consisted of a mixture of HGF-supplemented REGM with EBM plus 10 % of FBS.

### IV-2.7. Evaluation of cellular viability, proliferation and morphology

At 7, 14 and 21 days of culture, the viability of hRPCs was assessed using alamarBlue® (BioRad) assay. Membranes with seeded hRPCs were removed from the inserts, washed with DPBS and placed on new 24 well-plates with fresh cell medium containing 10 % of alamarBlue reagent. After an incubation period of 4 h at 37 °C, the supernatant was used to determine the fluorescence intensity in a microplate reader (excitation: 530/25 nm; emission: 590/25 nm). To evaluate hRPCs proliferation over time, dsDNA quantification was performed. Briefly, after the viability assay, constructs were rinsed in DPBS to release the alamarBlue dye. After, specimens were immersed in Milli-Q water and cells were lysed by thermal and osmotic shock. The resulting supernatant was used for the quantification with Picogreen dsDNA Kit. The fluorescence of each specimen was measured using a microplate reader (excitation: 485 nm; emission: 528 nm). The DNA concentration for each sample was calculated using a standard curve. The same supernatants were used to perform protein content measurements with Micro BCA protein assay kit (ThermoFisher) according to the manufacturer's instructions. After 2 h of sample incubation with the substrate, absorbance was measured at 562 nm in a microplate reader. The concentration of total protein in the samples was calculated using a standard curve of Bovine Serum Albumin.

To analyze cellular morphology and the formation of a monolayer, after 21 days of culture, membranes were washed with DPBS and fixed in 2.5 % glutaraldehyde (Sigma Aldrich) for 1 h at 4 °C. After the fixation step, they were washed again and dehydrated through the exposure to a gradient of

alcohol concentrations. Samples were sputter coated with gold prior to analysis and micrographs were obtained using a scanning electron microscope (SEM, JSM-6010 LV, JEOL).

### IV-2.8. Immunofluorescence of renal epithelial-related proteins

Both hRPCs and hRPTECs were fluorescently labeled with antibodies directed against markers for differentiated epithelia and transport proteins. Briefly, cell-loaded membranes were fixed with 10 % neutral buffered formalin for 1h at 4 °C and then washed in PBS. The blocking step was performed for 30 min incubating the membranes in 3 % bovine serum albumin (BSA, Sigma Aldrich) solution. Primary antibodies were diluted in blocking solution and incubated overnight at 4 °C. Epithelial protein analysis was evaluated with antibodies against the sodium-dependent glucose transporter (SGLT2, abcam, 1:30), aquaporin-1 (AQP-1, abcam, 1:100), chloride channel-Ka (CLC-NKA, Santa Cruz Biotechnology, 1:25) and Na/Cl cotransporter (NCC, Santa Cruz Biotechnology, 1:25). Samples were washed in PBS and incubated with fluorescent labeled secondary antibodies Alexa Fluor 488 against the specific primary antibody species at 1:500 concentration. DAPI (Sigma Aldrich, 1:1000) was incubated along with the secondary antibody. After several rinses in PBS, constructs were mounted with VECTASHIELD® (Vector Laboratories) and analyzed under Leica SP5 AOBS confocal microscope (Leica, Wetzlar, Germany) equipped with a Chameleon Ultra-II two-photon laser (Coherent, Milan, Italy). Images were recorded digitally and further processed using LASX software (Leica).

### IV-2.9. Real-time quantitative polymerase chain reaction (RT-PCR) of tubular-related genes

Total RNA was extracted using RNeasy Microkit (Qiagen) and quantified using a Nanodrop spectrophotometer (ThermoFisher Scientific). Briefly, after 7, 14 and 21 days, membranes with attached hRPCs in monoculture or in co-culture systems were removed from the inserts and immersed in buffer RTL (acquired from the kit) containing β-mercaptoethanol for efficient cell lysis. After extraction, 52 ng of RNA was retrotranscribed using TaqMan™ Reverse Transcription Reagents (ThermoFisher) following manufacturer's instructions, in a final volume of 17 µL. TaqMan RT-PCR was performed as previously described using a 7900HT Real Time PCR System (Applied Biosystems).[21] Na/K/Cl cotransporter (*SLC12A1*), amino acid transport protein (*SLC3A1*), γ-glutamyltranspeptidase (*GGT1*) and Na/H exchanger (*SLC9A3*) quantification was performed using commercially available Assay on Demand kits (Applied Biosystems). Fold expression (FE) was determined using the equation $FE = 2^{-\Delta\Delta Ct}$, where

$\Delta$Ct = Ct gene of interest – Ct housekeeping gene, glyceraldehyde-3-phosphate dehydrogenase (GAPDH), and $\Delta\Delta$Ct = Ct sample of interest – Ct control sample, which was considered the gene expression level at the seeding day.

### IV-2.10. Paracellular permeability and albumin reabsorption studies

At day 7 of co-culture of hRPTECs and HUVECs, 400 µL of media containing 25 µg $mL^{-1}$ of fluorescein isothiocyanate (FITC)-conjugated inulin (Sigma Aldrich) was applied to the top compartment, while 600 µL of medium was applied to the bottom compartment. Cells were incubated at 37 °C for 5 h. Every hour, samples were drawn from both compartments and fluorescence intensity was measured in a microplate reader (excitation: 485/25 nm; emission: 530/25 nm). For albumin uptake assay, FITC-conjugated human serum albumin (HSA) was applied to the top compartment at a concentration of 40 µg $mL^{-1}$ and the initial fluorescence was measured in the total volume of the well. After 5 h, inserts were drawn from the wells and the remaining concentration of HSA in the well was measured as above mentioned. The leakage and absorption studies were calculated as the percentage of the initial concentration.

### IV-2.11. Nephrotoxicity assessment

Cisplatin (Sigma Aldrich) was applied to the top compartment of confluent monocultures of hRPTEC and to co-cultures with HUVEC. 0, 50, 100 and 150 µM of cisplatin in REGM complete medium was added to the inserts after 7 days of cell culture. The range of values was selected according to previously published papers which also performed nephrotoxicity assays,[22, 23] with the main aim of evaluating cell response to the increasing concentration of cisplatin. Cellular viability was assessed by alamarBlue as previously described and presented as a percentage of control viability (the inserts that were subjected to 0 µM of cisplatin). To further evaluate cisplatin effect, live/dead assay with Calcein AM and propidium iodide (PI, both Sigma Aldrich) and immunofluorescence of DAPI and Phalloidin (ThermoFisher) were performed. The fluorescent dyes were incubated with the constructs at a concentration of 1 µg $mL^{-1}$ for PI and 2 µg $mL^{-1}$ for Calcein AM in DPBS for 30 min at 37 °C. Cell fixation and immunofluorescence staining was performed as previously described. The cell-loaded membranes were visualized using a confocal microscope (above mentioned).

### IV-2.12. Statistical analysis

Statistical analyses were performed with GraphPad Prism 8 (GraphPad Software, California, USA). Data were expressed as means ± standard deviation of experiments. Differences between groups were analyzed by unpaired t test or two-way analysis of variance (ANOVA) in case of experiments conducted over time, using Tukey test for post hoc assessments of the differences between samples. Statistical significance was defined as $p < 0.05$.

## IV-3. RESULTS

### IV-3.1. dKECM and dKECM-derived membrane characterization

To confirm that processing steps were not causing adverse effects on the protein content of kidney ECM, collagen content was assessed by immunofluorescence (IF) methods, being the major component of kidney ECM.[24] Fibronectin was additionally assessed as a well-known protein which mediates cell-substratum adhesion.[25] Preservation of collagen I, collagen IV and fibronectin was confirmed by green staining on the micrographs after sterilization process (Figure IV-2a, b and c respectively). No differences in fluorescence intensity were found between these micrographs and the ones obtained before sterilization process (data not shown), which confirms protein preservation after processing steps. Nuclear staining was also performed on IF sections by DAPI, although not visible on the micrographs, confirming effective removal of cellular content. Moreover, biochemical quantification of total protein content was performed (Figure IV-2d) and the difference on the quantity of protein per mg was found no significant after sterilization (with a mean of ~328 and ~261 $\mu g\ mL^{-1}$ for non-sterile and sterile conditions, respectively).

SEM micrographs of the electrospun meshes revealed a fibrous surface with randomly oriented fibers (Figure IV-2e and f). These micrographs reveal the nanostructure of these fibers, which present an average diameter of 0.242 ± 0.1 μm, following a normal distribution (Figure IV-2g). These nanofibers will potentially aid on cellular adhesion without compromising cellular proliferation, because of their large surface area. Thickness was measured from SEM micrographs by performing a cross section and placing the membrane at a 90° angle. The measured thickness was 22 ± 5.19 μm, which will allow for physical separation of hRPCs and endothelial cells, while maintaining the communication between the two cell types. Porosity measurements revealed the percentage of porous space existent in the membrane. We calculated a porosity value of 97 ± 1.28 %, which allows for the selective passage of solutes. These

models also require the maintenance of the ultrastructure and very low percentage of weight loss, which we tested during a 30-day degradation assay, where only ~3 % of the mass was lost, proving that our membrane has a strong ECM crosslink and also a good blend between decellularized matrix and PCL. This enables performing long-term studies with the membrane, being confident that its properties are not lost. Additionally, the membranes shown having a very high water uptake capacity of nearly 499 %, which further corroborates the high porosity results. The nanometer scale fibers will support higher cell attachment, while providing a solid substrate with high porosity and water uptake, enabling solute, oxygen and growth factors passage between the two compartments of the co-culture system.

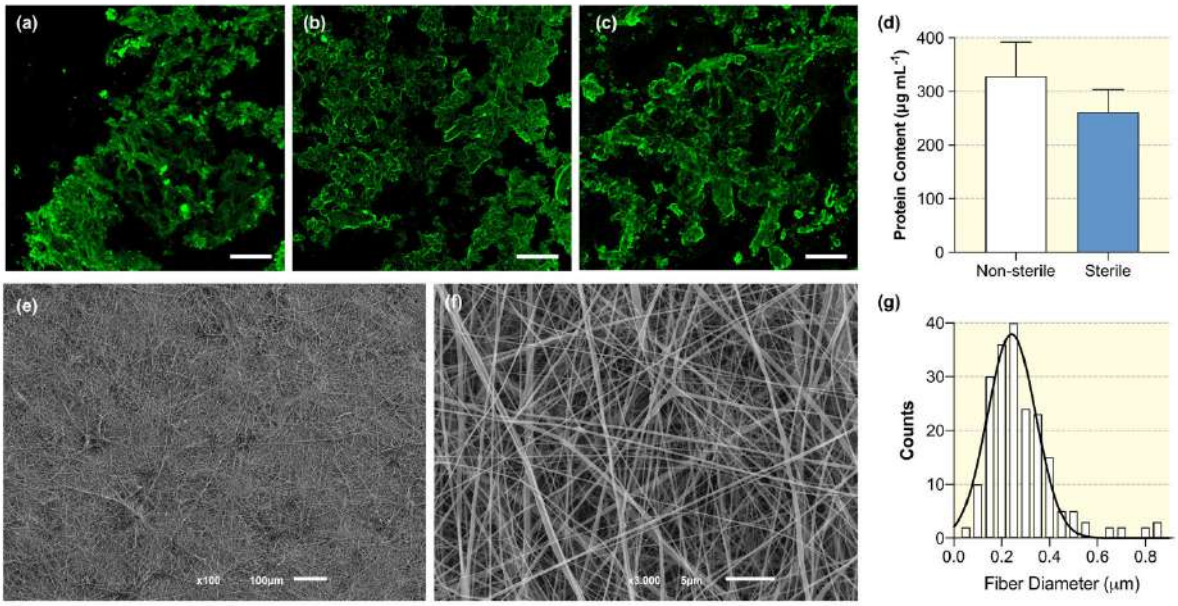


Figure IV-2 – dKECM characterization. (a-c) Immunofluorescence of ECM-related proteins (green) on cryosections of decellularized powder (a) Collagen type I, (b) Collagen type IV and (c) Fibronectin; (d) Protein quantification of decellularized powder demonstrates preservation of protein content after sterilization process; (e, f) SEM micrographs of the fibers at 100 and 3000x magnification, respectively; (g) Fiber diameter distribution was measured from 3 random sites on 3 different batches of electrospun membranes. Fibers are randomly distributed and present an average diameter of 0.242 µm. Scale bars: (a-c and e) 100 µm, (f) 5 µm.

### IV-3.2. Cellular behaviour of hRPCs on decellularized matrix membranes

Before all the experiments, hRPCs were characterized for simultaneous expression of CD133 and CD24 by flow cytometry. hRPCs between passages 1-3 from two different donors were used. All of the populations presented double positivity between 90-95 %, a signature preserved until passage 3. In this work, the construction of the bilayer model started with a simplistic study on our dKECM membranes where hRPCs growth and behavior was characterized in a culture time of 21 days. For that, it was necessary to physically separate the HUVECs from hRPCs. Figure IV-3 represents the results for cellular

metabolic activity (by alamarBlue assay – Figure IV-3a) and proliferation (by quantification of DNA content – Figure IV-3b) for mono and co-cultures. hRPCs were shown viable and proliferating in all timepoints when in contact with dKECM, with increasing values over time. Interestingly, we observed no statistical difference at 21 days of culture between mono and co-cultures for both assays. Indeed, results revealed that at 7 and 14 days, mean values and correspondent interquartile ranges were lower for co-cultures when comparing with monocultures, being this difference statistically relevant for DNA content measurements. These cells were already demonstrated to possess high clonogenic potential and self-renewal ability. In this work we demonstrate that this capacity is not influenced by the presence of the endothelial cells on the system. Indeed, the lower values observed in the first timepoints for co-cultures can be explained by the higher number of cells in the system for the same quantity of media. This allows higher proliferation in monocultures at early timepoints, reaching cell confluency faster. As a result, when comparing to co-cultures, a plateau phase is observed specially from day 14 to 21 for both assays in monocultures.

It was also important to evaluate how cells organize in this system. We previously observed the formation of a monolayer of epithelial cells on these membranes.[16] However, this work was a proof of concept performed with a cell line, having its limitations when mimicking an *in vivo* mechanism. Herein, we intended to assess if the hRPCs followed the same tendency as previously observed in monolayer cultures. Therefore, SEM was performed after 21 days on mono (Figure IV-3c and d) and co-cultures (Figure IV-3e and f). Contradicting the above-mentioned quantification results, we notice a huge difference on how cells organize in these membranes. In co-cultures, a homogenous and organized layer of cells was observed, with all cells oriented and resembling a natural epithelial monolayer. On the other hand, for monocultures, some parts of the fibers which compose the membranes can be seen, proving that cells were not able to form a homogeneous monolayer on this condition. Additionally, no cellular polarization is observed, being the cells present in a spiral and round-shaped morphology. In some sites, cells seem to be creating multilayered structures, which corroborates the higher values obtained for DNA content. Overall, these results demonstrate that hRPCs may be presenting a different phenotype when co-cultured with HUVECs.

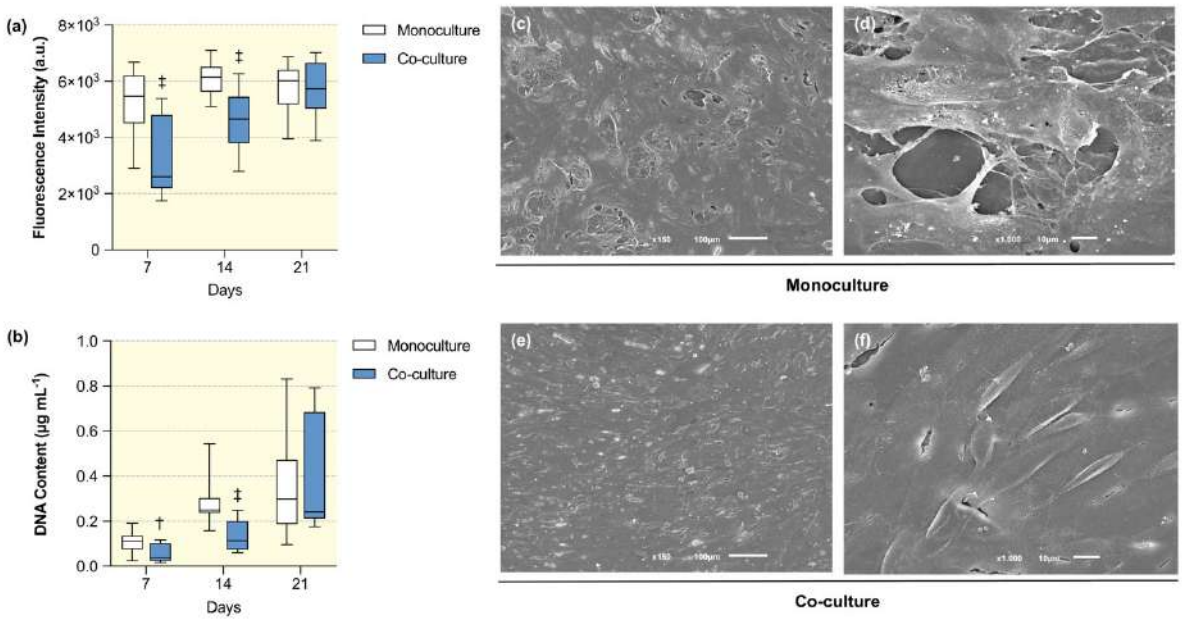


Figure IV-3 – Behavior of hRPC in contact with decellularized matrix membrane over 21 days. (a) Metabolic activity assay demonstrated by alamarBlue fluorescence after a 4 h incubation period. Monocultures are represented by white bars, whereas co-cultures are represented by blue bars. Monocultures present higher values at 7 and 14 days, whereas after 21 days mean values are equal on both; (b) Proliferation assay demonstrated by quantification of dsDNA over time. The same tendency as in viability assay is observed. Monocultures reach a plateau phase after 14 days culture, whereas in co-cultures values are increasing over time; †$p$<0.01, ‡$p$<0.001 vs. monoculture; (c-f) SEM was performed on fixed hRPCs to evaluate morphology and distribution after 21 days on the decellularized matrix membranes. Monocultures present a non-organized monolayer of cells, while in co-cultures hRPCs have organized themselves in a polarized manner, resembling natural epithelial organization and morphology. Scale bars: (c and e): 100 µm; (d and f): 10 µm.

## IV-3.3. Phenotypic characterization of hRPCs over time

To understand the response of progenitor cells to the created system, their phenotypic expression was characterized simultaneously by qPCR and IF stainings of relevant tubular markers. Gene expression was analyzed for genes encoding three different epithelial transporters: Na/K/Cl cotransporter (*SLC12A1*), amino acid transport protein (*SLC3A1*) and Na/H exchanger (*SLC9A3*). Not only the presence of transporters but also the recapitulation of physiological functions is important. For that, the expression γ-glutamyltranspeptidase (*GGT1*) was also measured, being this enzyme responsible for the supply of an adequate amount of glutathione, essential to maintain normal kidneys function.[7] As demonstrated (Figure IV-4a-d), all the genes are upregulated at day 21 for mono and co-cultures. We observe that the higher turnover happens essentially from day 14 to day 21 and that all of the genes follow the same tendency over time in mono and co-cultures. Indeed, between the two conditions, the only statistical difference happens in *GGT1* expression, which is probably due to variability between samples, since it is a unit fold difference between the two conditions. The higher fold expression happens on Na/K/Cl

cotransporter (with a mean of ~30-fold and ~21-fold expression for mono and co-cultures, respectively) and on Na/H exchanger (with a mean of ~13-fold and ~15-fold expression for mono and co-cultures, respectively). No differences in GAPDH expression were found with culture time and co-culture systems, validating our qPCR assay (Figure S IV-1b).

Afterwards, we used fluorescence microscopy to directly confirm the presence of tubular-related proteins in co-cultures (Figure IV-4e-h) and in monocultures (Figure S IV-1c-f). We could observe that the proximal tubular transporters aquaporin-1 (AQP-1) and sodium glucose transporter (SGLT2) have a more homogeneous fluorescent staining (Figure IV-4 e and f) when comparing to the distal convoluted tubule Na/Cl cotransporter (NCC) and the thick ascending limb chloride channel-Ka (CLC-NKA) (Figure IV-4g and h). Furthermore, by comparing with the immunofluorescent staining of the same transporters in monocultures (Figure S IV-1c-f), a much more diffuse staining is shown in all transporters, with several cells evidencing no signal. Indeed, no green staining is shown for CLC-NKA. We experienced difficulties in obtaining clear confocal images caused by the autofluorescence of the ECM that strongly absorbs DAPI stain.[16] Because of that, and since each membrane is different on its irregularity, we selected a representative site of the membrane in which we could obtain micrographs with sharper contrast. Protein content on the cell cultures was also measured over the 21 days of culture (Figure S IV-1a). No statistical differences were found between mono and co-cultures. However, an increase on protein content from day 7 to day 14 was observed for monocultures, which decreased after 21 days. Indeed, the same tendency was observed for the proliferation assay, and a plateau phase is observed from day 14 to 21 in monocultures. In contrast, proliferation in co-cultures was stable from day 14 to 21 and protein content values increased, a possible indicator of cellular differentiation.

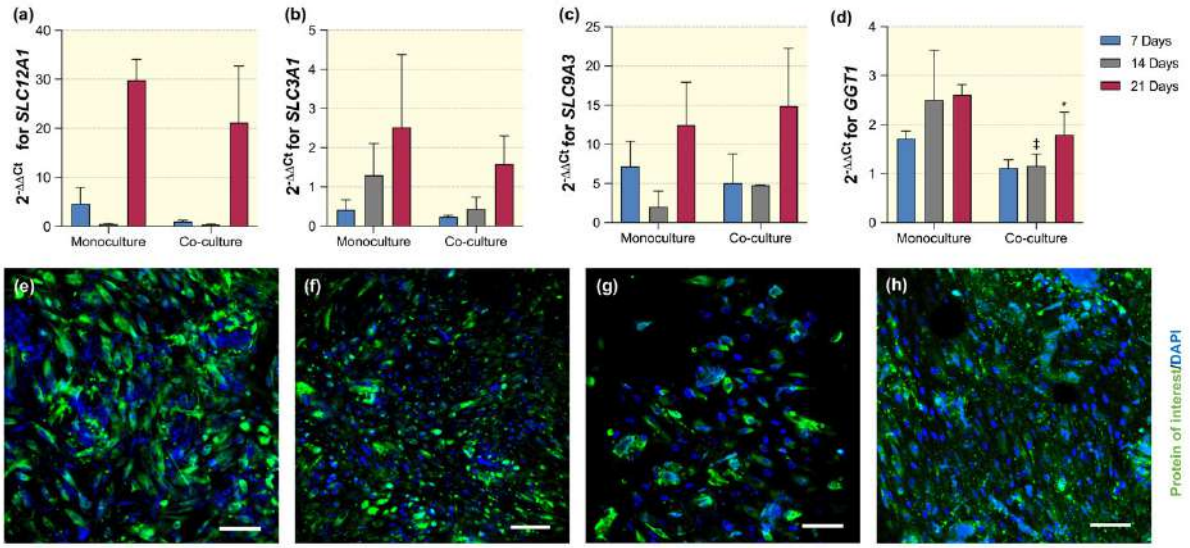


Figure IV-4 – Phenotypic characterization of hRPCs cultured on decellularized membranes. Gene expression of tubular related markers (a) *SCL12A1* (Na/K/Cl cotransporter), (b) *SLC3A1* (amino acid transport protein), (c) *SLC9A3* (Na/H exchanger) and (d) *GGT1* (γ-glutamyltranspeptidase); *$p$<0.05, ‡$p$<0.001 vs. monoculture; Tubular related markers protein assessment of (e) AQP-1 (aquaporin-1), (f) SGLT2 (sodium glucose transporter-2), (g) NCC (Na/Cl cotransporter) and (h) CLC-NKA (chloride channel-Ka) marked in green. Nuclei were stained with DAPI (blue). Scale bar: 100 μm. Both assays were performed simultaneously. All genes are upregulated at 21 days of culture with respect to their expression at day 0. Additionally, AQP-1 and SGLT2 had the most homogenous staining. These results suggest preferable differentiation of hRPCs on proximal tubular cells when in contact with the decellularized membranes.

## IV-3.4. Polarization and maturity assessment on proximal tubule cells

The ability of the RPTECs/HUVECs bilayer model to recapitulate renal function is highly dependent on the polarity and maturity of the seeded cells. For that, we have used imaging methods to analyze cellular organization and specific protein content after 7 days of bilayer seeding, corresponding to the 30$^{th}$ day of hRPCs differentiation stimulus. The previously detected phenomena for the hRPCs was also observed for hRPTECs, although the position of the endothelial cells had changed as well as the degree of differentiation of the hRPCs. As demonstrated in Figure IV-5a and b, epithelial morphology and distribution was highly influenced by the presence of the HUVECs, when comparing to monocultures (Figure S IV-2a and b). The endothelial cells enhanced the formation of a polarized monolayer of epithelial cells, typical of renal morphology.[14] SEM micrographs of higher magnification also revealed the formation of tight junctions connecting the neighboring cells (signaled by circles) and short microvilli at the apical surface (signaled by arrows), although much more present in co-cultures (Figure IV-5b), confirming epithelial cell polarization in this system. Indeed, we calculated the percentage of cells expressing microvilli on mono and co-cultures at 150× magnification SEM micrographs by ImageJ software (Figure IV-5d). The obtained values corroborate the above results, where ~83 % of the co-cultured

cells were found to present microvilli on their cell surface, contrasting with a value of ~21 % for monocultured hRPTECs.

After observing a positive effect of the presence of HUVECs on hRPTECs monolayer formation, we evaluated if in co-cultures we could observe signals of enhanced maturity by IF staining of tubular-related proteins. Similar to what was observed in hRPCs culture, we could notice higher fluorescence intensity signal and an overall more organized cellular distribution on co-cultures (Figure IV-5d-g) than for monocultures (Figure S IV-2c-f), which confirms the maturity observed in SEM micrographs. Also, fluorescence intensity differed for the different tubular segments, being much higher for proximal tubular markers in both conditions (AQP1 and SGLT2). However, in contrast to hRPCs culture, we could observe better fluorescence signal for NCC and CLC-NKA markers, indicative of simultaneous differentiation on epithelial cells of the distal tubule and the thick ascending limb of the loop of Henle. Overall these results suggest a good differentiation onto the renal tubular lineage on our co-culture system, with the presence of specialized cells of different segments of the tubule.

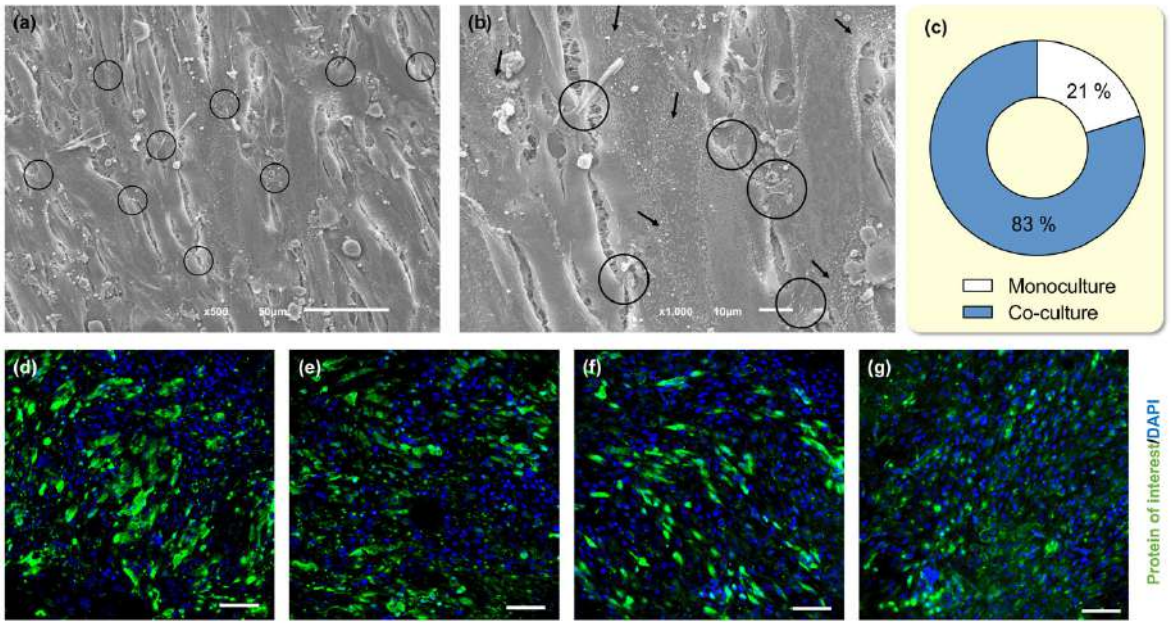


Figure IV-5 – Assessment of hRPTECs maturity and polarization after 7 days of bilayer assembling. (a-b) SEM micrographs of hRPTECs co-cultured with HUVECs. These cells organized in a homogenous oriented monolayer. Tight junctions characteristic of fully maturated epithelial tubular cells can be observed (indicated by circles) as well as microvilli (indicated by arrows). These micrographs suggest cellular polarization with the apical surface towards the top compartment, accurately mimicking tubular organization; (c) Percentage of cells expressing microvilli on mono (white) and co-cultures (blue). Values were obtained by cell counting on ImageJ software; (d-g) Tubular related markers protein assessment of (d) AQP1 (aquaporin-1), (e) SGLT2 (sodium glucose transporter-2), (f) NCC (Na/Cl cotransporter) and (g) CLC-NKA (chloride channel Ka) marked in green. Nuclei were stained with DAPI (blue). Results demonstrate the presence of proteins corresponding to several nephron segments on

hRPTECs, indicating successful maintenance of fully differentiated epithelial cells on our membranes. Scale bars: (a) 50 µm; (b) 10 µm; (d-g) 100 µm.

### IV-3.5. Characterization of proximal tubule physiological functions

To understand and characterize the developed system, we investigated Human Serum Albumin (HSA) and inulin transport (Figure IV-6a and b, respectively). These compounds were loaded into the upper compartment and their kinetics of diffusion was measured over time. We noticed that after 5 h, HSA uptake was more pronounced in co-cultures versus monocultures (~60 % versus ~40 % uptake). Inulin leakage was measured as an indicator of the barrier function. We noticed a slight increase of the leakage during the experiment both in mono and co-cultures, which was more pronounced in monocultures (~12 % versus ~8 % in co-cultures). However, this increase was expectable due to the over concentrated solution of inulin introduced in the system and the necessary manipulation of the system between the timepoints. It can also be observed that in all timepoints leakage values for monocultures are higher than in co-cultures, being statistically different at the 5 h timepoint. Comparing these results with the values obtained for non-seeded membranes, we noticed that there was no uptake of HSA, being the values around 0 % or negative, which could be explained by medium evaporation for the same amount of probe throughout the timepoints. Inulin leakage after 5 h was ~50 % for membranes with no cells (data not shown), which indicates that the membranes alone are also selectively permeable. The results obtained for cell-seeded membranes indicate selective reabsorption characteristics of our bilayer model.

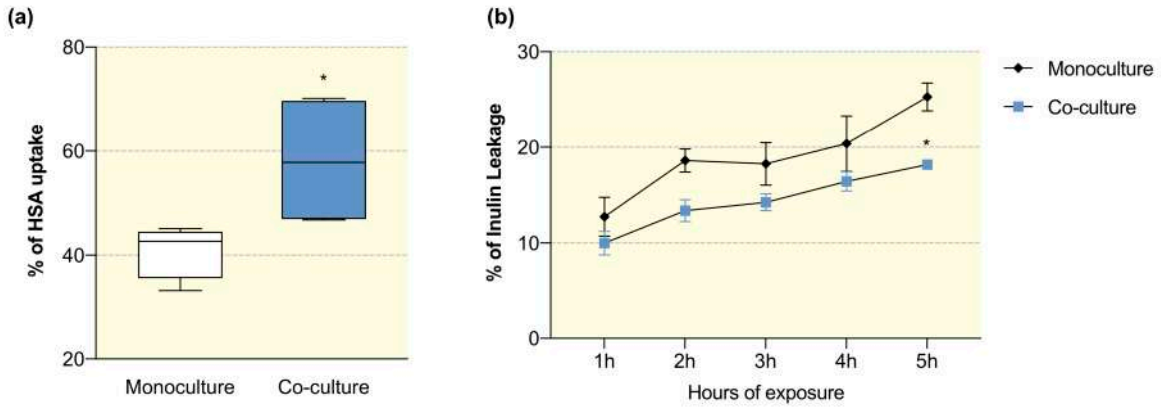


Figure IV-6 – Functional assays on the bilayer model. (a) Human serum albumin (HSA) uptake of hRPTECs cultured on mono or co-cultures. A solution of FITC-conjugated HSA with a known concentration was introduced on the top compartment. After 5 h, the concentration of the remaining compound was extrapolated from its fluorescence intensity; (b) Percentage of inulin leakage obtained for mono and co-cultures. FITC-conjugated inulin at a known concentration was introduced on the top compartment. Throughout the 5 h timepoints, the fluorescence intensity of the compound present on the bottom compartment

was measured; *$p$<0.05. These results are indicative of higher endocytic activity as well as higher resistance to compound leakage on epithelial cells cultured in the bilayer model, rather than in monocultures.

### IV-3.6. Model of drug-induced nephrotoxicity

A major goal in developing *in vitro* models is to have the recapitulation of physiological functions and disease phenotypes to better predict drug toxicity in humans. We therefore administered the known chemotherapeutic drug and nephrotoxin cisplatin in the top compartment of our co-culture system in different dosages. We evaluated cellular viability by live/dead assay in co-cultures (Figure IV-7a to d) and monocultures (Figure S IV-3a to d) and by MTS (Figure IV-7i), comparing to a control condition (0 µM of cisplatin). Phalloidin and DAPI staining was also performed on fixed mono (Figure S IV-3e to h) and co-cultures (Figure IV-7e to h). We could observe that, with the increasing concentration of cisplatin, cellular viability was reduced in ~80 % for monocultures and ~90 % for co-cultures when the higher concentration of the drug was administered. Although no significative differences were observed between both conditions, we could notice that co-cultured cells reacted quicker to the drug than in monocultures, which can be due to the higher abundance of active transporters mediating drug uptake. Live/dead micrographs indicate the abundance of dead cells by the internalization of propidium iodide. These micrographs corroborate the above MTS results, where a higher red and lower green fluorescence staining can be detected with the increasing concentration of cisplatin, comparing with the control condition (Figure IV-7a). Additionally, on monocultures (Figure S IV-3), some parts of the cellular body can still be distinguished even after the administration of a higher cisplatin dose, which does not happen in co-cultures, where scarce green staining appears. This is again indicative of a higher epithelial differentiation degree. However, the demonstrated green staining is often accompanied by red staining in the same cell, suggesting that cells may be entering apoptosis. Phalloidin and DAPI staining on fixed mono and co-cultures corroborates the above results, where lower red staining for phalloidin is observed with the increasing concentration of cisplatin.

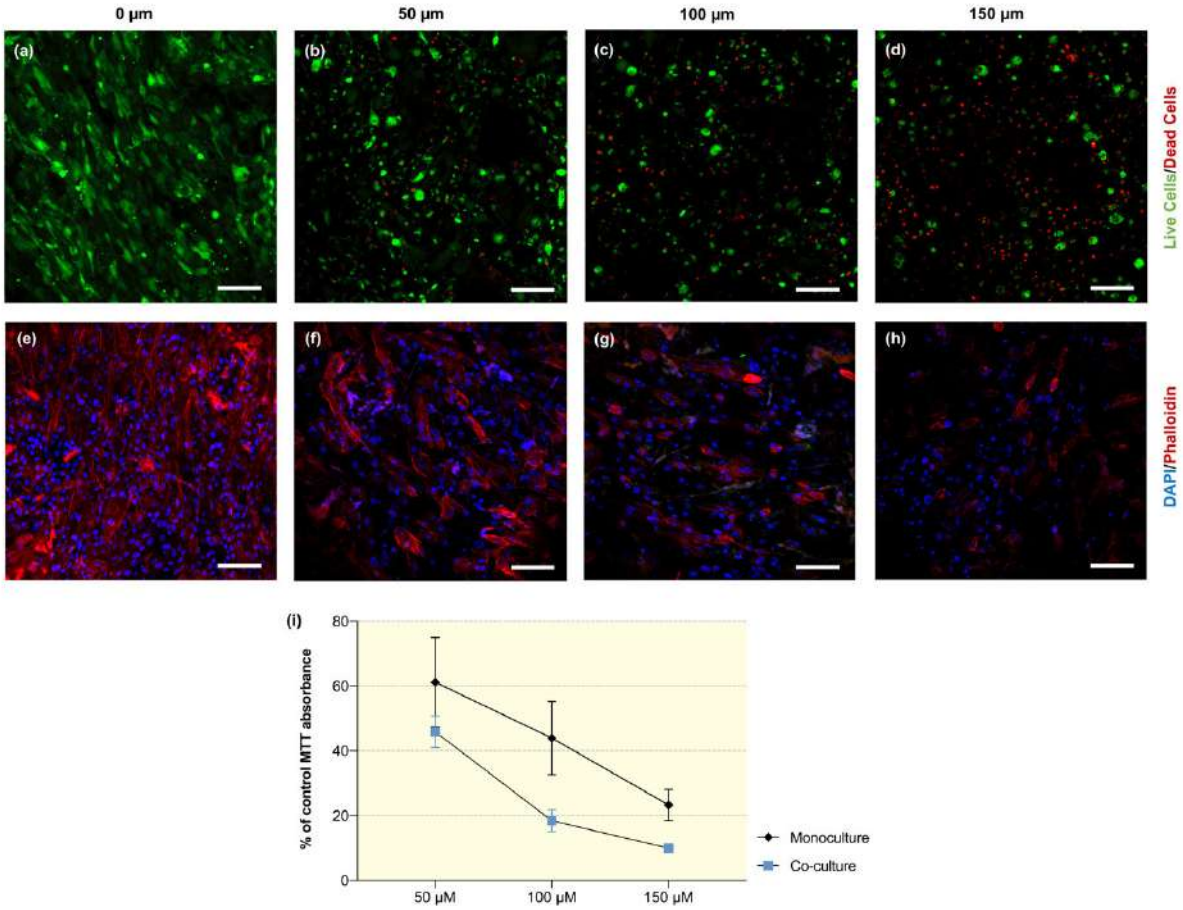


Figure IV-7 – Cisplatin-induced nephrotoxicity model. Cisplatin was dissolved in cell culture medium in different concentrations and introduced in the cell culture system to assess cellular damage. (a-h) Qualitative results for viability on co-cultures were obtained by immunofluorescence micrographs of live/dead assay and Phalloidin/DAPI staining of fixed cells. Cells were administered with 0 µM (a, e), 50 µM (b, f), 100 µM (c, g) and 150 µM (d, h) of cisplatin. Live/Dead assay was performed by incubating cells with Calcein AM (stains green for live cells) and PI (stains red for dead cells). DAPI/Phalloidin staining was performed after cell fixation in formalin. Cytoskeleton is stained by phalloidin (red) and nuclei are stained by DAPI (blue). (i) Quantitative results for viability were obtained by MTS assay. No significative differences were found between mono and co-cultures. These assays revealed that hRPTECs cultured on the bilayer model were more sensitive to the presence of cisplatin, which uptake occurs in proximal tubules. Scale bars: 100 µm.

## IV-4. DISCUSSION

In this work, we focused in developing and characterizing a physiologically relevant *in vitro* tubular bilayer model incorporating both endothelial and epithelial cells. By using an electrospun membrane, we intended to mimic orientation, separation, porosity and composition of the basement membrane found *in vivo* (Figure IV-2). The large surface area obtained by electrospinning processing has already demonstrated to allow stronger cell adhesion and proliferation,[26, 27] which was our main goal when fabricating these membranes. They were previously studied by our group, where we demonstrate

functionality of the proteins included on the membrane, by comparing cellular behavior on membranes which had no dKECM on their composition.[16] Herein, we intended to further explore their potential by using co-cultures of endothelial and renal progenitor cells (the precursors of tubular epithelial cells). The obtained results for quantitative cellular assays reveal that hRPCs do not demonstrate any kind of preference for being in co-culture or monoculture (Figure IV-3), which can be attributed to the lack of evidence showing any beneficial effect on having endothelial cells boosting the performance of renal progenitor cells. However, we demonstrated that the formation of monolayer was remarkably enhanced by adding endothelial cells to the system. The assessment of ultrastructure by SEM revealed hallmarks of an epithelial-like morphology, showing the importance of the co-cultures in this kind of studies. We also characterized the phenotypic expression by RT-PCR and IF staining methods. All genes were upregulated after 21 days, revealing hRPCs differentiation into tubular epithelial cells (Figure IV-4). The major fold increased expression was observed for *SLC12A1* and *SLC9A3*, which encode Na/K/Cl cotransporter and the Na/H exchanger, respectively. The upregulation of *SLC3A1* and *GGT1* was also demonstrated, which is indicative of a higher maturation of these cells, since both genes encode proteins responsible for amino acid transport on the tubular epithelial brush-border. IF revealed consistent staining of proximal tubular markers AQP-1 and SGLT2, whereas the signal for NCC and CLC-NKA, markers for the distal tubule and the thick ascending limb was lower. Furthermore, by comparing these results to that of the monocultures, we observe overall lower IF signal of all markers (Figure S IV-1). These findings demonstrate not only a preference for hRPCs differentiation into proximal tubular cells, but also increased phenotypic markers provoked by the presence of endothelial cells. Moreover, the cells were able to express tubular-related genes and proteins at day 21 of culture, contrasting with a previously published work, in which a 30-day culture was necessary for fully tubular differentiation of hRPCs.[17]

To further evaluate how hRPCs potentiate the use of the electrospun membrane as a model of a natural renal filtration barrier, we have also studied co-cultures of hRPTECs with HUVECs, by growth factor-induced differentiation of hRPCs. Figure IV-5 clearly demonstrates the ultrastructure, polarization and the presence of characteristic transporters of the renal epithelial cell lineage.[28] Brush border microvilli and tight junctions are abundant in all of the cells co-cultured on the membranes, which are polarized according to the organization of the *in vivo* tubule. We can observe the apical membrane turned to the top compartment which suggests the basolateral membrane to be in contact with the decellularized kidney ECM, similar to what happens with *in vivo* BMs. By IF, markers correspondent to different sections of the tubule were assessed to understand the heterogeneity of the population. Less fluorescence intensity was found on CLC-NKA, which is explained by the basolateral location. However, all of the markers were

found present on our membranes, showing differentiation towards other epithelial phenotypes rather than proximal tubule cells, which was not previously demonstrated with renal progenitor cells. Higher fluorescence intensity is always found with the presence of HUVECs on the system, comparing with monocultures (Figure S IV-2), demonstrating once more the value of the epithelial cells on modulating cellular phenotype.

The adopted polarized morphology of hRPTECs when in co-culture with HUVECs allowed the study of renal-specific transport functions across the bilayer model, similar to the complete pathway which water and solutes cross when reabsorbed from the tubular lumen to the blood flow. We have demonstrated consistent values for HSA uptake and inulin leakage (Figure IV-6). Indeed, we were able to obtain lower values for inulin leakage than what is reported in the literature for transwell systems.[10] We were also able to obtain higher values for HSA uptake comparing with tubule models including immortalized hRPTECs instead of primary lineages.[29]

One of the major goals on developing a reliable *in vitro* model of the tubule is to have a consistent response to drugs which are known to induce nephrotoxicity. In this way, it would be possible to predict drug toxicity on humans. Cisplatin is a known nephrotoxic drug that accumulates in the renal parenchyma by active transport into proximal tubular cells.[30, 31] Herein, we have demonstrated that hRPTECs exhibit a dose-dependent toxic response to cisplatin with higher fidelity when cultured on the bilayer model (Figure IV-7). Indeed, by live/dead assay micrographs we demonstrate that cisplatin induced less cellular damage in monocultures which was also corroborated by phalloidin cytoskeleton staining. These results suggest that our model should provide specific and reliable measurements of drug toxicities *in vitro*.

The main aim of an epithelial-endothelial bilayer system is having the formation of single layered epithelia and their maintenance for long periods of time. We were able not only to develop a system capable of recapitulating morphology and physiological functions, but also a system which is capable of maintaining the maturity of differentiated cells. Other authors developed different systems in order to mimic ECM compositions and spatial organization of the tubular basement membrane, including bioprintring,[29, 32, 33] microphysiological systems,[7] and tubule-on-a-chip technology.[22] Herein, we employ a different strategy, where a similar composition to the human kidney ECM is used to give a proper stimulus to the cultured cells. The importance of the ECM on the maintenance of these monolayers was already described.[5] Indeed, changes in the ECM in the tubule and the surrounding interstitium are associated with pathological conditions, including inflammatory processes and renal fibrosis. Our system enabled obtaining the *in vivo* variability by the incorporation of natural kidney ECM on electrospun

membranes. Besides, no additional treatment was necessary to mimic porosity, since that electrospinning enables obtaining porous membranes, suitable for solute and water passage between the two layers.[34] However, we do think that there are further developments to be performed, including employing specific renal endothelial cells, which could have recapitulated in a more relevant manner the organization and phenotype of an interface between tubular and vascular poles. Indeed, in the future, we intend to not only have a mature renal cellular phenotype on the bilayer, but also introduce flow-induced shear stress to the model, to better understand and mimic physiological conditions. We also will work on understanding what is the exact stimulus that the proteins present on our membrane are giving to the cells and which cellular pathways are being activated. Nevertheless, we do think that this biomimetic system constitutes a powerful tool not only for drug toxicity screening but also for increasing our knowledge on molecular mechanisms that underlie kidney function and disease. To the best of our knowledge, this is the first demonstration of a co-culture system on decellularized kidney membranes and also the first time that hRPC-derived epithelial cells were co-cultured and maintained in a differentiated state *in vitro*.

## Acknowledgments

The authors want to acknowledge the financial support obtained by the European Regional Development Fund (ERDF) on the project FROnTHERA (NORTE-01-0145-FEDER-000023) and the FCT PhD Grant on the Doctoral Program on Advanced Therapies for Health (PATH) (PD/BD/128102/2016).

## IV-5. REFERENCES

1. Scott RP, Quaggin SE (2015) The cell biology of renal filtration. J Cell Biol 209:199–210. https://doi.org/10.1083/jcb.201410017
2. Kirk A, Campbell S, Bass P, et al (2010) Differential expression of claudin tight junction proteins in the human cortical nephron. Nephrol Dial Transplant 25:2107–19. https://doi.org/10.1093/ndt/gfq006
3. Sun C-Y, Chang S-C, Wu M-S (2012) Uremic Toxins Induce Kidney Fibrosis by Activating Intrarenal Renin–Angiotensin–Aldosterone System Associated Epithelial-to-Mesenchymal Transition. PLoS One 7:e34026. https://doi.org/10.1371/journal.pone.0034026
4. Masereeuw R, Mutsaers HAM, Toyohara T, et al (2014) The Kidney and Uremic Toxin Removal: Glomerulus or Tubule? Semin Nephrol 34:191–208. https://doi.org/10.1016/j.semnephrol.2014.02.010
5. Zhang H, Tasnim F, Ying JY, Zink D (2009) The impact of extracellular matrix coatings on the performance of human renal cells applied in bioartificial kidneys. Biomaterials 30:2899–2911. https://doi.org/10.1016/J.BIOMATERIALS.2009.01.046

6. Prange JA, Bieri M, Segerer S, et al (2016) Human proximal tubule cells form functional microtissues. Pflügers Arch - Eur J Physiol 468:739–750. https://doi.org/10.1007/s00424-015-1771-8
7. Weber EJ, Chapron A, Chapron BD, et al (2016) Development of a microphysiological model of human kidney proximal tubule function. Kidney Int 90:627–637. https://doi.org/10.1016/j.kint.2016.06.011
8. Wilmer MJ, Ng CP, Lanz HL, et al (2016) Kidney-on-a-Chip Technology for Drug-Induced Nephrotoxicity Screening. Trends Biotechnol 34:156–170. https://doi.org/10.1016/j.tibtech.2015.11.001
9. Jansen J, De Napoli IE, Fedecostante M, et al (2015) Human proximal tubule epithelial cells cultured on hollow fibers: living membranes that actively transport organic cations. Sci Rep 5:16702. https://doi.org/10.1038/srep16702
10. Aydin S, Signorelli S, Lechleitner T, et al (2008) Influence of microvascular endothelial cells on transcriptional regulation of proximal tubular epithelial cells. Am J Physiol Physiol 294:C543–C554. https://doi.org/10.1152/ajpcell.00307.2007
11. Linas SL, Repine JE (1999) Endothelial cells regulate proximal tubule epithelial cell sodium transport. Kidney Int 55:1251–1258. https://doi.org/10.1046/J.1523-1755.1999.00360.X
12. Kim B-S, Chen J, Weinstein T, et al (2002) VEGF expression in hypoxia and hyperglycemia: reciprocal effect on branching angiogenesis in epithelial-endothelial co-cultures. J Am Soc Nephrol 13:2027–36. https://doi.org/10.1097/01.asn.0000024436.00520.d8
13. Tasnim F, Zink D (2012) Cross talk between primary human renal tubular cells and endothelial cells in cocultures. Am J Physiol Physiol 302:F1055–F1062. https://doi.org/10.1152/ajprenal.00621.2011
14. Vedula EM, Alonso JL, Arnaout MA, Charest JL (2017) A microfluidic renal proximal tubule with active reabsorptive function. PLoS One 12:e0184330. https://doi.org/10.1371/journal.pone.0184330
15. Sakolish CM, Mahler GJ (2017) A novel microfluidic device to model the human proximal tubule and glomerulus. RSC Adv 7:4216–4225. https://doi.org/10.1039/C6RA25641D
16. Sobreiro-Almeida R, Fonseca DR, Neves NM (2019) Extracellular matrix electrospun membranes for mimicking natural renal filtration barriers. Mater Sci Eng C 103:109866. https://doi.org/10.1016/J.MSEC.2019.109866
17. Sagrinati C, Netti GS, Mazzinghi B, et al (2006) Isolation and Characterization of Multipotent Progenitor Cells from the Bowman's Capsule of Adult Human Kidneys. J Am Soc Nephrol 17:2443–2456. https://doi.org/10.1681/ASN.2006010089
18. Ronconi E, Sagrinati C, Angelotti ML, et al (2009) Regeneration of glomerular podocytes by human renal progenitors. J Am Soc Nephrol 20:322–332. https://doi.org/10.1681/ASN.2008070709
19. Angelotti ML, Ronconi E, Ballerini L, et al (2012) Characterization of Renal Progenitors Committed Toward Tubular Lineage and Their Regenerative Potential in Renal Tubular Injury. Stem Cells 30:1714–1725. https://doi.org/10.1002/stem.1130
20. Salehi M, Naseri-Nosar M, Ghorbani S, et al (2017) Wet-electrospun PCL/PLLA Blend Scaffolds: Effects of Versatile Coagulation Baths on Physicochemical and Biological Properties of the Scaffolds. 2:1–7. https://doi.org/10.22037/rrr.v2i1.15431
21. Lazzeri E, Ronconi E, Angelotti ML, et al (2015) Human Urine-Derived Renal Progenitors for Personalized Modeling of Genetic Kidney Disorders. J Am Soc Nephrol 26:1961–1974. https://doi.org/10.1681/ASN.2014010057
22. Jang K-J, Mehr AP, Hamilton GA, et al (2013) Human kidney proximal tubule-on-a-chip for drug transport and nephrotoxicity assessment. Integr Biol 5:1119–1129. https://doi.org/10.1039/c3ib40049b

23. Czerniecki SM, Cruz NM, Harder JL, et al (2018) High-Throughput Screening Enhances Kidney Organoid Differentiation from Human Pluripotent Stem Cells and Enables Automated Multidimensional Phenotyping. Cell Stem Cell 22:929-940.e4. https://doi.org/10.1016/j.stem.2018.04.022
24. Nagao RJ, Xu J, Luo P, et al (2016) Decellularized Human Kidney Cortex Hydrogels Enhance Kidney Microvascular Endothelial Cell Maturation and Quiescence. Tissue Eng Part A 22:1140–1150. https://doi.org/10.1089/ten.TEA.2016.0213
25. Hynes RO (1992) Integrins: Versatility, modulation, and signaling in cell adhesion. Cell 69:11–25. https://doi.org/10.1016/0092-8674(92)90115-S
26. Denchai A, Tartarini D, Mele E (2018) Cellular response to surface morphology: Electrospinning and computational modeling. Front Bioeng Biotechnol 6:155. https://doi.org/10.3389/fbioe.2018.00155
27. Chen M, Patra PK, Lovett ML, et al (2009) Role of electrospun fibre diameter and corresponding specific surface area (SSA) on cell attachment. J Tissue Eng Regen Med 3:269–279. https://doi.org/10.1002/term.163
28. Molitoris BA, Wagner MC (1996) Surface membrane polarity of proximal tubular cells: Alterations as a basis for malfunction. Kidney Int 49:1592–1597. https://doi.org/10.1038/KI.1996.231
29. Lin NYC, Homan KA, Robinson SS, et al (2019) Renal reabsorption in 3D vascularized proximal tubule models. Proc Natl Acad Sci U S A 116:5399–5404. https://doi.org/10.1073/pnas.1815208116
30. Ishida S, Lee J, Thiele DJ, Herskowitz I (2002) Uptake of the anticancer drug cisplatin mediated by the copper transporter Ctr1 in yeast and mammals. Proc Natl Acad Sci 99:14298–14302. https://doi.org/10.1073/pnas.162491399
31. Ludwig T, Riethmüller C, Gekle M, et al (2004) Nephrotoxicity of platinum complexes is related to basolateral organic cation transport. Kidney Int 66:196–202. https://doi.org/10.1111/j.1523-1755.2004.00720.x
32. King SM, Higgins JW, Nino CR, et al (2017) 3D Proximal Tubule Tissues Recapitulate Key Aspects of Renal Physiology to Enable Nephrotoxicity Testing. Front Physiol 8:123. https://doi.org/10.3389/fphys.2017.00123
33. Nguyen DLG, King SM, Presnell SC (2019) US20190041381 - Engineered Renal Tissues, Arrays Thereof, and Methods of Making the Same
34. Prozialeck WC, Edwards JR, Lamar PC, Smith CS (2006) Epithelial barrier characteristics and expression of cell adhesion molecules in proximal tubule-derived cell lines commonly used for in vitro toxicity studies. Toxicol Vitr 20:942–953. https://doi.org/10.1016/j.tiv.2005.11.00634.

## IV-6. SUPPLEMENTARY INFORMATION

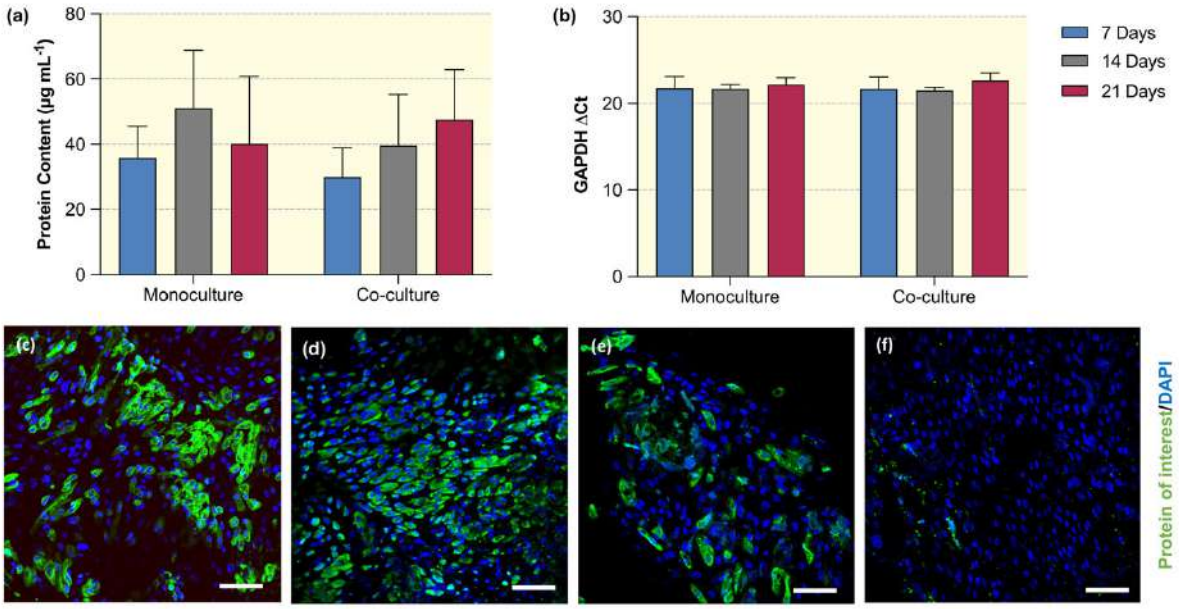


Figure S IV-1 – Human renal progenitor cells (hRPCs) behavior and phenotypic expression when cultured on the decellularized membranes. (a) Protein content was measured at 7, 14 and 21 days of culture by microBCA assay. Cells were submitted to an osmotic shock and proteins were quantified. Increasing values were obtained for co-cultures, whereas monocultures had a quantification peak at 14 days and a decrease at 21 days; (b) *GAPDH* ΔCt values for all of the timepoints and conditions. No differences in expression were found with time of incubation and/or co-culture; (c-f) Tubular related markers protein assessment of (c) AQP-1 (aquaporin-1), (d) SGLT2 (sodium glucose transporter-2), (e) NCC (Na/Cl cotransporter) and (f) CLC-NKA (chloride channel Ka) marked in green. Nuclei were stained with DAPI (blue). Diffuse expression of tubular related markers is found on these cells. Scale bars: 100 µm.

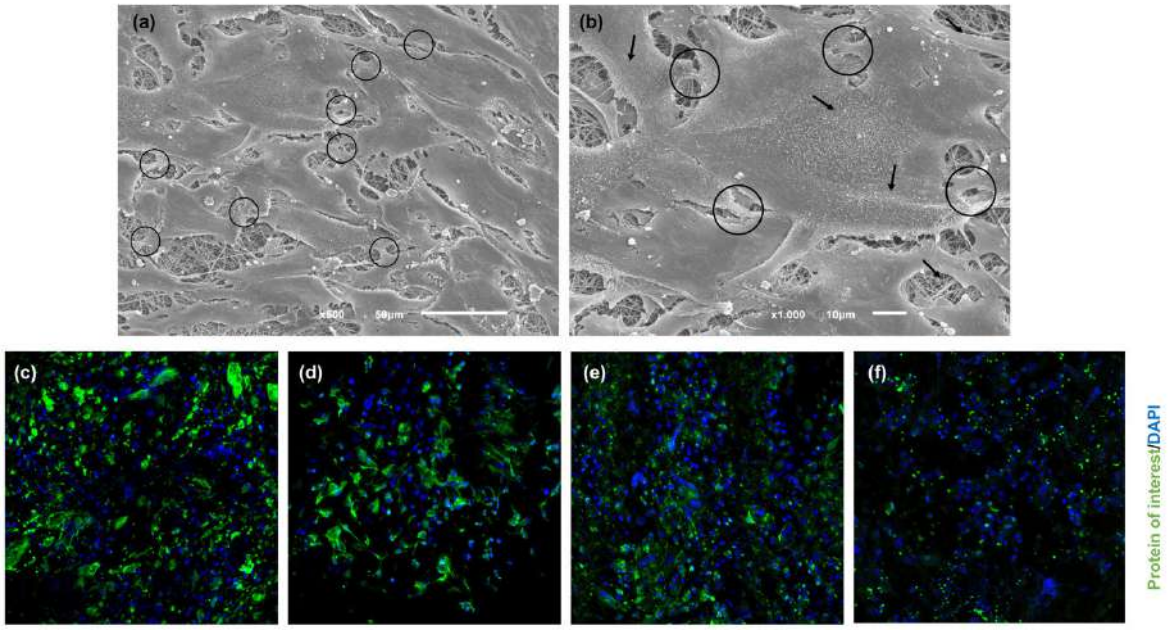


Figure S IV-2 – Assessment of hRPTECs maturity and polarization in the monolayer model. (a-b) SEM micrographs of hRPTECs. These cells are organized in a non-oriented monolayer. Tight junctions characteristic of maturated tubular cells can be spotted in some sites (indicated by circles) as well as microvilli (indicated by arrows), although not consistent in all of the membrane. (c-f) Tubular related markers protein assessment of (c) AQP-1 (aquaporin-1), (d) SGLT2 (sodium glucose transporter-2), (e) NCC (Na/Cl cotransporter) and (f) CLC-NKA (chloride channel Ka) marked in green. Nuclei were stained with DAPI (blue). Diffuse expression of proteins is found on monocultures of hRPTECs, indicating some epithelial maturation of the cells on our membranes. Scale bars: (a) 50 μm; (b) 10 μm; (c-f) 100 μm.

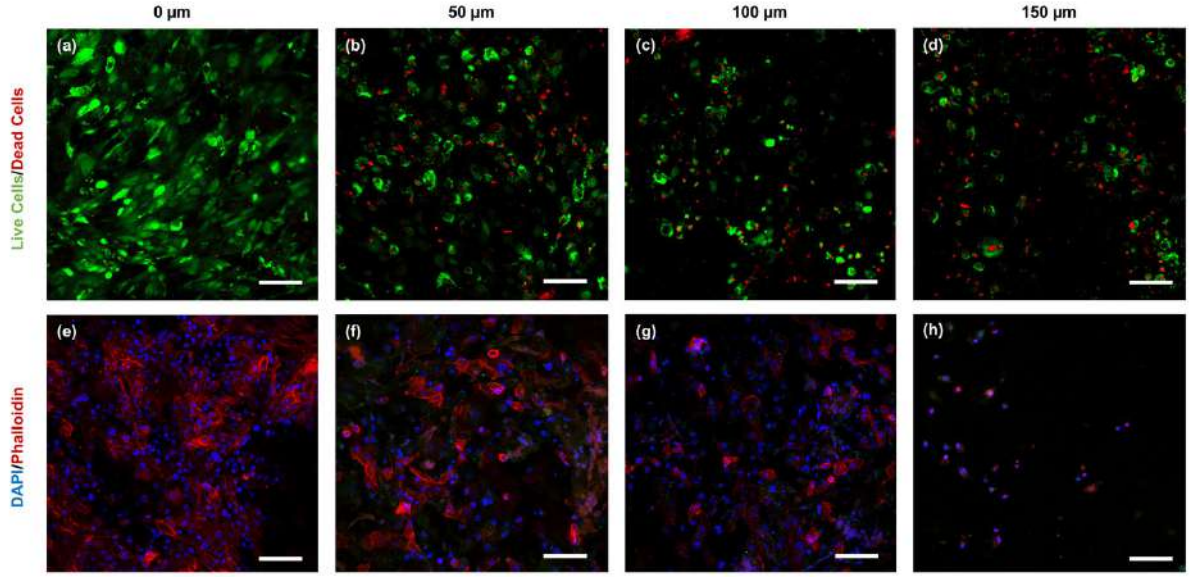


Figure S IV-3 – Nephrotoxicity assessment of cisplatin on monocultures. Qualitative results for viability were obtained by immunofluorescence micrographs of live/dead assay and Phalloidin/DAPI staining of fixed cells. Cells were administered with 0 µM (a, e), 50 µM (b, f), 100 µM (c, g) and 150 µM (d, h) of cisplatin. Live/Dead assay was performed by incubating cells with Calcein AM (stains green for live cells) and PI (stains red for dead cells). DAPI/Phalloidin staining was performed after cell fixation in formalin. Cytoskeleton is stained by phalloidin (red) and nuclei are stained by DAPI (blue). Cells in monoculture demonstrate a dose-dependent response to cisplatin, which is indicative of effective epithelial differentiation. Scale bars: 100 µm.

# Chapter V

# Retinoic acid benefits glomerular organotypic differentiation from adult renal progenitor cells *in vitro*

# Chapter V

## Retinoic acid benefits glomerular organotypic differentiation from adult renal progenitor cells *in vitro* [§]


### ABSTRACT

When in certain culture conditions, organotypic cultures are able to mimic developmental stages of an organ, generating higher-order structures containing functional subunits and progenitor niches. Despite the major advances in the area, researches have not been able to fully recapitulate the complexity of kidney tissue. Pluripotent stem cells are extensively used in the field, but very few studies refer the potential of using adult stem cells. Herein, we describe a simple and feasible method for achieving glomerular epithelial differentiation on an organotypic model comprising renal progenitor cells from adult kidney (hRPCs). Their glomerular differentiative potential was studied using retinoic acid (RA), a fundamental molecule for intermediate mesoderm induction on early embryogenesis. Immunofluorescence, specific cell surface markers expression and gene expression analysis confirm the glomerular differentiative potential of RA in a short-term culture. We also compared the potential of RA with a potent WNT agonist, CHIR99021, on the differentiative capacity of hRPCs. Gene expression and immunofluorescence analysis confirmed that hRPCs are more sensitive to RA stimulation when compared to CHIR9901. Endothelial cells were also included on the spheroids, resulting in a higher organizational level. The assembly potential of these cells and their selective stimulation will give new insights on adult organotypic cell culture studies and will hopefully guide more works in this important area of research.


[§] This chapter is based on the following publication:

**Sobreiro-Almeida, Rita;** Melica, Maria Elena; Lasagni, Laura; Romagnani, Paola; Neves, Nuno M. Retinoic acid benefits glomerular organotypic differentiation from adult renal progenitor cells *in vitro*. (Under review)

## V-1. INTRODUCTION

The human kidney is a complex organ working in very organized mechanisms. During its development, structures that allow the reproduction of crucial body functions are formed.[1] Each kidney is composed of nearly 1 million nephrons, each one comprising its own glomerulus.[2] Due to this complex architecture, mimicking its functional and physiological conditions *in vitro* is a very demanding challenge in the tissue engineering field. Currently, several tissue engineering strategies are being developed to overcome the limitations of 2D cell cultures, which include decellularization/recellularization strategies,[3, 4] microfluidics[5, 6] and 3D scaffolding technology.[7, 8] All of these strategies are promising to the evolution of the field, being able to demonstrate, even if only partially, tubular or glomerular function. However, the majority of the studies refer proof-of-concept experiments and the mechanisms regulating developmental and regeneration processes occurring in the kidney are still not well elucidated. For this reason, the research on cellular development and on the physical and molecular cues driving organogenesis is of extreme importance and can shed new light on kidney progenitor cells' migration, proliferation and differentiation.

Recently, researchers are performing studies on organoid cultures because these enable the study of developmental processes, drug screening, disease modeling and ultimately tissue remodeling and regeneration. These organoids are able to spatially restrict lineage commitments, since cells have the freedom to self-organize and differentiate similarly to *in vivo*,[9] not being restricted to the architecture of the substrate. Organoid cultures were already established for several different tissues including brain,[10] retina,[11] intestine,[12] lung,[13] liver,[14] and kidney.[15] They have a vast potential of applications and can lead us to uncover relevant knowledge for the development of new tissue engineering strategies. A critical aspect to enable the formation of a fully functional organoid is the potential to differentiate a cell into multiple cell types. Thus, the selection of cells is of critical importance.[16] Kidney organoids were already established from induced pluripotent stem cell (iPSC) [17, 18] and Embryonic Stem Cells (ESCs),[19, 20] demonstrating incorporation into developing renal tubules and generation of nephron structures. However, we must also be aware of the current constraints. A lot of ethical concerns are raised by the use of ESCs, and also the tumorigenic risk of using both of these cell types is well known.[21] Furthermore, non-kidney cells were already found in kidney organoids, such as neurons and muscle,[22] and all of the protocols tend to last more than 30 days to form a fully differentiated organoid, which limits the feasibility of clinical applications in the future.[15]

In an embryo, kidney development arises from intermediate mesoderm patterning (AP patterning) of the primitive streak. The AP patterning will allow the formation of a strip of intermediate mesoderm that extends along the axis of the embryo's trunk, which will later be specified as the metanephros. This phenomenon gives rise to the anterior and posterior intermediate mesoderm (AIM and PIM, respectively), in which cells migrate and are exposed to canonical WNTs, followed by FGF9 and retinoic acid (RA). Consequently, cells that migrate earlier will be exposed for a shorter period of time to WNTs, giving rise to the AIM, whereas longer exposure will result in the formation of the PIM.[23] Additionally, the spatiotemporal AP patterning contributes to the establishment of different portions of the urogenital system, being that AIM gives rise to the ureteric epithelium and PIM develops into the metanephric mesenchyme. These are the two structures that will respectively evolve to the branching collecting duct network of the kidney (AIM) and to mature nephrons and glomerular structures (PIM).[24] During the formation of the metanephros, a population of renal progenitors (RPCs) has been identified to present stemness features, such as self-renewal capacity and multipotency, characterized by the expression of the surface markers CD133 and CD24 and the absence of lineage specific markers of differentiation.[25, 26] Indeed, RPCs were first localized in the metanephric mesenchyme primordial structures and their expression is elevated during all stages of the metanephros formation. Additionally, when mature nephrons are formed, they decrease in number and are selectively located in the Bowman capsule or scattered in the tubules, acting as precursors to all renal epithelial cells and/or glomerular cell lineages.[27–29] The evidence that renal repair is mainly driven through endogenous cells and the fact that they do not present any tumorigenic risk strongly suggest them as valuable tool of cellular therapies for renal failure.[29, 30]

Herein, we propose to study the role of adult renal progenitor cells in an organotypic culture model and their differentiative potential. We aim to compare their response to different molecules when cultured in an organoid and in 2D substrates. Furthermore, we hypothesize that the required time for maturation and differentiation of human RPCs can be significantly shortened when comparing to iPSCs and ESCs. The expression of specific glomerular proteins will be studied, as well as the replication of the 3D structures and architecture.

## V-2. MATERIALS AND METHODS

### V-2.1. Human renal progenitor cells (hRPCs) isolation

Human kidney fragments were obtained in agreement with the Ethical Committee on human experimentation of the Azienda Ospedaliero-Universitaria Careggi, Florence, Italy. All subjects gave their informed consent for inclusion before they participated in the study. The study was conducted in accordance with the Declaration of Helsinki, and the protocol was approved by the Ethics Committee on Human Experimentation of the Azienda Ospedaliero-Universitaria Careggi, Florence, Italy (project identification code 2015/0009082 from 25/03/2015). Human RPCs were obtained and cultured as previously described [27] with minor modifications. Briefly, the cortex was minced before proceeding to an enzymatic digestion with collagenase solution type IV 750 U $ml^{-1}$ (Sigma Aldrich) for 45 min at 37 °C. After digestion, the solution was sieved through graded mesh screens (60 and 80 mesh). The cellular suspension was collected, washed and plated on petri dish containing complete medium. The medium is composed by Microvascular Endothelial Cell Growth Medium (EGM™-MV, Lonza) supplemented with 20 % HyClone™ Fetal Bovine Serum (FBS, GE Healthcare). After 4 to 5 days of culture, cells that adhered to the plate were subcultured.

### V-2.2. Spheroid formation and differentiation

hRPCs between P0 and P2 were used on this study. Cells were culture by hanging drop method [31]. Briefly, hRPCs were plated in hanging drops of 20 µL containing EGM-MV medium with 5, 10 and 20 × $10^3$ cells/drop. Podocyte differentiation was conducted with DMEM-F12 medium as previously described, with minor modifications [28]. DMEM-F12 (Sigma) was supplemented with 10 % FBS and all-trans retinoic acid (RA, 100 µM, Sigma) and applied to the spheroids for a maximum of 48 h. Similarly, an highly selective glycogen synthase kinase-3 (GSK-3) inhibitor, CHIR99021, was used as a WNT agonist to induce differentiation according to a previously published protocol [15]. Spheroid cultures were supplemented for 1 h in DMEM-F12 medium supplemented with 10 % FBS and 5 µM of CHIR99021 (R&D Systems). After, the medium was changed to include 10 % of FBS and 200 ng $mL^{-1}$ of FGF9 (R&D Systems) as supplements for 5 days. To obtain spheroid derived cells, spheroids were incubated with trypsin/EDTA for 5–20 min in a 37 °C water bath while pipetting every 2–3 min.

### V-2.3. Endothelial inclusion on the spheroids

For experiments using endothelial cells, we employed a human microvascular endothelial cell line, HMEC-1 (ATCC Cat# CRL-10636, RRID:CVCL 0307). Briefly, $5 \times 10^4$ HMEC-1 were mixed with $15 \times 10^4$ hRPCs and seeded on hanging drops as previously described. The culture was either maintained for 4 days in EGM-MV media or stimulated with DMEM-F12 RA-containing media after 2 days of seeding time, for 48h. After 4 days of co-culture, spheroids were retrieved for immunofluorescence or histology assessment.

### V-2.4. Viability and growth over time

At specific timepoints, the viability and growth rate of hRPCs aggregated as spheroids was assessed using MTT Cell Proliferation Assay Kit (ThermoFisher) and Picogreen dsDNA Kit (ThermoFisher). Briefly, spheroids were incubated with a mixture of 1:5 MTT reagent:DMEM-F12 and incubated for 4 h at 37 °C. After, the mixture was removed and 100 µL of DMSO (Sigma Aldrich) were used to dissolve the dye. Absorbance was read at 570 nm. For dsDNA quantification overtime, spheroids were immersed in Milli-Q water and cells were lysed by thermal and osmotic shock. The resulting supernatant was used for the quantification according to manufacturer's instructions. The fluorescence of each specimen was measured using a microplate reader (excitation: 485 nm; emission: 528 nm). Optical microscopy was used to take gross appearance photos and measure spheroid diameters.

### V-2.5. Flow cytometry characterization

Cultures were checked for simultaneous expression of CD133 and CD24 by flow cytometry at different passages, according to previously published methods for characterizing hRPCs [29]. Briefly, cells were washed with PBS containing 0.5% BSA and blocking was performed with FcR Blocking Reagent (Miltenyi Biotec). Primary antibodies anti-CD133/2 (Miltenyi Biotec) and anti-CD24 (Santa Cruz) were incubated for 15 min along with respective isotypes. Secondary antibodies added and incubated for 15 min in the dark. A total of $4 \times 10^4$ events for each sample were acquired. Dead cells were excluded by propidium iodide positive staining (Miltenyi Biotec). Only populations expressing > 90 % CD133+CD24+ cells were used on this study.

### V-2.6. Immunocytochemistry and immunohistochemistry

Spheroids were fluorescently labeled with antibodies directed against markers for undifferentiated hRPCs and podocyte lineages. To perform immunocytochemistry, they were fixed with 10 % neutral buffered formalin for 30 min at RT and then rinsed in PBS. Primary antibodies were diluted in 0.5 % TWEEN 20 (Sigma Aldrich) plus 3 % bovine serum albumin (BSA, Sigma Aldrich) and incubated overnight at 4 °C. Secondary antibodies Alexa Fluor 488 or 594 (1:500, Alfagene) were diluted in PBS plus 0.5 % TWEEN 20 and incubated overnight at 4 °C in the dark. When required, DAPI (1:500, Sigma Aldrich) and Phalloidin (1:200, Alfagene) were incubated along with the secondary antibody. After several rinses in PBS, spheroids were mounted with VECTASHIELD® (Vector Laboratories) and analyzed under Leica SP5 AOBS confocal microscope (Leica, Wetzlar, Germany) equipped with a Chameleon Ultra-II two-photon laser (Coherent, Milan, Italy). Images were recorded digitally and further processed using LASX software (Leica).

Immunohistochemistry was also performed after the fixation step. Briefly, spheroids were embedded in Histogel™ (ThermoFisher) before being processed and embedded in paraffin for sectioning. 5 µm thick sections were stained with Hematoxylin & Eosin (H&E) or deparaffinized and rehydrated to perform immunofluorescence. Blocking step was performed with 3 % BSA and primary antibodies were incubated for 1 h at RT in 0.5 % TWEEN 20. Secondary antibodies Alexa Fluor 488 or 594 were incubated among with DAPI and Phalloidin for 1 h in the dark. After several rinses in PBS, slides were mounted with VECTASHIELD® and visualized under a confocal microscope.

### V-2.7. Gene expression analysis

Total RNA was extracted using RNeasy Microkit (Qiagen) and quantified using a Nanodrop spectrophotometer (ThermoFisher Scientific). Briefly, 50 spheroids for each condition were centrifuged, trypsinized and frozen until analysis. After, cells were resuspended in buffer RTL (acquired from the kit) containing β-mercaptoethanol for efficient cell lysis. RNA correspondent to the same number of cells per condition was used. After extraction, RNA was retrotranscribed using TaqMan™ Reverse Transcription Reagents (ThermoFisher) following manufacturer's instructions. TaqMan RT-PCR was performed as previously described using a 7900HT Real Time PCR System (Applied Biosystems).[32, 33] Paired box2 (*PAX2*), Octamer-binding transcription factor 4 (*OCT4*), Wilms tumor 1 (*WT1*), Synaptopodin (*SYNPO*) and Nephrin (*NPHS1*) quantification was performed using commercially available Assay on Demand kits

(Applied Biosystems). Fold expression (FE) was determined using the equation FE=2^(-ΔΔCt), where ΔCt = Ct gene of interest – Ct housekeeping gene, glyceraldehyde-3-phosphate dehydrogenase (*GAPDH*), and ΔΔCt = Ct sample of interest – Ct control sample, which was considered the gene expression level at the seeding day.

### V-2.8. Statistical analysis

Statistical analyses were performed with GraphPad Prism 8 (GraphPad Software, California, USA). Data were expressed as means ± standard deviation of experiments with at least three independent assays. Differences between groups were analyzed by unpaired t test or two-way analysis of variance (ANOVA) in case of experiments conducted over time, using Tukey test for post hoc assessments of the differences between samples. Statistical significance was defined as $p < 0.05$.

## V-3. RESULTS

### V-3.1. Spheroids remain viable and intact during long-time cultures

After hRPCs isolation, spheroids were formed by hanging drop method for 48 h. They have shown to aggregate and shape into a spheroid in all seeding concentrations (Figure V-1-A). As expected, their diameter was shown to be dependent of the initial seeding concentration (Figure V-1-B), being larger when higher cell concentrations were used. A reduction on the size was also observed over time, particularly in the higher seeding concentration (20K). We also evaluated the viability and proliferation over time by means of metabolic and DNA quantification, respectively. Spheroids were shown viable along a 28-day culture time, with increasing values over time (Figure V-1-C). Results also demonstrate that metabolic activity is dependent on seeding concentration, with higher absorbance values for higher concentrations. DNA content demonstrate that cells proliferate in the beginning of the culture, but then reach a plateau phase from day 7 until the end of culture time (Figure V-1-D). This result suggests that cells cannot further proliferate when aggregated. Immunofluorescent images of the cytoskeleton demonstrate once more the decrease in diameter with culture time (Figure V-1-E, F and G). Overall, cytoskeleton staining demonstrates that, after 2 days, hRPCs aggregated, forming round structures. However, after 5 days, the organization in the spheroid is more evident, and small round structures can be found, forming little organized niches, indicating some type of structural organization. 5K spheroids demonstrate an

inconsistent morphology, with some cellular disaggregation. The lower viability and reproducibility demonstrated by the 5K spheroids left us to proceed for the following assays only with 10K and 20K seeding concentrations.

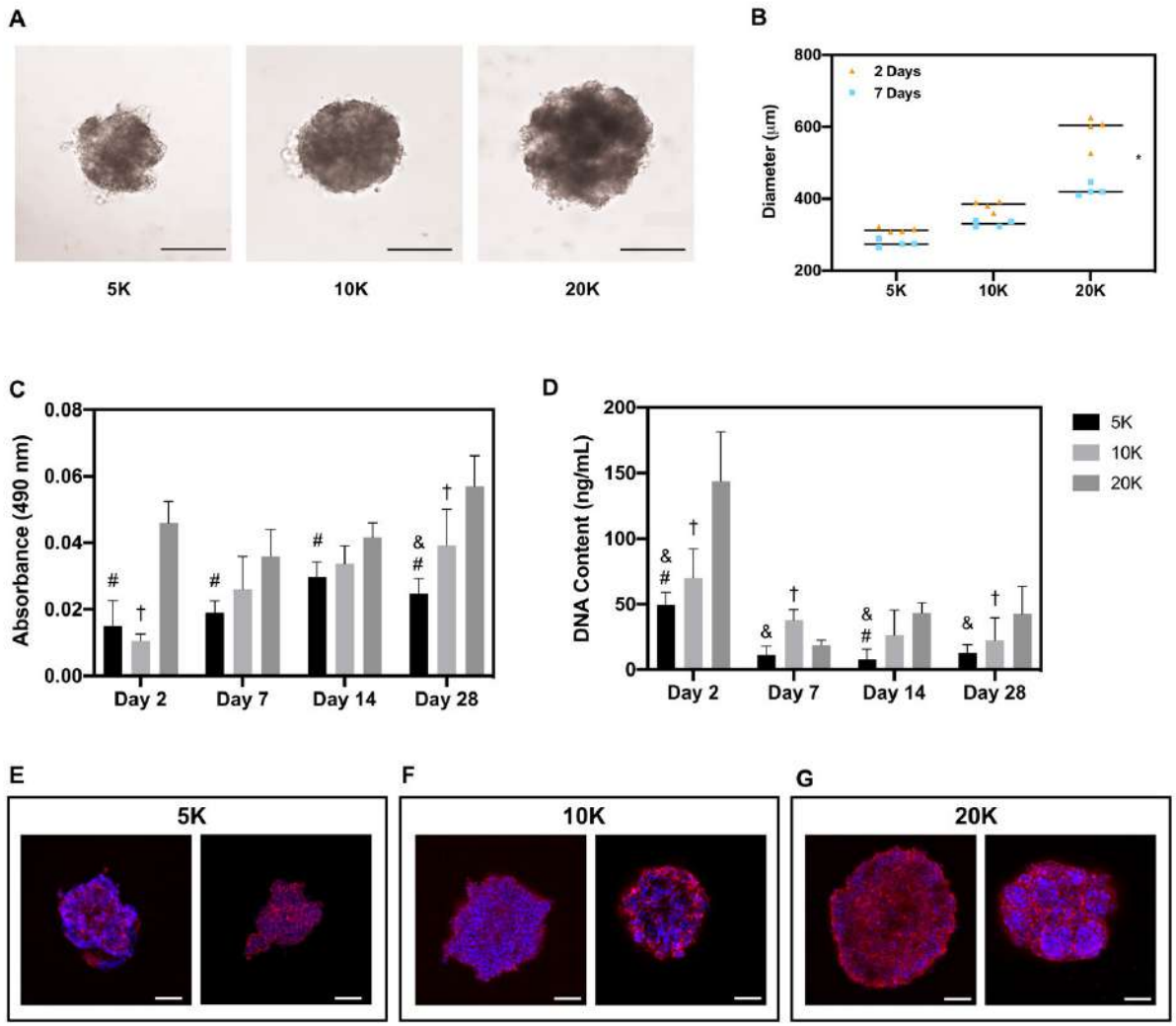


Figure V-1 – Spheroids remain viable and intact during long-time cultures. (A) Optical microscopy micrographs of spheroids after 48h of cell seeding. Scale bar: 200 µm; (B) Spheroid diameter after 2 (orange) and 7 days (blue) of cell seeding. *$p$<0.0001; (C) MTS absorbance values for a 28-day spheroid cell culture, indicating increasing viability values over time; (D) DNA content values for a 28-day spheroid cell culture, indicating that cells are not proliferating overtime, reaching a plateau phase. #$p$<0.05 vs. 20K; &$p$<0.05 vs. 10K; †$p$< 0.05 vs. 20K.; (E-G) Immunofluorescent images of phalloidin (red) and DAPI (blue), demonstrating cytoskeleton organization and nuclei after 2 (left image) and 5 days (right image) of cell seeding. 5K (E), 10K (F) and 20K (G) spheroids. Scale bar: 100 µm.

## V-3.2. Short maturation time potentiates the effect of retinoic acid

For studying the effect of RA on spheroid differentiation, two protocols were tested, in which the stimulus was given in different times of spheroid maturation - Day 2 and Day 7 after seeding (Figure V-2-

A). After 48h of stimulus, spheroids were retrieved for analyzing the presence of PAX2 (Figure V-2-B to G) and nephrin (Figure V-2-H to M). We noticed that, by using protocol 2, the spheroids adopted an inconsistent morphology, mostly on 10K seeding concentration. By using this protocol, the 20K seeding density revealed better structural maintenance after 9 days of culture, comparing with the 10K spheroids. Indeed, the overall structure of the 10K spheroids was sometimes lost, with disintegration and loss of structure, indicating that cells may be losing their viability. Instead, by applying protocol 1, spheroids maintained the overall structure, with some inconsistencies on the 10K spheroids (Figure V-2-C, D, J). In addition, a more marked presence of nephrin was noted, especially for 20K concentration (Figure V-2-K to M). Regarding the staining observed for PAX2, it was less evident with the prolonged culture time on 20K spheroids, regardless of the protocol, demonstrating a tendency of hRPCs to change phenotypic expression with 3D culture (Figure V-2-C, D, F, G). Weaker staining for PAX2 and stronger staining for nephrin was found on 20K spheroids differentiated using protocol 1 (Figure V-2-F, L). Due to these findings, we have selected this protocol to continue with the experiments, in which we evaluated the metabolic activity and the expression of specific stem markers.

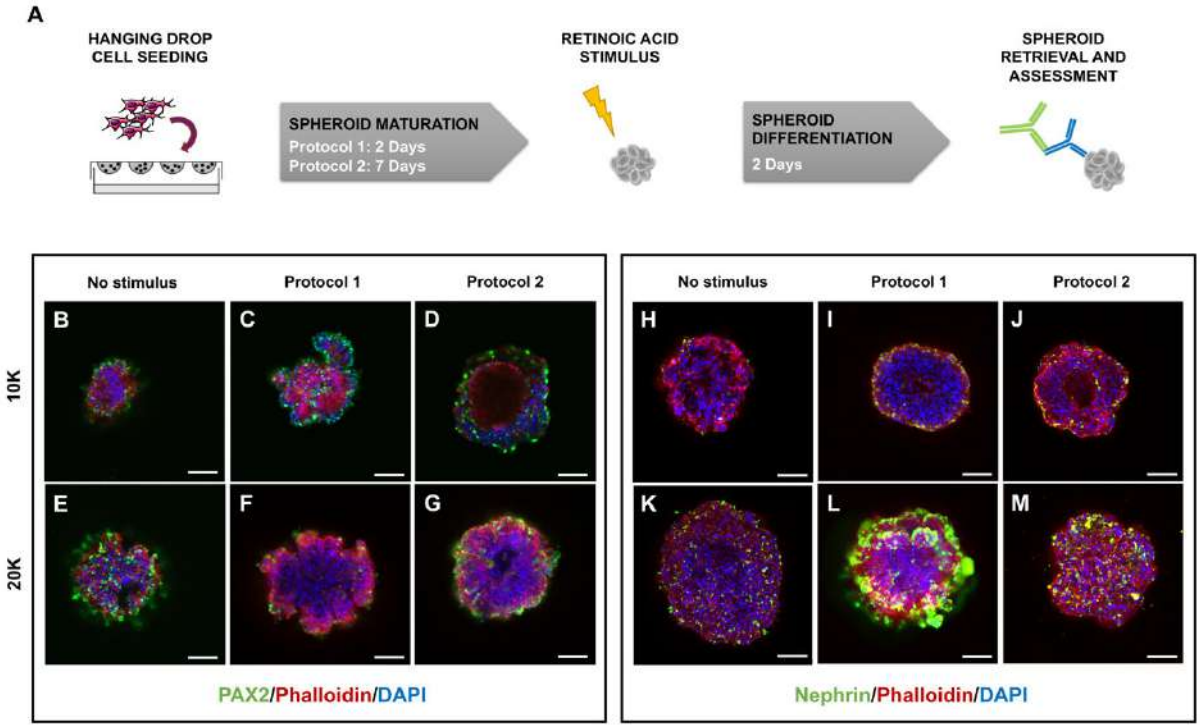


Figure V-2 – Short maturation time potentiates the effect of retinoic acid. (A) Schematic representation of the applied strategy, where the time between spheroid seeding and stimulation was varied from 2 to 7 days. (B-C) Immunofluorescence against (B) PAX2 and (C) Nephrin (green), cytoskeleton (red) and nuclei (blue), varying spheroid maturation time before RA stimulus from

2 (protocol 1) to 7 days (protocol 2). The protocols were tested in two different seeding densities, 10K and 20K. The provided images refer to the end of culture time. Scale bar: 100 µm.

### V-3.3. Specific markers expression is dependent of the seeding concentration

Flow cytometry analysis reveals, as previously published, that hRPCs are > 95 % double positive for CD133/CD24 (Figure V-3-A).[27] Herein, we hypothesized that this value would decrease with cell culture conditions and RA stimulation. Indeed, a huge decrease on the double positivity of CD133/CD24 was observed only by changing hRPCs from a 2D (before seeding) to a 3D (spheroid) environment, which corroborates with PAX2 staining (Figure V-3-A). Additionally, this double positivity was significantly affected when spheroids were stimulated with RA. For the 10K seeding concentration, the double positivity decreased in ~9.59 %, whereas for 20K the decrease was ~26.8 %, revealing once more that the higher seeding concentration is more sensible to the RA stimulus (Figure V-3-B). Control conditions for each seeding concentration and respective isotype controls of FACS analysis are shown in Figure S V-1and Figure S V-2.

To further validate this protocol, the effect of RA on viability was assessed by MTT assay, and values were compared to spheroids which were not stimulated. We have noticed that spheroids were intact and easy to manipulate in both conditions. No significative differences were found between 10K and 20K spheroids viability and a decrease on the values was observed for all stimulated conditions comparing with their control (Figure V-3-C).

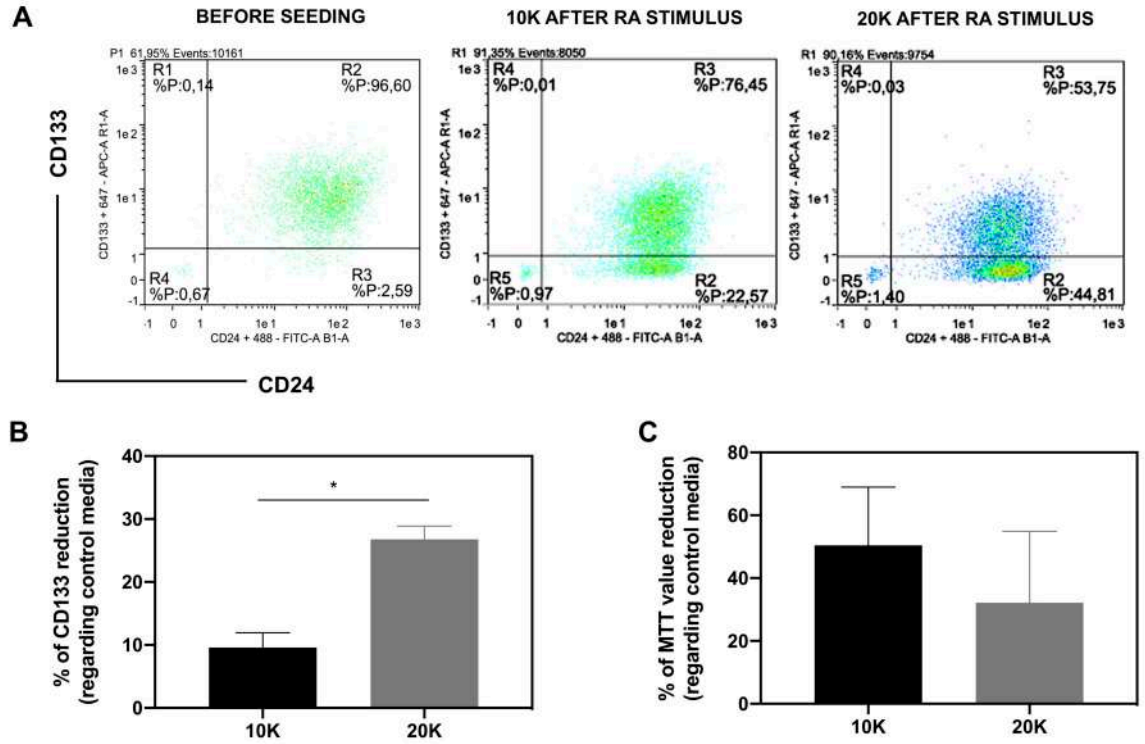


Figure V-3 – Specific markers expression is dependent of the seeding concentration. (A) Flow Cytometry (FC) analysis for the simultaneous expression of CD133 and CD24 before seeding and after RA stimulus in 10K and 20K seeding concentrations. Control conditions for each seeding concentration and isotype controls are shown in Figure S V-1and Figure S V-2; (B) Percentage of CD133 reduction when comparing RA stimulation to non-stimulated spheroids at the same timepoint. *$p$<0.016; (C) Percentage of the reduction in viability caused by RA stimulus. Values were calculated dividing MTT absorbance values of spheroids submitted to RA stimulation by non-stimulated spheroids at the same timepoint.

## V-3.4. Retinoic acid outstands CHIR99021 on spheroid glomerular differentiation

For analyzing the potential of RA on glomerular differentiation, we compared this stimulus with a known GSK-3 inhibitor, CHIR99021.[34] This molecule has been used by several researchers to induce the differentiation of pluripotent cells into specific lineages, including in spheroids, demonstrating effective results in spheroid differentiation.[15] Herein, we analyzed the GSK-3 inhibitor as a late differentiation molecule and the stimulus was maintained for a short period of time, after which FGF-9 was used to maintain the spheroid culture (Figure V-4-A). Gene expression was assessed before the stimulus (T0) and after the culture times (T2 and T5) and normalized to the expression at the seeding day (Figure V-4-B). *PAX2* and *OCT4* were assessed as relevant stem cell markers. A significant decrease in the expression of the stem marker *PAX2* in RA induction was observed, which did not happen for CHIR99021 induction. *OCT4* revealed maintenance of expression values independent of stimulus or culture time, although values were all upregulated comparing with the seeding time. Podocytes are characterized by persistent

expression of *WT1*, synaptopodin (*SYNPO*) and nephrin (*NPHS1*). *WT1* was found significantly upregulated upon RA induction, comparing with the stimulus day (T0) which was not observe with CHIR99021 induction. *SYNPO* was found significantly upregulated in both induction conditions, comparing with hRPCs in initial seeding expression and also T0. At last, *NPHS1* has a marked increase in expression by 6 thousand-fold upon RA stimulus, which was also observed upon CHIR99021 induction, but to a minor extent (3 thousand-fold), which suggests that RA has the strongest differentiative capacity on 3D culture of adult renal progenitor cells.

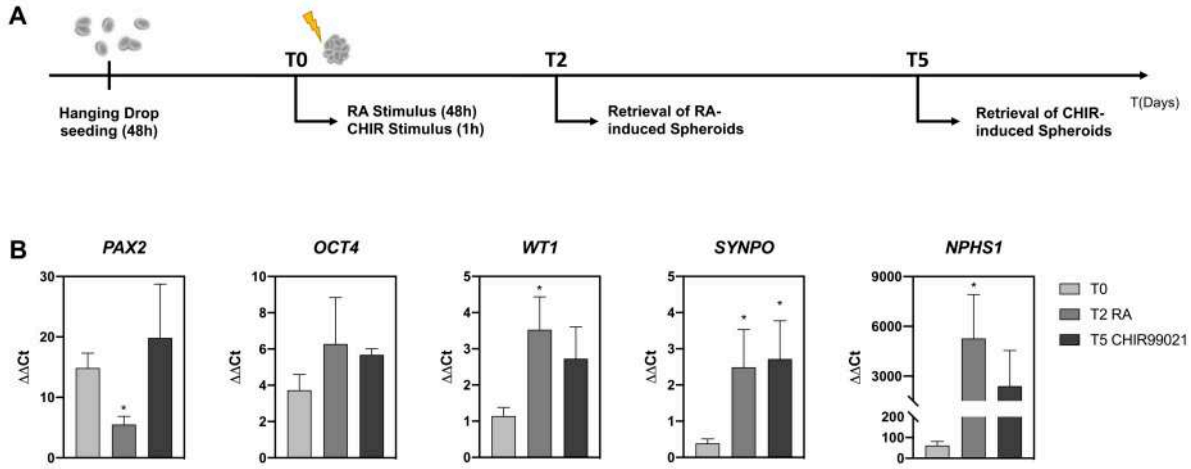


Figure V-4 – Retinoic acid outstands CHIR99021 on spheroid glomerular differentiation. (A) Schematic representation of the differentiation protocols applied for the two molecules. After spheroid formation (48h), RA stimulus was applied for another 48 h, whereas CHIR99021 stimulus was only applied for 1 h, followed by FGF9-supplemented culture for 5 more days. (B) Gene expression analysis for Paired box2 (*PAX2*), Octamer-binding transcription factor 4 (*OCT4*), Wilms tumor 1 (*WT1*), Synaptopodin (*SYNPO*) and Nephrin (*NPHS1*). Expression is compared before (T0) and after the stimulus (T2 and T5) and normalized to hRPCs expression at the seeding day. *$p$<0.05 vs. T0.

To confirm the obtained results, the presence of the most relevant podocyte proteins was also assessed by immunofluorescence staining. The stem marker PAX2 was again evaluated as a control and the podocyte markers synaptopodin, nephrin and podocin were used to compare the differentiation induction capacity of the two molecules (Figure V-5-A, C, E). Our results show, as corroborated by previous assays, that the 3D environment is sufficient to induce some degree of differentiation. Indeed, podocyte markers are already present in the non-induced condition. Comparing the two induction molecules, it was noticed that the staining for podocyte markers was more evident on RA-induced spheroids rather than on CHIR-induced spheroids, especially for nephrin and podocin. Quantification of fluorescence intensity corroborates these results (Figure V-5-B, D, F) by showing a significative difference between the fluorescence intensities of RA and CHIR-stimulated spheroids on nephrin and podocin. Synaptopodin does

not demonstrate this difference, which corroborates the PCR results. The results reveal consistency and a preference for glomerular differentiation upon RA stimulation.

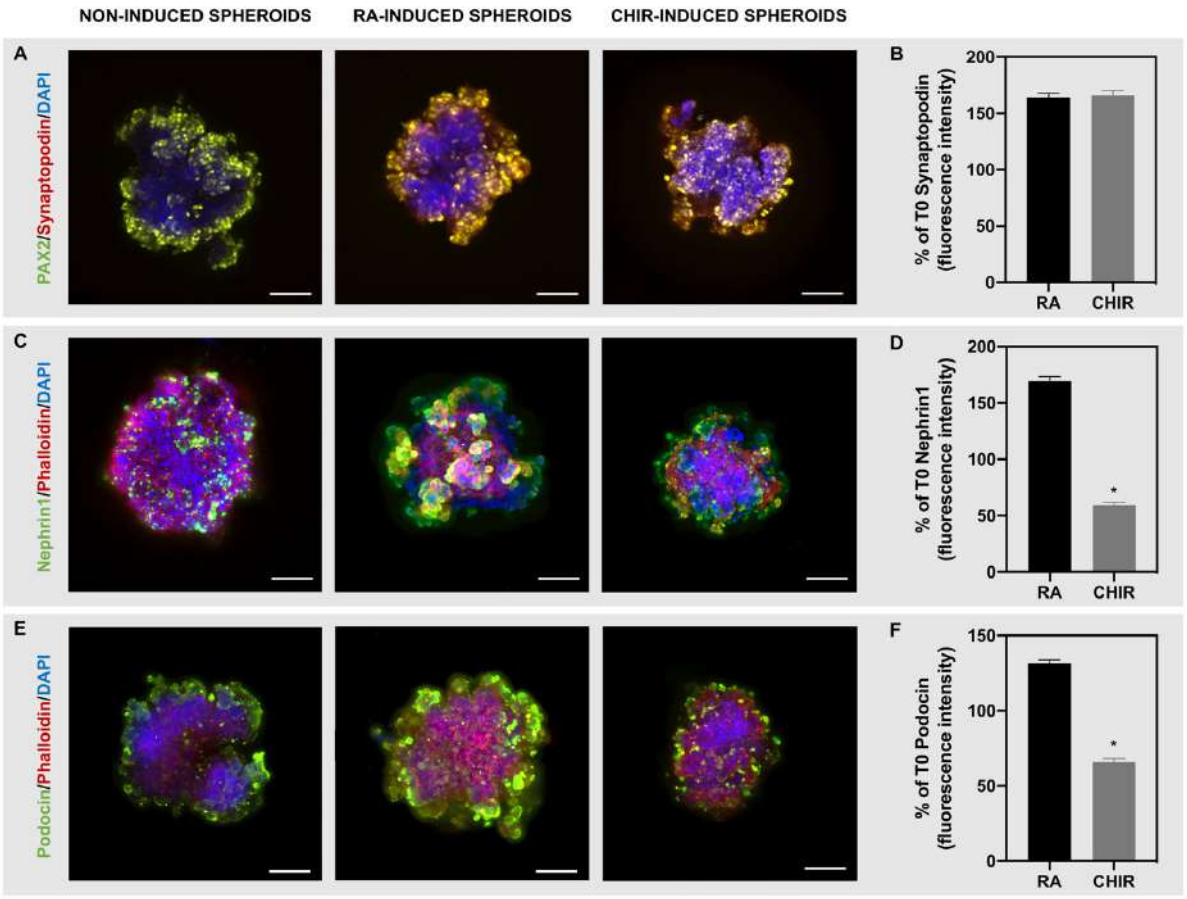


Figure V-5 – Retinoic acid outstands CHIR99021 on spheroid glomerular differentiation. Immunofluorescent staining of hRPC-related markers (A) PAX2 (green) and of the podocyte-related markers (A) synaptopodin (red), (C) nephrin (green) and (E) podocin (green). DAPI and Phalloidin stain for nuclei and cytoskeleton in blue and red, respectively. Scale bars: 100 µm. Quantification of fluorescence intensity of podocyte-related markers synaptopodin (B), nephrin (D) and podocin (F). Quantification was performed in ImageJ and divided to the fluorescence intensity of non-stimulated spheroids. *$p$<0.0001 vs. RA fluorescence intensity.

## V-3.5. Endothelial inclusion allows for a higher spheroid organizational level

Human microvascular endothelial cells were included in the spheroids to evaluate their interaction with hRPCs. Herein, we intended to evaluate morphological and phenotypic changes by immunofluorescence of von Willebrand Factor (vWF) (Figure V-6-A, B, C) and hematoxylin and eosin (H&E) histological staining (Figure V-6A, B, C). RA was also added to the culture media to observe its effect in deeper spheroid layers.

An overall change in morphology is shown only by including the endothelial cells. Spheroids switch form an irregular shape, in which the outer layers demonstrate a loose interaction (Figure V-6-A, D), into organized round and compact shapes (Figure V-6- B, C, E, F). VWF immunofluorescence demonstrates that endothelial cells are mostly located in the outer layers (Figure V-6-E, blue arrow). Round and non-nucleated structures appear only after endothelial inclusion inside the spheroids (circles). Also, cells demonstrate a higher organizational degree, and some hollow spaces can be spotted (black arrows). After RA stimulation, the hollow spaces become more evident (Figure V-6-F). Additionally, bigger cells with long cytoplasmic projections are demonstrated around the spheroids, which is similar to a podocyte morphology (Figure V-6-F, green arrow). Figure S V-3 demonstrates higher magnification images with evident nephrin expression only present on the RA-stimulated spheroids. Although these stained sections demonstrate a small portion of the spheroids, images show that the expression is not confined to the outer layers and is also present in the center of the spheroids. Moreover, endothelial cells seem to be intercalating with podocytes, a typical interaction of *in vivo* glomerular systems. These results demonstrate a successful inclusion of HMEC-1 cells in hRPC-derived spheroids, in which a higher organizational degree is achieved.

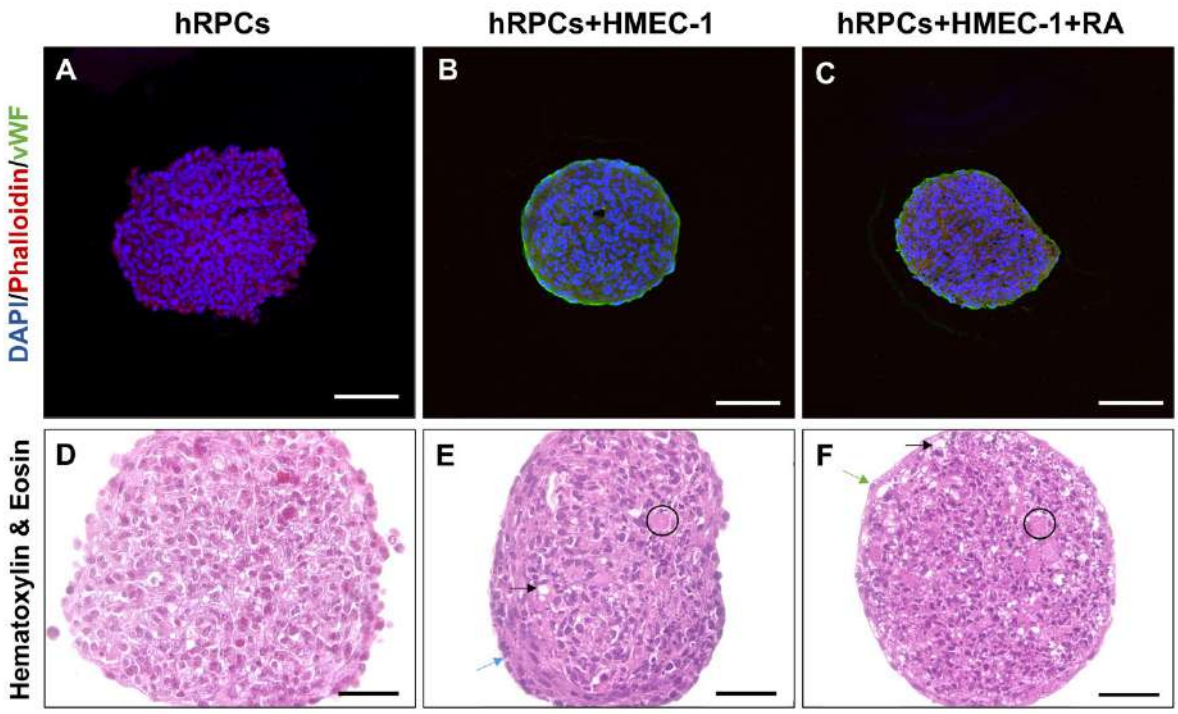


Figure V-6 – Endothelial inclusion allows for a higher spheroid organizational level. (A-C) Immunofluorescent staining of endothelial-related marker von Willebrand Factor (vWF) in green, cytoskeleton marker phalloidin in red and nuclei in blue. Scale bars: 100 μm; (D-F) Hematoxylin and Eosin staining. Circles and arrows denote morphological changes regarding the

control condition without endothelial cells. Circles indicate non-nucleated structures, black arrows indicate hollow spaces, blue and green cells indicate elongated cells. Scale bars: 50 μm.

## V-4. DISCUSSION

Organotypic cell cultures have emerged with the increasing knowledge on embryonic development. Being able to recapitulate developmental stages *in vitro* is a huge scientific advance that will give scientists valuable insights for developing new regenerative strategies. Although adult stem cells cannot rearrange in order to recapitulate whole organs, as pluripotent cells theoretically do, they enable molecular and cellular analysis, disease modeling and drug screening. Herein, we focused on obtaining adult renal cell-derived spheroids and to optimize its glomerular differentiation. We were also focused on assessing the best conditions for spheroid formation and on developing an adequate protocol for their differentiation.

Primarily, spheroids were tested for three different cell seeding densities. Their viability, proliferation, diameter and overall morphology were assessed. There was a significant reduction of 20K spheroids diameter from day 2 to day 7. This can be a result of the time that hRPCs require for self-spatial organization into a viable spheroid, which was observed in a less extent for the 5K and 10K concentrations. Also, the diffusion of nutrients and metabolites to the center of the spheroid is more difficult as cell density increases, and this can also explain the reduction of the 20K spheroid size. Although lower concentrations require less time for self-organization, we have noticed that after some time in culture, the 5K spheroids lose viability or even start to disintegrate, resulting in a very difficult manipulation and assessment. Regarding quantification assays, day 2 demonstrates higher values comparing with the rest of culture time. This effect also suggests that spheroids require some self-organization time, which is only achieved between day 2 and 7, after which the values are maintained or increasing at a lower rate. Moreover, at day 2, the first medium change after the seeding is performed. We postulate that this medium change removes non-adhered cells, therefore diminishing the number of metabolic active cells. There is also a disparity between MTS values and DNA content values. Although MTS reveals an increase in metabolic activity over time, this tendency is not followed by the mitogenic activity of the cells. This can be reflection of hRPCs differentiation within the spheroids. As these cells may be entering its final stages of differentiation, they stop proliferating, therefore reflecting different tendencies for metabolic activity and proliferative capacity. Overall, we postulate that hRPCs need at least

48 h of organizational time, in which some cells are lost, and others aggregate, forming a compact spheroid, mainly on 10K and 20K cell concentrations (Figure V-1).

In order to observe if maturation time influences overall morphology and, consequently, differentiation of hRPCs, spheroids were kept for 2 or 7 days in expansion media before being changed to differentiation media. Overall, hRPCs demonstrated to be more sensitive to retinoic acid when applied after 2 days of seeding (protocol 1) than after 7 days (protocol 2) (Figure V-2-B and C). These findings suggest a more homogeneous differentiation by using protocol 1. Instead, by using protocol 2 cellular organization changes, demonstrating no fluorescence for nuclei and cytoskeleton in the center of the spheroid (Figure V-2-B and C). This effect will have influence on the effect of retinoic acid, concentrating its effect on the cells placed in the outside layers, as can be seen by nephrin immunostaining.

To have a deeper insight on cell phenotype, we analyzed the cell surface markers CD133 and CD24 by flow cytometry before and after RA differentiation (Figure V-3). The differentiation effect of RA in the spheroids was once more confirmed by a percentual reduction on the presence of CD133/CD24 markers in almost 50 % on the 20K seeding concentration. This differentiation kinetics was already observed in 2D surfaces, where a subset of $CD24^{-}CD133^{-}$ cells were shown to be derived from $CD24^{+}CD133^{+}$ cells, i.e., hRPCs.[28, 35]

The metabolic activity of the spheroids demonstrated being always higher after 48h comparing with the rest of the culture time. RA induction has demonstrated do decrease metabolic activity for all conditions (Figure V-3-C), which was already observed by retinoic acid stimulation in hRPCs.[28] Because RA induces hRPCs into terminally differentiated podocytes, these cells cannot further proliferate and divide, demonstrating a limited survival capacity, and thereby affecting its metabolic activity. The results obtained for immunostaining and flow cytometry were balanced with overall spheroid survival, viability and maintenance of structure, suggesting that higher cell seeding concentrations and shorter time of maturation stimulate the effect of retinoic acid on its differentiation induction.

In an embryo, during the intermediate mesoderm AP patterning, cells are exposed to canonical WNTs, FGF9 and RA.[36] These cells will further maturate into more specific structures, such as the metanephric mesenchyme and the ureteric bud, later developing into mature nephrons. A potent WNT agonist is CHIR99021, a glycogen synthase kinase (GSK-3) inhibitor. It has been extensively used to induce nephrogenesis and to differentiate pluripotent and embryonic stem cells into kidney specialized structures.[15, 18, 37, 38] Results have shown that the time of exposure to CHIR99021 influences the induction into anterior and/or posterior intermediate mesoderm, a result that is also dependent on the

origin of the cells.[39] Herein, we employed adult stem cells, a subset of multipotent progenitors also existent in the kidney from early developmental stages.[40] A recent study with adult stem cell-derived tubuloids in Matrigel® revealed prolonged maintenance of proximal as well as distal nephron segments in culture and were also able to recapitulate disease phenotypes.[41] Although the regenerative potential of these cells was already proved by recovering kidney function in diseased animals,[26, 27] the glomerular differentiation of hRPCs in 3D organoids was yet to be studied. Human renal progenitor cells were already identified in the metanephric mesenchyme during renal organogenesis.[26] However, in adulthood, they become selectively located in the Bowman's capsule or scattered along the tubules. These cells were found to be the precursors of glomerular and tubular epithelial cells, thus actively participating in the *in vivo* remodeling of kidney tissue.[29, 42] RA has already shown to promote hRPCs differentiation into podocytes by upregulating specific podocyte genes, through the activation of RA response elements on their promoters.[28] Herein, we were able to study the effect of two different nephrogenic molecules existent *in vivo* on the phenotype of adult renal progenitor cells in a 3D culture. CHIR99021 differentiation protocol was adapted from Takasato *et al.*[15]. Given that hRPCs possess a further step of differentiation compared with pluripotent stem cells, we started the protocol after the intermediate mesoderm induction, in which a pulse of CHIR99021 was followed by 5 days of supplementation with FGF9. FGF9 is a growth factor required for nephron progenitor growth *in vivo*, directing the differentiation of the primitive streak into the intermediate mesoderm.[43, 44] It has also shown its efficiency on directing renal development in organoids, by using both CHIR99021 and FGF9 supplementation.[15, 45] Herein, we analyzed if this strategy could be more effective than RA supplementation to generate podocytes from adult hRPCs in 3D organotypic cultures. Overall, RA stimulation demonstrated better differentiative capacity than CHIR99021, as evidenced by gene expression (Figure V-4-B) and immunofluorescence analysis (Figure V-5). *PAX2* and *OCT4* were analyzed as key regulatory genes of kidney stem cells.[46, 47] *WT1* is a tumor suppressor gene known to be expressed in kidney progenitor cells (together with *PAX2* and *Six2*), in epithelial precursors of renal cells and also on podocytes, being a good indicator that cells are not differentiating into epithelial tubular lineages. Indeed, its expression has significantly increased in RA-induced spheroids, while *PAX2* has significantly decreased (Figure V-4). Additionally, *NPHS1* fold expression indicates the successful differentiation of these spheroids into glomerular epithelial cells, being its product (nephrin) a transmembrane protein which composes the core of the glomerular filtration barrier. Figure V-5 immunofluorescent assays corroborate these results, in which the podocyte markers nephrin and podocin demonstrate higher cell fluorescence intensity by using RA rather than CHIR99021. Synaptopodin was

present in the two conditions without significative differences, which may be a result of its nature, as an actin binding protein. Comparing with nephrin and podocin, which are components of the filtration slits of podocytes, their expression is only present in fully differentiated podocytes. In this way, synaptopodin expression may be present in a premature point of differentiation, therefore being present in the two conditions. Overall, these results suggest that RA is able to stimulate hRPCs differentiation more homogeneously than CHIR99021, validating our initial hypothesis.

The inclusion of endothelial cells indicates a higher organizational degree (Figure V-6), with new structures forming inside the spheroids. We were able to successfully demonstrate that these spheroids can be further explored to form mature glomerular structures. However, we do think that culture time and conditions have to be further optimized to achieve this mature state. Nevertheless, RA stimulation seems to be successful in achieving deeper layers of cells (Figure S V-2), which is a strong evidence supporting our initial hypothesis. Future studies may be focused on studying matrix deposition and also the formation of more established glomerular structures.

Although we were not able to perform functional analysis on these spheroids, we believe that this work will help researchers understanding the mechanisms guiding the differentiation of a population of progenitor cells existent from embryogenesis to adulthood in the kidney. Also, this work helps on establishing the proper cell culture conditions for other works following our rationale.

## V-5. Conclusion

The existence of a population of renal progenitor cells in adult kidney has already proved to be beneficial for the *in vivo* remodeling of kidney tissue upon injury. Herein, we hypothesize that organotypic cell cultures could be established from these cells and that glomerular differentiation could be achieved in 3D spheroid cultures. Taking together our results, we established adequate culture conditions for the maintenance and differentiation of these cells in spheroids for long periods. We compared the effect of two embryonic molecules on renal progenitor cells, confirming the potent effect of RA on glomerular differentiation of 3D cultures. We have also successfully validated endothelial inclusion on the spheroids. Future studies may explore high-order organ structures, in which functional analysis could be performed. Although we have not achieved the complexity of the kidney tissue, we have focused our work on simplicity and practicability, achieving a 4-day protocol with reasonable growth factor stimulation. This balance

between complexity and feasibility provides an attractive starting point for the development of adult stem cell-derived organoids focusing on therapeutic discovery, toxicology and regenerative medicine.

### Acknowledgements

We would like to acknowledge the Portuguese Foundation of Technology (FCT) for PhD Grant on the Doctoral Program on Advanced Therapies for Health (PATH) (PD/BD/128102/2016) and for the funding on the project Cells4_IDs (PTDC/BTM-SAL/28882/2017), under the Compete2020 Funding Program.

## V-6. REFERENCES

1. Zeidel ML, Hoenig MP, Palevsky PM (2014) A new CJASN series: Renal physiology for the clinician. Clin J Am Soc Nephrol 9:1271. https://doi.org/10.2215/CJN.10191012
2. Bertram JF, Douglas-Denton RN, Diouf B, et al (2011) Human nephron number: Implications for health and disease. Pediatr Nephrol 26:1529–1533. https://doi.org/10.1007/s00467-011-1843-8
3. Abolbashari M, Agcaoili SM, Lee M-KK, et al (2016) Repopulation of porcine kidney scaffold using porcine primary renal cells. Acta Biomater 29:52–61. https://doi.org/10.1016/j.actbio.2015.11.026
4. Song JJ, Guyette JP, Gilpin SE, et al (2013) Regeneration and experimental orthotopic transplantation of a bioengineered kidney. Nat Med 19:646–51. https://doi.org/10.1038/nm.3154
5. Sakolish CM, Mahler GJ (2017) A novel microfluidic device to model the human proximal tubule and glomerulus. RSC Adv 7:4216–4225. https://doi.org/10.1039/C6RA25641D
6. Lin NYC, Homan KA, Robinson SS, et al (2019) Renal reabsorption in 3D vascularized proximal tubule models. Proc Natl Acad Sci U S A 116:5399–5404. https://doi.org/10.1073/pnas.1815208116
7. Nagao RJ, Xu J, Luo P, et al (2016) Decellularized Human Kidney Cortex Hydrogels Enhance Kidney Microvascular Endothelial Cell Maturation and Quiescence. Tissue Eng Part A 22:1140–1150. https://doi.org/10.1089/ten.TEA.2016.0213
8. O'Neill JD, Freytes DO, Anandappa AJ, et al (2013) The regulation of growth and metabolism of kidney stem cells with regional specificity using extracellular matrix derived from kidney. Biomaterials 34:9830–9841. https://doi.org/10.1016/j.biomaterials.2013.09.022
9. Lancaster MA, Knoblich JA (2014) Organogenesis in a dish: Modeling development and disease using organoid technologies. Science (80- ) 345:1247125–1247125. https://doi.org/10.1126/science.1247125
10. Lancaster MA, Renner M, Martin CA, et al (2013) Cerebral organoids model human brain development and microcephaly. Nature 501:373–379. https://doi.org/10.1038/nature12517
11. Eiraku M, Takata N, Ishibashi H, et al (2011) Self-organizing optic-cup morphogenesis in three-dimensional culture. Nature 472:51–58. https://doi.org/10.1038/nature09941
12. McCracken KW, Catá EM, Crawford CM, et al (2014) Modelling human development and disease in pluripotent stem-cell-derived gastric organoids. Nature 516:400–404. https://doi.org/10.1038/nature13863

13. Dye BR, Hill DR, Ferguson MA, et al (2015) In vitro generation of human pluripotent stem cell derived lung organoids. Elife 2015:1–25. https://doi.org/10.7554/eLife.05098
14. Takebe T, Sekine K, Enomura M, et al (2013) Vascularized and functional human liver from an iPSC-derived organ bud transplant. Nature 499:481–484. https://doi.org/10.1038/nature12271
15. Takasato M, Er PX, Chiu HS, Little MH (2016) Generation of kidney organoids from human pluripotent stem cells. Nat Protoc 11:1681–1692. https://doi.org/10.1038/nprot.2016.098
16. Sagrinati C, Ronconi E, Lazzeri E, et al (2008) Stem-cell approaches for kidney repair: choosing the right cells. Trends Mol Med 14:277–285. https://doi.org/10.1016/j.molmed.2008.05.005
17. Freedman BS, Brooks CR, Lam AQ, et al (2015) Modelling kidney disease with CRISPR-mutant kidney organoids derived from human pluripotent epiblast spheroids. Nat Commun 6:8715. https://doi.org/10.1038/ncomms9715
18. Morizane R, Lam AQ, Freedman BS, et al (2015) Nephron organoids derived from human pluripotent stem cells model kidney development and injury. Nat Biotechnol 33:1193–1200. https://doi.org/10.1038/nbt.3392
19. Tan Z, Shan J, Rak-Raszewska A, Vainio SJ (2018) Embryonic Stem Cells Derived Kidney Organoids as Faithful Models to Target Programmed Nephrogenesis. Sci Rep 8:16618. https://doi.org/10.1038/s41598-018-34995-3
20. Kim D, Dressler GR (2005) Nephrogenic factors promote differentiation of mouse embryonic stem cells into renal epithelia. J Am Soc Nephrol 16:3527–3534. https://doi.org/10.1681/ASN.2005050544
21. Lo B, Parham L (2009) Ethical issues in stem cell research. Endocr Rev 30:204–213. https://doi.org/10.1210/er.2008-0031
22. Freedman BS (2019) Better Being Single? Omics Improves Kidney Organoids. Nephron 141:128–132. https://doi.org/10.1159/000496009
23. Takasato M, Little MH (2015) The origin of the mammalian kidney: Implications for recreating the kidney in vitro. Development 142:1937–1947. https://doi.org/10.1242/dev.104802
24. Little MH, Combes AN, Takasato M (2016) Understanding kidney morphogenesis to guide renal tissue regeneration. Nat Rev Nephrol 12:624–635. https://doi.org/10.1038/nrneph.2016.126
25. Kobayashi A, Valerius MT, Mugford JW, et al (2008) Six2 Defines and Regulates a Multipotent Self-Renewing Nephron Progenitor Population throughout Mammalian Kidney Development. Cell Stem Cell 3:169–181. https://doi.org/10.1016/j.stem.2008.05.020
26. Lazzeri E, Crescioli C, Ronconi E, et al (2007) Regenerative potential of embryonic renal multipotent progenitors in acute renal failure. J Am Soc Nephrol 18:3128–3138. https://doi.org/10.1681/ASN.2007020210
27. Sagrinati C, Netti GS, Mazzinghi B, et al (2006) Isolation and Characterization of Multipotent Progenitor Cells from the Bowman's Capsule of Adult Human Kidneys. J Am Soc Nephrol 17:2443–2456. https://doi.org/10.1681/ASN.2006010089
28. Ronconi E, Sagrinati C, Angelotti ML, et al (2009) Regeneration of glomerular podocytes by human renal progenitors. J Am Soc Nephrol 20:322–332. https://doi.org/10.1681/ASN.2008070709
29. Angelotti ML, Ronconi E, Ballerini L, et al (2012) Characterization of Renal Progenitors Committed Toward Tubular Lineage and Their Regenerative Potential in Renal Tubular Injury. Stem Cells 30:1714–1725. https://doi.org/10.1002/stem.1130
30. Mazzinghi B, Ronconi E, Lazzeri E, et al (2008) Essential but differential role for CXCR4 and CXCR7 in the therapeutic homing of human renal progenitor cells. J Exp Med 205:479–490. https://doi.org/10.1084/jem.20071903
31. Bartosh TJ, Ylöstalo JH, Mohammadipoor A, et al (2010) Aggregation of human mesenchymal stromal cells (MSCs) into 3D spheroids enhances their antiinflammatory properties. Proc Natl Acad Sci U S A 107:13724–13729. https://doi.org/10.1073/pnas.1008117107

32. Lazzeri E, Ronconi E, Angelotti ML, et al (2015) Human Urine-Derived Renal Progenitors for Personalized Modeling of Genetic Kidney Disorders. J Am Soc Nephrol 26:1961–1974. https://doi.org/10.1681/ASN.2014010057
33. Sobreiro‐Almeida R, Elena Melica M, Lasagni L, et al (2020) Co‐cultures of renal progenitors and endothelial cells on kidney decellularized matrices replicate the renal tubular environment in vitro. Acta Physiol 230:e13491. https://doi.org/10.1111/apha.13491
34. Lam AQ, Freedman BS, Morizane R, et al (2014) Rapid and efficient differentiation of human pluripotent stem cells into intermediate mesoderm that forms tubules expressing kidney proximal tubular markers. J Am Soc Nephrol 25:1211–1225. https://doi.org/10.1681/ASN.2013080831
35. Peired A, Angelotti ML, Ronconi E, et al (2013) Proteinuria impairs podocyte regeneration by sequestering retinoic acid. J Am Soc Nephrol 24:1756–1768. https://doi.org/10.1681/ASN.2012090950
36. M. Chambers J, A. McKee R, E. Drummond B, A. Wingert R (2016) Evolving technology: creating kidney organoids from stem cells. AIMS Bioeng 3:305–318. https://doi.org/10.3934/bioeng.2016.3.305
37. Czerniecki SM, Cruz NM, Harder JL, et al (2018) High-Throughput Screening Enhances Kidney Organoid Differentiation from Human Pluripotent Stem Cells and Enables Automated Multidimensional Phenotyping. Cell Stem Cell 22:929-940.e4. https://doi.org/10.1016/j.stem.2018.04.022
38. Hale LJ, Howden SE, Phipson B, et al (2018) 3D organoid-derived human glomeruli for personalised podocyte disease modelling and drug screening. Nat Commun 9:5167. https://doi.org/10.1038/s41467-018-07594-z
39. Takasato M, Er PX, Chiu HS, et al (2015) Kidney organoids from human iPS cells contain multiple lineages and model human nephrogenesis. Nature 526:564–568. https://doi.org/10.1038/nature15695
40. Angelotti ML, Becherucci F, Mazzinghi B, et al (2017) Principles of Kidney Regeneration. In: Kidney Transplantation, Bioengineering, and Regeneration: Kidney Transplantation in the Regenerative Medicine Era, 1st ed. Academic Press, p 1252
41. Schutgens F, Rookmaaker MB, Margaritis T, et al (2019) Tubuloids derived from human adult kidney and urine for personalized disease modeling. Nat Biotechnol 37:303–313. https://doi.org/10.1038/s41587-019-0048-8
42. Lasagni L, Angelotti ML, Ronconi E, et al (2015) Podocyte Regeneration Driven by Renal Progenitors Determines Glomerular Disease Remission and Can Be Pharmacologically Enhanced. Stem Cell Reports 5:248–263. https://doi.org/10.1016/j.stemcr.2015.07.003
43. Colvin JS, Feldman B, Nadeau JH, et al (1999) Genomic organization and embryonic expression of the mouse fibroblast growth factor 9 gene. Dev Dyn 216:72–88. https://doi.org/10.1002/(SICI)1097-0177(199909)216:1<72::AID-DVDY9>3.0.CO;2-9
44. Barak H, Huh SH, Chen S, et al (2012) FGF9 and FGF20 Maintain the Stemness of Nephron Progenitors in Mice and Man. Dev Cell 22:1191–1207. https://doi.org/10.1016/j.devcel.2012.04.018
45. Taguchi A, Nishinakamura R (2017) Higher-Order Kidney Organogenesis from Pluripotent Stem Cells. Cell Stem Cell 21:730–746. https://doi.org/10.1016/j.stem.2017.10.011
46. Rasti A, Mehrazma M, Madjd Z, et al (2018) Co-expression of Cancer Stem Cell Markers OCT4 and NANOG Predicts Poor Prognosis in Renal Cell Carcinomas. Sci Rep 8:11739. https://doi.org/10.1038/s41598-018-30168-4
47. Sharma R, Sanchez-Ferras O, Bouchard M (2015) Pax genes in renal development, disease and regeneration. Semin Cell Dev Biol 44:97–106. https://doi.org/10.1016/j.semcdb.2015.09.01647.

## V-7. SUPPLEMENTARY INFORMATION

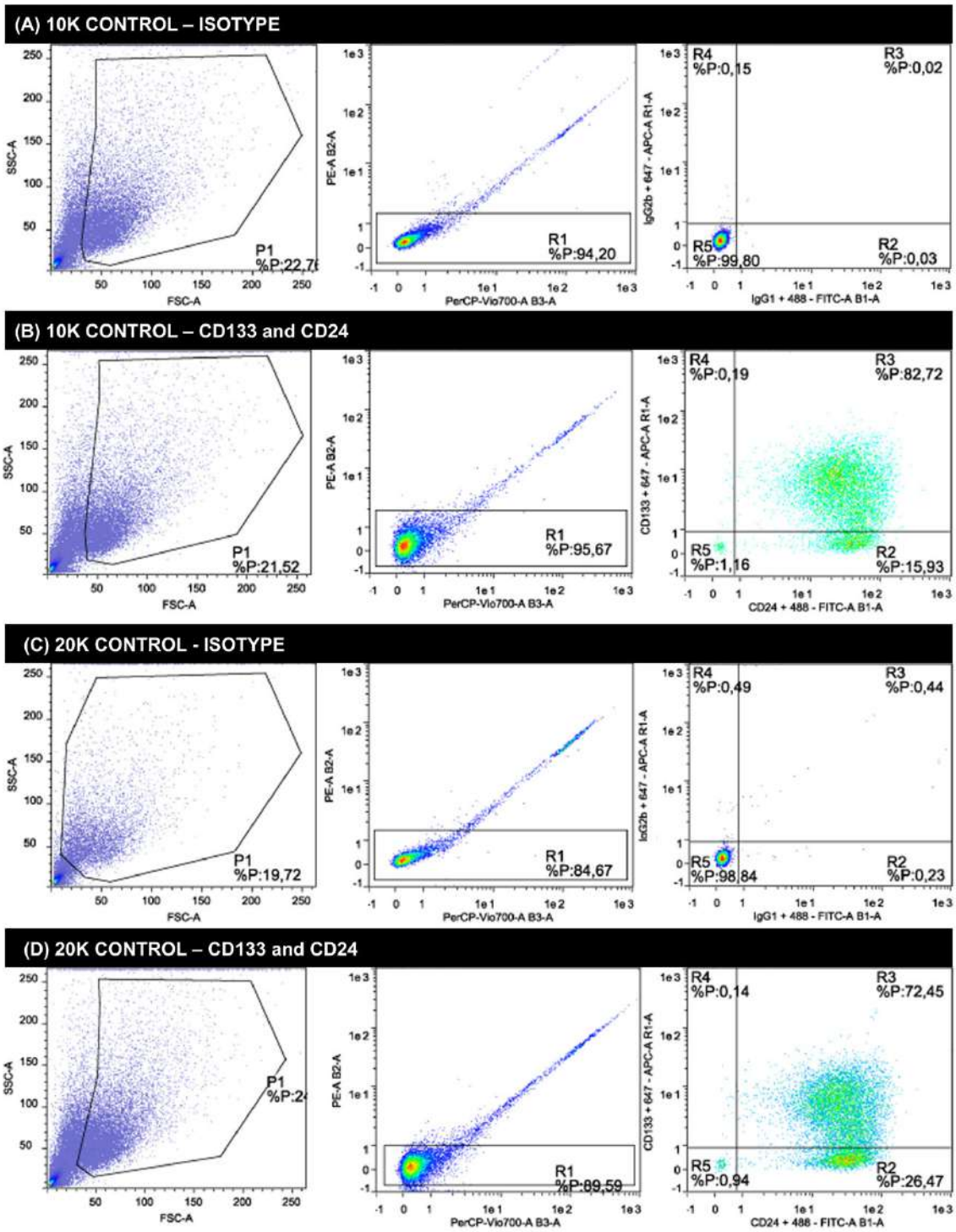


Figure S V-1 – Flow cytometry analysis for non-stimulated conditions. Density plots indicate the used gating for live cells - left and middle dot plots - excluding debris and PI-positive stained cells, respectively. Right plots indicate fluorescence of specific antibodies. (A) Gating for 10K isotype control condition demonstrates 94 % live cells and 0.02 % Alexa Fluor 647 IgG2b and Alexa Fluor 488 IgG1 double positive cells; (B) Gating for 10K stained control condition demonstrates 96 % live cells and 83 % CD133 and CD24 double positive cells; (D) Gating for 20K isotype control condition demonstrates 85 % live cells and 0.44 %

Alexa Fluor 647 IgG2b and Alexa Fluor 488 IgG1 double positive cells; (B) Gating for 20K stained control condition demonstrates 90 % live cells and 73 % CD133 and CD24 double positive cells.

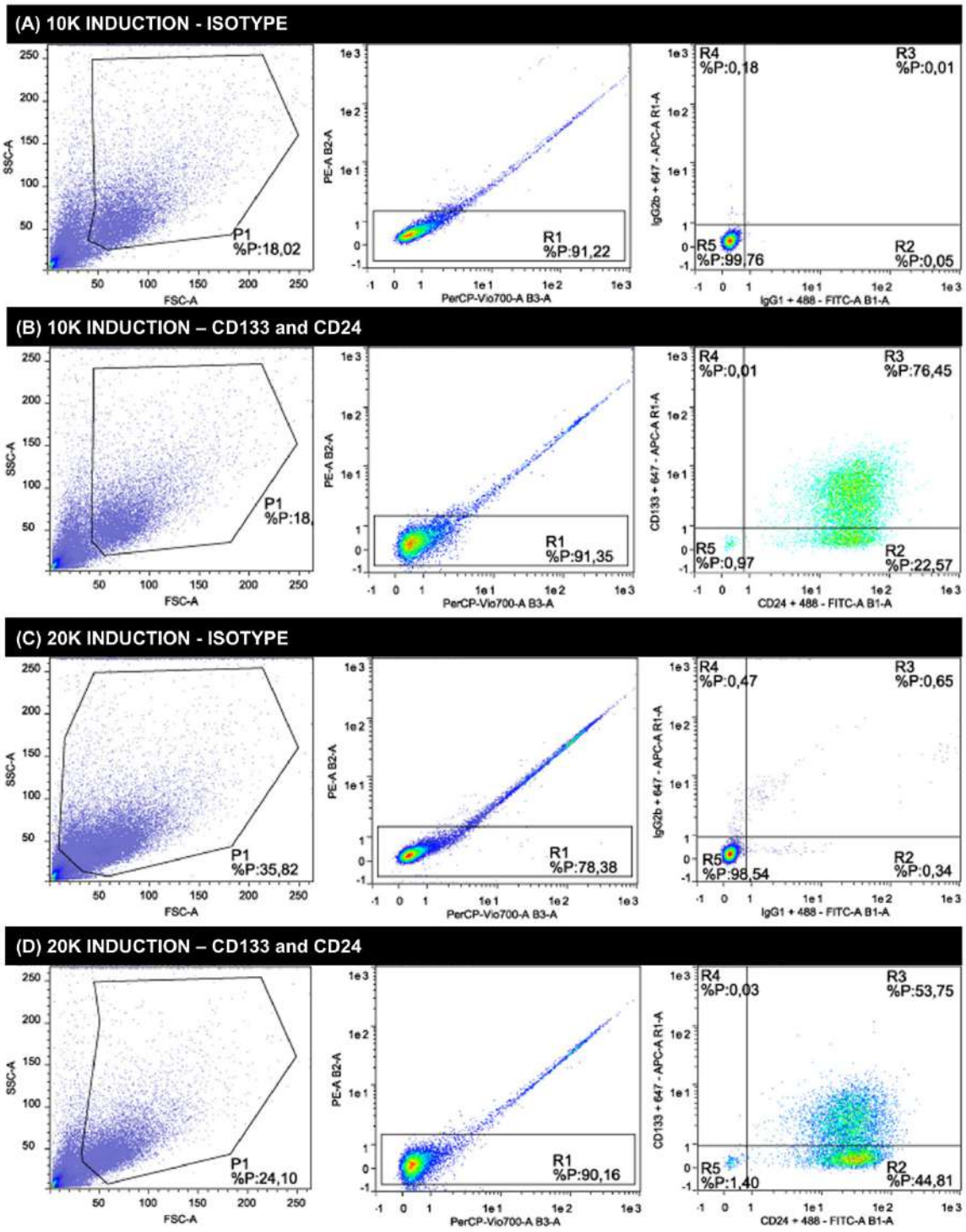


Figure S V-2 – Flow cytometry analysis for retinoic acid-stimulated conditions (induction). Density plots indicate the used gating for live cells - left and middle dot plots - excluding debris and PI-positive stained cells, respectively. Right plots indicate fluorescence of specific antibodies. (A) Gating for 10K isotype induction condition demonstrates 91 % live cells and 0.01 % Alexa Fluor 647 IgG2b and Alexa Fluor 488 IgG1 double positive cells; (B) Gating for 10K stained induction condition demonstrates 91 % live cells and 77 % CD133 and CD24 double positive cells; (D) Gating for 20K isotype induction condition

demonstrates 78 % live cells and 0.65 % Alexa Fluor 647 IgG2b and Alexa Fluor 488 IgG1 double positive cells; (B) Gating for 20K stained induction condition demonstrates 90 % live cells and 54 % CD133 and CD24 double positive cells.

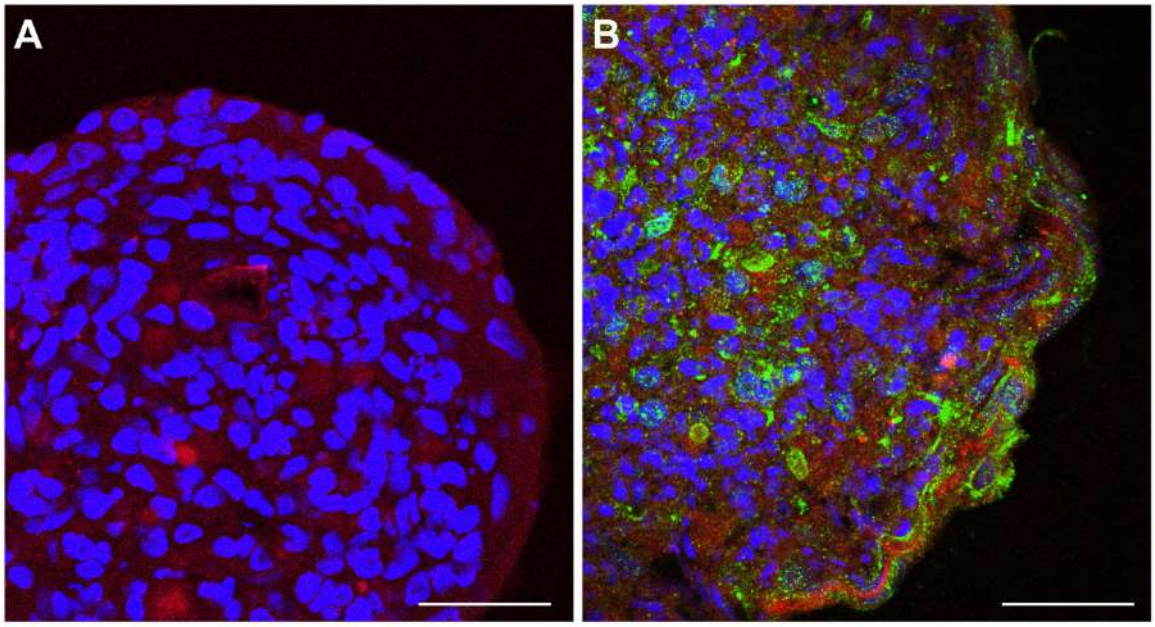


Figure S V-3 – Higher magnification (x63) images of hRPC spheroids with endothelial cells. Immunofluorescent staining of podocyte-related marker Nephrin (green) and of endothelial-related marker von Willebrand Factor (red). Images demonstrate spheroids composed of hRPCs + HMEC-1 without (A) and with (B) RA stimulation. Scale bar: 40 μm.

# SECTION 4

# STRATEGIES FOR RENAL REGENERATION

# Chapter VI

# Particulate kidney extracellular matrix: bioactivity and proteomic analysis of a novel scaffold from porcine origin

# Chapter VI

## Particulate kidney extracellular matrix: bioactivity and proteomic analysis of a novel scaffold from porcine origin[5]


### ABSTRACT

Decellularized matrices are attractive substrates, being able to retain growth factors and proteins present in the native tissue. Several biomaterials can be produced by processing these matrices. However, new substrates capable of being injected and reverse local kidney injuries are currently scarce. Herein, we hypothesized that decellularized particulate kidney porcine ECM (pKECM) could support renal progenitor cell cultures for posterior implantation. Briefly, kidneys are cut into pieces, decellularized by immersion on detergent solutions, lyophilized and reduced into particles. Then, ECM particles are analyzed for nuclear material remainings by DNA quantification and histological examination, molecular conformation by FITR and structural morphology by SEM. Protein extraction is also optimized for posterior identification and quantification by mass spectrometry. The results obtained confirm the collagenous structure and composition of the ECM, the effective removal of nucleic material and the preservation of ECM proteins with great similarity to the human kidney. Human renal progenitor cells (hRPCs) are seeded in different ratios with pKECM, on 3D suspensions. The conducted assays for cell viability, proliferation and distribution over 7 days of culture suggest these matrices as biocompatible and bioactive substrates for hRPCs. Also, by analyzing CD133 expression, an optimal ratio for specific phenotypic expression is revealed, demonstrating the potential of these substrates to modulate cellular behavior. The initial hypothesis of developing and characterizing a particulate ECM biomaterial as a consistent substrate for 3D cultures is successfully validated. The findings on this manuscript suggest these particles as valuable tools for regenerative nephrology by minimizing surgeries and locally reverse small injuries which can lead to chronic renal disfunction.


[5] This chapter is based on the following publication:

**Sobreiro-Almeida, Rita**; Melica, Maria Elena; Lasagni, Laura; Osório, Hugo; Romagnani, Paola; Neves, Nuno M. Particulate kidney extracellular matrix: bioactivity and proteomic analysis of a novel scaffold from porcine origin. *Biomaterials Science*, ahead of print, doi: 10.1039/D0BM01272F, 2020

## VI-1. INTRODUCTION

The extracellular matrix (ECM) is known to directly influence cell adhesion, migration, proliferation and differentiation. It is a specific product of resident cells providing not only support, but also biochemical cues crucial for determining cell fate and survival.[1, 2] Thus, tissue engineers have been trying to mimic not only the morphology but also the composition of the ECM for promoting repair and regeneration of tissues. Many studies refer candidate biomaterials by using micro- and nanofibrillar fabrication techniques, such as electrospinning[3–5] and/or supramolecular self-assembly.[6–8] However, these materials are often composed by synthetic polymers, which fail to reproduce the intricate network of proteins, growth factors, glycosaminoglycans and cytokines, inherent to the natural ECM.[9, 10]

In the past few years, decellularized tissues have been extensively studied because they enable retaining proteins and other components present in the native tissue. This naturally-occurring ECM has shown to be biocompatible, lacking immunogenic cell membrane proteins, and to promote site-specific remodeling of tissues, minimizing scar formation.[11, 12] Decellularized tissues are also advantageous because of the high degree of evolutionary conservation of many ECM components, which allows for the use of xenogeneic sources. These matrices are currently being studied as an alternative source for organ transplantation, where whole-organ decellularization, repopulation,[13, 14] and posterior *in vivo* implantation is achieved by using perfusion strategies.[15, 16] Despite the promising results obtained, a number of concerns remain to be addressed to translate this technique to the clinical practice. It is also important to consider new solutions for initial-stage repetitive episodes of Acute Kidney Injury (AKI), which can lead to irreversible renal damage and evolve into Chronic Kidney Disease (CKD).[17]

Several authors already reported the use of decellularized and processed kidney extracellular matrix to obtain several ECM-derived biomaterials, suitable for addressing early symptoms of kidney disease. Kidney ECM hydrogels from human origin were already developed and characterized for their properties and ability to support kidney endothelial cell culture.[18, 19] Other authors also studied the growth and metabolism of kidney stem cells when seeded on hydrogels from three different regions of the kidney, revealing tissue and region-specificity.[20] However, cells were seeded on top of the hydrogels and, therefore, in 2D. Another approach is to combine kidney-derived ECM with other components (natural or synthetic) in order to enhance its limited mechanical properties. For instance, a small portion (10 %) of porcine derived kidney ECM was combined with a synthetic polymer to fabricate a porous scaffold. This scaffold was implanted in a partially nephrectomized mice *in vivo*, demonstrating regeneration of renal glomerular tissue, with some inflammatory response.[21] Other works have also followed this rationale,

developing alginate and gelatin-based hydrogels in combination with kidney matrices as new bioinks for 3D printing.[22, 23] Although hybrid biomaterials can provide diverse cellular responses, it is also important to study the composition-related response of the host tissues. Having a particulate form of ECM can also be of advantage because of their small size and shape, which allows for their implantation by non-invasive techniques, such as injections,[24] enabling cell delivery on a specific defect and/or injury of any size or shape.[25] This particulate ECM can also circumvent the problems of low cellular migration on hydrogels, allowing for a more efficient cell spreading. Some studies were published in the past few years using particulate ECM as a cell carrier for regeneration of several tissues, such as cartilage,[25] adipose tissue[26] and bone.[27]

In this work, we hypothesized that decellularized porcine kidney ECM particles possess similar composition to the human kidney, enabling the 3D culture of human-origin cells, without changing their phenotypic expression. To the best of our knowledge this is the first time that porcine kidney matrix is fully characterized by proteomic analysis and also the first time that renal progenitor cells are cultured in 3D with natural ECM. We believe that this substrate can be promising for cell delivery and, ultimately, to promote kidney regeneration.

## VI-2. MATERIALS AND METHODS

Expanded methods for morphological, structural, histological and biochemical analysis of particulate kidney ECM as well as the nano-liquid chromatography–tandem mass spectrometry (nanoLC-MS/MS) methodology for characterization and relative quantification of protein composition can be found in Supplementary Experimental Section. Detailed information about the isolation and characterization of human renal progenitor cells (hRPC) is also provided.

### VI-2.1. Processing and characterization of kidney ECM derived powders (pKECM)

#### VI-2.1.1. Kidney decellularization and pKECM preparation

A schematic representation of the whole process is shown on Figure VI-1. Fresh porcine kidneys obtained from a local slaughterhouse were decellularized according to a previously described method with minor modifications.[28, 29] After removing renal capsules and pelvis, kidney was sectioned (A). After, portions were immersed in a solution of 1 % SDS before being changed to another solution of 1 %

Triton X-100 and washed for removal of residual detergent with Milli-Q water for 7 days (B). The whole process was performed at 4 °C. The portions were frozen at -80 °C before being freeze-dried (C). Next, the pKECM was obtained by milling with a cryogenic grinder (SamplePrep Freezer/Mill, SPEXSamplePrep) and sterilized by ethylene oxide (D). Sterile pKECM was stored at 4 °C until further use.


Figure VI-1 – Sequence of procedures used in the preparation of pKECM. (A) Porcine kidneys were obtained in a local slaughterhouse and cut into sagittal sections before being washed in distilled water. (B) Sections were immersed in detergent solutions of 1 % SDS and 1 % Triton X-100 and placed on an orbital shaker for 7 days. Decellularization was achieved by frequent renewal of the solutions. (C) The decellularized tissue was freeze-dried. (D) pKECM was obtained using a cryogenic mill. Scale bar: 1 cm.

### VI-2.1.2. Protein extraction from pKECM substrates

Decellularized kidney particulate protein was extracted in three fractions. A brief scheme of the whole process is represented in Figure VI-3. Approximately 5 mg of pKECM was processed in triplicate. One mL of Urea Extraction Buffer (8 M Urea, 10 mM ammonium bicarbonate and 25 mM of tris(2-carboxyethyl)phosphine, pH 8.0) supplemented with 10 mg $mL^{-1}$ of dithiothreitol (abcr GmbH) and 20 µL $mL^{-1}$ of protease inhibitors (Sigma Aldrich) were used to homogenize the matrix with a tissue grinder (Nippon Genetics). After, the matrix was incubated with the buffer overnight in agitation. The homogenized pKECM was centrifuged at 12700 rpm and the supernatant, referred as Fraction 1, was removed and saved. The pellet was once again homogenized and centrifuged. The resultant supernatant was joined to the soluble Fraction 1 (F1). Urea extraction buffer was again added to the resultant pellet and vortexed. The mixture was sonicated at 40 % amplitude while being refrigerated. After centrifuging, the supernatant was saved as Fraction 2 (F2). The remaining pellet was digested with trypsin as described in section 2.2.5. to yield Fraction 3 (F3).

## VI-2.2. *In vitro* renal progenitor cell culture studies on pKECM

### VI-2.2.1. Preparation of the constructs and cell seeding

The effect of pKECM on cell behavior was analyzed having 3 different ratios of pKECM to hRPCs. Suspension tissue culture 48-well plates were used in this study. In order to perform non-adherent cultures, plates were coated with a thin layer of 1.5 % agarose gel which was left to gelify overnight at 4 °C. After that, 1, 2 and 4 mg of pKECM were weighted and added to each well before being rehydrated with complete medium for 30 min at 37 °C. A cell suspension of 50 µL containing $10^5$ hRPC was added to each well and left 30 min at 37 °C to adhere to pKECM substrates. After that, complete medium composed by Microvascular Endothelial Cell Growth Medium (EGM-MV, Lonza) supplemented with 20 % HyClone™ Fetal Bovine Serum (FBS, GE Healthcare) was added. The same cell concentration was seeded without the presence of pKECM in tissue culture treated polystyrene plates for the adherent cultures (2D control). The medium was changed every 2 or 3 days.

### VI-2.2.2. hRPC viability and proliferation

The viability of hRPCs was evaluated both by indirect and direct culture method. For the first, conditioned medium (EGM-MV exposed to pKECM during 24h) was added to hRPCs cultured on tissue culture plastic. Macroscopic evaluation of cells' morphology and growth was evaluated after 2 and 24 h of plating, comparing with cells cultured in EGM-MV media. Direct evaluation of pKECM viability was performed on cell+pKECM suspensions after 1, 2, 4 and 7 days of culture using alamarBlue (BioRad) assay. Culture medium was removed and replaced with fresh medium supplemented with 10 % of alamarBlue reagent. After an incubation period of 7 h at 37 °C, the supernatant was used to determine the fluorescence intensity in a microplate reader (excitation: 530/25 nm; emission: 590/25 nm). For the evaluation of the effect of the different ratio of cells/pKECM on cell viability, a live/dead assay was performed using PI and Calcein, AM (Thermo Fisher). The fluorescent dyes were incubated with the constructs at a concentration of 1 µg $mL^{-1}$ for PI and 2 µg $mL^{-1}$ for Calcein, AM in DPBS for 30 min at 37 °C. After this time, the constructs were visualized using a SP5 AOBS confocal microscope (Leica, Wetzlar, Germany) equipped with a Chameleon Ultra-II two-photon laser (Coherent, Milan, Italy). Images were recorded digitally and further processed using LASX software (Leica).

To evaluate hRPCs proliferation on the different cell/matrix ratios, dsDNA quantification was performed. After the viability assay, constructs were rinsed in DPBS to release the alamarBlue dye. After, specimens were immersed in Milli-Q water and cells were lysed by thermal and osmotic shock. The resulting supernatant was used for DNA quantification with Quanti-iT Picogreen dsDNA assay kit (ThermoFisher). The fluorescence of each specimen was measured using a microplate reader (excitation: 485 nm; emission: 528 nm). The DNA concentration for each sample was calculated using a standard curve.

### VI-2.2.3. hRPC distribution and stemness potential

For microstructure analysis of the cellular adhesion onto different quantities of pKECM, after 7 days of culture, constructs were washed with DPBS and fixed in 2.5 % glutaraldehyde (Sigma Aldrich) for 1 h at 4 °C. After the fixation step, they were washed again and dehydrated through an alcohol series. Samples were sputter coated with gold prior to analysis and micrographs were obtained using a scanning electron microscope (SEM, JSM-6010 LV, JEOL).

For the histological analysis of the distribution of cells on the matrix after 7 days, constructs were fixed in 10 % neutral buffered formalin and embedded in OCT compound for cryosectioning. H&E and MT stainings were performed on the constructs. Staining intensity and cell distribution were observed under light microscopy (DM750, Leica).

The stemness potential of hRPCs cultured in pKECM was evaluated by immunocytochemistry after 7 days of culture. Briefly, constructs were fixed with 10 % neutral buffered formalin for 1 h at 4 °C and then washed in PBS. Cells were further incubated with antibody against CD133 marker for hRPCs (Miltenyi Biotec; 1:2.5 diluted in 3% BSA/PBS) for 1 h at RT. Samples were washed with PBS and incubated with the secondary antibody Alexa Fluor 488 (Alfagene; 1:500 diluted in PBS) at RT in the dark for 1h. DAPI (Sigma Aldrich, 1:500) and Alexa Fluor 546 Phalloidin (Alfagene; 1:200) were incubated along with the secondary antibody. After several rinses in PBS, constructs were analyzed under a Leica SP5 AOBS confocal microscope. Cells cultured in conventional polystyrene plates without pKECM were used as control. Images were recorded digitally and further processed using LASX software (Leica).

### VI-2.3. Statistical analysis

Statistical analyses were performed with GraphPad Prism 8 (GraphPad Software, California, USA). Data were expressed as means ± standard deviation of experiments with at least three independent assays. Differences between groups were analyzed by unpaired t test or two-way analysis of variance (ANOVA) in case of experiments conducted over time, using Tukey test for post hoc assessments of the differences between samples. Statistical significance was defined as $p < 0.05$.

## VI-3. RESULTS

Naturally occurring ECM has been gaining interest in the past few years in the tissue engineering field. This matrix, in a particulate form, enables developing injectable advanced therapies. Herein, we aim at characterizing the ECM particulate morphology, composition and bioactivity when supplemented in cultures of specific renal progenitor cells.

### VI-3.1. Evaluation of pKECM substrates

This section will report on the studies aiming at characterizing the particulate ECM structure and morphology. Its protein and DNA content are compared with those of native kidney tissue. Also, the effects of ethylene oxide sterilization on thermal and conformational behavior were evaluated. Its protein composition was extensively characterized by mass spectrometry and further compared with human renal proteomic content.

#### VI-3.1.1. pKECM biological and structural characterization

ECM particles were obtained with minor modifications of a published protocol.[28, 29] The macroscopic structure of the decellularized kidneys shows being intact, with effective cell removal with minor loss of collagen. In the present study, we focused on characterizing the structure of the powders to show bioactivity even after processing by milling and freeze-drying. In Figure VI-2-A, we can observe the gross appearance of the obtained powders. By microscopic evaluation with SEM (Figure VI-2-B and C) we can notice highly irregular size and shape. Particles with size ranges from 10 to 100 µm can be found on the micrographs, presenting a sheet-like shape, characteristic of collagenous material.[24, 30]

To assess the effect of decellularization and processing of the matrix on the molecular composition, ATR-FTIR analysis was performed to native, decellularized and sterile pKECM samples (Figure VI-2-D). The spectra, characteristic of collagenous components, presents several bands and peaks that will be herein described. The band at 3284 $cm^{-1}$ is characteristic of amide A for NH stretching. Also, the peaks at 2848 and 2916 $cm^{-1}$ are characteristic of OH, $NH_2$, and NH stretching vibration in the amide group. The peaks at 1631 and 1537 $cm^{-1}$, respectively, are characteristic of the C=O (amide I) stretching vibration and to the bending and stretching vibration of NH and CN (amide II).[31] The peak at and 1232 $cm^{-1}$ is relative to the NH plane bending from amide linkages (amide III), associated with the secondary conformation of collagen. The peak identified at 1450 $cm^{-1}$ and the region in the range of 1,417–1,360 $cm^{-1}$ corresponds to the stereochemistry of the pyrrolidine rings of proline and hydroxyproline.[32] No significative difference was found between the spectra of native kidney, pKECM and pKECM submitted to EO sterilization process, suggesting that the molecular conformation of ECM and collagen does not change by decellularization and/or sterilization process.

Differential Scanning Calorimetry (DSC) was used to compare the thermal properties of pKECM substrates before and after sterilization process and compared to the thermal properties of native samples (Figure VI-2-E). In all samples the matrix demonstrates a broad transition temperature from approximately 15 °C to 140 °C, with one distinct endothermic peak. Enthalpy has a shift from 181 to 306 J/g when samples are decellularized. The melting temperature (Tm) peaks range from approximately 73 to 77 °C, which are within the range of collagen melting temperature. Additionally, another endothermic peak appears around 225 °C for both decellularized conditions and also for native samples, but in a minor extent.

To assess effective removal of cellular content, specimens were embedded in OCT and the obtained cryosections were stained with H&E and MT. Also, dsDNA quantification enables a quantitative measurement of the effectiveness of the decellularization process. H&E micrographs demonstrate no violet staining for nucleus (Figure VI-2-G), representing a successful decellularization, in comparison to the native tissue (Figure VI-2-H). As eosin Y binds to positively charged amino-acid side chains such as lysine and arginine, we found that the pKECM stains positive for it, evidencing their protein content and structure in 2D. This staining is comparable to the native tissue (Figure VI-2-H), where the pink color can also be found surrounding the nucleus, evidencing the cytoplasm and ECM. Corroborating these results, MT staining for pKECM revealed no red staining for Weigert's iron hematoxylin (Figure VI-2-I), comparing with the native tissue (Figure VI-2-J). Double-stranded DNA quantification confirms an effective removal

of > 90 % of the nucleic material when comparing with the native tissue, confirming an adequate protocol for kidney decellularization (Figure VI-2-F).

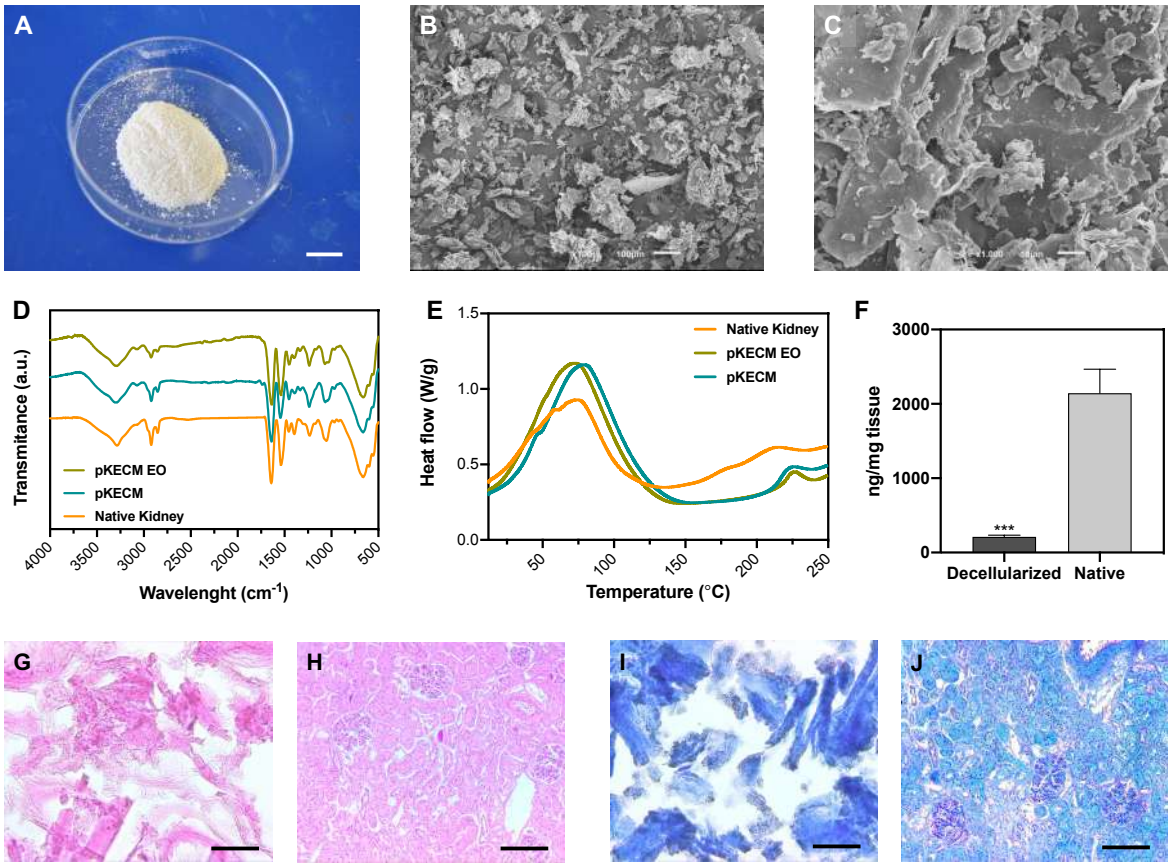


Figure VI-2 – Particulate kidney matrix characterization. (A) Gross appearance of the powders obtained after decellularization, freeze-drying and milling process. Scale bar: 1 cm; (B-C) Scanning electron microscopy micrographs of the powders. A broad distribution of sizes is presented, with collagen-characteristic sheet-like conformation. Scale bars: 100 and 10 µm. (D) Fourier Transformed Infrared Spectroscopy and (E) Differential Scanning Calorimetry characterization of native kidney (orange), decellularized matrix (pKECM, blue) and decellularized matrix submitted to Ethylene Oxide sterilization (pKECM EO, green). Results suggest maintenance of molecular composition and thermal properties of the matrix after decellularization and after ethylene oxide sterilization process. (F) DNA quantification of decellularized and native tissue demonstrating a ~90% decrease on dsDNA content (n = 3). ***p<0.001 vs native; (G-H) Hematoxylin and Eosin and (I-J) Masson's Trichrome staining on cryosections of native tissue (H-J) and decellularized matrix (G and I). Nuclear staining is not present on decellularized matrix sections and collagenous staining is seen (blue). Scale bars: (G- I): 50 µm, (H- J): 200 µm.

### VI-3.1.2. Proteomic analysis of decellularized pKECM

In order to provide a complete characterization of the proteomic profile of porcine kidneys after decellularization, we did a 3-fraction proteomic extraction and analyzed the content in each one of these fractions. For this study, 3 different decellularized kidneys were used as representative of sample variability. The workflow, represented in Figure IV-3-A, was optimized to yield the maximum quantity of

protein without compromising protein stability and avoiding degradation. Therefore, a higher amount of proteins is expected in Fraction 1 (F1) compared to the other fractions. With this study, we aim to evaluate this protocol in extracting the proteins present in the insoluble part of the decellularized ECM and also to avoid the effect of the initial sonication and enzymatic digestion on more sensible proteins. Together we were able to identify 77 relevant ECM proteins, in which 43 of them were common to the 3 fractions, which corresponds to ~ 56 % of total ECM proteins (Figure IV-3-B). Moreover, only 6 new proteins were identified in F2 and F3, which include collagen alpha-1 (V) chain, elastin and fibulin 5. A tendency was observed regarding the total number of proteins identified; 364 in F1, 208 in F2 and 119 in F3, which represents a drop of ~67 % on the total amount of proteins identified from F1 to F3.

To better categorize the proteins that are present in each fraction, we performed gene ontology analysis of the characterized ECM proteins. This categorization was not completely automatic because the UniProt database for porcine (*Sus scrofa*) is less informative than that of the human (*Homo sapiens*). Therefore, and because some proteins were still "uncharacterized", the majority were confirmed and classified manually. The most abundant of them is collagen type IV, which is herein named as "COL4*" because the NC1 domain could not be identified. We have noticed that although we were able to extract the majority of proteins in F1 (59 out of 77), they did not represent the abundance expected from a naturally-sourced biological kidney matrix. So, we graphed all of the identified proteins as a percentage of the total protein abundance by gene ontology classification (Figure IV-3-C). From this analysis we could observe that fibrillar collagen only constitutes ~10 % of the proteins identified in F1, while matricellular proteins account for ~37 % of whole protein abundance. Furthermore, by analyzing F2 and F3, ~69 % and ~55 % of their content is composed of fibrillar collagen, and ~23 % and ~41 % is composed of basement membrane proteins, respectively. Accordingly, the amount of proteins representing ECM regulators, FACIT collagens, secreted and matricellular proteins decrease radically from F1 to F3. Indeed, in F3, only ~4 % of the proteins correspond to this kind of proteins, being the remaining ~96 % basement membrane and fibrillar collagen proteins. These results support our initial hypothesis; the chaotropic insoluble pellet, which is typically discarded in proteomic analysis of this kind, is mainly composed of fibrillar collagen and basement membrane proteins, essential components of the ECM. Encouragingly, cytoskeletal components represent less than 1 % of the total amount of proteins, which confirms once more a successful protocol of decellularization.

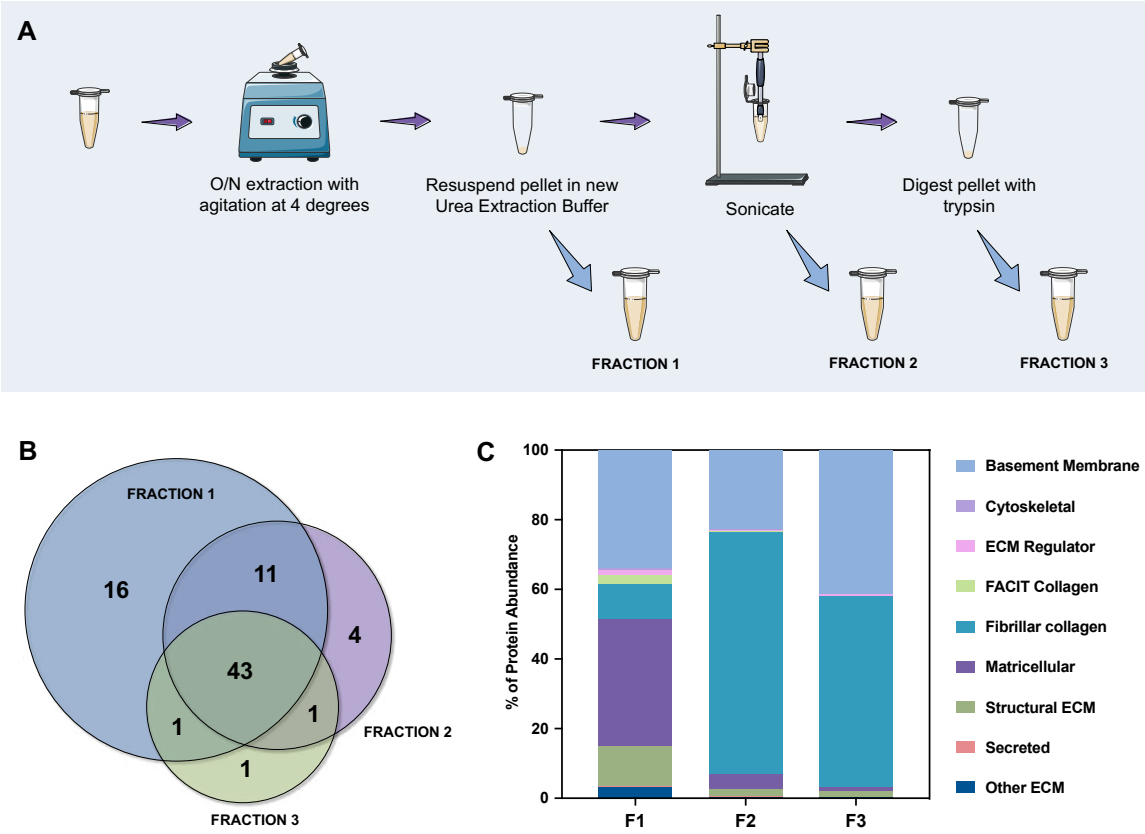


Figure VI-3 – Schematic representation of the methodology and the unique profile of the ECM fractions. (A) Fraction 1 was obtained by homogenization with Urea Extraction Buffer, Fraction 2 was obtained after sonication of the remaining pellet and Fraction 3 was obtained after tryptic digestion of the Fraction 2 pellet; (B) 43 proteins are common to the three fractions being most proteins identified on fraction 1 (F1), while only 6 new proteins were found in fraction 2 and 3 (F2 and F3). (C) F2 and F3 are mainly composed by basement membrane proteins and fibrillar collagen, which lead us to conclude that F1 abundances do not correspond to the total protein isolated, and that several steps of protein homogenization are required to extract the total amount of protein.

A more detailed description of the identified proteins is shown on Table S VI-1. The percentages of each protein present on each analyzed kidney sample (K1, K2 and K3) and their coefficient of variation (CV) were calculated. We could notice that high variances (greater than 1) were mainly detected on ECM regulators family of proteins, rather than in the most abundant components of the matrix. This feature is expectable due to the decellularization process, in which those proteins are more easily removed. In proteins such as collagen type IV, collagen type I, collagen type VI, perlecan and nidogens, CV calculated values were lower than 0.5.

Absolute quantitative abundances of the 30 more expressed ECM proteins were graphed in a heat map for each separate sample that was analyzed by MS (Figure S VI-1), where *green* represents the lowest abundances, *red* represents the higher abundances and *black* denotes the middle-term. We managed to extract the majority of proteins in F1, a consistent result within the 3 replicas. However, as

previously noticed in Figure IV-3-C, the extraction of fibrillar (collagens type I and III) and basement membrane collagens (collagen type IV) revealed higher abundances in F2 and F3 extractions. On the contrary, matricellular collagens (collagen type VI) have a decrease in abundance from F1 to F3. The same phenomena occurred for all of the remaining proteins identified. We couldn't notice the presence of nidogen-1 in F3, which was the only protein in this set which could not be detected in the 3 fractions. The overall profile denotes that chaotrope protein extraction may give us a reasonable idea of the group of proteins that constitute the matrix, but cannot give us a rigorous quantification, which was only possible when separating the fractions and quantifying separately.

To have a stronger analysis of our protein profile, we have performed pie chart analysis for total ECM components of the kidney considering the three independent tissue replicas (Figure VI-4). Percentages were obtained by dividing the individual abundance of each identified protein by the total ECM abundance content. Fibrillar collagens, basement membrane and matricellular proteins were further analyzed, and a sub-pie chart is presented for each one of these categories, given that together they constitute more than 92 % of the total protein content. As expected, the main component of basement membranes is collagen type IV (70 %). Matricellular protein analysis revealed that collagen type VI composes 76 % of the total amount of identified proteins and collagen type I composes 92 % of fibrillar collagen existent in porcine kidneys.

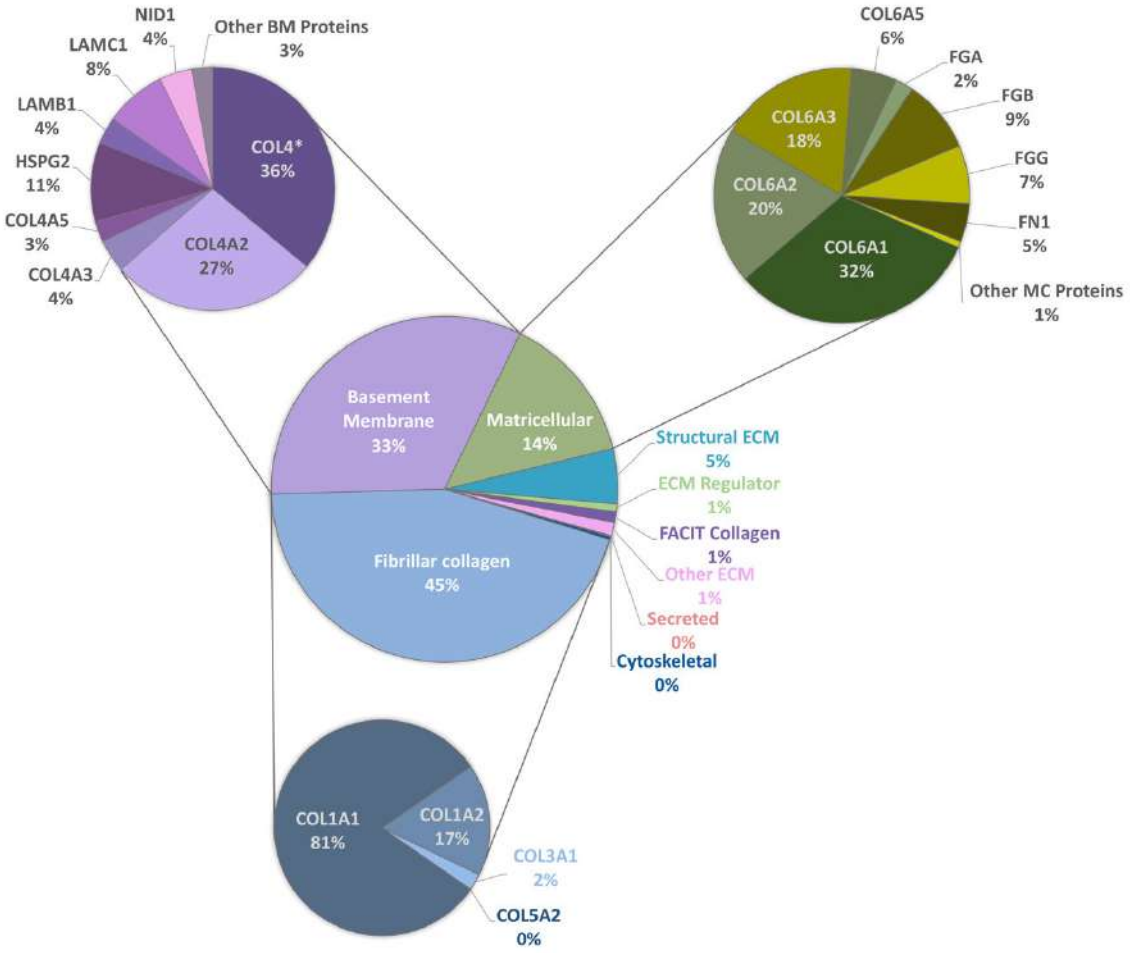


Figure VI-4 – Quantitative assessment of proteomic profile of pKECM by LC-MS/MS. A sub graph is demonstrated for the most abundant ECM categories: fibrillar collagens (blue), basement membrane proteins (purple/pink) and matricellular proteins (green). Quantitative proteomics demonstrate that collagen type IV composes nearly 70 % of basement membranes; collagen type I composes 92 % of total fibrillar collagen content and collagen type VI is 76 % of total matricellular proteins. Proteins are identified with the respective gene name. This proteomic analysis enlightens the three major collagenous components of the porcine kidney ECM.

## VI-3.2. 3D culture of renal progenitor cells and pKECM

This section includes the evaluation of the bioactivity of particulate ECM to stimulate specific renal progenitor cells in a 3D culture. Cytocompatibility and cell proliferation were evaluated, as well as the capacity of the ECM to guide phenotypic changes.

### VI-3.2.1. hRPC viability and proliferation studies

hRPCs were obtained from the mechanical enzymatic digestion of kidney fragments. They were isolated for their unique capacity of self-renewal and high clonogenic potential, which does not occur for terminally differentiated cells, such as those composing the renal tubule or the Bowman's capsule. Flow Cytometry (FC) analysis was also performed and we were able to demonstrate that the recovered population homogeneously exhibit the presence of CD24 and CD133 (~ 94 %), known to be specific stem cell markers which when co-expressed identify this population of cells (Figure S VI-2).[33]

To assess pKECM cytotoxicity, we first evaluated cell viability when in contact with pKECM conditioned medium. Figure VI-5-B and D demonstrates cells after 2 and 24 h of conditioned culture, respectively. No morphological differences are observed between these cells and cells submitted to regular culture medium (Figure VI-5-A and C), giving a first insight on the biocompatibility of this matrix. Next, the matrix was directly cultured with particulate ECM for 7 Days and live/dead staining was performed with Calcein AM and PI to 1, 2 and 4 mg of pKECM (Figure VI-5-E, F and G, respectively). No significant red staining is visible, indicative of the biocompatibility of this substrate, regardless of the quantity used for the assays. However, a higher quantity of cells can be seen on 1 and 2 mg of matrix comparing with 4 mg. Also, an alteration on morphology is present, being that cells cultured on 4 mg of matrix are bigger and rounder, suggesting lack of adhesion points to the pKECM. On the other hand, cells cultured with lower quantities of matrix demonstrate evenly distribution and a higher amount of green staining, also suggesting higher cell viability and proliferation. Quantification of fluorescence intensity was also performed, corroborating the previous findings (Figure VI-5-H). Although not significant, PI staining is only visible on cells cultured on 1 mg of pKECM. This can be explained due to the high proliferation and higher cell confluence present on these constructs, which can lead to cell death. As the quantity of matrix increases, the cell number diminishes and, as a consequence, the number of live and dead cells also decrease, leading to no dead cells quantified on 4 mg of pKECM.

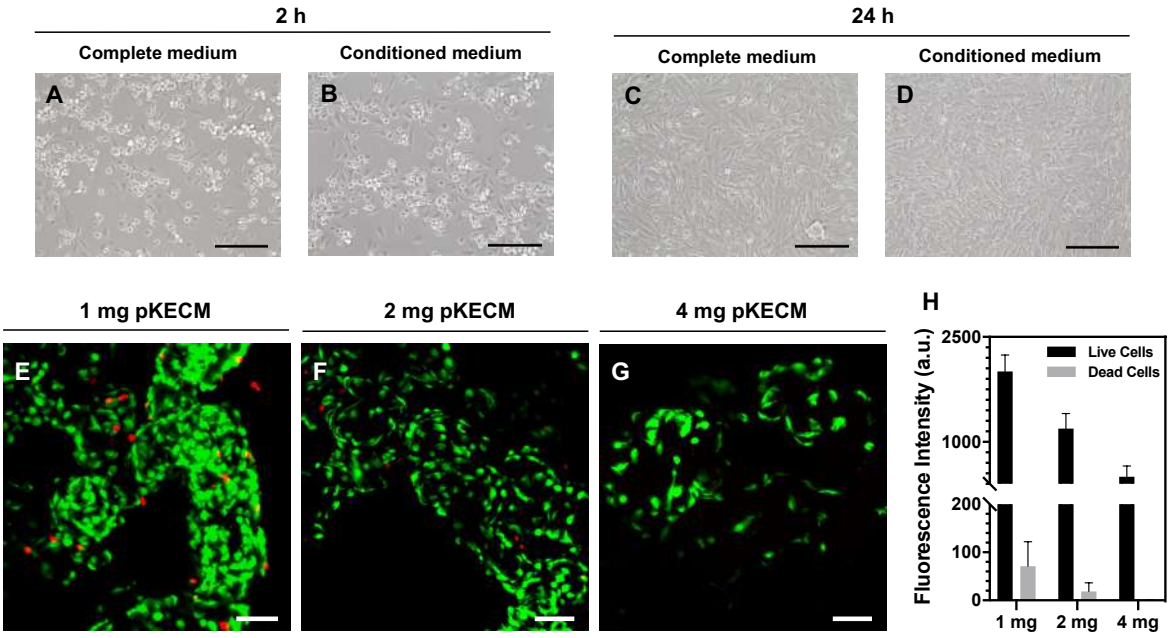


Figure VI-5 – Cytocompatibility of human renal progenitor cells. (A-D) Optical microscope images of hRPCs after 2 and 24 h of seeding in complete medium (EGM-MV) or conditioned medium (EGM-MV prior exposed to pKECM during 24 h). Conditioned medium cultures (B and D) demonstrate no morphological changes on the hRPCs comparing with complete medium cultures (A and C). Scale bar: 200 µm; Qualitative results for viability were obtained by immunofluorescence micrographs of live/dead assay for hRPCs after a 7-day culture time with (E) 1 mg, (F) 2 mg and (G) 4 mg of matrix. Cells were incubated with Calcein AM (stains green for live cells) and PI (stains red for dead cells). Scale bar: 100 µm; (H) Quantification of fluorescence intensity of live and dead cells was performed on ImageJ, corroborating Live/Dead stainings (n = 3).

As a corroborative assay, hRPCs metabolic activity was quantitatively assessed overtime using alamarBlue on hRPCs seeded on pKECM substrates (1, 2 and 4 mg) and on tissue culture plastic (0 mg) (Figure VI-6-A). We noticed that hRPC shown viable in all timepoints when in contact with pKECM, revealing no cytotoxicity. We can additionally notice a common tendency for a peak increase in intermediate culture times and then a decrease of the metabolic activity after 7 days of culture. We hypothesized this event to be a result of achieving cell confluence after 4 days, reducing cellular metabolic activity. We can also observe that after 2 days of culture, cells were shown more metabolically active when cultured on intermediate amounts of matrix (2 mg), which was also observed at day 4, being statistically different from all the other conditions. At day 7, cells are shown more metabolically active when cultured on the higher amount of matrix, which is also attributed to the lack of cell confluence on these substrates.

Cellular proliferative capacity was inferred from the quantification of double-stranded DNA present on hRPCs (Figure VI-6-B). After 24 h, RPCs cultured on 0 and 4 mg substrates present the higher proliferation capacity. However, throughout the timepoints, cells seem to not be proliferating on the 4 mg

condition, being the concentration of dsDNA maintained after 7 days of culture on the substrates. Nevertheless, there is a tendency for the increasing of DNA content from day 1 to day 7 on the cells cultured on lower amounts of pKECM (1 and 2 mg). This is a good indicator of cells preference towards lower quantities of particulate matrix. It is also important to notice a tendency from day 4 to day 7 of higher proliferation capacity of the cells when cultured on 1 mg instead of 2 mg of pKECM. This can be again explained by the lower quantity of substrate, which enables higher surface area for cells to attach and proliferate. Instead, in 2 mg of matrix, although cells can proliferate in between the ECM particles, this effect becomes reduced as the amount of matrix increases. This can also be corroborated by the lower DNA content demonstrated on 4 mg of pKECM. The increasing values observed for 0 mg condition translate the proliferating capacity of these cells on tissue culture plastic, although it cannot be directly compared with our 3D suspension conditions.

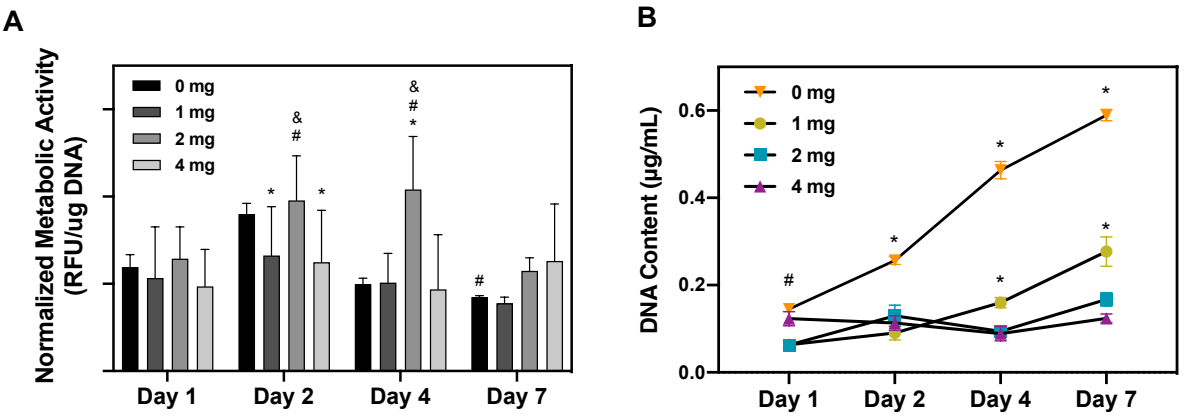


Figure VI-6 – Quantitative analysis of viability and proliferation of hRPCs cultured on pKECM. (A) Viability assay demonstrated by alamarBlue fluorescence over 7 days timepoints. Control condition (0 mg) represents hRPCs cultured on tissue culture plastic; RFU = Relative Fluorescence Units; (*) statistically different from 0 mg; (&) statistically different from 1 mg; (#) statistically different from 4 mg (n = 9); (B) Proliferation assay demonstrated by quantification of DNA over time. (*) statistically different from all conditions; (#) statistically different from 1 and 2 mg conditions; (n = 9).

### VI-3.2.2. Evaluation of morphology and phenotype

To assess cellular phenotype when cultured on these substrates, we evaluated the presence of a known hRPC marker, CD133. Also, alteration on the morphology of the cells was evaluated by IHC and SEM to detect phenotype changes. H&E and MT stainings are shown on Figure VI-7-A, B, C and Figure VI-7-D, E, F, respectively. These stainings reveal maintenance of the collagenous content and the attachment of hRPCs to the matrix. The pKECM substrates stain pink in H&E and blue in MT staining, indicative of their collagenous nature. These substrates can be seen covered with cells, which stain purple

on H&E and red on MT staining. A higher amount of nucleus can be found with lower quantities of pKECM used in the culture, as observed previously. Regarding the CD133 staining, the marker was only present on cells seeded on 1 and 2 mg of pKECM (Figure VI-7-G and H). No CD133 expression was found on cells cultured on 4 mg of matrix (Figure VI-7-I), as well as on 2D cultures of hRPCs in tissue culture plastic (data not shown). Evaluating the morphology and distribution adopted by the cells around the matrix by SEM micrographs, we can observe a confluent culture and full coverage of this surface with cells when cultured on 1 mg of pKECM (Figure VI-7-J), being slightly lower when comparing with cells cultured on 2 mg of pKECM (Figure VI-7-K). These micrographs corroborate the IF images shown, which also suggest a lower number of cells and different distribution when cultured on 4 mg of pKECM (Figure VI-7-L), as well as altered overall cellular and nuclear size of the cells, which was confirmed by phalloidin (Figure VI-7-I) and Calcein-AM staining (Figure VI-5-G).

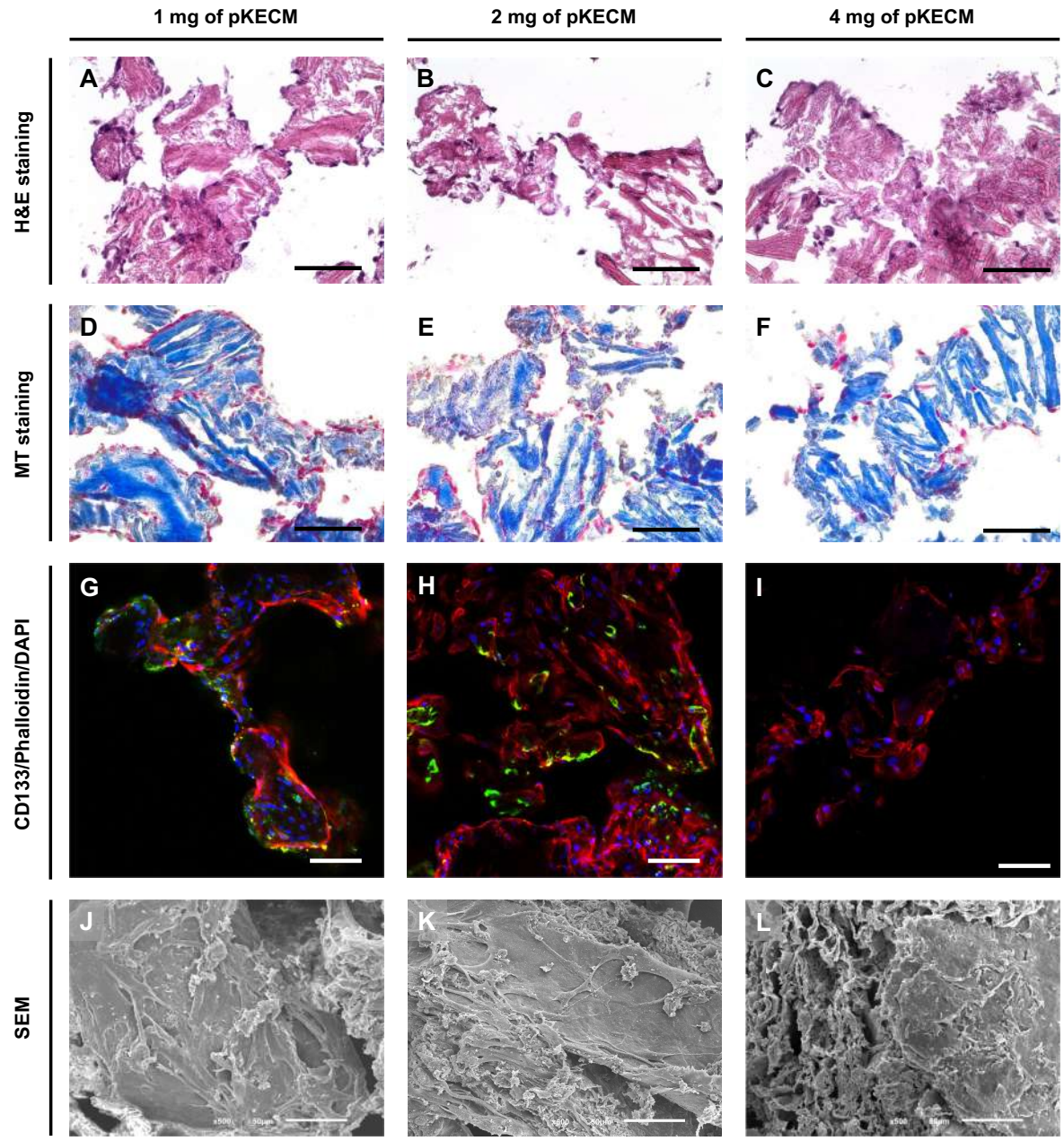


Figure VI-7 – Spatial distribution of hRPCs cultured on pKECM substrates. Immunohistochemistry on matrix cryosections for Hematoxylin and Eosin (A-C) and Masson's Trichrome (D-F) demonstrate good cellular coverage around the powders mainly on 1 and 2 mg of pKECM after 7 days of culture. Scale bars: 100 µm. (G-I) Immunofluorescence of CD133 (green), phalloidin for cytoskeleton (red) and DAPI for nuclei (blue) demonstrate greater fluorescence of the stem marker on 2 mg of pKECM. Scale bar: 100 µm. (J-L) Scanning Electron Microscopy images of hRPCs cultured on matrix after being fixed and dehydrated. After 7 days, overall cell coverage of the substrate is found on 1 and 2 mg of pKECM. Scale bar: 50 µm.

## VI-4. DISCUSSION

This work was focused on developing a particulate kidney matrix to act as a new advanced therapy for kidney diseases. We performed structural, morphological and proteomic characterization and as a second aim, we optimized a strategy to culture cells of human origin *in vitro* with the matrix. We suggest that decellularized kidney particles retain the biological efficacy needed to maintain the stemness of renal progenitor cells. The injection of cells alone has a number of shortcomings. Without a substrate to attach, a lot of cells are lost in the process or migrate out of the intended site of action and frequently there is insufficient cell engraftment to obtain clinically relevant efficacy. Therefore, we propose a synergistic effect of using pKECM as a substrate in which hRPCs could be delivered, helping in the renal repair after injury.

To ensure that the cells can interact, attach and proliferate in the particulate matrix, it is important to evaluate the structure and composition of the ECM. SEM micrographs (Figure VI-2-B and C), allow detecting two distinct surface ultrastructures within the particles: smooth surfaces, demonstrating the sheet conformation of basement membranes and fibrous surfaces, which can be assigned to the interstitial matrix.[24] We also noticed the resemblance of the matrix to those of other previously published works.[30] By ATR-FTIR we could not detect any alterations in molecular conformation between native and decellularized samples (Figure VI-2-D), indicating the preservation of the structure. Moreover, we can infer from the FTIR spectrum that the integrity of the triple helix was conserved by the ratio of 1235 $cm^{-1}$ (amide III) and 1450 $cm^{-1}$ (pyrrolidine ring) bands, which is close to 1 in both samples.[34] By DSC, we could confirm that decellularization and sterilization did not change the thermal properties of the native tissue. Additionally, the broad transition temperature range presented in the DSC thermogram, indicates the specific distribution of the collagenous population in the particulate matrix.[31] The difference observed between melting peaks (4 °C range) is attributed to variability between samples, since they were not performed on the same kidney sample. The enthalpy values also differ between native and decellularized samples. To the best of our knowledge, this is the first report on the thermal behavior between native and decellularized samples of kidney tissue. We suggest that this difference is due to the natural plasticizer effect of the cells, which reduces the forces of attraction between ECM fibers, thereby reducing the enthalpy needed for denaturation, as previously reported.[35] We also investigated the remainings of cellular and nuclear materials by DNA quantification and hematoxylin staining of pKECM frozen sections. We demonstrated that > 90% of the nucleic material was removed after powder digestion (Figure VI-2-F). Additionally, no hematoxylin staining for DNA was found on IHC stainings (Figure VI-2-G and I). By comparing our findings with previously published results, we were able to notice structural,

morphological and thermal properties very similar to other decellularized matrices.[30, 36] Thus, we were able to validate our developed particulate matrix in terms of particle size, collagenous content, thermal properties and immunogenic content.

The proteomic content of our matrices was investigated by nanoLC-MS/MS. Herein, we employed for the first time an ECM targeted homogenization method and proteomic analysis to define the molecular components of porcine-derived renal matrices at a quantitative level. We demonstrate the presence of essential ECM proteins in the pellets that arise from protein homogenization, which are typically discarded. We also considered the biological variability existing between kidney donors, and thus we analyzed three kidneys representative of different animals which were independently submitted to the decellularization process. The variability between ECM components of each kidney presented on Table S1 can be attributed to donor-to-donor variability, since it is dependent on donor age, species of origin and also the history of stimulus/insults that each kidney experienced.[37] By applying this methodology, we were able to identify proteins which are typically lost during decellularization procedures, such as some glycoproteins, proteoglycans and other secreted factors. These proteins are extremely important on stabilizing elastin and collagen networks being therefore essential to maintain the basement membrane stability and integrity.[38] We were also able to retain the majority of renal basement proteins, such as collagen type IV and laminins, important because of their abundant binding sites for both endothelial and epithelial cells and their capacity of regulating cellular migration and proliferation.[39] We have also noticed the preservation of fibrillar collagens, which provide tensile strength to the organs, including the kidney.

Until now, our understanding of matrix composition of renal decellularized matrices was relying on a previous mass spectrometry study.[18] However, this study does not describe donor-to-donor variability and no gene ontology classification was performed. Other authors also performed a fractioned proteomic analysis in lung and myocardial tissues.[40, 41] Unlike those reports, we didn't use toxic digesting agents and we managed to extract the majority of proteins in F1, a consistent result within the 3 replicas (Figure S VI-1). The results presented on Figure S VI-1 suggest that subpopulations of proteins are able to solubilize according with their location in the matrix as well as their interactions with other matrix proteins, making some of them insoluble in the commonly used buffer solutions.[42]

Comparing our results with a recently published study by Louzao-Martinez *et al.*,[43] where the human kidney proteome was analyzed, we can detect proteomic similarities between porcine and human kidney, where 49 proteins were common to both proteomes (Figure S VI-3). However, we also could

notice that a lot of essential proteins are not present in the human kidney proteomic analysis, such as alpha-3, 4, 5 and 6 chains of collagen type IV, alpha-1 and 2 chains of collagen type V and even apha-1 laminin. Being collagen type IV and laminins the main components of human kidney basement membranes,[44] and collagen type V a fibrillar collagen that compose the majority of the interstitial ECM,[45] these should have been detected and identified in the human proteomic analysis. As aforementioned, we noticed that fibrillar and more crosslinked collagens could only be extracted in its total abundance in the fractions F2 and F3, with a more severe method of homogenization. We hypothesize that the different extraction protocols may be responsible for the differences found when comparing human and porcine kidney proteomics. Therefore, an accurate comparison cannot be performed on this study between porcine and human kidney ECM. We have additionally noticed that we are lacking the identification of some renal ECM proteins on porcine kidney, such as laminin alpha-4 and 5 and small proteoglycans such as biglycan and decorin. Instead, we identified other 5 sub-domains of laminin and the core proteins of heparan sulfate lumican, perlecan, collagen type XVIII and agrin (Table S1).[45]

As a second aim, we investigated the bioactivity of particulate ECM by evaluating the growth, proliferation, morphology and phenotypic changes of hRPCs. These cells represent a subset of multipotent progenitors present in the Bowman's capsule. They can be purified from cultured kidney fragments, revealing self-renewal potential and a high cloning efficiency.[46] When injected into SCID mice with acute renal failure, hRPCs have demonstrated to ameliorate the morphologic and functional kidney damage.[33] Our results demonstrate high biocompatibility and mitogenic activity on a 3D culture with ECM particles (Figure VI-5 and 6). We also noticed the presence of cell-cell and cell-substrate interactions when cultured on 1 and 2 mg of matrix (Figure VI-7), indicative of good cellular environment adaptation by 7 days of *in vitro* culture. The IHC micrographs are the result of a 10 µm section of the whole 3D culture, being not representative of the cell-cell interactions but on how cells are distributed. We could notice the cells surrounding the matrix, creating an evenly distributed monolayer when cultured on 1 and 2 mg of matrix. On the contrary, when augmenting the quantity of matrix to 4 mg, but with the same cell concentration, the cells lose their cell-to-cell interactions. Consequently, very few cells or no cells can be spotted on IHC micrographs. However, they can be found when performing a z-stack on IF micrographs. Regarding CD133 expression (Figure VI-7-G, I), it was interesting to spot a change on morphology and size of the cells with the increasing content of matrix. This change consequently caused the loss of CD133 expression on 4 mg of pKECM. Additionally, very few CD133 expression is found on cells cultured on 1 mg of matrix, suggesting that cell-cell and cell-matrix interactions lead the guidance of phenotypic

expression, where a mild proliferation capacity together with a mild cell-cell interaction lead to maintenance of stemness by using 2 mg of matrix. A 3D reconstruction of cellular organization around the matrix can be seen in Figure S VI-4. Although these results are promising and consistent with each other in terms of cell distribution, morphology and interaction with the substrate, the stem nature of hRPCs is only confirmed by immunofluorescence. In the future, we intend to do a follow-up of the cell markers CD133 and CD24 by flow cytometry, which will enable for a stronger evaluation of cellular phenotype. Moreover, in a future *in vivo* work, we intend not only to perform injectability tests but also functional analysis assays in order to evaluate the full potential of our therapy.

These findings suggest an optimal ratio for the maintenance cell phenotype and an optimal cell-cell interaction. The particulate matrix has shown to be highly supportive for a 3D progenitor cell culture, suggesting that a scaled-up culture of these cells with pKECM could be achieved *in vitro* for posterior patient engraftment.

## VI-5. CONCLUSIONS

This work highlights the potential of ECM-based biomaterials from porcine origin for kidney advanced therapies. We successfully confirmed our initial hypothesis of developing and characterizing a particulate extracellular matrix biomaterial as a consistent substrate for 3D cultures of adherent renal progenitor cells. We herein shown a similar protein composition with the human kidney. Indeed, the matrix demonstrated being an excellent substrate for supporting renal progenitor cell attachment, proliferation and growth. Moreover, it was shown to modulate the morphology and phenotypic expression of renal progenitor cells. To the best of our knowledge, this the first report investigating particulate kidney ECM as a promising 3D substrate for cell cultures. Our results suggest that this particulate ECM together with reparative progenitor cells may become a powerful tool to address renal pathologies in its early stages.

## Acknowledgements

Authors would like to acknowledge the funding. This work was supported by the European Regional Development Fund (ERDF) on the project FROnTHERA (NORTE-01-0145-FEDER-000023) and the FCT PhD Grant on the Doctoral Program on Advanced Therapies for Health (PATH) (PD/BD/128102/2016). Mass spectrometry and proteomics was performed at the Proteomics i3S Scientific Platform with the assistance of Hugo Osório. This work was supported by the Portuguese Mass Spectrometry Network,

integrated in the National Roadmap of Research Infrastructures of Strategic Relevance (ROTEIRO/0028/2013; LISBOA-01-0145-FEDER-022125).

## VI-6. REFERENCES

1. Discher DE, Mooney DJ, Zandstra PW (2009) Growth factors, matrices, and forces combine and control stem cells. Science (80- ) 324:1673–1677. https://doi.org/10.1126/science.1171643
2. Philp D, Chen SS, Fitzgerald W, et al (2005) Complex Extracellular Matrices Promote Tissue-Specific Stem Cell Differentiation. Stem Cells 23:288–296. https://doi.org/10.1634/stemcells.2002-0109
3. Kenawy E-R, Layman JM, Watkins JR, et al (2003) Electrospinning of poly(ethylene-co-vinyl alcohol) fibers. Biomaterials 24:907–913. https://doi.org/10.1016/S0142-9612(02)00422-2
4. Alves da Silva M, Martins A, Costa-Pinto AR, et al (2017) Electrospun Nanofibrous Meshes Cultured With Wharton's Jelly Stem Cell: An Alternative for Cartilage Regeneration, Without the Need of Growth Factors. Biotechnol J 12:1700073. https://doi.org/10.1002/biot.201700073
5. Martins A, Reis RL, Neves NM (2008) Electrospinning: processing technique for tissue engineering scaffolding. Int Mater Rev 53:257–274. https://doi.org/10.1179/174328008X353547
6. Jayawarna V, Ali M, Jowitt TA, et al (2006) Nanostructured Hydrogels for Three-Dimensional Cell Culture Through Self-Assembly of Fluorenylmethoxycarbonyl–Dipeptides. Adv Mater 18:611–614. https://doi.org/10.1002/adma.200501522
7. Tysseling-Mattiace VM, Sahni V, Niece KL, et al (2008) Self-assembling nanofibers inhibit glial scar formation and promote axon elongation after spinal cord injury. J Neurosci 28:3814–23. https://doi.org/10.1523/JNEUROSCI.0143-08.2008
8. Jiménez G, Venkateswaran S, López-Ruiz E, et al (2019) A soft 3D polyacrylate hydrogel recapitulates the cartilage niche and allows growth-factor free tissue engineering of human articular cartilage. Acta Biomater 90:146–156. https://doi.org/10.1016/j.actbio.2019.03.040
9. Carretero A, Soares da Costa D, Reis RL, Pashkuleva I (2017) Extracellular matrix-inspired assembly of glycosaminoglycan–collagen fibers. J Mater Chem B 5:3103–3106. https://doi.org/10.1039/C7TB00704C
10. O'Brien FJ, Harley BA, Yannas IV, Gibson LJ (2005) The effect of pore size on cell adhesion in collagen-GAG scaffolds. Biomaterials 26:433–441. https://doi.org/10.1016/J.BIOMATERIALS.2004.02.052
11. Orlando G, Booth C, Wang Z, et al (2013) Discarded human kidneys as a source of ECM scaffold for kidney regeneration technologies. Biomaterials 34:5915–5925. https://doi.org/10.1016/j.biomaterials.2013.04.033
12. Yu YL, Shao YK, Ding YQ, et al (2014) Decellularized kidney scaffold-mediated renal regeneration. Biomaterials 35:6822–6828. https://doi.org/10.1016/j.biomaterials.2014.04.074
13. Ott HC, Matthiesen TS, Goh S-K, et al (2008) Perfusion-decellularized matrix: using nature's platform to engineer a bioartificial heart. Nat Med 14:213–221. https://doi.org/10.1038/nm1684
14. Abolbashari M, Agcaoili SM, Lee M-KK, et al (2016) Repopulation of porcine kidney scaffold using porcine primary renal cells. Acta Biomater 29:52–61. https://doi.org/10.1016/j.actbio.2015.11.026
15. Ko IK, Abolbashari M, Huling J, et al (2014) Enhanced re-endothelialization of acellular kidney scaffolds for whole organ engineering via antibody conjugation of vasculatures. TECHNOLOGY 02:243–253. https://doi.org/10.1142/s2339547814500228

16. Song JJ, Guyette JP, Gilpin SE, et al (2013) Regeneration and experimental orthotopic transplantation of a bioengineered kidney. Nat Med 19:646–51. https://doi.org/10.1038/nm.3154
17. Hoste EAJ, Kellum JA, Selby NM, et al (2018) Global epidemiology and outcomes of acute kidney injury. Nat Rev Nephrol 14:607–625. https://doi.org/10.1038/s41581-018-0052-0
18. Nagao RJ, Xu J, Luo P, et al (2016) Decellularized Human Kidney Cortex Hydrogels Enhance Kidney Microvascular Endothelial Cell Maturation and Quiescence. Tissue Eng Part A 22:1140–1150. https://doi.org/10.1089/ten.TEA.2016.0213
19. Su J, Satchell SC, Shah RN, Wertheim JA (2018) Kidney decellularized extracellular matrix hydrogels: Rheological characterization and human glomerular endothelial cell response to encapsulation. J Biomed Mater Res - Part A 106A:2448–2462. https://doi.org/10.1002/jbm.a.36439
20. O'Neill JD, Freytes DO, Anandappa AJ, et al (2013) The regulation of growth and metabolism of kidney stem cells with regional specificity using extracellular matrix derived from kidney. Biomaterials 34:9830–9841. https://doi.org/10.1016/j.biomaterials.2013.09.022
21. Lih E, Park W, Park KW, et al (2019) A Bioinspired Scaffold with Anti-Inflammatory Magnesium Hydroxide and Decellularized Extracellular Matrix for Renal Tissue Regeneration. ACS Cent Sci 5:458–467. https://doi.org/10.1021/acscentsci.8b00812
22. Singh NK, Han W, Nam SA, et al (2020) Three-dimensional cell-printing of advanced renal tubular tissue analogue. Biomaterials 232:119734. https://doi.org/10.1016/j.biomaterials.2019.119734
23. Ali M, Anil Kumar PR, Yoo JJ, et al (2019) A Photo-Crosslinkable Kidney ECM-Derived Bioink Accelerates Renal Tissue Formation. Adv Healthc Mater 8(7):e1800992. https://doi.org/10.1002/adhm.201800992
24. Gilbert TW, Stolz DB, Biancaniello F, et al (2005) Production and characterization of ECM powder: implications for tissue engineering applications. Biomaterials 26:1431–1435. https://doi.org/10.1016/j.biomaterials.2004.04.042
25. Yin H, Wang Y, Sun Z, et al (2016) Induction of mesenchymal stem cell chondrogenic differentiation and functional cartilage microtissue formation for in vivo cartilage regeneration by cartilage extracellular matrix-derived particles. Acta Biomater 33:96–109. https://doi.org/10.1016/j.actbio.2016.01.024
26. Choi JS, Yang H-J, Kim BS, et al (2009) Human extracellular matrix (ECM) powders for injectable cell delivery and adipose tissue engineering. J Control Release 139:2–7. https://doi.org/10.1016/j.jconrel.2009.05.034
27. Penolazzi L, Mazzitelli S, Vecchiatini R, et al (2012) Human mesenchymal stem cells seeded on extracellular matrix-scaffold: Viability and osteogenic potential. J Cell Physiol 227:857–866. https://doi.org/10.1002/jcp.22983
28. Sobreiro-Almeida R, Fonseca DR, Neves NM (2019) Extracellular matrix electrospun membranes for mimicking natural renal filtration barriers. Mater Sci Eng C 103:109866. https://doi.org/10.1016/J.MSEC.2019.109866
29. Sobreiro‐Almeida R, Elena Melica M, Lasagni L, et al (2020) Co‐cultures of renal progenitors and endothelial cells on kidney decellularized matrices replicate the renal tubular environment in vitro. Acta Physiol 230:e13491. https://doi.org/10.1111/apha.13491
30. Zahiri S, Masaeli E, Poorazizi E, Nasr-Esfahani MH (2018) Chondrogenic response in presence of cartilage extracellular matrix nanoparticles. J Biomed Mater Res Part A 106:2463–2471. https://doi.org/10.1002/jbm.a.36440
31. Bottino MC, Jose M V., Thomas V, et al (2009) Freeze-dried acellular dermal matrix graft: Effects of rehydration on physical, chemical, and mechanical properties. Dent Mater 25:1109–1115. https://doi.org/10.1016/J.DENTAL.2009.03.007

32. Movasaghi Z, Rehman S, ur Rehman DI (2008) Fourier Transform Infrared (FTIR) Spectroscopy of Biological Tissues. Appl Spectrosc Rev 43:134–179. https://doi.org/10.1080/05704920701829043
33. Sagrinati C, Netti GS, Mazzinghi B, et al (2006) Isolation and Characterization of Multipotent Progenitor Cells from the Bowman's Capsule of Adult Human Kidneys. J Am Soc Nephrol 17:2443–2456. https://doi.org/10.1681/ASN.2006010089
34. Riaz T, Zeeshan R, Zarif F, et al (2018) FTIR analysis of natural and synthetic collagen. Appl Spectrosc Rev 53:703–746. https://doi.org/10.1080/05704928.2018.1426595
35. Chi Ting Au-Yeung G, Sarig U, Sarig H, et al (2017) Restoring the biophysical properties of decellularized patches through recellularization. Biomater Sci 5 (6):1183–1194. https://doi.org/10.1039/c7bm00208d
36. Baiguera S, Del Gaudio C, Lucatelli E, et al (2014) Electrospun gelatin scaffolds incorporating rat decellularized brain extracellular matrix for neural tissue engineering. Biomaterials 35:1205–1214. https://doi.org/10.1016/j.biomaterials.2013.10.060
37. Dziki JL, Badylak SF (2019) Acellular Biologic Scaffolds in Regenerative Medicine: Unacceptable Variability with Acceptable Results. Regen Eng Transl Med 5:414–419. https://doi.org/10.1007/s40883-019-00106-5
38. Couchman JR, Abrahamson DR, McCarthy KJ (1993) Basement membrane proteoglycans and development. Kidney Int 43:79–84. https://doi.org/10.1038/ki.1993.14
39. Cameron JD, Skubitz APN, Furcht LT (1991) Type IV collagen and corneal epithelial adhesion and migration: Effects of type IV collagen fragments and synthetic peptides on rabbit corneal epithelial cell adhesion and migration in vitro. Investig Ophthalmol Vis Sci 32:2766–2773
40. Hill RC, Calle EA, Dzieciatkowska M, et al (2015) Quantification of extracellular matrix proteins from a rat lung scaffold to provide a molecular readout for tissue engineering. Mol Cell Proteomics 14:961–973. https://doi.org/10.1074/mcp.M114.045260
41. Johnson TD, Hill RC, Dzieciatkowska M, et al (2016) Quantification of decellularized human myocardial matrix: A comparison of six patients. Proteomics - Clin Appl 10:75–83. https://doi.org/10.1002/prca.201500048
42. Eyre DR, Paz MA, Gallop PM (1984) Cross-Linking in Collagen and Elastin. Annu Rev Biochem 53:717–748. https://doi.org/10.1146/annurev.bi.53.070184.003441
43. Louzao-Martinez L, van Dijk CGM, Xu YJ, et al (2019) A proteome comparison between human fetal and mature renal extracellular matrix identifies EMILIN1 as a regulator of renal epithelial cell adhesion. Matrix Biol Plus 4:100011. https://doi.org/10.1016/j.mbplus.2019.100011
44. Furness PN (1996) Extracellular matrix and the kidney. J Clin Pathol 49:355–359. https://doi.org/10.1136/jcp.49.5.355
45. Genovese F, Manresa AA, Leeming DJ, et al (2014) The extracellular matrix in the kidney: A source of novel non-invasive biomarkers of kidney fibrosis? Fibrogenes Tissue Repair 7:4. https://doi.org/10.1186/1755-1536-7-4
46. Angelotti ML, Ronconi E, Ballerini L, et al (2012) Characterization of Renal Progenitors Committed Toward Tubular Lineage and Their Regenerative Potential in Renal Tubular Injury. Stem Cells 30:1714–1725. https://doi.org/10.1002/stem.113046.

# VI-7. SUPPLEMENTARY INFORMATION

## VI-7.1. Supplementary methods

### VI-7.1.1. Morphological and structural analysis of pKECM

After fixation with 2.5 % glutaraldehyde dehydration in a graded ethanol series, pKECM structure was analyzed by Scanning Electron Microscopy (SEM; JSM-6010 LV, JEOL, Japan). Samples were sputter coated with gold (coater 108 A, Cressington, United States) prior to examination. Micrographs were obtained at an accelerating voltage of 10 kV. The infrared spectra of pKECM before and after sterilization was analyzed by Attenuated total reflection-Fourier transform infrared spectroscopy (ATR-FITR, IRPrestige 21, Shimadzu), with a spectral range of 500-3000 $cm^{-1}$ in reflection mode to characterize the composition and molecular conformation of the pKECM. Thermal properties of the pKECM substrates before and after sterilization were characterized by differential scanning calorimetry (DSC, Q100, TA Instruments). Approximately 2 mg of sterile and non-sterile pKECM were transferred into an aluminum pan and the sample was scanned with a modulated heating method. First, pKECM was heated until 250 °C at a heating rate of 10 °C $min^{-1}$ and then cooled down to 10 °C. The sample chamber was purged with nitrogen at a flow rate of 50 mL $h^{-1}$.

### VI-7.1.2. Histological and biochemical analysis of pKECM

pKECM substrate was assessed by Hematoxylin & Eosin (H&E) and Masson's Trichrome (MT) stainings of frozen sections. The samples were fixed for 30 min with 10 % neutral-buffered formalin before being embedded in OCT compound (Bio-optica). After this, they were snap-freezed in liquid nitrogen and cut into 10 µm sections using a cryostat. Sections were stained with working solutions of H&E and a MT kit according to manufacturer's instructions (Bio-optica), dehydrated through a series of ethanol and mounted. For the detection of dsDNA, pKECM was digested for 2 h at 56 °C with proteinase K and the remaining DNA extraction was performed using DNeasy blood and tissue kit (Qiagen) according to manufacturer's instructions. The digested samples were quantified using Quanti-iT PicoGreen dsDNA assay kit (Invitrogen) according to the manufacturer's protocol. Values were extrapolated using a standard curve of dsDNA and sample fluorescence was read in a microplate reader (excitation: 485/20 nm; emission: 530/25 nm).

### VI-7.1.3. Characterization and relative quantification of protein composition by nano-liquid chromatography–tandem mass spectrometry (nanoLC- MS/MS)

Each sample was reduced and alkylated and processed for proteomics analysis following the solid-phase-enhanced sample-preparation (SP3) protocol as described in PMID30464214.[1] Enzymatic digestion was performed with Trypsin/LysC (2 µg) overnight at 37 ºC at 1000 rpm.

Protein identification and quantitation was performed by nanoLC-MS/MS. This equipment is composed by an Ultimate 3000 liquid chromatography system coupled to a Q-Exactive Hybrid Quadrupole-Orbitrap mass spectrometer (Thermo Scientific, Bremen, Germany). Samples were loaded onto a trapping cartridge (Acclaim PepMap C18 100Å, 5 mm x 300 µm i.d., 160454, Thermo Scientific) in a mobile phase of 2 % acetonitrile (ACN), 0.1 % formic acid (FA) at 10 µL $min^{-1}$. After 3 min loading, the trap column was switched in-line to a 50 cm by 75 µm inner diameter EASY-Spray column (ES803, PepMap RSLC, C18, 2 µm, Thermo Scientific, Bremen, Germany) at 250 nL $min^{-1}$. Separation was generated by mixing A: 0.1 % FA, and B: 80 % ACN, with the following gradient: 5 min (2.5 % B to 10 % B), 120 min (10 % B to 30 % B), 20 min (30 % B to 50 % B), 5 min (50 % B to 99 % B) and 10 min (hold 99 % B). Subsequently, the column was equilibrated with 2.5 % B for 17 min. Data acquisition was controlled by Xcalibur 4.0 and Tune 2.9 software (Thermo Scientific, Bremen, Germany).

The mass spectrometer was operated in data-dependent (dd) positive acquisition mode alternating between a full scan (m/z 380-1580) and subsequent HCD MS/MS of the 10 most intense peaks from full scan (normalized collision energy of 27 %). ESI spray voltage was 1.9 kV. Global settings: use lock masses best (m/z 445.12003), lock mass injection Full MS, chrom. peak width (FWHM) 15 s. Full scan settings: 70 k resolution (m/z 200), AGC target 3E6, maximum injection time 120 ms. dd settings: minimum AGC target 8E3, intensity threshold 7.3E4, charge exclusion: unassigned, 1, 8, > 8, peptide match preferred, exclude isotopes on, dynamic exclusion 45vs. MS2 settings: microscans 1, resolution 35 k (m/z 200), AGC target 2E5, maximum injection time 110 ms, isolation window 2.0 m/z, isolation offset 0.0 m/z, spectrum data type profile.

The raw data was processed using Proteome Discoverer 2.4.0.305 software (Thermo Scientific) and searched against the UniProt database for the Sus scrofa Proteome 2019_11. The Sequest HT search engine was used to identify tryptic peptides. The ion mass tolerance was 10 ppm for precursor ions and 0.02 Da for fragment ions. Maximum allowed missing cleavage sites was set 2. Cysteine carbamidomethylation was defined as constant modification. Methionine oxidation and protein N-terminus

acetylation were defined as variable modifications. Peptide confidence was set to high. The processing node Percolator was enabled with the following settings: maximum delta Cn 0.05; decoy database search target FDR 1 %, validation based on q-value. Protein label free quantitation was performed with the Minora feature detector node at the consensus step. Precursor ions quantification was performing at the processing step with the following parameters: unique plus razor peptides were considered for quantification, precursor abundance was based on intensity and normalization was based on total peptide amount.

The total number of proteins identified in each fraction was obtained by filtering peptide identifications at > 95.0 % confidence interval with at least two peptides per protein. Gene ontology analysis (GO) was performed manually using AmiGO online platform.[2, 3] Following categorization, non-ECM proteins were excluded to perform graphical analysis. Coefficient of variation (CV) values were calculated by dividing standard deviation by mean values of the ECM proteins identified on each kidney sample. The mass spectrometry proteomics data have been deposited to the ProteomeXchange Consortium via the PRIDE [4] partner repository with the dataset identifier PXD019122.

### VI-7.1.4. Isolation and characterization of human renal progenitor cells (hRPC)

Human kidney fragments were obtained in agreement with the Ethical Committee on human experimentation of the Azienda Ospedaliero-Universitaria Careggi, Florence, Italy. All subjects gave their informed consent for inclusion before they participated in the study. The study was conducted in accordance with the Declaration of Helsinki, and the protocol was approved by the Ethics Committee on Human Experimentation of the Azienda Ospedaliero-Universitaria Careggi, Florence, Italy (project identification code 2015/0009082 from 25/03/2015). Human RPCs were obtained and cultured as previously described,[5] with minor modifications. Briefly, we minced the cortex and we performed an enzymatic digestion with collagenase solution type IV 750 U $mL^{-1}$ (Sigma Aldrich) in PBS for 45 min at 37 °C. After digestion, we filtered the solution by a standard sieving technique through graded mesh screens (60 and 80 mesh). Subsequently, we performed red blood cell lysis by incubating with lysis buffer ($NH_4Cl$ 0.087 %) for 4 min at 37 °C. The cellular suspension was collected, washed and plated on petri dish containing complete medium. The medium is composed by Microvascular Endothelial Cell Growth Medium (EGM™-MV, Lonza) supplemented with 20 % HyClone™ Fetal Bovine Serum (FBS, GE Healthcare). After 4 to 5 days of culture, cells that adhered to the plate were subcultured. Cultures were checked for simultaneous expression of CD133 and CD24 by flow cytometry, according to previously

published methods for characterizing hRPC.[6] For the analysis, total hRPCs population was gated on a forward scatter (FSC)/side scatter (SSC) plot and dead cells were excluded by Propidium Iodide (PI) staining. Live cells (PI negative) were gated for CD133 and CD24 expression. Only cells between passage 1-3 and expressing > 90 % CD24/CD133 double positivity were used in this study.

## VI-7.2. References

1. Hughes CS, Moggridge S, Müller T, et al (2019) Single-pot, solid-phase-enhanced sample preparation for proteomics experiments. Nat Protoc 14:68–85. https://doi.org/10.1038/s41596-018-0082-x
2. Carbon S, Ireland A, Mungall CJ, et al (2009) AmiGO: Online access to ontology and annotation data. Bioinformatics 25:288–289. https://doi.org/10.1093/bioinformatics/btn615
3. Carbon S, Douglass E, Dunn N, et al (2019) The Gene Ontology Resource: 20 years and still GOing strong. Nucleic Acids Res 47:D330–D338. https://doi.org/10.1093/nar/gky1055
4. Perez-Riverol Y, Csordas A, Bai J, et al (2019) The PRIDE database and related tools and resources in 2019: Improving support for quantification data. Nucleic Acids Res 47:D442–D450. https://doi.org/10.1093/nar/gky1106
5. Sagrinati C, Netti GS, Mazzinghi B, et al (2006) Isolation and Characterization of Multipotent Progenitor Cells from the Bowman's Capsule of Adult Human Kidneys. J Am Soc Nephrol 17:2443–2456. https://doi.org/10.1681/ASN.2006010089
6. Angelotti ML, Ronconi E, Ballerini L, et al (2012) Characterization of Renal Progenitors Committed Toward Tubular Lineage and Their Regenerative Potential in Renal Tubular Injury. Stem Cells 30:1714–1725. https://doi.org/10.1002/stem.11306.

## VI-7.3. Supplementary Figures and Tables

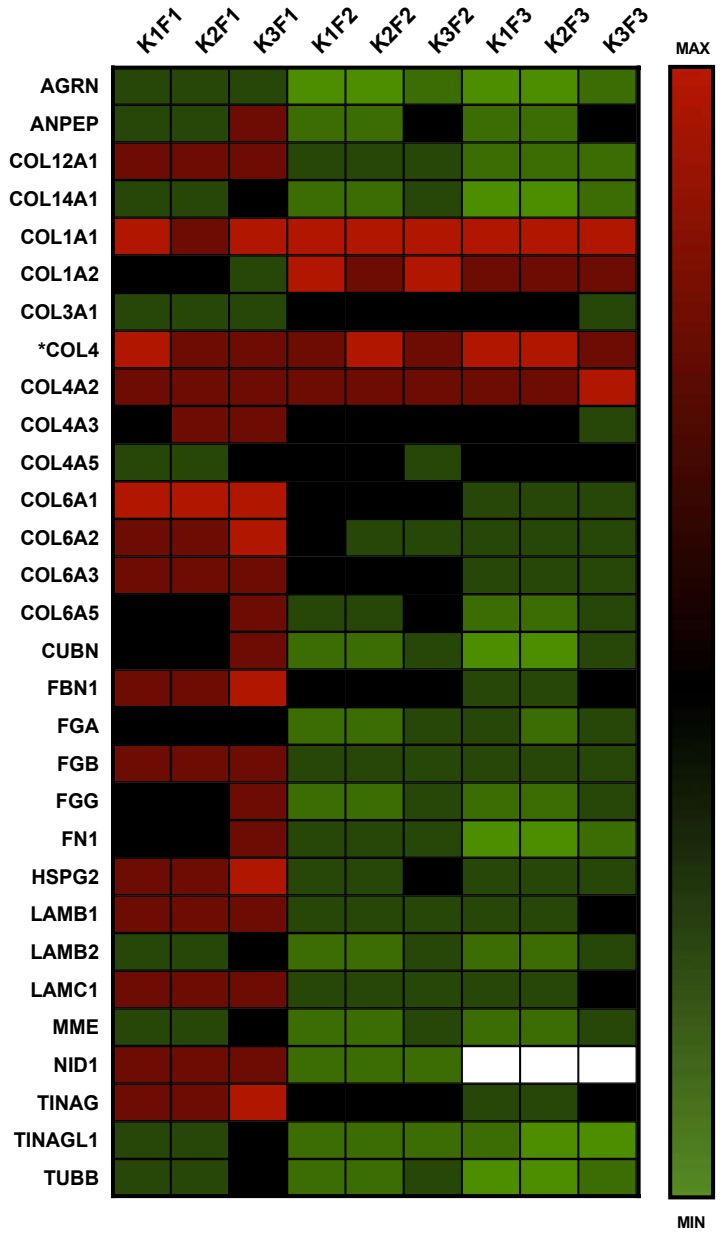


Figure S VI-1 – Quantitative proteomic analysis of the 30 most abundant proteins on decellularized porcine matrix. Heat map representing the absolute abundance per each fraction (F - detailed at Scheme 2), present on each kidney (K). Red boxes correlate with higher abundances of proteins while green boxes to lower. Proteins are identified with the respective gene name. The majority of protein present higher abundance values in F1, with the exception of some collagens.

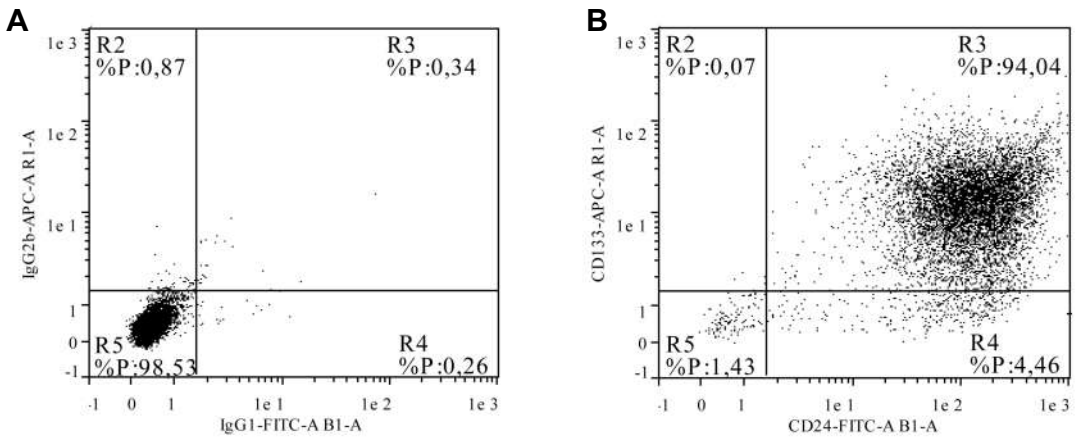


Figure S VI-2 – Flow cytometry characterization of hRPCs. CD133 and CD24 markers expression in human renal progenitor cells confirm that double-positive cells represent a homogeneous population with ~94% double positivity. Images represent (A) Isotype control and (B) double-stained cells.

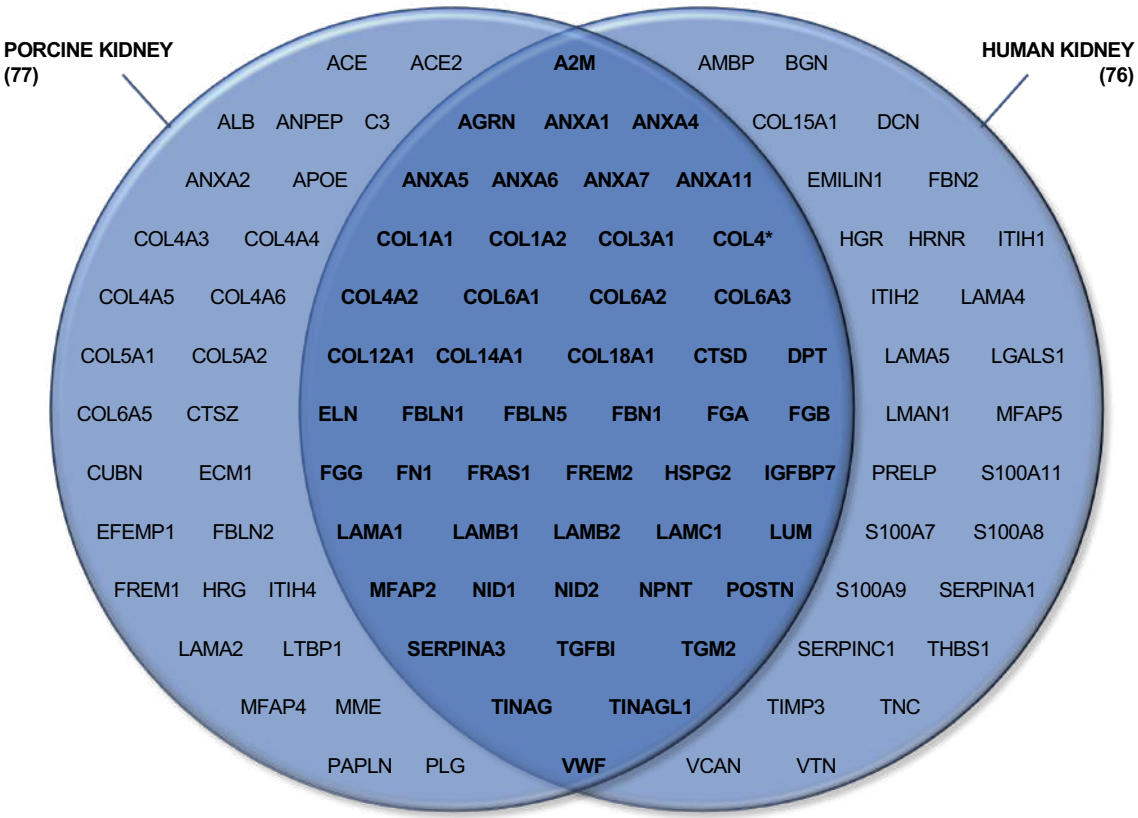


Figure S VI-3 – Venn diagram representing the overlap and differences between the human and porcine kidney ECM proteome as identified by the study of Louzao-martinez et al. Each word represents a single protein that is labeled with the gene name.

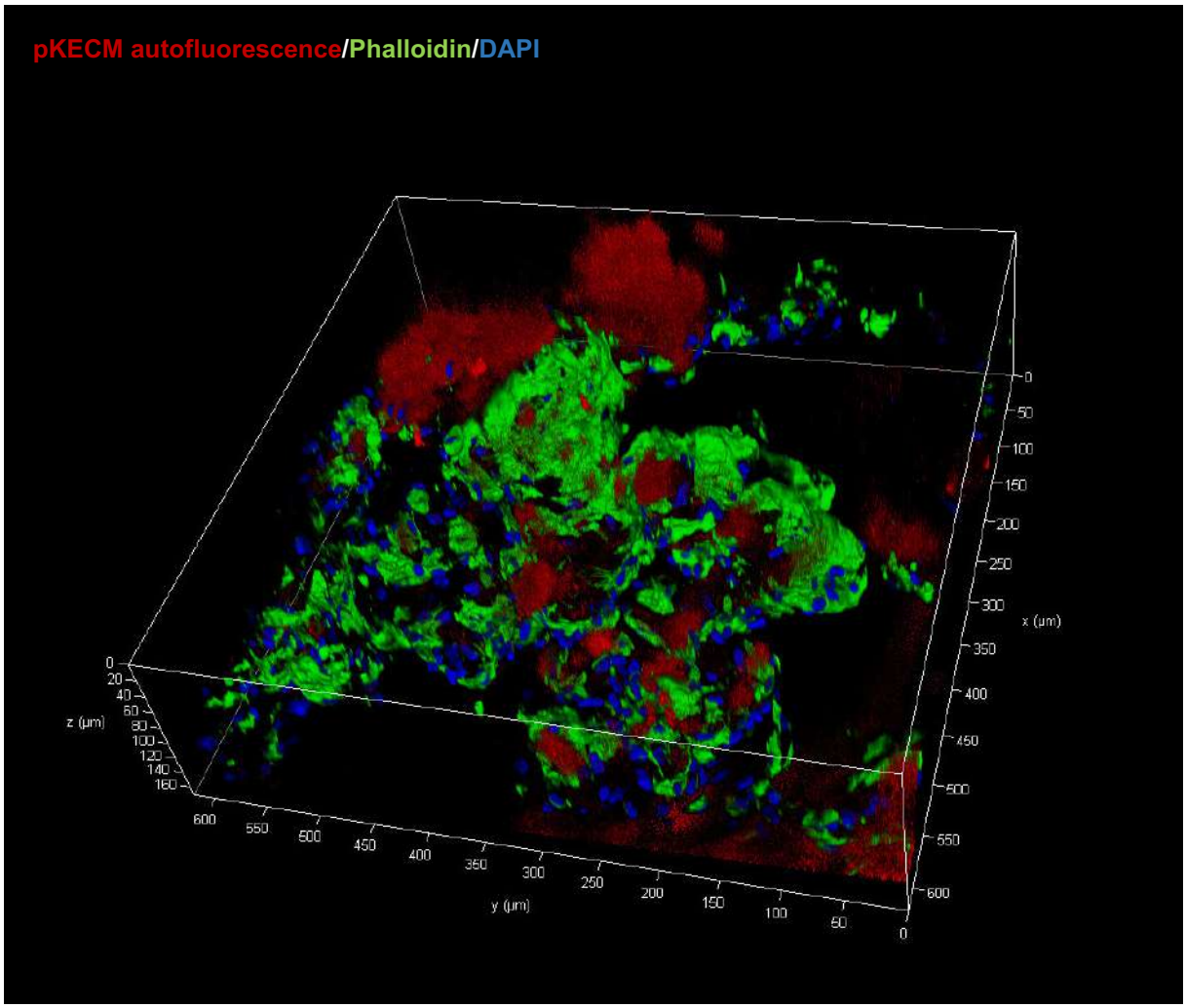


Figure S VI-4 – 3D micrograph of the hRPCs distribution on the pKECM. Immunofluorescence of phalloidin for cytoskeleton (green) and DAPI for nuclei (blue). Matrix autofluorescence appears in red. Numbers are displayed in µm.

Table S VI-1 – Quantitative proteomic analysis of decellularized porcine kidney ECM. Protein description and accession numbers are relative to Sus scrofa database from UniProt. Functional classification was obtained in AmiGO database. The abundance percentage was obtained by dividing each protein abundance to the total abundance of ECM proteins relative to each kidney (K).

| Protein | Gene | Accession | Functional Classification | % (vs. Total ECM Proteins) | | | CV |
|---|---|---|---|---|---|---|---|
| | | | | K1 | K2 | K3 | |
| Agrin | AGRN | A0A287AN50 | Basement Membrane | 0,186 | 0,199 | 0,142 | 0,045 |
| Collagen type XVIII alpha-1 chain | COL18A1 | A0A286ZIL9 | Basement Membrane | 0,010 | 0,012 | 0,012 | 0,325 |
| Similar to Collagen NC1 domain containing protein (IV) | COL4 | A0A5G2QEJ2 | Basement Membrane | 15,738 | 15,903 | 5,842 | 0,313 |
| Collagen alpha-2 (IV) chain | COL4A2 | A0A5G2RJ53 | Basement Membrane | 8,468 | 7,891 | 9,799 | 0,352 |
| Collagen alpha-3 (IV) chain | COL4A3 | F1SNP0 | Basement Membrane | 1,450 | 1,875 | 1,089 | 0,104 |
| Collagen alpha-4 (IV) chain | COL4A4 | A0A287BI02 | Basement Membrane | 0,070 | 0,085 | 0,108 | 0,455 |
| Collagen alpha-5 (IV) chain | COL4A5 | A0A287A007 | Basement Membrane | 1,143 | 1,025 | 0,601 | 0,145 |
| Collagen alpha-6 (IV) chain | COL4A6 | F1RXI3 | Basement Membrane | 0,065 | 0,077 | 0,044 | 0,078 |
| Fraser extracellular matrix complex subunit 1 | FRAS1 | F1RYS0 | Basement Membrane | 0,019 | 0,022 | 0,021 | 0,247 |
| FRAS1 related extracellular matrix 1 | FREM1 | A0A287BGJ4 | Basement Membrane | 0,004 | 0,008 | 0,008 | 0,453 |
| FRAS1 related extracellular matrix 2 | FREM2 | F1RS31 | Basement Membrane | 0,022 | 0,029 | 0,045 | 0,603 |
| Perlecan | HSPG2 | A0A287ATP0 | Basement Membrane | 2,683 | 2,983 | 4,180 | 0,486 |
| Laminin subunit alpha 1 | LAMA1 | A0A287AG36 | Basement Membrane | 0,013 | 0,015 | 0,012 | 0,147 |
| Laminin subunit alpha 2 | LAMA2 | A0A287A027 | Basement Membrane | 0,008 | 0,017 | 0,023 | 0,669 |
| Laminin beta-1 | LAMB1 | F1SAE9 | Basement Membrane | 1,217 | 1,187 | 1,049 | 0,152 |
| Laminin beta-2 | LAMB2 | A0A287AWV5 | Basement Membrane | 0,220 | 0,259 | 0,567 | 0,784 |
| Laminin gamma-1 | LAMC1 | F1S663 | Basement Membrane | 1,742 | 2,259 | 3,520 | 0,604 |
| Nidogen-1 | NID1 | F1RGY5 | Basement Membrane | 1,271 | 1,520 | 1,383 | 0,235 |
| Nidogen-2 | NID2 | A0A287AKJ2 | Basement Membrane | 0,103 | 0,145 | 0,086 | 0,142 |
| Nephronectin | NPNT | A0A5G2QQZ6 | Basement Membrane | 0,055 | 0,067 | 0,033 | 0,143 |
| Papilin, proteoglycan like sulfated glycoprotein | PAPLN | F1S3J7 | Basement Membrane | 0,013 | 0,020 | 0,014 | 0,201 |
| Aminopeptidase N | ANPEP | A0A5G2QPR2 | ECM Regulator | 0,076 | 0,096 | 1,637 | 1,559 |
| Inter-alpha-trypsin inhibitor heavy chain H4 | ITIH4 | A0A286ZN24 | ECM Regulator | 0,006 | 0,006 | 0,053 | 1,393 |

| | | | | | | | |
|---|---|---|---|---|---|---|---|
| Latent transforming growth factor beta binding protein 1 | LTBP1 | A0A286ZWQ1 | ECM Regulator | 0,005 | 0,006 | 0,011 | 0,692 |
| Transglutaminase 2 | TGM2 | A0A5G2R416 | ECM Regulator | 0,021 | 0,019 | 0,190 | 1,405 |
| Insulin-like growth factor-binding protein 7 | IGFBP7 | A0A287B8M8 | ECM Regulator | 0,013 | 0,009 | 0,219 | 1,566 |
| Alpha-2-macroglobulin | A2M | A0A5G2Q8I9 | ECM Regulator | 0,003 | 0,004 | 0,033 | 1,384 |
| Cathepsin D | CTSD | A0A286ZX26 | ECM Regulator | 0,000 | 0,000 | 0,001 | 1,529 |
| Cathepsin Z | CTSZ | A5GFX7 | ECM Regulator | 0,001 | 0,001 | 0,005 | 1,288 |
| Histidine-rich glycoprotein | HRG | F1SFI5 | ECM Regulator | 0,002 | 0,002 | 0,018 | 1,338 |
| Collagen apha-1 (XII) chain | COL12A1 | F1RQI0 | FACIT Collagen | 1,012 | 1,311 | 1,167 | 0,254 |
| Collagen apha-1 (XIV) chain | COL14A1 | A0A287BGV6 | FACIT Collagen | 0,106 | 0,137 | 0,206 | 0,580 |
| Collagen alpha-1 (I) chain | COL1A1 | A0A287A1S6 | Fibrillar collagen | 35,036 | 32,737 | 27,141 | 0,111 |
| Collagen alpha-2 (I) chain | COL1A2 | F1SFA7 | Fibrillar collagen | 7,601 | 4,560 | 6,945 | 0,387 |
| Collagen alpha-1(III) chain preproprotein | COL3A1 | F1RYI8 | Fibrillar collagen | 1,229 | 1,249 | 0,561 | 0,220 |
| Collagen apha-1 (V) chain | COL5A1 | F1S021 | Fibrillar collagen | 0,026 | 0,018 | 0,027 | 0,408 |
| Collagen apha-2 (V) chain | COL5A2 | A0A287BPM1 | Fibrillar collagen | 0,031 | 0,037 | 0,021 | 0,069 |
| Collagen apha-1 (VI) chain | COL6A1 | A0A5G2QW87 | Matricellular | 5,231 | 6,294 | 6,255 | 0,292 |
| Collagen apha-2 (VI) chain | COL6A2 | I3LQ84 | Matricellular | 3,212 | 3,923 | 3,852 | 0,290 |
| Collagen apha-3 (VI) chain | COL6A3 | I3LUR7 | Matricellular | 3,366 | 3,965 | 2,821 | 0,089 |
| Collagen apha-5 (VI) chain | COL6A5 | A0A287BK35 | Matricellular | 0,680 | 0,876 | 1,477 | 0,651 |
| Dermatopontin | DPT | A0A286ZVB7 | Matricellular | 0,031 | 0,034 | 0,101 | 0,943 |
| Fibulin 3 | EFEMP1 | F1SQL2 | Matricellular | 0,022 | 0,032 | 0,047 | 0,601 |
| Fibulin 1 | FBLN1 | A0A286ZLN2 | Matricellular | 0,014 | 0,015 | 0,019 | 0,414 |
| Fibulin 2 | FBLN2 | A0A287B5Q1 | Matricellular | 0,003 | 0,004 | 0,005 | 0,477 |
| Fibulin 5 | FBLN5 | A0A480ZQ94 | Matricellular | 0,015 | 0,017 | 0,002 | 0,628 |
| Fibrinogen alpha chain | FGA | F1RX36 | Matricellular | 0,289 | 0,366 | 0,566 | 0,591 |
| Fibrinogen beta chain | FGB | A0A5G2RHA4 | Matricellular | 1,005 | 1,229 | 2,588 | 0,772 |
| Fibrinogen gamma chain | FGG | F1RX35 | Matricellular | 0,491 | 0,631 | 2,480 | 1,122 |
| Fibronectin 1 | FN1 | A0A286ZY95 | Matricellular | 0,700 | 0,787 | 1,137 | 0,509 |

| | | | | | | | |
|---|---|---|---|---|---|---|---|
| Lumican | LUM | F1SQ09 | Matricellular | 0,038 | 0,037 | 0,068 | 0,619 |
| Periostin | POSTN | A0A5G2R015 | Matricellular | 0,001 | 0,002 | 0,013 | 1,341 |
| Angiotensin-converting enzyme | ACE | A0A5G2QTW5 | Other ECM | 0,005 | 0,006 | 0,016 | 0,865 |
| Angiotensin-converting enzyme 2 | ACE2 | K7GLM4 | Other ECM | 0,002 | 0,003 | 0,034 | 1,467 |
| Serum albumin | ALB | A0A287BAY9 | Other ECM | 0,011 | 0,024 | 0,059 | 0,992 |
| Annexin A11 | ANXA11 | A0A5K1UZZ4 | Other ECM | 0,005 | 0,007 | 0,031 | 1,205 |
| Annexin A2 | ANXA2 | A0A5G2QCF9 | Other ECM | 0,004 | 0,004 | 0,015 | 1,045 |
| Cubilin | CUBN | F1RWC3 | Other ECM | 0,655 | 0,832 | 1,790 | 0,796 |
| Extracellular matrix protein 1 | ECM1 | I3LC64 | Other ECM | 0,003 | 0,005 | 0,009 | 0,747 |
| Neprilysin | MME | A0A287BPD6 | Other ECM | 0,057 | 0,071 | 0,448 | 1,310 |
| Plasminogen | PLG | P06867 | Other ECM | 0,114 | 0,124 | 0,151 | 0,387 |
| Annexin A7 | ANXA7 | F1SU59 | Other ECM | 0,000 | 0,001 | 0,002 | 0,826 |
| Annexin A4 | ANXA4 | A0A287AYJ2 | Other ECM | 0,001 | 0,001 | 0,003 | 1,178 |
| Annexin A5 | ANXA5 | F2Z5C1 | Other ECM | 0,000 | 0,000 | 0,001 | 1,350 |
| Annexin A6 | ANXA6 | A0A5G2RBI3 | Other ECM | 0,004 | 0,005 | 0,019 | 1,082 |
| Annexin A1 | ANXA1 | F1SJB5 | Other ECM | 0,000 | 0,000 | 0,003 | 1,284 |
| Apolipoprotein E | APOE | F1RM45 | Secreted | 0,001 | 0,001 | 0,003 | 1,044 |
| Complement C3 | C3 | F1SBS4 | Secreted | 0,041 | 0,044 | 0,162 | 1,052 |
| Transforming growth factor-beta-induced protein ig-h3 | TGFBI | A0A5G2QXN3 | Secreted | 0,033 | 0,038 | 0,059 | 0,565 |
| von Willebrand factor (Fragment) | VWF | Q28833 | Secreted | 0,005 | 0,005 | 0,004 | 0,159 |
| SERPIN domain-containing protein | SERPINA3-2 | F1SCC6 | Secreted | 0,000 | 0,000 | 0,003 | 1,732 |
| Elastin | ELN | A0A5G2Q717 | Structural ECM | 0,022 | 0,029 | 0,007 | 0,469 |
| Fibrillin 1 | FBN1 | F1SN67 | Structural ECM | 1,658 | 1,824 | 4,354 | 0,816 |
| Microfibril associated protein 2 | MFAP2 | F1SUS0 | Structural ECM | 0,030 | 0,046 | 0,087 | 0,781 |
| Tubulointerstitial nephritis antigen | TINAG | I3L9E7 | Structural ECM | 2,422 | 2,730 | 4,222 | 0,554 |
| Tubulointerstitial nephritis antigen like 1 | TINAGL1 | A0A287ANT6 | Structural ECM | 0,155 | 0,199 | 0,268 | 0,510 |
| Microfibril associated protein 4 | MFAP4 | A0A287AZP0 | Structural ECM | 0,001 | 0,001 | 0,004 | 1,168 |

# Chapter VII

# Decellularized kidney extracellular matrix bioinks recapitulate renal 3D microenvironment *in vitro*

# Chapter VII

## Decellularized kidney extracellular matrix bioinks recapitulate renal 3D microenvironment *in vitro*[††]


### ABSTRACT

In the past few years, the use of decellularized matrices as bioinks has been gaining interest. They are able to provide the necessary and specific cues for remodeling and maturation of tissue-specific cells and have already demonstrated being highly versatile when mixing them with other components for bioprinting. However, researchers have not yet been able to produce a bioink uniquely composed of decellularized kidney matrix, mainly due to its limited viscoelastic properties. Herein, we have optimized the bioprinting process using an agarose microparticle support bath containing transglutaminase for printing. This methodology has shown being highly effective to obtain constructs with good printing resolution and structural integrity. Herein, porcine kidneys were decellularized, lyophilized and digested over 48 h to yield a viscous solution that is able to crosslink after neutralization and incubation at physiological temperature. The viscoelastic properties of the decellularized kidney matrix (dKECM) were tested as well as its printability. Moreover, encapsulation of primary renal progenitor cells was performed, which resulted in high cell viability, with the creation of 3D complex structures over time. This tissue-specific matrix has also shown to influence cellular growth, maturation and differentiation over time. Taken together, these results demonstrate that these bioinks have great potential for bioengineering renal tissue, with numerous applications for the future of regenerative medicine and 3D *in vitro* modeling systems.


[††] This chapter is based on the following publication:

**Sobreiro-Almeida, Rita**; Gómez-Florit, Manuel; Quinteira, Rita; Reis, Rui L.; Gomes, Manuela E.; Neves, Nuno M. Decellularized kidney extracellular matrix bioinks recapitulate renal 3D microenvironment *in vitro*. (Under review).

## VII-1. INTRODUCTION

Renal diseases represent a concerning health-care issue. When kidney fails to perform its normal function, patients have to resort to lifelong dialysis treatments or renal transplantation.[1, 2] Last decades' advances in the biomedical field disclosed new routes to improve current renal replacement therapies. Novel bioengineering techniques, such as 3D printing,[3] decellularization[4, 5] or microfluidics[6] enabled the production of new advanced therapy strategies aiming at kidney regeneration. In such a context, researchers are now applying this knowledge with the ultimate goal of developing functional full-size organs. Nonetheless, kidney's anatomic and cellular complexity combined with its extensive homeostatic function, represent an important tissue engineering challenge.

Tridimensional bioprinting is an emerging technology that consists in the layer-by-layer deposition of cells embedded in a biomaterial. This high precision technology, allows the construction of structures that partially reproduce the architecture and function of the native tissue.[7] However, printing a fully functional kidney represents a higher complexity level and is currently beyond our current capabilities. Numerous challenges can be pointed out, including the technical difficulty of assembling the structures into nephrons, the vascularization requirements, and the selection of biomaterials.[8] Although current 3D bioprinting technology has allowed researchers to produce small portions of nephrons for the future integration in a macroscale organ,[9] the choice of the adequate bioink for kidney tissue engineering is still under extensive research. The ideal bioink needs to keep a good balance between printability (allow extrusion and physical integrity of printed structure with good shape fidelity) and biocompatibility (allow cell encapsulation and normal proliferation), while mimicking the tissue-specific microenvironment.[10] In order to print with bioinks less suited for use as fabrication materials, due to low viscosity or weak mechanical strength, 3D printing in suspension baths has emerged as a promising alternative.[11]

Recently, natural-derived hydrogels were explored as adequate biomaterials to produce bioinks.[12, 13] However, the high complexity and tissue specificity of the extracellular matrix (ECM) are not well represented in the majority of the developed bioinks. Tissue decellularization is the most truthful way to recapitulate the tissue microenvironment, providing all the native biological cues for cell survival and proliferation.[14] Advances in decellularization procedures allowed for an efficient separation of the cellular components from the ECM, which enable the development of biomaterials based on decellularized ECM, including in the kidney.[5, 15, 16] The production of hydrogels from decellularized kidney ECM (dKECM) was already reported.[16–18] These works enabled scientists to understand the electrostatic and hydrophobic interactions that promote collagen fibers to naturally crosslink, when brought to

physiological pH.[19] The soft gel that is formed can have several therapeutic applications, such as studying tissue-specific response, for *in vivo* implantation or as a bioink for 3D bioprinting. Indeed, 3D-printed tissue models from decellularized visceral organs such as heart, liver and pancreas, have been successfully developed in the last few years.[20–22] However, ECM-derived bioinks generally lack mechanical strength, and possess weak mechanical properties which is an important feature specially for weight-bearing tissues.[23] Additionally, they demonstrate slow gelation/crosslinking kinetics, which does not allow to print using the typical layer-by-layer technologies. Despite all concerns, researchers have already been able to print dKECM-derived bioinks, by adding other biomaterials to provide additional support and improve printability.[9, 24] Both works offer innovative and promising concepts for renal regeneration research, but there is room for further development, including in the bioink composition. Little advantage is taken of inherent bioactive and biomimetic properties of the decellularized tissue, by using less than 50 % of dKECM on their bioinks. Furthermore, these works were proposed with the main goal of developing disease models or for *in vitro* biocompatibility.

Herein, we hypothesize that a bioink can be developed by using just dKECM and that it reunites the adequate properties to print kidney tissue structures. Additionally, we propose using these bioinks to promote renal differentiation *in situ* and cell growth over a long-time culture. For that, the most relevant physicochemical properties of the bioinks are adjusted and a printing support bath impregnated with an enzymatic crosslinking agent is developed. To the best of our knowledge, this is the first report of bioinks composed uniquely of decellularized kidney matrix and also the first time studying the growth and differentiation of encapsulated renal progenitor cells. We believe that this work gives a valuable insight on the development of decellularized tissue-derived bioinks and that the developed constructs can be used as advanced therapies to promote kidney regeneration.

## VII-2. METHODS

### VII-2.1. Tissue decellularization and characterization

Porcine kidneys were obtained from a local slaughterhouse according to the national ethical animal guidelines. After removal of the renal capsule and pelvis, two detergent solutions were used to achieve cell removal and matrix preservation. Kidneys were immersed in solutions of 1 % sodium dodecyl sulfate (SDS) and 1 % Triton-X100 for cellular removal under agitation. Following, 1x PBS was used to eliminate detergent residues for 7 days. Remnants of nucleic acid material were further removed with 0.0025 w/w%

DNase and 10 mM of magnesium chloride overnight. Magnesium chloride is essential to potentiate the action of DNase, as this enzyme requires activation through divalent metals for hydrolyzing double-stranded DNA.[25] All the processes were conducted in a sterile environment. Decellularized kidneys were immediately processed after the decellularization process.

To evaluate the efficacy of the decellularization, histological and DAPI stainings were performed. Briefly, kidney sections were immersed in a 10 % neutral buffered formalin solution (Thermo Scientific) for 24 h at room temperature. Pieces of decellularized and native tissues were embedded in paraffin and cut into 5 µm thick sections. These sections were deparaffinized, rehydrated and stained with working solutions of Hematoxylin and Eosin, Alcian blue or with a Masson Trichrome staining kit (Bio-optica), according to manufacturer instructions. Sections were also stained with DAPI (VWR) (diluted 1:1000) for 10 min in the dark. The slides were further analyzed by optical or fluorescence microscopy.

### VII-2.2. Bioink development and characterization

Decellularized kidney extracellular matrix (dKECM) was further cut into pieces and frozen at -80 °C overnight. After, a freeze-dryer was used to lyophilize the tissues for 48 h. dKECM was further processed into a powder by using a cryogenic grinder (SPEX SamplePrep). At this point, the fine powder was stored at -20 °C until further use. The fabrication of the bioinks was performed by digesting the dKECM in acidic environment. Two concentrations were produced to test injectability and rheological properties. 1 and 2 w/v% dKECM were digested for 48 h in 0.01 M hydrochloric acid together with 0.1 or 0.2 w/w% of pepsin, respectively. All the solutions were passed through a 0.22 µm filter before use. After 48 h, the matrix was brought-up to physiological pH by the addition of 1/9 v/v% of 10 x PBS (Sigma Aldrich) and 1/10 v/v% of 0.1 N NaOH (Enzymatic). After neutralization, the solutions were immediately used for bioprinting.

Evaluation of the bioink rheological properties was performed on 1 and 2 % dKECM using a rheometer (Kinexus Prot, Malvern). 20 mm diameter parallel plates and 1 mm gap size was used for all the measurements. To mimic crosslinking conditions after bioprinting, microbial transglutaminase (Ajinomoto) was added at a final concentration of 10 mg $mL^{-1}$ of dKECM neutralized solution. The gelation kinetics of the samples was measured by temperature sweep, following a previously reported protocol.[20] Briefly, dKECM bioinks were subjected to oscillatory shear stress (by setting the strain to 1% and angular frequency to 10 rad $s^{-1}$) during heating from 4 to 37 °C. A linear ramp of 5 °C $min^{-1}$ was set, while there were two incubation periods at 15 °C and 37 °C for 5 and 40 min, respectively. Dynamic frequency sweep analysis was performed after a 30 min incubation at 37 °C, by setting the applied strain

at 1% and sweeping the frequency from 100 to 0.1 rad $s^{-1}$. Finally, shear rate sweeps were conducted to assess the viscosity, by varying the shear rate from 0.01 to 500 $s^{-1}$ at room temperature. Mineral oil (Fisher Scientific) was used as solvent trap.

The overall morphology and the internal structure of the hydrogels was assessed by Scanning Electron Microscopy (SEM). Briefly, all samples were fixed in 2.5 % glutaraldehyde (VWR), washed with PBS and frozen with liquid nitrogen before freeze-drying for 24 h. After dehydration, samples were sputter coated with gold and analyzed under a SEM equipment (JSM-6010 LV, JEOL) at an acceleration voltage of 10 kV.

### VII-2.3. Cellular encapsulation on dKECM bioinks

Before bioprinting, dKECM bioinks were centrifuged at 4000 rpm to pellet non-digested pieces. Human renal progenitor cells (hRPCs) were kindly provided by Prof. Paola Romagnani (Department of Biomedical, Experimental and Clinical Medicine, University of Florence, Italy). They were used from passage 1 to 3 and isolated as previously described.[5, 15, 26] HRPCs were cultured and expanded in Microvascular Endothelial Cell Growth Medium (EGM™-MV, Lonza) supplemented with 20 % HyClone™ Fetal Bovine Serum (FBS, GE Healthcare). Cells were trypsinized with TrypLE Express (ThermoFisher) before being suspended on fresh media, counted and centrifuged at 1500 rpm. $10^6$ cells were resuspended in each 1 mL of 2% dKECM matrix. Cell-laden bioinks were loaded in sterile cartridges (CELLINK) for printing. Gelatin-laden bioinks were used as a control. Briefly, a 10 % gelatin solution (Sigma Aldrich) was dissolved in PBS under constant stirring at 60 °C for 30 min and then cooled to 37 °C, before being mixed with $10^6$ hRPCs per mL and loaded in sterile cartridges.

### VII-2.4. Printing of cell-laden constructs

Constructs were printed using a bioprinter (BioX, CELLINK). All printing models were post-processed by the BioX HeartOS (V2.0, CELLINK). The bioprinting was performed using a support bath, as previously described.[12] Briefly, a 0.5 % agarose solution (Lonza) containing 11 mM $CaCl_2$ (Sigma-Aldrich) was prepared and autoclaved. Immediately after, the solution was cooled down to room temperature under constant agitation at 700 rpm to form agarose microparticles. The solution was stored at 4 °C or used directly after cooling. 0.5 w/v % of microbial transglutaminase (Ajinomoto) was added to the agarose bath and left to solubilize for 20 min before printing. Printability was tested using a 25 G needle with a printing

speed varying from 8 to 14 mm $s^{-1}$ and pressure varying from 5 to 10 kPa. The gelatin-containing printhead was heated at 37 °C, and hRPCs-laden gelatin was printed at a constant pressure of 5 kPa and a printing speed of 10 mm $s^{-1}$. Based on the printability tests, a square solid construct of 10 x 10 x 1 $mm^3$ was printed inside sterile plates loaded with the support bath. After printing, the constructs were crosslinked by incubation at 37 °C for 2 h, followed by agarose bath removal and fresh culture media addition. Cultures were maintained for 30 days, with specific timepoints to evaluate the evolution of cellular performance.

### VII-2.5. Evaluation of cellular performance

The metabolic activity of encapsulated hRPCs was evaluated on constructs after 1, 5 and 12 days after bioprinting using alamarBlue (BioRad) assay. Culture medium was removed and replaced with fresh medium supplemented with 10 % of alamarBlue reagent. After an incubation period of 4 h at 37 °C, the supernatant was used to determine the fluorescence intensity in a microplate reader (excitation: 530/25 nm; emission: 590/25 nm). For the evaluation of the effect of the printing process on cell viability, a live/dead assay was performed using PI and Calcein, AM (ThermoFisher). The fluorescent dyes were incubated with the constructs at a concentration of 1 µg $mL^{-1}$ for PI and 2 µg $mL^{-1}$ for Calcein, AM in DPBS for 30 min at 37 °C. After this time, the constructs were analyzed using a TCS SP8 confocal microscope (Leica, Wetzlar, Germany). Images were recorded digitally and further processed using LASX software (Leica). For the histological analysis of the distribution of cells on the matrix, the printed constructs were fixed in 10 % neutral buffered formalin, and embedded in Histogel™ (ThermoFisher) before being processed and embedded in paraffin for sectioning. 5 µm sections were stained with Hematoxylin & Eosin, and observed under light microscopy (DM750, Leica).

### VII-2.6. Evaluation of cellular phenotype

The potential of dKECM bioinks to modulate hRPCs phenotype was evaluated by immunocytochemistry after 21 and 30 days of culture. Briefly, the printed constructs were fixed with 10 % neutral buffered formalin for at 4 °C and washed with PBS. Constructs were further incubated with blocking solution 3 % bovine serum albumin (BSA, Laborspirit) for 30 min, after which the primary antibodies against Paired box gene 2 (PAX2, Abcam, 1:100), Nephrin (NPHS1, Citomed, 1:200) and Tamm–Horsfall protein (THP, Santa Cruz, 1:25) were incubated in blocking solution overnight at 4 °C. Samples were washed with PBS and incubated with the secondary antibody Alexa Fluor 488 (Alfagene;

1:500 diluted in PBS) at RT in the dark for 1h. DAPI (Sigma Aldrich, 1:500) and Alexa Fluor 546 Phalloidin (Alfagene; 1:200) were incubated along with the secondary antibody. After several rinses in PBS, constructs were analyzed under a Leica SP8 confocal microscope. Images were recorded digitally and further processed using LASX software.

### VII-2.7. Development of the glomerular model

The glomerulus 3D model was created using AutoCAD (Adobe, USA) and exported to STL format, which was converted to G-code using HeartWare (CELLINK). The design of the model was inspired in the human glomerular architecture, in order to comprise two cell types: endothelial cells and podocytes. Human umbilical vein endothelial cells (HUVECs) were obtained from Cascade Biologics® and encapsulated in dKECM as previously described at a density of $2 \times 10^6$ cells $mL^{-1}$. To obtain primary podocytes, hRPCs were cultured for two days in DMEM-F12 media (Sigma), supplemented with 10 % FBS and all-trans retinoic acid (100 µM, Sigma) for 48 hours before encapsulation, as previously reported.[27] These cells were encapsulated at a density of $1 \times 10^6$ cells $mL^{-1}$. The printing of cell laden constructs was performed as previously described and cultures were maintained for a maximum of 2 days. For cell tracking purposes, cells were incubated with CellTrace™ dyes (ThermoFisher) for 30 min at 37 °C before being encapsulated.

### VII-2.8. Statistical Analysis

Statistical analyses were performed with GraphPad Prism 8 (GraphPad Software, California, USA). Data were expressed as means ± standard deviation of experiments with at least three independent assays. Differences between groups were analyzed by unpaired t test or two-way analysis of variance (ANOVA) in case of experiments conducted over time, using Tukey test for post hoc assessments of differences between samples. Statistical significance was defined as $p < 0.05$.

## VII-3. RESULTS

### VII-3.1. Tissue processing and evaluation of decellularization

In this study, porcine kidneys were decellularized using solutions of an anionic (SDS) and non-ionic detergent (Triton X-100), followed by DNase to remove the remainings of nucleic material. This protocol

was previously described by our group,[5, 15] where we have shown that contents of dsDNA were successfully removed and that collagen and glycosaminoglycan's contents were preserved in the decellularized tissue.[15] Herein, we proceeded to histological analysis of native versus decellularized tissue to corroborate these findings. In comparison to the native kidney (Figure VII-1-A), the decellularized tissues appear whiteish and with smaller overall volume (Figure VII-1-F). Histomorphological analysis reveals nucleic material removal and preservation of structures on the decellularized tissues, including capillaries, glomerular and tubular structures (Figure VII-1-G, H, I). Masson trichrome and Alcian Blue stainings reveal preservation of collagen and glycosaminoglycans of the decellularized tissue (Figure VII-1-H, I), respectively. No DAPI staining for nucleic material is found after the decellularization process (Figure VII-1-J), which corroborates our previous findings. Overall, we have successfully demonstrated a reproducible decellularization protocol that renders a good balance between nucleic material removal and preservation of kidney structures and its major components.

To obtain decellularized kidney ECM (dKECM) bioinks, the matrix was dehydrated and cryo-milled (Figure VII-1-K). The resulting particulate matrix was already characterized by our group.[14] Then, it was enzymatically digested in acidic environment (pH = 2), creating a viscous solution (Figure VII-1-L). After solution neutralization, the crosslinking process using microbial transglutaminase (mTG) and temperature enables to obtain a gel consistency, which viscoelastic properties were further characterized.

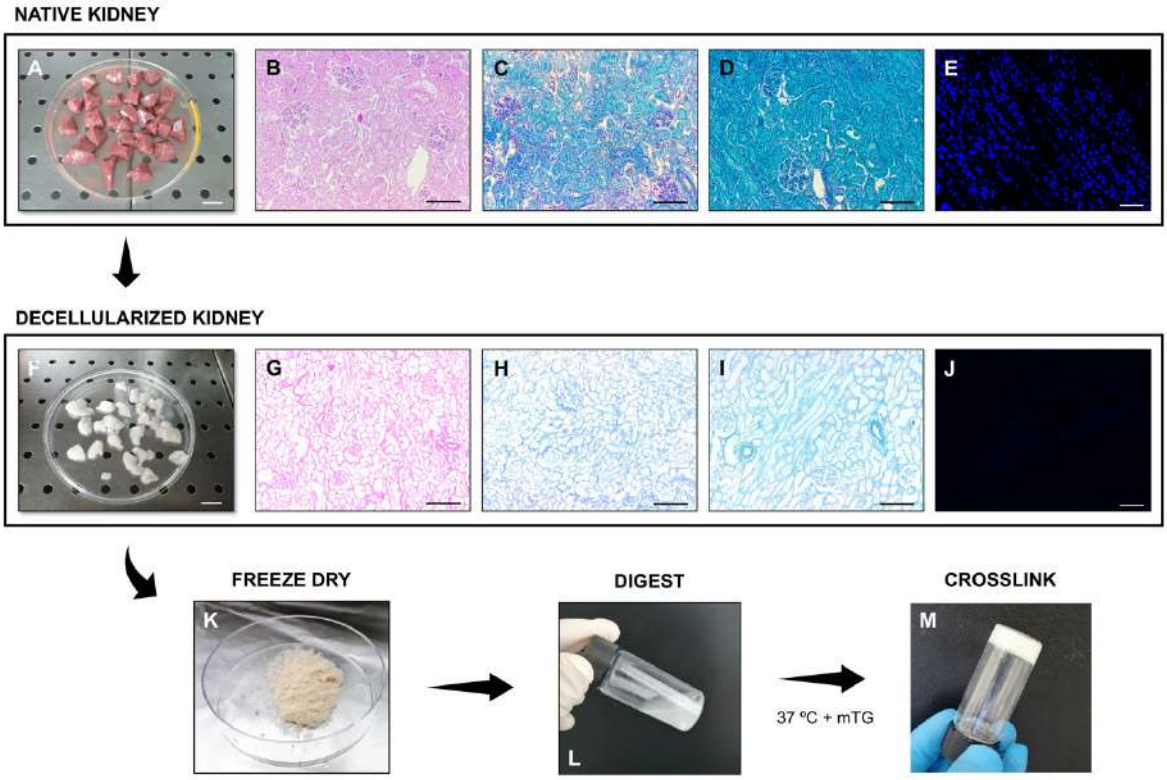


Figure VII-1 – Representative micrographs of native and decellularized kidney tissue and macroscopic representations of post-decellularization processing. (A) Representation of kidney sections before decellularization. (B) Hematoxylin and Eosin, (C) Masson's Trichrome, (D) Alcian Blue and (E) DAPI stainings of native tissue. (F) Representation of kidney sections after decellularization. (G) Hematoxylin and Eosin, (H) Masson's trichrome, (I) Alcian Blue and (J) DAPI stainings of decellularized tissue. (K) Appearance of decellularized kidney after freeze-drying and milling. (L) Representative micrograph of the digested matrix. (M) Representative micrograph of sol to gel transition of dKECM after thermal (37 ºC) and enzymatic (mTG - microbial transglutaminase) crosslinking. Scale bars: A, F = 1.5 cm; B-D, G-I = 500 µm; E, J = 50 µm.

## VII-3.2. Effect of dKECM bioink concentration on structural and rheological properties

The flow behavior of the dKECM bioinks was measured at room temperature, to mimic printing conditions. Both concentrations demonstrate shear thinning behavior in the shear stress range of 0.01 to 500 $s^{-1}$ (Figure VII-2-A), indicating that viscosity decreases as the shear rates increase. Additionally, the increase in concentration results in higher viscosity values for all shear rates. Because dKECM bioinks are printed in an agarose support bath, we also evaluated its rheological properties upon inclusion of mTG (Figure S VII-1). The agarose bath demonstrates shear thinning behavior even after mTG inclusion, which allows for a smooth printing process, and healing upon nozzle movement, as previously shown.[12, 28]

In addition, we also evaluated the gelation kinetics by varying the temperature from 4 to 37 °C and measured its influence on the storage modulus (Figure VII-2-B, C). The increasing concentration of dKECM

results in increasing storage modulus both before and after crosslinking. The inclusion of mTG had the same effect regardless of the concentration. It is interesting to note that the time required for reaching the higher modulus peak was higher for gels containing mTG in its composition. In addition, upon reaching 37 °C, the storage modulus of 2 % dKECM is already increasing, whereas for 1 % dKECM, the storage modulus has a slight decrease in its values within the temperature ramp from 15 to 37 °C, particularly in the condition without mTG. This indicates that the assembly of collagen fibrils in 2 % dKECM is triggered before reaching 37 °C, starting an earlier gelation. Nevertheless, all four conditions formed a fully crosslinked hydrogel after 30 min incubation at 37 °C.

The stability of the dKECM hydrogels was measured by frequency sweeps in both concentrations (Figure VII-2-D, E). This measurement was performed after thermal crosslinking and the influence of enzymatic crosslinking (inclusion of mTG) was also evaluated on the gel behavior. The inclusion of mTG results in increasing storage modulus of the network over all frequencies in both concentrations. However, 1 % dKECM concentration demonstrates a huge increase in the storage modulus upon higher angular frequencies (Figure VII-2-D), which does not happen with 2 % dKECM concentration (Figure VII-2-E). This indicates that elastic behavior becomes dominant, whereas the influence of the viscous behavior is diminished.[29] Besides, the storage modulus (G') documented for 1 % concentration is at all frequencies lower than 2 % concentration, which can be correlated with greater stability of the 2 % dKECM gel after crosslinking. Additionally, these results confirm the gel-like behavior of all samples, since they demonstrate a higher storage modulus (G') than loss modulus (G") (data not shown).

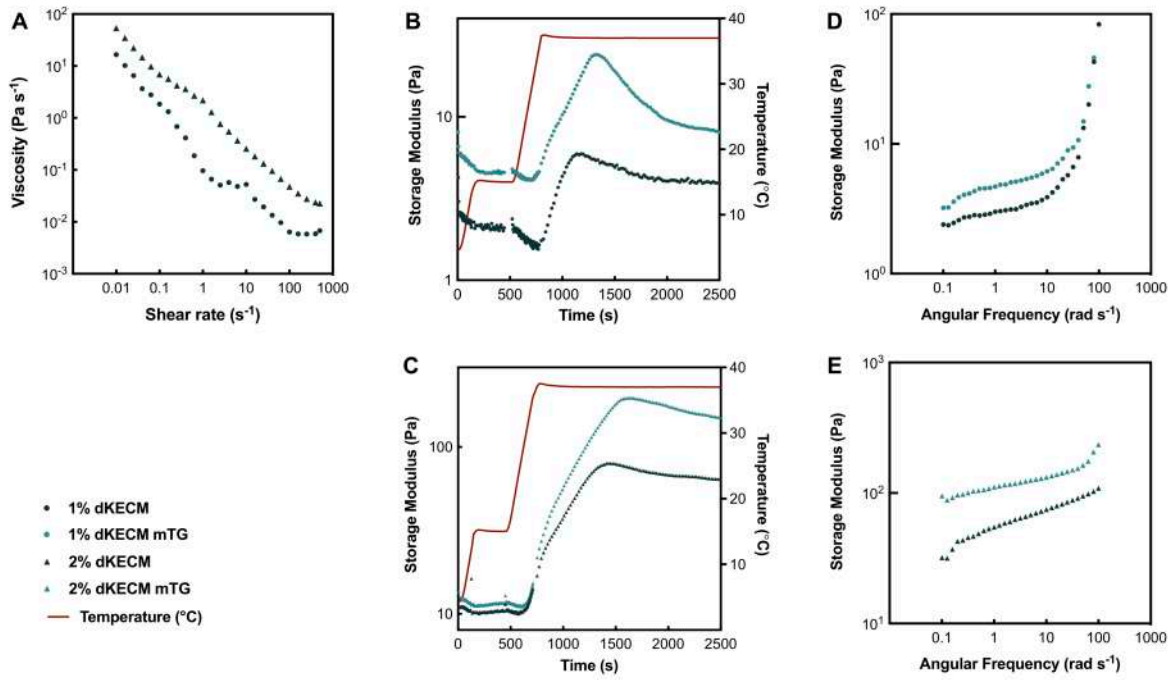


Figure VII-2 – Rheological characterization of dKECM bioinks using different concentrations. (A) Flow behavior of dKECM bioinks measured at RT. Viscosity was measured by increasing shear rates on 1 and 2 % dKECM (black symbols). (B, C) Storage modulus of 1 and 2 % crosslinked dKECM bioinks at varying frequencies, respectively. The inclusion of mTG (blue symbols) was performed in situ in order to mimic post-printing conditions. (D, E) Gelation kinetics of 1 and 2 % dKECM, respectively, with (blue) and without mTG (black). The gelation kinetics was measured from 4 to 37 °C in four stages (red line), comprising one first increment from 4 to 15 °C (at 5 °C/min), a 5 min incubation at 15 °C, a second increment from 15 to 37 °C and finally 30 min incubation at 37 °C.

The structural properties of the dKECM hydrogels were also evaluated by SEM (Figure S VII-2). Herein, we intend to evaluate the changes in fibril organization upon the increase in concentration and the inclusion of mTG. Upon dehydration of the gels, they form lamellar sheets, particularly in the 1 % dKECM concentration (Figure S VII-2-A, E), which is a characteristic of collagenous hydrogels. Moreover, all conditions demonstrate porous structure and an intrinsic fibril network. The increase in concentration results in a denser network, as expected by the increasing protein content (Figure S VII-2-C, G). The inclusion of mTG results in interconnected pores and rearrangement of the network, forming a more cohesive ultrastructure, which corroborates with the rheology values observed for these hydrogels (Figure S VII-2-D, H).

Analyzing the obtained results, the 2 % dKECM concentration yields better results regarding hydrogel stability and viscoelastic properties, with no significant changes in their ultrastructure. This stability is highly correlated with maintenance of the shape and mechanical integrity after printing. Based on this outcome, the printability and biological response of the dKECM bioink was evaluated using only 2 % dKECM gels.

### VII-3.3. Printability of dKECM bioink using a support bath

To demonstrate the printability properties of the dKECM bioink, we printed constructs of different kinds with increasing complex geometry and evaluated the differences after crosslinking and support bath removal (Figure VII-3). The 3D models used for printing are represented in Figure VII-3-A to D. Using our printing methodology, we are not only able to print in the $x$ and $y$ axis directions, creating straight lines (Figure VII-3-E), but also in oblique angles, creating curved lines (Figure VII-3-F, G). Additionally, we are able to print constructs with unsupported layer deposition (90° rotation from the previous layer, Figure VII-3-G), without losing the integrity of the construct after support bath removal (Figure VII-3-K). Our major goal with the support bath was to provide a stable bed to print a bioink with slow gelation kinetics to allow the self-assembly of collagen, while supplying the right amount of transglutaminase in order to obtain stable constructs with shape-fidelity and mechanical integrity after changing the support bath for culture media. In addition, this strategy allows the crosslinking between the deposited layers, which is difficult using bioinks that crosslink right after extrusion, resulting in structures with high shape and mechanical integrity not limited by the number of layers. Herein, we are able to print structures from 4 (~1 mm height) to at least 18 layers (~4.5 mm height), without losing its integrity, even after crosslinking and agarose removal (Figure VII-3-H). In Figure S VII-3, we can observe the effect of printing the same constructs without including mTG in the support bath. Although some filaments are still preserved (Figure S VII-3-A), the overall structure and geometry is lost, and the printed constructs disintegrate after agarose removal, which reinforces the need to have an external crosslinking agent.

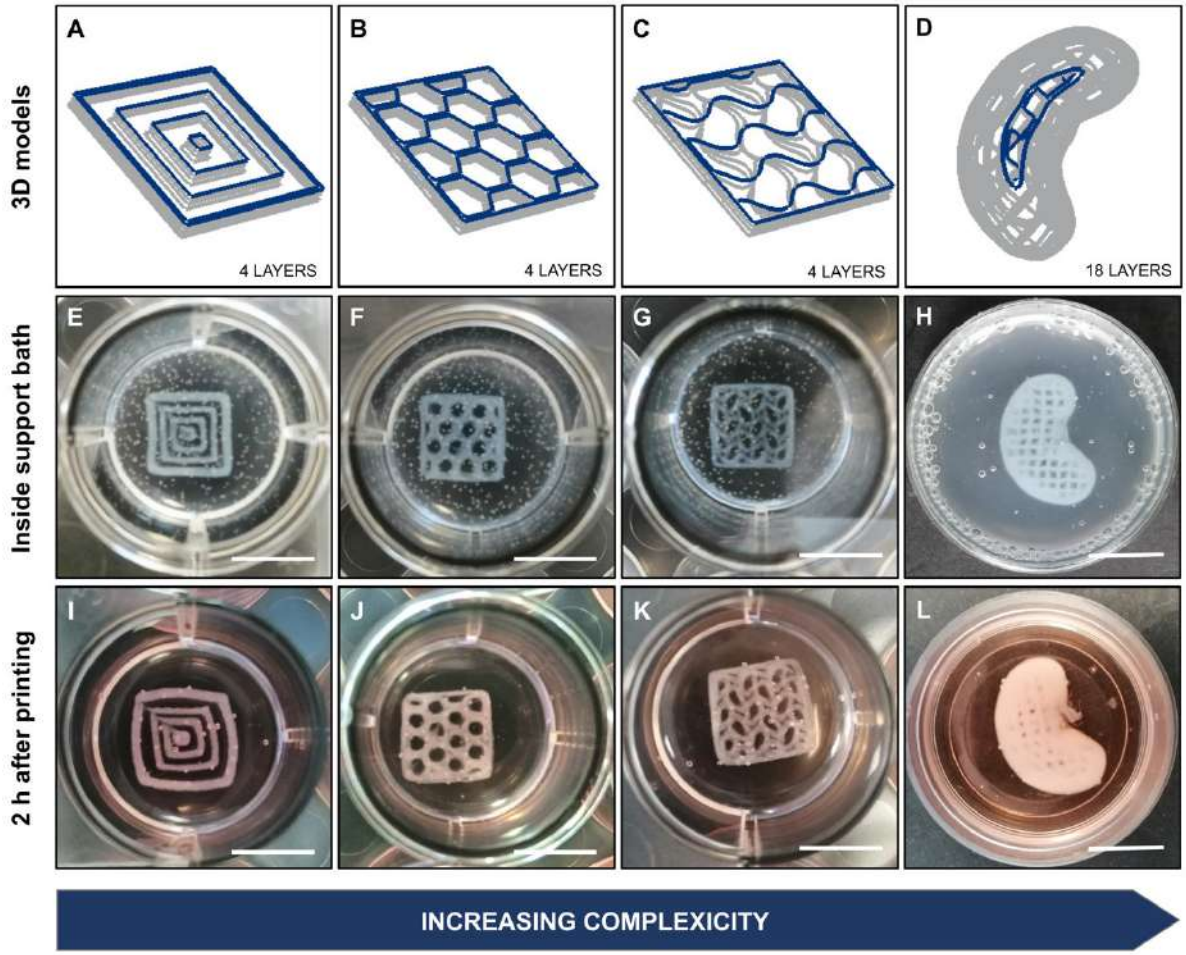


Figure VII-3 – Macroscopic printability evaluation using different 3D models. (A-D) 3D models used for printability assessment; (E-H) Representative images of the constructs right after printing process, inside the agarose support bath; (I-L) Representative images of the constructs after a 2 h incubation at 37 °C, removal of the agarose support bath and addition of media. Scale bars: 1 cm.

The printability precision was evaluated using a standard square model with four layers and intercalated orientation (rotating 90° between each layer deposition). For that, we established a constant pressure for extrusion (8 kPa), which enabled uniform extrusion without needle clogging. The increasing printing speed from 8 to 14 mm $s^{-1}$ enables obtaining solid constructs with macroscopic differences in size (Figure VII-4-A to D). Microscopic evaluation of line-crossing points demonstrates that the intercalated orientation printing does not drag the deposited material from the bottom layer, creating thinner filaments and resulting in higher resolution with the increasing printing speeds (Figure VII-4-E to H). Quantitative data corroborates the macroscopic evaluation, being that printing speeds of 8, 10, 12 and 14 mm $s^{-1}$ results in mean filament widths of 667, 569, 465 and 440 µm (Figure VII-4-I), and mean areas of 1.39, 1.28, 1.18 and 1.10 $cm^2$ (Figure VII-4-J), respectively. We noticed that 8 mm $s^{-1}$ printing speed yields constructs very variable in size, with filament widths more than 2.5 times the nozzle diameter, which indicates excessive extrusion of material. Additionally, the 14 mm $s^{-1}$ printing speed yields constructs with

higher resolution, but low stability, in which the outer filaments become separated from the original construct, probably due to insufficient flow of material (Figure VII-4-D). We also notice that upon small fluctuations in temperature, it is necessary to increase or decrease the printing speed, based on the variation of the viscoelastic properties of dKECM, as aforementioned. Based on these findings, we have proceeded to biological assays using a printing speed range between 10 and 12 mm $s^{-1}$.

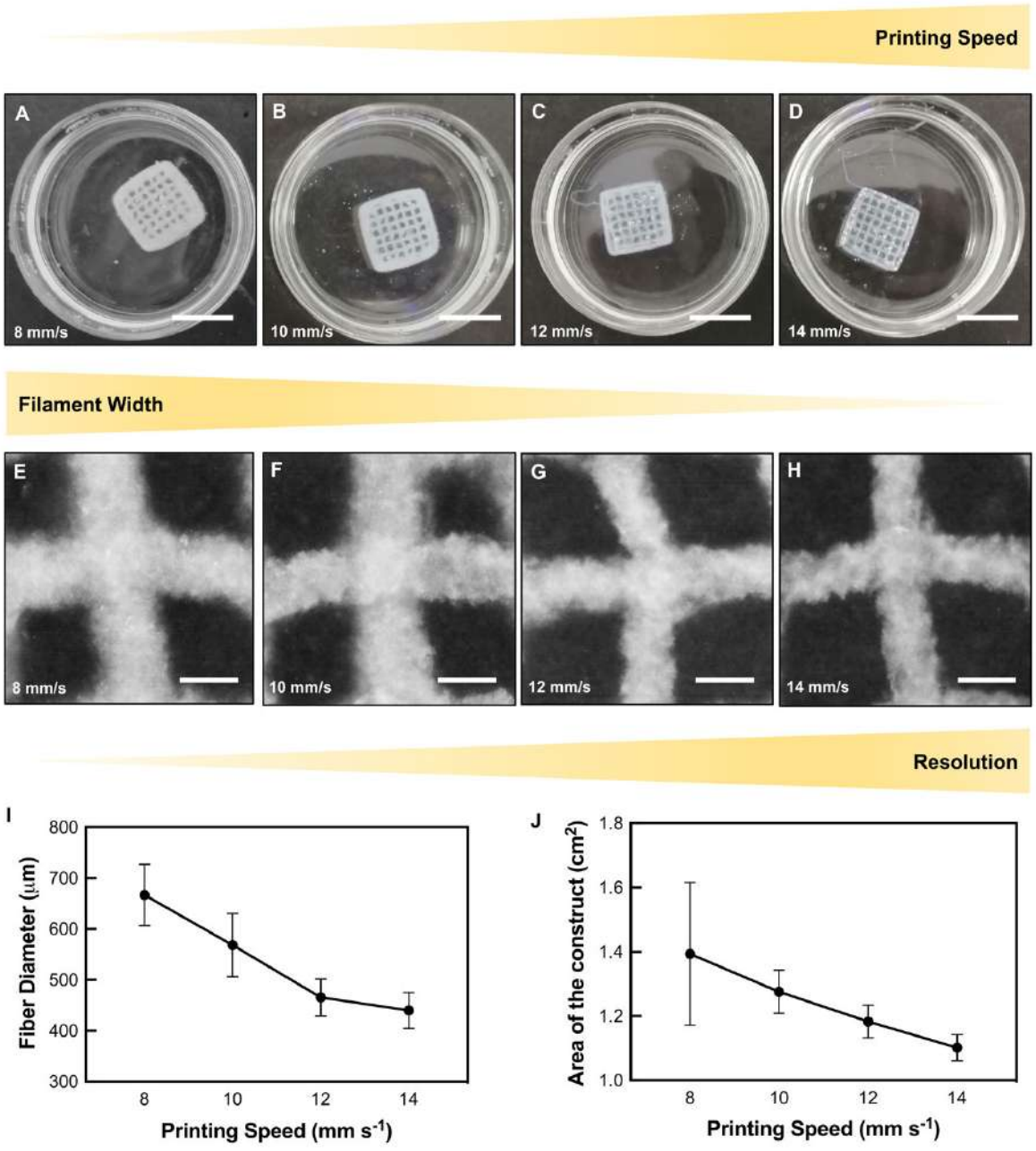


Figure VII-4 – Printability of the dKECM bioinks depending of the printing speed. (A-D) Macroscopic view of the constructs printed with increasing speed after crosslinking and agarose removal. Scale bar: 1 cm; (E-H) Microscopic view of line-crossing

points with increasing printing speed. Scale bar: 500 µm. (I) Quantitative analysis of the fiber diameter and (J) area of the constructs upon increasing printing speeds. Measurements were performed using ImageJ Software.

### VII-3.4. Biological evaluation of dKECM bioinks

One of the most important criteria for a bioink is that it enables extrusion without loss of cell viability and the growth of tissue-specific cellular phenotypes. For that, we used gelatin as a control, a natural origin protein derived from collagen hydrolysis.[30] Gelatin-based biomaterials have already been developed in combination with several biomaterials and stem cells, and have demonstrated great versatility for biomedical applications.[31] Herein, we employed human renal progenitor cells (hRPCs) to study matrix-induced changes on cellular behavior. Therefore, after bioprinting, we evaluated bioinks' cytocompatibility by qualitative (live/dead assay) and quantitative methods (alamarBlue assay) over 12 days with hRPCs (Figure VII-5).

Live/dead assay results are shown in Figure VII-5 for dKECM and gelatin-encapsulated cells after printed and removed from the support bath. Cells demonstrate being viable and evenly distributed in the printed hydrogels throughout the assay, regardless of the bioink in which they were encapsulated. Day 1 micrographs (Figure VII-5-A, D) do not demonstrate substantial microscopic differences between dKECM and gelatin-encapsulated cells. Indeed, after 24 h, cells are still round-shaped and very few dead cells (red staining) can be observed (< 5 %). However, after 5 days in culture (Figure VII-5-B, E) some differences between control condition and dKECM can be observed, especially regarding cellular morphology. Cells encapsulated in dKECM start to elongate, whereas hRPCs encapsulated in gelatin do not demonstrate the same behavior, remaining round-shaped during all the assay. Indeed, after 12 days in culture (Figure VII-5-C, F), these differences are even more evident, a result which is corroborated by the quantification of live cells fluorescence (Figure VII-5-G). Herein, the increase in fluorescence intensity is observed overtime for dKECM-encapsulated cells, indicating that the percentage of live cells is increasing, but the exact opposite effect is observed for gelatin-encapsulated cells, being the difference in values statistically different at day 5 and day 12. Cellular metabolic activity was evaluated by alamarBlue assay (Figure VII-5-H). Although these results can give an insight on cellular behavior over time, it is not possible to infer that all the encapsulated cells were metabolizing the compound and therefore this was considered as a corroborative assay for the live/dead analysis. Indeed, the results are correlated with the viability assay, demonstrating that metabolic activity is maintained overtime for dKECM and gelatin-encapsulated cells, being the difference in values statistically relevant at day 5.

To evaluate the inner organization of encapsulated cells on dKECM constructs, we have performed H&E staining on 5 µm paraffin slices of constructs cultured for 12 days (Figure S VII-4). During culture time, it is possible to observe that the inner cellular density is increasing and that cells are changing from a round shape to an elongated morphology, which corroborates the observation of the live/dead assay. Indeed, it is also possible to observe that cells migrate and evolve from isolated single cells to agglomerates of two or more cells (Figure S VII-4-F). It is not possible to show similar H&E micrographs of gelatin constructs due to the excessive dye absorbance of the gelatin.

We also analyzed the stability of the constructs after 30 days in culture (Figure VII-5-I-L). Constructs were printed with relatively low infill and high porosity, allowing for nutrients and waste exchange. Even though, it was possible to observe high structural integrity over long-term cultures. Representative images of the hRPCs-laden dKECM and gelatin constructs at day 1 and day 30 of culture are shown in Figure VII-5-I, K and Figure VII-5-J, L, respectively. After quantifying the area occupied by the constructs, we are able to demonstrate that the percentage of shrinkage was significantly higher for the dKECM constructs rather than for the gelatin constructs (22.8 % versus 9.8 %). Therefore, we hypothesize that while hRPCs on specific kidney ECM are able to grow, proliferate and secrete their own matrix, cells on gelatin would remain more static, resulting in low matrix remodeling. The contraction of the construct can be an indirect measurement of ECM remodeling.[32]

These results indicate that dKECM bioinks are highly cytocompatible, and that the mechanical properties were adequate to maintain the structural integrity of the constructs and, at the same time, provide a stable environment for the encapsulated cells to remain viable and organize inside the construct.

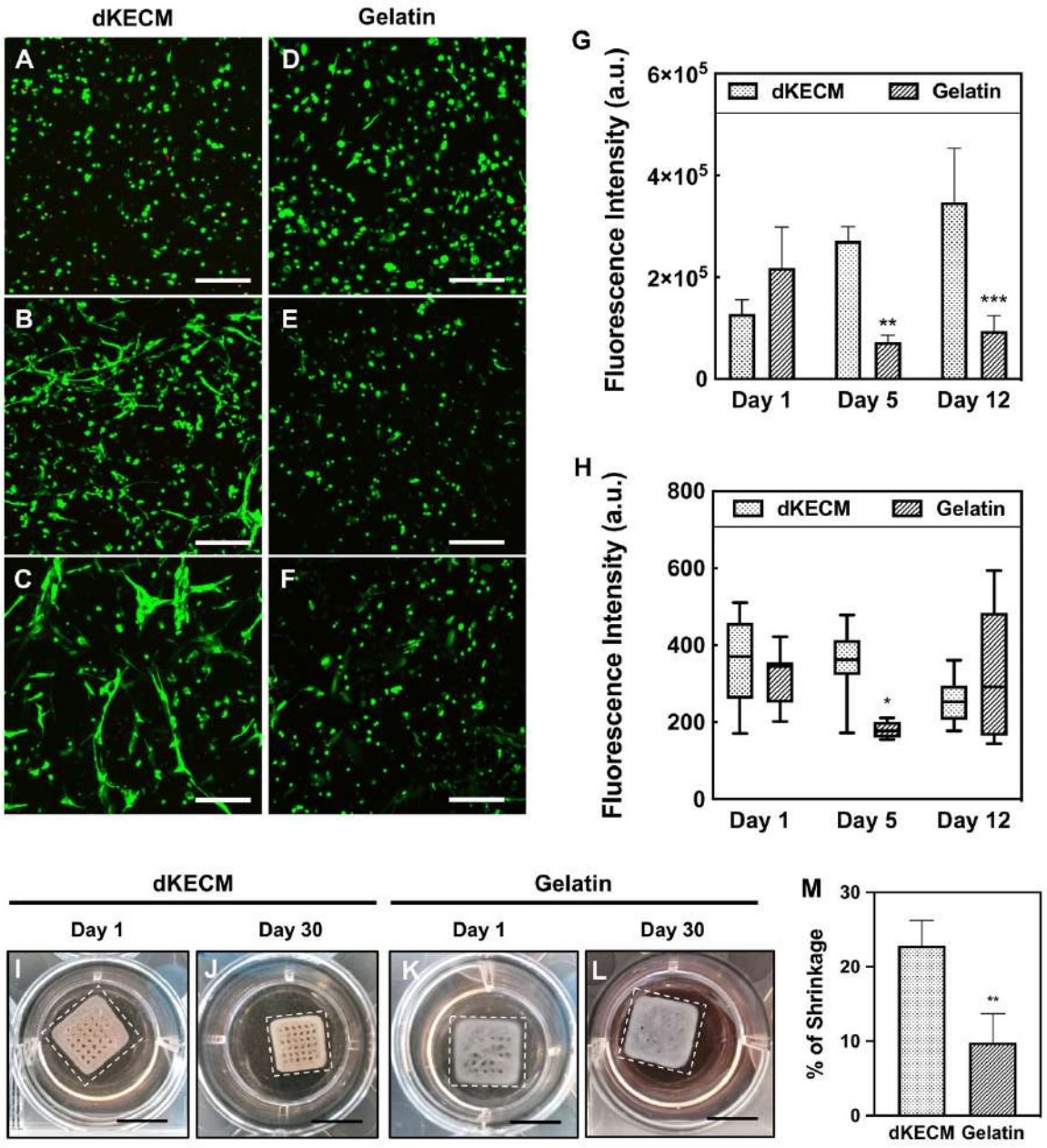


Figure VII-5 – Cytocompatibility assessment of dKECM and gelatin-encapsulated hRPCs. (A, B, C) Live/dead assay of dKECM and (D, E, F) gelatin-encapsulated hRPCs at day 1, day 5 and day 12, respectively. Cells were incubated with Calcein AM (stains green for live cells) and PI (stains red for dead cells). Scale bar: 250 μm; (G) Quantification of fluorescence intensity of live cells performed on ImageJ, corroborating Live/Dead stainings; (H) Metabolic activity assay demonstrated by alamarBlue fluorescence over 12 days timepoints; (I, J) Representative images of the dKECM and (K, L) gelatin constructs after 1 and 30 days of cell culture, respectively. Scale bar: 1 cm; (M) Percentage of shrinkage observed after 30 days of cell culture. The percentage was calculated by diving the area of the construct at day 30 by the area at day 1. *$p$<0.05, **$p$<0.01, ***$p$<0.001 vs. dKECM at the same day.

### VII-3.5. Tissue-specific proteins on encapsulated hRPCs

After the initial cytocompatibility assessment, it is important to examine if the dKECM bioinks can support progenitor cells differentiation into renal specific phenotypes. For that, immunocytochemistry (ICC) was performed on dKECM and gelatin bioprinted constructs. The presence of the stem cell marker PAX2, the tubular marker THP and the glomerular marker NPHS1 were assessed at 21 (Figure S VII-5) and 30 days of culture (Figure VII-6). The first insight reveals a confluent and highly interconnected network of cells present on dKECM bioink, whereas the majority of the gelatin-encapsulated cells remain round-shaped with no network formation. Moreover, the presence of renal specific markers is only microscopically detected on the dKECM constructs, whereas in gelatin constructs the detected fluorescence is ascribed to phalloidin (*red*) and DAPI (*blue*), which mark cytoskeleton and nuclei, respectively. These observations are also valid for 21-day ICC assays (Figure S VII-5). For a more accurate evaluation, we performed quantification of fluorescence intensity of PAX2, THP and NPHS1 markers on dKECM constructs (Figure VII-6-G) and on gelatin constructs (Figure VII-6-H) and evaluated their evolution overtime. Quantification results reveal higher fluorescence intensity for all markers on dKECM-encapsulated cells at all timepoints. Additionally, THP demonstrates higher fluorescence intensity over the stem cell maker PAX2 and the glomerular marker NPHS1. These findings are observed at both timepoints, which can reveal a preference for cellular differentiation towards tubular lineage in dKECM. Additionally, THP presence increases overtime, being significantly different from day 21 to day 30. Nevertheless, NPHS1 expression is also found on the constructs, but the expression decreases from day 21 to day 30, although without significant differences. PAX2 shows a constant expression over culture time, indicating that some cells are still undifferentiated. Regarding gelatin-encapsulated cells (Figure VII-6-H), the highest fluorescence is noted for PAX2 marker, regardless of the culture time, indicating that cells remained undifferentiated over 30 days. No THP presence was noted and NPHS1 presence was very reduced, corroborating ICC micrographs.

These results reveal that dKECM bioinks can provide an appropriate environment for the growth, migration, self-assembly and specific differentiation of human renal progenitor cells, with the formation of a highly intrinsic network of matrix and cells.

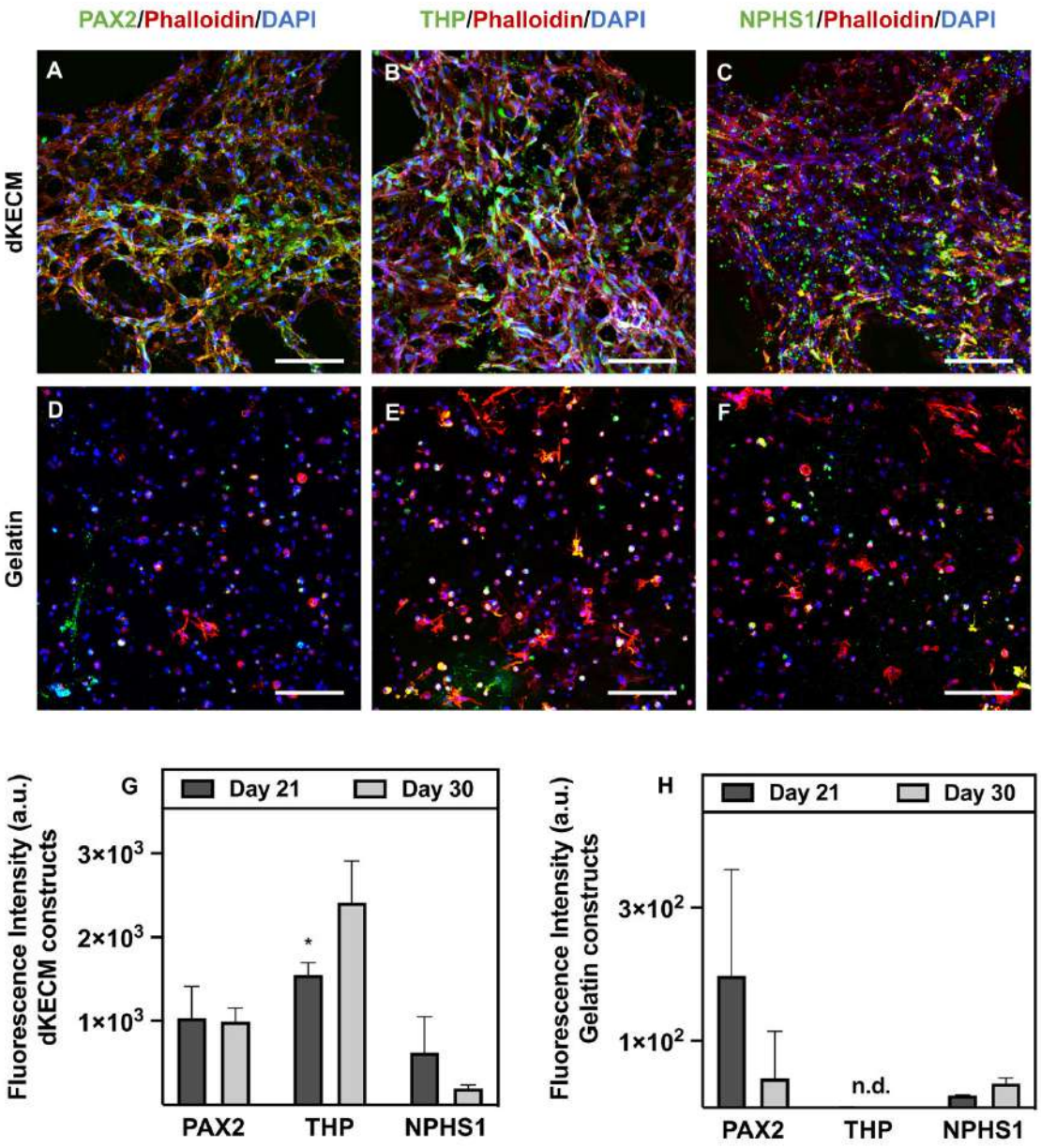


Figure VII-6 – Evaluation of differentiation into renal-specific lineages and overall maturation of the constructs. (A-F) ICC micrographs of renal-specific markers PAX2, THP and NPHS1 on dKECM and gelatin-encapsulated cells after 30 days of culture. Green stains for specific cell marker, phalloidin (red) stains for cytoskeleton and DAPI (blue) stains for nuclei. Scale bar: 250 µm; (G-H) Quantification of green fluorescence intensity on dKECM and gelatin constructs after 21 and 30 days performed on ImageJ software. *p<0.05 vs. 30 days. n.d. = not detected.

### VII-3.6. 3D Printing of a pre-glomerular model

As a practical application of the bioprinting system, we have also envisioned using the dKECM bioink as a substrate for fabricating renal model systems. We demonstrated the versatility and the adequate viscoelastic properties of this bioink, which enabled optimizing the printing conditions for two cell types

in the same model. A glomerular model would have to be composed of, at least, three components: endothelial cells (Figure VII-7-A *red cells*), the glomerular basement membrane and parietal epithelial cells, i.e. podocytes (Figure VII-7-A *blue cells*). Our 3D model was designed to obtain a microarchitecture similar to the glomerulus, in which there is an inner part composed of an intricate network of endothelial cells, and an outer part composed of podocytes (Figure VII-7-B). The glomerular basement membrane would be provided by our decellularized matrix. For the printing process, two printing tools were prepared for extruding dKECM bioink, one containing podocytes (Tool 1-*blue*), and the other endothelial cells (Tool 2-*red*). The macroscopic view of the printed model is shown in Figure VII-7-C. A supplementary video related to the printing of this construct can be found in the supplementary material (Video S1). Overall, we were able to successfully bioprint a model mimicking the human glomerular microarchitecture in a macro scale, which allows for scaled-up reproduction and multiple testing at the same time. This model was maintained for 48 hours, mainly because primary podocytes are terminally differentiated cells unable of dividing or proliferate. After 48 h, HUVECs and podocytes remain viable and evenly distributed inside the bioink (Figure VII-7-D and E, respectively). Indeed, podocytes are elongating inside the dKECM constructs, which is not unusual given our previous findings. Although there is room for improvement, labeling of the cells with appropriate cell trackers allowed us to demonstrate that interface studies could be performed in this system, not only for toxicology analyses but also to study the glomerular barrier with appropriate and patient-specific primary cells (Figure VII-7-F).

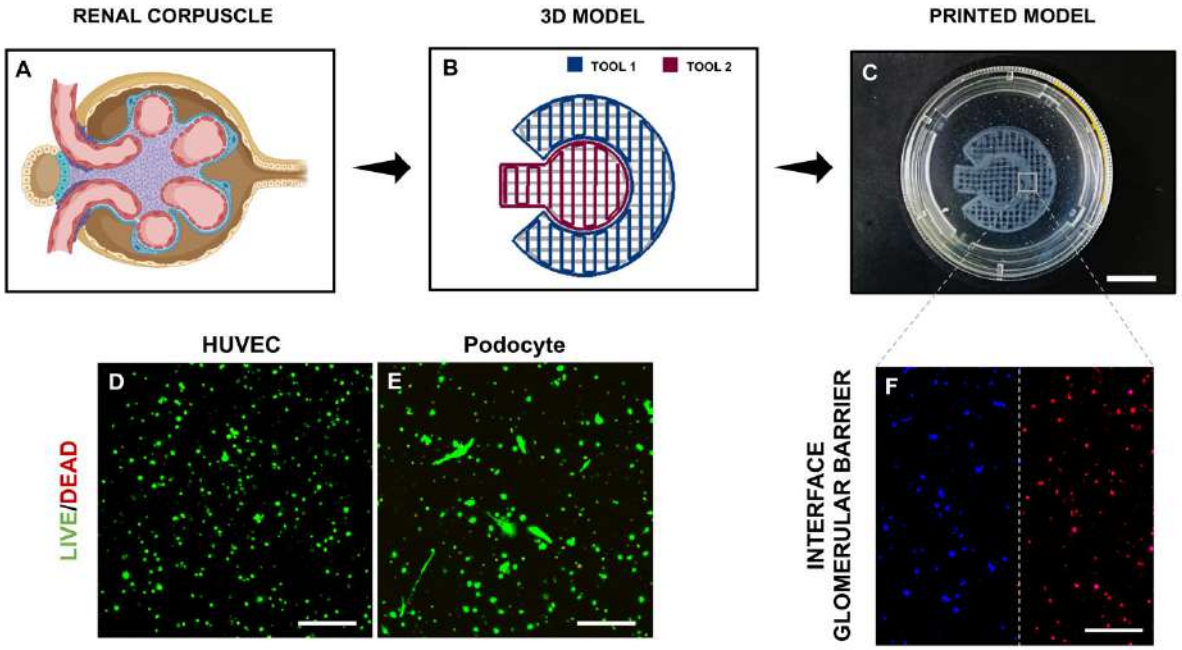


Figure VII-7 – Development of a pre-glomerular model. (A) Schematic representation of the renal corpuscle, where mesangial cells are represented in purple, endothelial cells are represented in red and podocytes are represented in blue. The Bowmans capsule is surrounding the intricate network and is presented in light brown; (B) Representation of the model used as a printing

code for the development of the model. Blue indicates where the podocyte-containing bioink will be printed and red indicates where the HUVEC-containing bioink will be printed; (C) Macroscopic image of the glomerular model after printing. Scale bar: 1 cm; (D-E) Live/dead micrographs of HUVEC and podocyte-encapsulated dKECM 48 h after printing. Cells were incubated with Calcein, AM (stains green for live cells) and PI (stains red for dead cells).; (F) ICC micrograph representing the interface between podocytes (blue) and HUVECs (red), using appropriate cell trackers. Scale bars: 250 μm.

## VII-4. DISCUSSION

The main goal of tissue decellularization is to have maximal cellular material removal without compromising the ECM content, including proteins and growth factors.[33] Our group has already established and improved kidney decellularization process in tissue sections.[5, 14, 15] Although perfusion decellularization has gained interest in the past years, decellularizing a whole porcine kidney is still a challenge. Therefore, one of our goals was to demonstrate that the ECM from porcine kidneys can be obtained by other feasible means. The final outcome of the decellularization process greatly depends on the employed protocol and on the nature of the tissue.[34] Therefore, it is essential to characterize the histomorphological properties and the presence of nucleic material after each decellularization process. We were able to successfully preserve the major morphological characteristics of the kidney tissue (glomerular and tubular compartments, and capillaries) and the main components of the ECM, collagen and GAG's, corroborating our previous findings and that of several others.[35–37] Another concern of exploring decellularized tissues is regarding the immune reaction to xenogeneic material. This reaction is mainly caused by the $\alpha$-Gal epitope existent in the cellular membrane, which can cause immunogenicity in humans.[38] However, the use of porcine-derived ECM has already demonstrated having no adverse immune response upon implantation over 45 days.[39] Therefore, we expect no evidence of sensitization upon implantation of our porcine-derived dKECM. Besides the usual detergent selection for the decellularization procedure, we have also employed enzymatic treatment with DNase to remove any residual cellular material, which ensures an efficient decellularization process. We have previously shown that the nucleic acid material remaining on kidney tissue after decellularization is adequate for tissue engineering applications (20.95 ± 13.25 ng/mg of tissue),[15] which corroborates the obtained results. In addition, we also demonstrated that even after lyophilization and digestion of the decellularized tissue, the growth factors and proteins are still preserved,[14, 15] ensuring that the dKECM remains bioactive.

In the present work, our objective was to develop a bioink composed of dKECM uniquely, in order to benefit from the intrinsic bioactivity of decellularized tissues to reproduce the native tissue

microenvironment. Therefore, we proceeded to the digestion of dKECM in order to obtain a printable viscous solution, which required the tunning and characterization of its viscoelastic properties. Pepsin digestion in acidic environment has been widely used to solubilize ECM-based materials, which upon readjustment to physiological pH and temperature yields ECM-based hydrogels.[16–18] This enzyme cleaves the telopeptide bonds of collagen triple helix, unraveling collagen chains which become available for a self-assembly phenomenon after neutralization.[40] The neutralization is an essential step to ensure inactivation of the enzyme. Nevertheless, decellularized matrices are known to possess low structural integrity and stability, requiring chemical modifications and/or mixing with other materials to enhance its mechanical properties. For example, previous works employed a process of photo-crosslinkable methacrylation of dECM,[24, 41] co-printing with a poly(caprolactone),[20] mixing with alginate and ionic crosslinking with calcium chloride,[9] mixing with a photocurable methacrylated gelatin (GelMA),[21] and/or combined them with other biodegradable materials.[24] Herein, we aimed to minimize the modifications to the matrix composition, and, although the dKECM was extruded through printing nozzles, its low viscosity and gelation kinetics did not allow to use the typical layer-by-layer 3D printing. To overcome this, we used an agarose microparticle support bath, which behaves as a viscoelastic fluid (Figure S VII-1) and can self-heal after nozzle movement and deposition of the bioink, as previously shown.[12, 28] Although we were able to print complex 3D constructs with high resolution by using this method, the low mechanical properties of the constructs after the gelation did not allow to retrieve them from the support bath (Figure S VII-3). In order to obtain constructs with higher mechanical stability, we followed the rationale of diffusing a natural crosslinking agent through the support bath. Transglutaminases are responsible for several biological events such as epidermal keratinization, blood coagulation, and regulation of erythrocyte membranes. The polymerization of proteins by microbial transglutaminase (mTG) can be achieved as a result of the formation of intermolecular or intramolecular ε-(γ-glutamyl)lysine bonds.[42] Therefore, dKECM bioinks were characterized with and without incorporation of mTG to evaluate changes in their viscoelastic properties (Figure VII-2). The density of the collagen fibers was shown to influence the flow behavior of the dKECM bioinks, indicating that higher concentrations are less sensitive to fluctuations in the shear rate. One of the most important characteristics of a bioink is to endure stress fluctuations during printing, which will then protect cellular viability during the printing process. Another prerequisite for cell-printed constructs is the maintenance of their shape and form. For that, we applied frequency sweep analysis, which revealed that increasing the density of collagen fibers resulted in increasing storage modulus, a phenomenon which was already reported in tendon tissue.[43] The inclusion of mTG also increased the modulus, as well as the gelation

time, probably because collagen fibrils take more time to reorganize into a stiffer gel. Overall, these results demonstrate that the inclusion of mTG resulted in stiffer gels with a branched ultrastructure, demonstrating ideal properties not only for bioprinting, but also for long-term stability after crosslinking. This outcome contradicts previously reported results using decellularized kidney matrix as a bioink, in which constructs were completely dissolved after 24 h of printing.[24]

Our printability data demonstrates that by our adapted methodology, we are able to print constructs from thin to thick dimensions without losing structure and integrity. We are also able to tune filament width and the quantity of material extruded by area, which revealed to be important for the overall size of the printed constructs. Moreover, constructs of anatomically relevant size can be bioprinted with specific cells, demonstrating a homogenous distribution. We have additionally demonstrated that the stress caused by printing pressure and velocity did not cause cell apoptosis, which resulted in high cell viability. A long-time culture enabled cell growth and the production of matrix by hRPCs, which was corroborated by construct shrinking after 30 days of culture. Tissue-specific decellularized ECM was already demonstrated to influence the growth, proliferation and differentiation of cells through the preservation of specific growth factors, secreted factors and several proteins.[44, 45] There is now strong evidence supporting the hypothesis that the interactions existent between cells and ECM can trigger signaling events controlling cellular fate.[46] Therefore, it was important for us to evaluate changes in the phenotypic expression with tissue-specific renal progenitor cells over the culture period. These cells are classified as a subset of multipotent progenitors existent in the adult kidney since embryogenesis, and have already demonstrated to possess regenerative properties *in vivo*.[26, 47] They have also demonstrated their clinical potential by differentiating into the most relevant kidney cellular phenotypes: parietal epithelial cells, or podocytes,[48] and tubular epithelial cells.[49] Our results indicate differentiation of hRPCs towards these two tissue-specific phenotypes, whereas gelatin-encapsulated cells remained undifferentiated, demonstrating the potential of the dKECM to provide relevant signals (Figure VII-6). Additionally, we noted a preference towards tubular commitment of hRPCs by THP higher fluorescence intensity. Indeed, its presence is increasing overtime, which was not observed for the glomerular protein NPHS1. This can be explained by two rationales: the first being the ratio between tubular and glomerular tissue existent in the kidney, the second being that podocytes are very sensitive cells with no proliferative capacity, which makes their survival difficult throughout a 30-day culture time.[27] Overall, our results show a synergistic effect of the decellularized matrix combined with tissue-specific cells and a construct with tailored porosity, which enables favorable cell growth, organization and differentiation inside the printed filaments. These tissue-engineered constructs demonstrate being

renotropic, guiding tissue morphogenesis through the modulation of cell-cell and cell-matrix interactions. Future studies will be focused on the functionality assessment of these constructs and posterior *in vivo* implantation in a kidney diseased animal model.

Another potential application of this tissue analogue would be their application on tissue-engineered modeling systems. The human kidney filters almost 180 L of plasma every day, which makes it one of the most susceptible organs to injury. Indeed, nephrotoxic drugs and interruptions of blood flow into the kidneys represent the major causes of small kidney injuries.[50] An accurate modeling system would be extremely valuable to predict the outcomes of potential toxic exposures to certain drugs, while at the same time recreating histomorphological changes which would enable the study of kidney pathophysiology. Other authors have already recreated a tubular analogue using cell printing with kidney decellularized matrices.[9] Herein, we were able to recreate a pre-glomerular model, consisting on the co-printing of two types of cells that compose the glomerular filtration barrier: parietal epithelial cells and endothelial cells, along with the glomerular basement membrane. Both cell types remained viable after 48 h, which is sufficient time to assess the diffusion of a certain compound on the glomerular barrier, due to the high porosity of the constructs. Although there is still room for improving cellular placement in order to study the barrier function, this study demonstrates the potential of dKECM bioinks to produce a macro interpretation of a glomerular barrier and is an attractive starting point for *in vitro* tissue reconstruction.

## VII-5. Conclusions

We have successfully developed an optimized a bioink uniquely composed of kidney decellularized matrix. The mechanical properties of the bioink have shown being highly favorable for bioprinting and its structural integrity has shown being dependent on the utilization of a support bath with diffusion of transglutaminase. Cellular encapsulation was successfully achieved, with high cell viability. More importantly, we were able to demonstrate that cellular fate is dependent on the substrate in which they are cultured. Overall, the bioink preserved and provided the kidney specific microenvironment necessary for the migration, maturation and differentiation of reparative renal progenitor cells. Our printing strategy opens a new avenue not only for the reconstruction of renal tissue analogues for regenerative medicine, but also for the development of new *in vitro* models enabling studying the human physiology and pathology with great potential to develop a new understanding of the kidney structure and function.

## Acknowledgements

The authors wish to acknowledge Prof. Paola Romagnani for providing the cells to conduct this study. Moreover, authors also wish to acknowledge the funding provided by the Portuguese Foundation of Technology (FCT) on the PhD Grants on the Doctoral Program on Advanced Therapies for Health (PATH) (PD/BD/128102/2016, PD/BD/150518/2019), on the individual grant on the scientific employment stimulus (CEECIND/01375/2017) and on the project Cells4_IDs (PTDC/BTM-SAL/28882/2017), under the Compete2020 Funding Program.

## VII-6. REFERENCES

1. Liyanage T, Ninomiya T, Jha V, et al (2015) Worldwide access to treatment for end-stage kidney disease: A systematic review. Lancet 385:P1975-1982. https://doi.org/10.1016/S0140-6736(14)61601-9
2. Wang H, Naghavi M, Allen C, et al (2016) Global, regional, and national life expectancy, all-cause mortality, and cause-specific mortality for 249 causes of death, 1980-2015: a systematic analysis for the Global Burden of Disease Study 2015. Lancet 388:1459–1544. https://doi.org/10.1016/S0140-6736(16)31012-1
3. Fonseca DR, Sobreiro-Almeida R, Sol PC, Neves NM (2018) Development of non-orthogonal 3D-printed scaffolds to enhance their osteogenic performance. Biomater Sci 6:1569–1579. https://doi.org/10.1039/c8bm00073e
4. Frazão LP, Vieira-de-Castro J, Nogueira-Silva C, Neves NM (2020) Method to decellularize the human chorion membrane. In: Cell-Derived Matrices Part B, 1st ed. Academic Press, pp 23–35
5. Sobreiro‐Almeida R, Elena Melica M, Lasagni L, et al (2020) Co‐cultures of renal progenitors and endothelial cells on kidney decellularized matrices replicate the renal tubular environment in vitro. Acta Physiol 230:e13491. https://doi.org/10.1111/apha.13491
6. Lin NYC, Homan KA, Robinson SS, et al (2019) Renal reabsorption in 3D vascularized proximal tubule models. Proc Natl Acad Sci U S A 116:5399–5404. https://doi.org/10.1073/pnas.1815208116
7. Gomes ME, Rodrigues MT, Domingues RMA, Reis RL (2017) Tissue engineering and regenerative medicine: new trends and directions - A year in review. Tissue Eng - Part B Rev 23:211–224. https://doi.org/10.1089/ten.teb.2017.0081
8. Montserrat N, Garreta E, Izpisua Belmonte JC (2016) Regenerative strategies for kidney engineering. FEBS J 283:3303–3324. https://doi.org/10.1111/febs.13704
9. Singh NK, Han W, Nam SA, et al (2020) Three-dimensional cell-printing of advanced renal tubular tissue analogue. Biomaterials 232:119734. https://doi.org/10.1016/j.biomaterials.2019.119734
10. Chimene D, Lennox KK, Kaunas RR, Gaharwar AK (2016) Advanced Bioinks for 3D Printing: A Materials Science Perspective. Ann Biomed Eng 44:2090–2102. https://doi.org/10.1007/s10439-016-1638-y
11. McCormack A, Highley CB, Leslie NR, Melchels FPW (2020) 3D Printing in Suspension Baths: Keeping the Promises of Bioprinting Afloat. Trends Biotechnol 38:584–593. https://doi.org/10.1016/j.tibtech.2019.12.020

12. Mendes BB, Gómez-Florit M, Hamilton AG, et al (2020) Human platelet lysate-based nanocomposite bioink for bioprinting hierarchical fibrillar structures. Biofabrication 12:015012. https://doi.org/10.1088/1758-5090/ab33e8
13. Choudhury D, Tun HW, Wang T, Naing MW (2018) Organ-Derived Decellularized Extracellular Matrix: A Game Changer for Bioink Manufacturing? Trends Biotechnol 36:787–805. https://doi.org/10.1016/j.tibtech.2018.03.003
14. Sobreiro-Almeida R, Melica ME, Lasagni L, et al (2020) Cytocompatibility, Bioactivity and Proteomic Analysis of Particulate Porcine Kidney Extracellular Matrix. Advance Ar: https://doi.org/10.1039/D0BM01272F
15. Sobreiro-Almeida R, Fonseca DR, Neves NM (2019) Extracellular matrix electrospun membranes for mimicking natural renal filtration barriers. Mater Sci Eng C 103:109866. https://doi.org/10.1016/J.MSEC.2019.109866
16. O'Neill JD, Freytes DO, Anandappa AJ, et al (2013) The regulation of growth and metabolism of kidney stem cells with regional specificity using extracellular matrix derived from kidney. Biomaterials 34:9830–9841. https://doi.org/10.1016/j.biomaterials.2013.09.022
17. Su J, Satchell SC, Shah RN, Wertheim JA (2018) Kidney decellularized extracellular matrix hydrogels: Rheological characterization and human glomerular endothelial cell response to encapsulation. J Biomed Mater Res - Part A 106A:2448–2462. https://doi.org/10.1002/jbm.a.36439
18. Nagao RJ, Xu J, Luo P, et al (2016) Decellularized Human Kidney Cortex Hydrogels Enhance Kidney Microvascular Endothelial Cell Maturation and Quiescence. Tissue Eng Part A 22:1140–1150. https://doi.org/10.1089/ten.TEA.2016.0213
19. Claudio-Rizo JA, Delgado J, Quintero-Ortega IA, et al (2018) Decellularized ECM-Derived Hydrogels: Modification and Properties. In: Hydrogels, 1st ed. IntechOpen, pp 3–22
20. Pati F, Jang J, Ha DH, et al (2014) Printing three-dimensional tissue analogues with decellularized extracellular matrix bioink. Nat Commun 5:3935. https://doi.org/10.1038/ncomms4935
21. Mao Q, Wang Y, Li Y, et al (2020) Fabrication of liver microtissue with liver decellularized extracellular matrix (dECM) bioink by digital light processing (DLP) bioprinting. Mater Sci Eng C 109:110625. https://doi.org/10.1016/j.msec.2020.110625
22. Kim J, Shim IK, Hwang DG, et al (2019) 3D cell printing of islet-laden pancreatic tissue-derived extracellular matrix bioink constructs for enhancing pancreatic functions. J Mater Chem B 7:1773–1781. https://doi.org/10.1039/c8tb02787k
23. Badylak SF, Freytes DO, Gilbert TW (2015) Reprint of: Extracellular matrix as a biological scaffold material: Structure and function. Acta Biomater 23:S17–S26. https://doi.org/10.1016/j.actbio.2015.07.016
24. Ali M, Anil Kumar PR, Yoo JJ, et al (2019) A Photo-Crosslinkable Kidney ECM-Derived Bioink Accelerates Renal Tissue Formation. Adv Healthc Mater 8(7):e1800992. https://doi.org/10.1002/adhm.201800992
25. Guéroult M, Picot D, Abi-Ghanem J, et al (2010) How cations can assist dnase i in DNA binding and hydrolysis. PLoS Comput Biol 6:e1001000. https://doi.org/10.1371/journal.pcbi.1001000
26. Sagrinati C, Netti GS, Mazzinghi B, et al (2006) Isolation and Characterization of Multipotent Progenitor Cells from the Bowman's Capsule of Adult Human Kidneys. J Am Soc Nephrol 17:2443–2456. https://doi.org/10.1681/ASN.2006010089
27. Vaughan MR, Pippin JW, Griffin S V., et al (2005) ATRA induces podocyte differentiation and alters nephrin and podocin expression in vitro and in vivo. Kidney Int 68:133–144. https://doi.org/10.1111/j.1523-1755.2005.00387.x
28. Moxon SR, Cooke ME, Cox SC, et al (2017) Suspended Manufacture of Biological Structures. Adv Mater 29:. https://doi.org/10.1002/adma.201605594

29. Böhning M, Frasca D, Schulze D, Schartel B (2019) Multilayer graphene/elastomer nanocomposites. In: Carbon-Based Nanofillers and Their Rubber Nanocomposites: Fundamentals and Applications, 1st ed. Elsevier, pp 139–200
30. Echave MC, Burgo LS, Pedraz JL, Orive G (2017) Gelatin as Biomaterial for Tissue Engineering. Curr Pharm Des 23:3567–3584. https://doi.org/10.2174/0929867324666170511123101
31. Echave MC, Domingues RMA, Gómez-Florit M, et al (2019) Biphasic Hydrogels Integrating Mineralized and Anisotropic Features for Interfacial Tissue Engineering. ACS Appl Mater Interfaces 11:47771–47784. https://doi.org/10.1021/acsami.9b17826
32. Jin GZ, Kim HW (2017) Effects of Type I Collagen Concentration in Hydrogel on the Growth and Phenotypic Expression of Rat Chondrocytes. Tissue Eng Regen Med 14:383–391. https://doi.org/10.1007/s13770-017-0060-3
33. Orlando G, Farney AC, Iskandar SS, et al (2012) Production and implantation of renal extracellular matrix scaffolds from porcine kidneys as a platform for renal bioengineering investigations. Ann Surg 256:363–370. https://doi.org/10.1097/SLA.0b013e31825a02ab
34. He M, Callanan A, Lagaras K, et al (2017) Optimization of SDS exposure on preservation of ECM characteristics in whole organ decellularization of rat kidneys. J Biomed Mater Res - Part B Appl Biomater 105:1352–1360. https://doi.org/10.1002/jbm.b.33668
35. Nakayama KH, Batchelder CA, Lee CI, Tarantal AF (2010) Decellularized rhesus monkey kidney as a three-dimensional scaffold for renal tissue engineering. Tissue Eng - Part A 16:2207–2216. https://doi.org/10.1089/ten.tea.2009.0602
36. Orlando G, Booth C, Wang Z, et al (2013) Discarded human kidneys as a source of ECM scaffold for kidney regeneration technologies. Biomaterials 34:5915–5925. https://doi.org/10.1016/j.biomaterials.2013.04.033
37. Poornejad N, Momtahan N, Salehi ASM, et al (2016) Efficient decellularization of whole porcine kidneys improves reseeded cell behavior. Biomed Mater 11:025003. https://doi.org/10.1088/1748-6041/11/2/025003
38. Badylak SF, Gilbert TW (2008) Immune response to biologic scaffold materials. Semin Immunol 20:109–116. https://doi.org/10.1016/j.smim.2007.11.003
39. Daly KA, Stewart-Akers AM, Hara H, et al (2009) Effect of the $\alpha$ gal epitope on the response to small intestinal submucosa extracellular matrix in a nonhuman primate model. Tissue Eng - Part A 15:3877–3888. https://doi.org/10.1089/ten.tea.2009.0089
40. Lynn AK, Yannas I V., Bonfield W (2004) Antigenicity and immunogenicity of collagen. J Biomed Mater Res - Part B Appl Biomater 71:343–354. https://doi.org/10.1002/jbm.b.30096
41. Kim WJ, Lee H, Lee JU, et al (2020) Efficient myotube formation in 3D bioprinted tissue construct by biochemical and topographical cues. Biomaterials 230:119632. https://doi.org/10.1016/j.biomaterials.2019.119632
42. Cozzolino A, Di Pierro P, Mariniello L, et al (2003) Incorporation of whey proteins into cheese curd by using transglutaminase. Biotechnol Appl Biochem 38:289–295. https://doi.org/10.1042/ba20030102
43. Toprakhisar B, Nadernezhad A, Bakirci E, et al (2018) Development of Bioink from Decellularized Tendon Extracellular Matrix for 3D Bioprinting. Macromol Biosci 18:e1800024. https://doi.org/10.1002/mabi.201800024
44. Lennon R (2017) Extracellular Matrix Biology Applied to the Kidney. In: Kidney Transplantation, Bioengineering, and Regeneration: Kidney Transplantation in the Regenerative Medicine Era, 1st ed. Academic Press, p 1252
45. Ullah I, Busch JF, Rabien A, et al (2020) Adult Tissue Extracellular Matrix Determines Tissue Specification of Human iPSC-Derived Embryonic Stage Mesodermal Precursor Cells. Adv Sci 7:1901198. https://doi.org/10.1002/advs.201901198

46. Guilak F, Cohen DM, Estes BT, et al (2009) Control of Stem Cell Fate by Physical Interactions with the Extracellular Matrix. Cell Stem Cell 5:17–26. https://doi.org/10.1016/j.stem.2009.06.016
47. Lazzeri E, Crescioli C, Ronconi E, et al (2007) Regenerative potential of embryonic renal multipotent progenitors in acute renal failure. J Am Soc Nephrol 18:3128–3138. https://doi.org/10.1681/ASN.2007020210
48. Lasagni L, Angelotti ML, Ronconi E, et al (2015) Podocyte Regeneration Driven by Renal Progenitors Determines Glomerular Disease Remission and Can Be Pharmacologically Enhanced. Stem Cell Reports 5:248–263. https://doi.org/10.1016/j.stemcr.2015.07.003
49. Angelotti ML, Ronconi E, Ballerini L, et al (2012) Characterization of Renal Progenitors Committed Toward Tubular Lineage and Their Regenerative Potential in Renal Tubular Injury. Stem Cells 30:1714–1725. https://doi.org/10.1002/stem.1130
50. Bellomo R, Kellum JA, Ronco C, et al (2012) Acute kidney injury. Lancet 380:756–66. https://doi.org/10.1016/S0140-6736(11)61454-250.

## VII-7. SUPPLEMENTARY INFORMATION

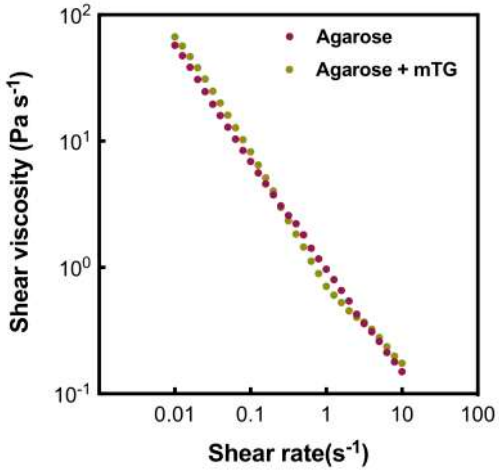


Figure S VII-1 – Rheological characterization of the agarose support bath. Flow behavior of the agarose support bath measured at RT. Viscosity was measured by increasing shear rates on samples with (yellow dots) and without microbial transglutaminase (mTG, red dots).

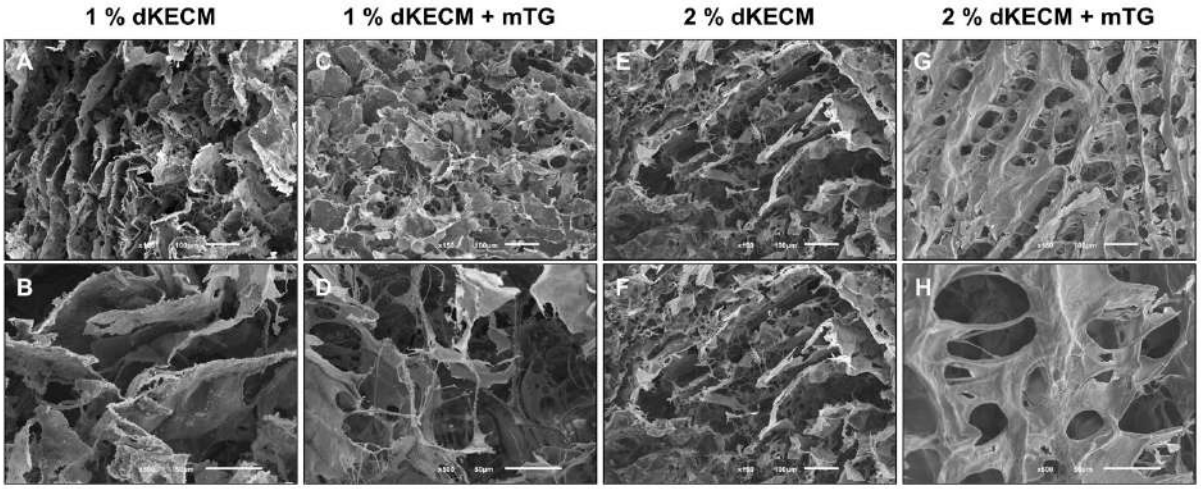


Figure S VII-2 – Scanning Electron micrographs of 1 and 2 % dKECM concentrations with and without microbial transglutaminase (mTG). (A-D) 150× magnification. Scale bar: 100 µm; (E-G) 500× magnification. Scale bar: 500 µm.

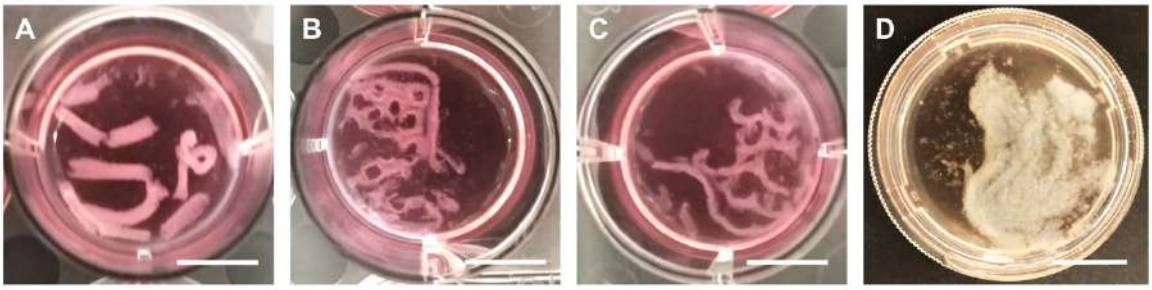


Figure S VII-3 – Macroscopic printability evaluation using different 3D models. (A-D) Representative images of the constructs printed without addition of transglutaminase to the support bath. Photos were taken after a 2 h incubation at 37 °C, removal of the support bath and addition of media. Scale bars: 1 cm.

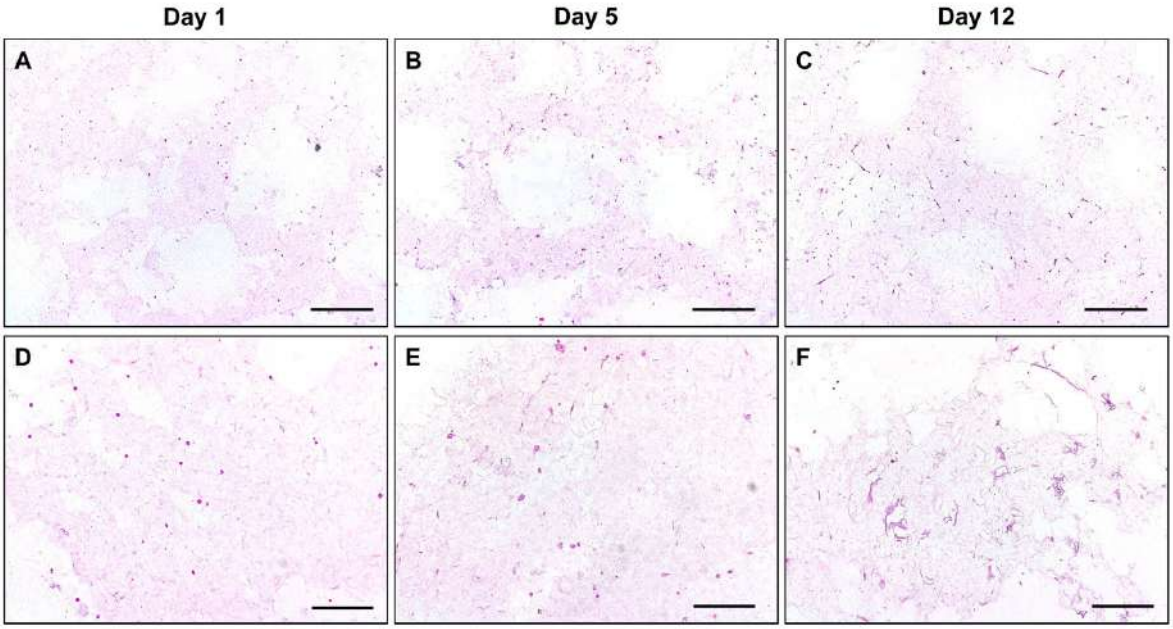


Figure S VII-4 – Histological evaluation of cellular performance inside the dKECM constructs. Hematoxylin and Eosin staining on 5 µm paraffin slices, after inclusion on Histogel®. (A-C) Scale bar: 500 µm; (D-F) Scale bar: 200 µm.

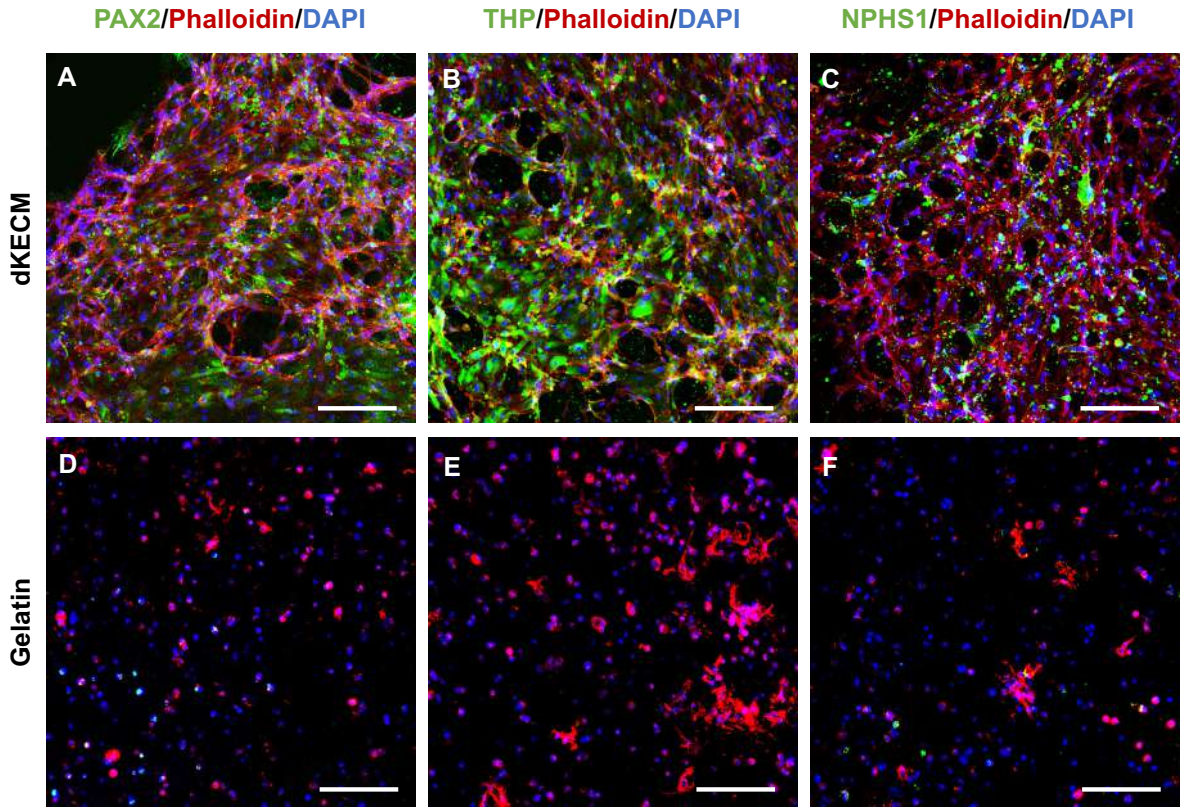


Figure S VII-5 – Evaluation of differentiation into renal-specific lineages and overall maturation of the constructs. (A-F) ICC micrographs of renal-specific markers PAX2, THP and NPHS1 on dKECM and gelatin-encapsulated cells after 21 days of culture. Green stains for specific cell marker, phalloidin (red) stains for cytoskeleton and DAPI (blue) stains for nuclei. Scale bar: 250 µm.

# SECTION 5

# GENERAL CONCLUSIONS

# Chapter VIII

# General Conclusions and Future Perspectives

# Chapter VIII

# General Conclusions and Future Perspectives

## VIII-1. GENERAL CONCLUSIONS

Kidney-related diseases constitute one of the most important health challenges in modern society. Although science has developed new and innovating advanced therapies for treatment of other devasting diseases, no solutions have emerged so far for the initial repetitive stages of renal dysfunction. Diseased patients are in an irreversible situation dependent on renal replacement therapies, which account with 3 to 5 % of annual government healthcare budgets. Besides, each patient needs to wait in average 3.6 years for a kidney transplant, which claims for new therapeutic solutions. The work performed under the scope of this thesis aimed to propose new solutions for the treatment of kidney diseases, namely the development of new tissue-engineered kidney models, and the development of new advanced therapies to treat initial repetitive episodes of kidney injury. For that, we used decellularized matrices, which are known for their potential as a virtually infinite source for organ transplantation. As these are very versatile materials, we used these matrices as a basis for the fabrication of various bioactive substrates. We also emphasized the use of human renal progenitor cells, a subset of reparative cells existing in the adult kidney. The proposed approaches aim to overcome the current limitations on the treatment of kidney diseases, and to avoid reaching end-stage renal disease, by intervening for an early treatment.

We first focused our efforts on the development of new tissue engineered kidney models. Although these models will not replace the traditional experimental methodologies of cell therapies and animal models, they can provide relevant information, enabling a proper testing with more predictive value. Additionally, these models will help researchers to go from experimental assays to clinical trials, which is a critical step. Therefore, we explored both tubular and glomerular models, as the process of filtration is entirely different, from the architecture and composition of the filtration barrier, to the filtrated molecules. Most filtration membranes composing bioartificial kidney devices are composed of synthetic polymers. In these works, we proposed using decellularized matrix as components of these membranes. Indeed, we were able to demonstrate the biological benefit of having a higher fraction of matrix in detriment of polymeric material for allowing tubule functionality. By further exploring these membranes, we were able

to recapitulate not only morphological and physiological functions but also a system capable of maintaining the maturity of differentiated cells. Since changes in ECM composition are tightly related with pathological conditions, we concluded that having a very similar composition to the human kidney helps on the maintenance of phenotype and therefore on the development of accurate tissue engineered tubular models. Additionally, we were also able to validate the chemical modulation of nephrotoxicity on this epithelium-endothelium model, which may significantly contribute for the future investigation of advanced therapies for kidney diseases.

A different type of tissue engineered model, an organotypic model, was also developed in this thesis. This model relies on the use of simple building blocks that consist of a single cell type in a 3D environment, mimicking early developmental stages. Besides establishing adequate cell culture conditions, we confirmed the potent effect of retinoic acid on the glomerular differentiation of renal progenitor cells' 3D cultures, which may have a huge impact in this area of research. These cells, which can be isolated through tissue or urine samples of patients, demonstrated being a valuable resource to compose these systems, revealing 3D spatial organization and specific renal differentiation. Indeed, we concluded that organotypic cultures developed from primary adult cells are scarce but may be the answer for connecting the current existing gap between tissue models and personalized medicine. We also demonstrated that it is possible to include endothelial cells on these models. The normal function of the glomerular and peritubular endothelium is crucial for the preservation of renal structure and function. Therefore, its inclusion of tissue engineered models may be very valuable for therapeutic strategies aimed at preserving and/or restoring the integrity of the endothelial glycocalyx as well as for developmental and toxicological studies.

The versatility of the decellularized extracellular matrix allowed us to propose this biomaterial for integrated renal advanced therapies. For that, we processed it into a particulate form, which allowed us to fabricate several biomaterial structures. When developing tissue engineered substitutes for renal regeneration, it is crucial to understand kidney architecture, organization and disease in order to produce an adequate biomaterial in terms of structure, mechanical properties and biological activity. Therefore, we fabricated two moldable versions, appropriate for *in vivo* implantation, both composed uniquely of decellularized kidney matrix. With these studies, we have concluded that the particulate matrix and the bioinks are excellent substrates for supporting renal progenitor cell attachment, proliferation and growth in 3D cultures. We confirmed that the matrix preserved and provided the renal specific microenvironment necessary for the migration, maturation and differentiation of renal progenitor cells. Moreover, the matrix

has shown having a similar protein composition to the human kidney, a finding which allowed us to propose this biomaterial as a strong candidate to be used for regenerative medicine therapies, with promising patient engraftment. Our tissue engineering strategies based on decellularized kidney matrix opened a new era of research on natural-origin biomaterials for kidney regeneration and also open new possibilities for addressing renal pathologies in its early stages, which are currently inexistent.

Altogether, the work developed under this thesis enabled obtaining a significant advance in the field of kidney decellularized biomaterials. We not only fully characterize the porcine decellularized matrix, as we demonstrate its intrinsic bioactivity, a comprehensive work that was missing in the literature. Our search for a strategy envisioning functional recovery of the injured kidney is just in its beginning, but we paved the way for all researchers working in this area of investigation. As a general conclusion, the work developed in this thesis represents a step forward towards the development of new tissue engineered approaches for the treatment of kidney injuries.

## VIII-2. Future Perspectives

The findings of this thesis allowed obtaining a deeper understanding of the potential of using extracellular matrices as biomaterials, being only the first step of an ambitious process. As these biomaterials revealed being promising, a full array of validations has to be performed in order demonstrate their value, including *in vivo* implantation and immunogenicity studies.

This thesis emphasizes the use of adult human renal progenitor cells as an easily available source, capable of differentiating into several renal phenotypes. However, there is still room to further study the reparative potential of these cells. Their secretome and extracellular vesicles would enable defining the proteomic profile of these cells and hopefully characterize the mechanisms of kidney remodeling and regeneration after injury. Regarding their inclusion on organotypic models, the replication of functional characteristics on a self-organizational model is still a very difficult task. Future studies can rely on inclusion of other cell types comprising the glomerulus and on the self-assembly of more established glomerular structures.

Regarding the tissue engineered models, there is also a need for major improvement. Because kidney microenvironment is so complex, it is one of the organ systems more difficult to reproduce *in vitro*. Although we replicated some functional aspects of the tubular barrier, a more complex system with other cell types and flow-induced shear stress would be essential to better understand and mimic the

physiological conditions. An advanced possibility would be integrating both glomerular and tubular models in a microphysiological system comprising both capillaries and filtration units.

Another important aspect to be studied relies on the standardization of the decellularization process, so that the employed methodology enables to obtaining raw materials with consistent properties. This can be performed by developing a perfusion decellularization system. This system would enable shortening the decellularization time and also increase the efficacy in removing all residual kidney cellular material. Another important study regarding the use of decellularized matrices could rely on exploring by which mechanisms they stimulate differentiation of stem or progenitor cells. Although decellularized matrices already demonstrated tissue and site-specificity in terms of composition, it is crucial to understand which differences directly influence the cell fate and differentiation.

Although porcine-derived decellularized matrices have already been approved for human use, each organ is unique by itself, and further *in vivo* validation as a kidney-derived material needs to be demonstrated. There is also the need to understand the difference in inflammatory responses and remodeling upon implantation of different structures of decellularized matrices. However, the currently available animal models do not replicate the extent of chronic kidney injury, composed mainly of fibrotic tissue. Instead, the most used animal model of chronic kidney injury relies on a 5/6 nephrectomy, which is not ideal for applying a regenerative strategy nor representative of kidney diseases.

Overall, the use of kidney matrix-derived biomaterials opens a new area of research which is still in its youth. There is a whole list of research questions and hypothesis yet to be answered and validated, making this a promising biomaterial for further exploring.